Vegetation change detection and soil erosion risk assessment modelling in the Man River basin, Central India

THAKUR, JITENDRA

Vegetation change detection and soil erosion risk modelling in the Man River basin, Central India

---

Jitendra Thakur

Department of Geography

Durham University

This thesis is submitted in accordance with the regulations for the degree of Doctor of Philosophy at Durham University,

Department of Geography, 2015

Declaration

I confirm that no part of the material presented in this thesis has previously been submitted by me or any other person for a degree in this or any other university. In all cases, where it is relevant, material from the work of others has been acknowledged.

Signed

Data

Statement of Copyright

Abstract

Land use change directly increased soil erosion risk, which is a very sensitive environmental issue in Central India. To evaluate the response of land use changes on soil erosion risk, research was implemented using remote sensing techniques, coupled with ground information, to develop an integrated modelling approach to study the factors driving land use changes in the Man River basin, Central India. Results were used to assess the impact of land use change on soil erosion risk.

First, a series of sub methods were applied to monitor and verify land use land cover change in the study area which included pre-processing, classification and assessment of land use transaction from 1971 to 2013 using Landsat time series imagery. Additionally, an independent spatial assessment of deforestation, forest degradation and responsible drivers for the period 2009-2013 was conducted to enable a deeper analysis of forestry activates using the GIS based direct interpretation approach. The research also developed a robust accuracy assessment method to check the quality of the 2009 and 2013 classification maps using good quality Google Earth ™ imagery and a field measured GPS dataset. These approaches were largely based on the GOFC- GOLD (2010) and IPCC good recommendations for land use land cover mapping and verification. The information obtained from an accuracy assessment was also used to estimate deforestation area and construct confidence intervals that reflect the uncertainty of the area estimates obtained. Such analysis is rarely applied in current published verification assessments.

In the second phase of the study, a Geo-spatial interface for process-based Water Erosion Prediction Project (GeoWEPP) was implemented, to estimate the response of land use and land cover change on soil erosion risk in several scenarios derived from both ground and satellite based precipitation, DEMs and vegetation change. GeoWEPP was used at the hillslope scale in three selected watersheds within the Man River basin using Landsat, LISS-III, Cartosat-1, ASTER, SRTM, TRMM and ground based datasets.

The results highlight that the study developed a realistic approach using remote sensing techniques to understand the pattern and process of landscape change in the Man River basin and its response on soil erosion risk. Over the last four decades, forest and agriculture areas were found to be the most dynamic land use /land cover categories. During the last four decades, around 54200 ha (33.7 %) forest area has been decreased due to the expansion of agriculture, forest harvesting and infrastructure development. The direct interpretation approach estimated similar patterns of deforestation and forest degradation associated with

drivers for the 2009 to 2013 time period, but this approach also provided more accurate and location specific information than automatic analysis. The overall correspondence between the map and reference data are a good measure for 2009 and 2013; 94.03 % and 92.8 % respectively. User's and producer's accuracies of individual classes range from 75 % to 99 %. Using the accuracy assessment data and a simple set of equations, an error-adjusted estimate of the area of deforestation was obtained (± 95% confidence interval) of 23382 ± 550 ha.

The estimated average annual soil loss for all three watersheds is 21 T/ha which was found to be comparable to similar studies carried out in the study region. The highest soil loss rates occurred in areas of agriculture (301 T. /ha /yr) and fallow land (158 T/ha/yr), while the lowest rates were recorded in forest land (33.45 T/ha/yr). Agriculture extension (316.5 ha) due to forest harvesting (234 ha) in the last four decades is one of the significant drivers to speed up soil erosion (7.37 T/ha/yr.) in all three watersheds. The spatial pattern of erosion risk indicates that areas with forest cover have minimum rates of soil erosion, while areas with extensive human intervention such as agriculture and fallow land, have high estimated rates of soil erosion. The different DEMs generated varied topographic and hydrologic attributes, which in turn led to significantly different erosion simulations. GeoWEPP using Cartosat-1 (30 m) and SRTM (90 m) produced the most accurate estimation of soil loss which was close to similar already published studies in the area. TRMM rainfall data has good to use as a rainfall parameter for soil erosion risk mapping in study area.

Overall, the integrated approach using remote sensing and GIS allowed a clear understanding of the factors that drive land use/land cover change to be developed and enabled the impact of this change on soil erosion risk in the Man River basin, Central India to be assessed.

Acknowledgements

I would like to express my special appreciation and thanks to my supervisor Professor Danny Donoghue and Louise Bracken, you have been tremendous mentors for me. Your guidance, support and encouragement on both researches as well as during my difficult time have been priceless. It has been an honour for me to work with you as a PhD student in Durham University. I am forever grateful to Professor Thomas Scholten for his support to my short research visit and his invite for me to work at Tubingen University, Germany .I truly appreciate the guidance he offered to improve the quality of my research. I will forever be thankful to my former supervisor, Professor Venu Trivedi, University of Indore, India for her inspiration and support at starting of PhD Project.

I would especially like to thank supporting staff at Geography Department. All of you have been there to support me when I need your help.

I am very grateful to all my friends in the Department of Geography and friends outside the University campus for their encouragement and making me feel at home while being thousands of miles away from my home. I would especially like to thank my GIS lab friends for their valuable support and making priceless and beautiful memories whilst in the GIS lab and Gordon Manley Room. I would also like to thank all of my cousins and Indian friends who supported me in my field work in Central India and incited me to strive towards my goal.

A special thanks to my family. Words cannot express how grateful I am to my family for all of the sacrifices that you've made on my behalf. Your prayer for me was what sustained me thus far.

Dedication

This thesis is dedicated in memory of my late parents **Mr Gabbusingh Thakur** and **Mrs Kundana Thakur** for their blessing and unconditional love.

“Parents don’t go anywhere, it just feels like they left, but they never leave they live on in our mannerisms, smiles, values and lifestyle forever. Parents, through us, and our children
will live for generations to come.”

Vegetation change detection and soil erosion risk assessment modelling in the Man River basin, Central India

Contents

Chapter -3: Study area and data sources

Chapter – 4: Methods use for Vegetation Change Detection

List of Appendices

List of Figures

List of Tables

List of Equations

Symbols and constants

$\hat{A}_j$ = stratified estimator

$A_{m,\ i}$ = mapped area of category i

A_{tot} = Total area of map

CSA = Critical Source Area (Garbrecht and Martz 1997)

DEM = Digital Elevation Model

EVI = Enhance Vegetation Index

i = Map Category

j = Reference category

L1T = Level One Terrain Corrected Data

MSCL = Mean Source Channel Length

NDVI = Normalized Difference Vegetation Index

$\hat{O}$ = overall accuracy

OFE = Overland Flow Elements

$\hat{p}$ = Produced accuracy

$\hat{P}_{ij}$ = proportion of area

RMSE = Root Mean Square Error

$S(\hat{A}_j)$ = Standard error of the error – adjusted estimated area

$S(\hat{p}_j)$ = Estimated standard error of the estimated area proportion

SWIR = Short Wave Infrared

TSL = Tolerable soil loss

$\hat{U}$ = User accuracy

VIS = Visible Infared shortwave

VNIR = Visible Near Infrared

W_i = Known area proportions of the map classes

ASCII = American Standard Code for Information Interchange

Chapter 1 Introduction

1.1. Introduction

Land degradation is a major concern in many parts of India due to natural and human induced causes. The varying degrees and types of land degradation stem mainly from unsustainable land use and inappropriate land management practices (Indian Government Report on Environment, 2009).The Man River basin in Central India suffers from a number of land degradation problems concerning land use resource exploitation. These include; land use changes through clearing of forests and shifting agriculture, and accelerated rates of soil erosion consequent upon deforestation (The Times of India, March 2014; Irrigation Project Report NVDA, 2008; Londhe, 1995; Madhya Pradesh Forest Department Report, 2007; Tamgadge et al., 2001). Managers of the Man River basin are therefore looking for effective conservation and management of forests and soils which requires collection and analysis of a great deal of information on the physical relationship of vegetation-soil-land management to ensure eco-friendly development of the basin.

Despite this relevance, quantitative information on deforestation, forest degradation and soil erosion are widely unknown due to unavailability of quality data and mapping techniques. Thus it is difficult to answer the question of how much, or what fraction of land degradation, is caused by a specific driver in the Man River basin and other similar basins in India. The application of remote sensing for land surface surveys and mapping is gaining importance, largely because of its ability to provide rapid and reliable data within a given time framework (Lu et al., 2007, Gao and Liu, 2008). GIS is an excellent tool for the management of large bodies of spatially extensive data with all the advantages of a computer environment: precision, consistency and absence of computational error (Ugur and Gunay, 2007; Prabaharan, 2010).

In this study, an approach using remote sensing and digital mapping techniques combined with ground information has been applied to map vegetation change in detail for identifying areas of forest degraded and eroded land in the Man River basin, Central India.

Figure 1.1: Deforestation and Soil erosion issue in news highlighting the important of environmental degradation in the study region.

The Man River basin was chosen because of the following sensitive environmental issues which made this study both challenging and interesting.

- The basin has a large forest area which is facing serious loss of trees and degradation over recent decades due to population pressure and cultivation activities (Figure 1.1).
- There is a significant tribal population which has increased in the last few decades and whom are mostly dependent on subsistence agriculture.
- There is a serious problem of soil erosion risk in the basin arising mainly from the forest loss and cultivating forest areas and hill regions (Figure 1.2).
- There are a number of small dams, a large dam, canals and ponds in the basin promoting cultivation and forest loss.
- Data availability and quality are limited and appropriate mapping technology is lacking.

Thus, these issues produced an interesting and challenging environmental dimension to the study of vegetation change and soil erosion using RS and GIS techniques in the Man River basin, Central India.

Figure 1.2: Pati, a cluster of villages in the central Indian state of Madhya Pradesh, was once dotted with lush forests. In recent years, deforestation has turned the place virtually into a desert, Photo-2006. Sources: BBC News 2014 by SohrabHura 2006.

1.2. Research Questions

To understand the process by which land cover change leads to soil erosion, this study focused around the following research questions:

1. Can landscape dynamics be mapped from satellite data and if so are appropriate data available for the period from 1970 to the present day?
2. What are the factors that have driven land cover change in the Man river basin over the last four decades?
3. How can modern soil erosion modelling techniques help to estimate erosion risk at different scales using satellite data?

1.3. Aim

The aim of research is to apply a soil erosion model to estimate erosion risk at the watershed scale in the Man Basin using remotely sensed data in an area where vegetation change has been wide spread over the last four decades.

1.4. Objectives

(1) To establish a decadal time series of ortho-rectified Landsat images from 1972 to the present day and further satellite datasets to support erosion modelling.

(2) To analyse four decades of vegetation changes in order to identify major drivers of landscape change in the Man River basin.

(3) To test the sensitivity of the GeoWEPP model to different parameterizations.

(4) To produce a soil erosion risk map to provide information for effective soil erosion conservation in selected watersheds in the Man River basin.

1.5. Thesis structure

As already noted there are two substantive themes to this research: vegetation change detection and soil erosion modelling (Figure 3.1). To cover these themes in detail the thesis is organised around these themes. The first chapter of the thesis explains the background to the research issue including the research problem, research questions, aim and objectives of the study. Chapter 2 reviews the relevant literature to establish an effective approach to evaluate the effect of land use change on soil erosion risk for the Man River basin where land use changes is very sensitive issue due to a range of drivers. The third chapter of the thesis provides background information on the study area, detailed description of remote sensing data, and the spatial datasets used to support digital input for vegetation change and erosion risk modelling. Six different types of remote sensing datasets were acquired and processed over the study area to extract spatial and temporal information for modelling. A single methodology chapter is not presented, but rather the substantive themes are treated independently. Thus Chapter 4 describes the methodological process used to employ Landsat data with field measurement and aerial imagery to monitor and verify landscape change, especially forestry activities. These methodological steps include: 1) Digital image processing for Landsat; 2) advance change matrix analysis from 1972 to 2015; 3) GIS based wall to wall direct interpretation mapping for deforestation and forest degradation associate with responsible mechanisms; 4) Robust accuracy assessment to verify thematic error of the

2009 and 2013 maps; and 5) and use of accuracy data to estimate area of land cover change and construct confidence intervals that reflect the uncertainty of the area estimation. Chapter 5 presents vegetation change detection results and discusses the ability of Landsat data to estimate land use land cover change and process going on beyond this change. First, the accuracy of thematic maps for 2009 and 2013 is discussed followed by outputs of change detection analysis based on a transition matrix of the classification maps from 1972 to 2013. Finally, the area estimation of deforestation and forest degradation associate with responsible drivers' area discussed which is based on GIS – based direct interpretation approach.

Chapter 6 then turns attention to the soil erosion modelling and presents the implementation process of the GeoWEPP model to simulate soil loss in several land use/land cover and remote sensing data scenarios for three selected watershed in Man River basin. The Geo-spatial interface for WEPP (GeoWEPP) was used to characterise soil erosion behaviour based on their land use/land cover, soil, slope and climate profiles. These characteristics were used as inputs for the WEPP model to estimate run off and soil loss for four scenarios: land use/land cover (senario1), land use/land cover change (scenario 2), DEM effects (scenario 3) and rainfall effects (scenario 4). Chapter 7 then presents the results and discussion of runoff and soil loss simulation under the four scenarios, including effects of land use/land cover on runoff and soil loss, effects of historical vegetation change on runoff and soil loss, impacts of DEMs, TRMM and ground rainfall data on runoff and soil loss. The limitations of GeoWEPP model for current application were also discussed in this chapter. Finally, Chapter 8 and 9 brings the results from the two substantive themes together and evaluates the research objectives, provides conclusions and recommendations, and suggests futures research.

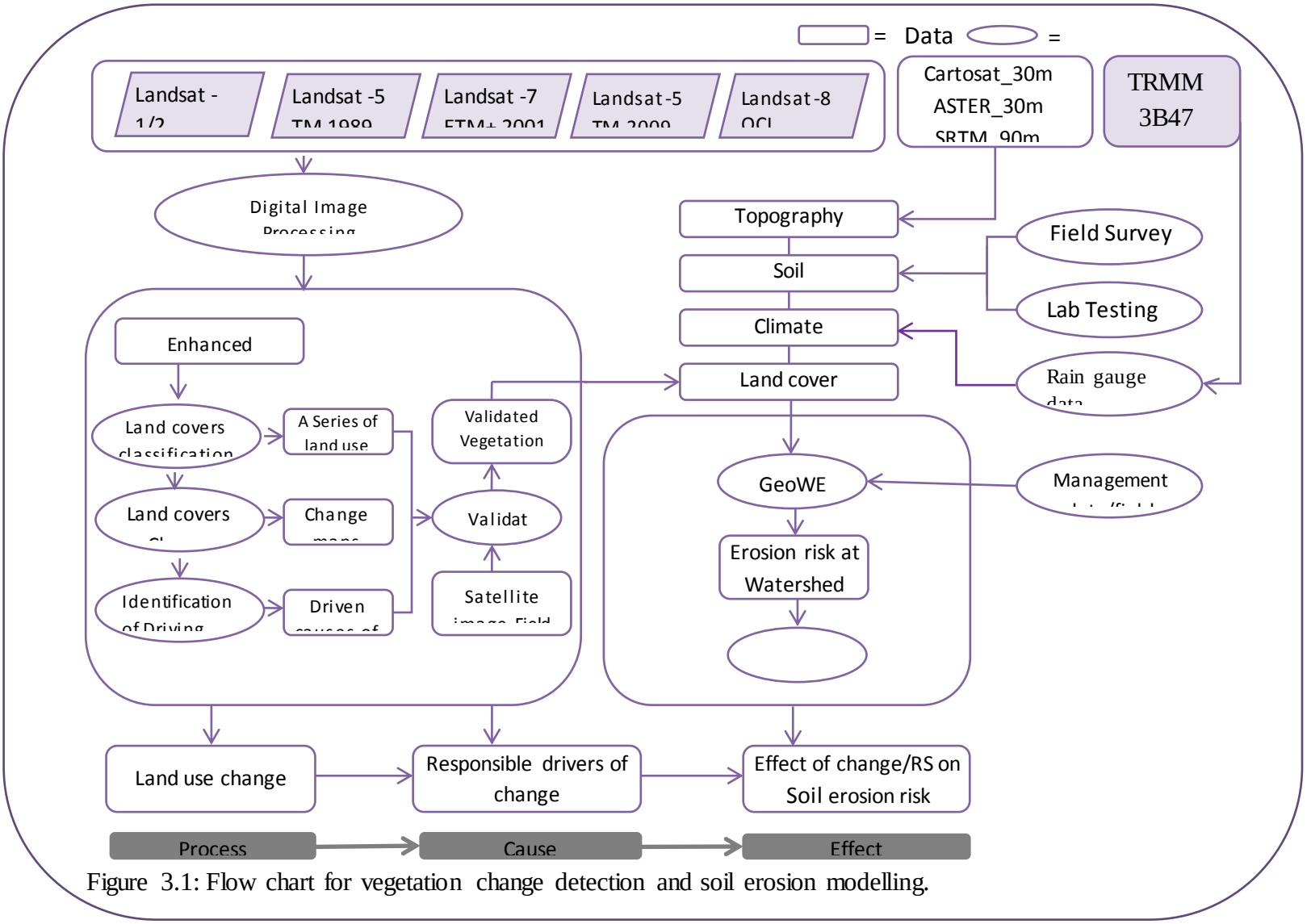

Figure 3.1: Flow chart for vegetation change detection and soil erosion modelling.

Chapter 2 Literature Review

2.1. Introduction

Soil erosion is one of the most significant forms of land degradation, greatly influenced by land use and management (Bini et al., 2006). A wide variety of research has reported that soil erosion is significantly related to land use (Del et al., 1998; Meng et al., 2001; Hessel et al., 2003; Fu et al., 2004; Bakker et al., 2005; Mutua et al., 2006; Sharma et al., 2011). Many researchers have used models and laboratory experiments to identify the relationship between land use and soil erosion (Hanson et al., 2004; Long et al., 2006; Xu et al., 2008). Several studies have also specialised in combining remotely sensed data with ground based data to understand the link between soil erosion and land use /land cover change. However, knowledge of the specific relationship between land use and soil erosion is unknown in the Man River basin, Central India, due to the lack of data and appropriate techniques. Therefore, this research focuses on the development and interrelationship of two major themes: a) Vegetation change detection modelling and b) Soil erosion risk assessment modelling based on remote sensing data. The two themes are used to understand the nature of drastic land use experienced causing distinct soil erosion in the Man River basin, Central India. This chapter outlines a wide range of existing research related to the process of vegetation change detection including specific techniques that are employed in the research, but also approaches to modelling soil erosion.

2.2. Advance change Matrix approach for change detection

A wide variety of techniques for mapping and monitoring the land use/land cover change using remote sensing and geographical information systems are reported in the scientific literature which have enhanced the efficiency of the techniques. The post-classification technique is widely adopted as it provides a matrix of land transitions among categories (Manandhar et al., 2010; Yuan et al., 2005). A post-classification change detection technique generally provides a “From-to” change matrix comprising two-dimensional (Jensen, 2005). However, traditional analysis of the change matrix is not sufficient to provide systematic signals of change and fail to indicate the intensity of the land use land cover change (LULCC) transitions (Manandhar el at., 2010; Weng, 2002; Currit, 2005). Therefore, there is a need for an updated approach to study LULCC transitions in order to detect systematic landscape changes based

on deviations of observed patterns of change. Pontius et al. (2004) was the first to introduce the methodology for determining systematic transitions and a few other studies have realized its importance and thus have adopted and extended the procedure (Braimoh, 2006; Alo and Pontius, 2008; Versace et al., 2008; Manandhar et al., 2010). Extending the traditional transition matrices beyond the size of each transition can reveal information that is important for detecting important signals of LULCC (Manandhar et al., 2010; Teferi et al., 2013). The enhanced transition matrix approach allows improved understanding of the processes of LULCC for identifying explanatory factors for further in-depth analysis as well as for practical interventions for planning and management (Teferi et al., 2013). The approach is also useful for investigating the possible drivers of transitions, and hence to propose site specific and targeted preventative measures to avoid undesirable impacts of land cover change (Pontius, 2004; Braimoh, 2006).

However, approaches using remote sensing also have the potential to provide accurate information on LULCC, but numerous problems may be encountered and the adequacy of this information has been questioned (Townshend et al., 1992; Wilkinson, 1996, Wilkinson, 2005). The enhanced transition matrix provides some additional clues to the understanding of the drivers of change, but uncertainty in the information is a further issue (Manandhar et al., 2010). Therefore, development of robust accuracy assessment is an unavoidable attribute for LULCC analysis which helps to better understand and quantify the uncertainty for the type of landscape change. It is also useful to prioritize efforts for their further development.

Foody G.M. (2002) and Stehman & Czaplewski (1998) highlighted some useful suggestions in their literature review on the current status of land cover classification accuracy assessment such as the research community does not universally adopt the approaches that are often recommended for accuracy assessment which perhaps results in several problems in accuracy assessment and means research has failed to achieve the accuracy targets commonly specified. A statistically rigorous assessment requires both a probability sampling design and statistically consistent estimators of accuracy parameters, along with a response design determined in accordance with features of the mapping and classification process such as the land-cover classification scheme, minimum mapping unit, and spatial scale of the mapping (Stehman & Czaplewski 1998). The IPCC (2004) and GOFC GOLD (2010) handbook provide a widely accepted set of good practice guidelines for dealing with uncertainty in proper manner for LULCC from satellite derived data. Information obtained from accuracy assessment sampling also helps to estimate areas of land cover or land use change and to construct confidence intervals that reflect the uncertainty of the area estimates mapped. A variety of methods exist in literature for error adjusted area estimation using information obtained from accuracy assessment sample (Card, 1982; Czaplewski, 1992; McRoberts, 2011; Stehman, 2009). These methods address the applications and concerns on use of accuracy

assessment sample for error adjusted area estimation (Olofsson, 2013). Card (1982) introduced the stratified estimator for area estimation which used in many studies (Olofsson et al, 2013; Olofsson et al, 2011, Jeon et al, 2014).

Thus, the enhanced change matrix method with Landsat time series data was used to estimate spatial and temporal trend in land use and forest change in the Man River basin, over four decades from 1972 to 2013 associating uncertainty in LULCC modelling.

2.3. Estimation of deforestation and forest degradation associated with responsible drivers.

The change matrix approach identifies tracking of land use changes between categories and is necessary to understand historical patterns and processes of landscape change. However the approach does not provide accurate information on deforestation and forest degradation linked to with responsible drivers at large spatial scales (Manandhar et al., 2010). Deeper explanation of the driving factors of LULCC dynamics is the subject of further study. Change matrix approaches based on automatic pixel analysis (the indirect approach) also contain a high level of error with deforestation mapping. Therefore, it is necessary to establish an advanced and best mapping technique to assess deforestation and forest degradation associate with responsible drivers for the Man River basin.

There is still debate internationally over the definition of degradation, a commonly adopted definition outlined in IPCC (2003) is:
"A direct human induced long term loss (persisting for X year or more) of at least Y % of forest carbon stocks (and forest values) since time T and not qualifying as deforestation or an elected activity under Article 3.4 of the Kyoto Protocol."

2.3.1. Characteristics of forest land degradation in the basin

In the Man River basin, forest degradation is define by permanent agriculture encroachment on forest areas which do not turn into forest land due to permanent ownership provided by the government. Agriculture is a major source of livelihood for tribal populations in the region which is promoted by the government to increase agriculture production through providing agriculture subsidies and facilities such as water, electricity, hybrid seeds, chemical fertilizers and pesticides (Banerjee, 2010). Government forest policy also allows farmers to extend agricultural land on the protected forest area through land ownership license of cultivated land. Farmers are mostly marginal and small farmers undertake

cultivation without soil and water conservation measures. Recently, most agricultural land has been converted from forest land, which is a permanent change in land category and the areas do not return to forest land. This permanent agriculture extension does not represent a shifting agriculture pattern as some publications suggest (GOI –UNDP-GEF 2007). Continued unsustainable cultivation reduces permanent productive capacity of the land; this forest land becomes degraded and cannot be used for any cultivation or plantation practices (see figure 2.1.). In this context, it is important to review operational methods and research that have used optical datasets to characterize degradation.

Figure 2.1.Historically, degraded areas were covered with forest which have been occupied by local formers for cultivation activities. These areas have been completely degraded.

2.3.2. Forest degradation methods

Scientific and forest policy literature contains a range of methodological approaches that have been used to identify and quantify the spatial and temporal pattern of deforestation and forest degradation (Lambin, 1999; Ringrose et al,1990; Hellden, 1991; Tucker et al., 1991; Prins and Kikula, 1996). Accurate mapping of deforestation and forest degradation is a difficult task and contains very high levels of error. Mapping forest degradation using remote sensing methods is also more difficult than mapping deforestation in the field because degraded forests are often a complex mix of different land cover types (vegetation, dead trees, soil and shade) that result from different human interventions. In optical imagery, the reflectivity

and the spectral signature of degradation can change very quickly making identification dependent on the timing and season of image acquisition (GOFC-GOLD, 2008).

2.3.3. Remote sensing methods

Remote sensing approaches provide important tools to map forest degradation at spatial and temporal scale (Eiumnoh, 2001, Symeonakis and Drake, 2004, Wessels et al., 2004) but it is also commonly agreed that mapping forest degradation using remote sensing methods is complex and more difficult than assessing deforestation because degraded forests result from different human interventions and are often a complex mix of different land cover such as vegetation, dead trees, soil and shade (Lambin, 1999; Souza et al., 2003). Remote sensing is more problematic for indicators of degradation drivers such as local wood collection or forest grazing. High resolution and ground data are required, with no widely accepted methods for mapping these types of degradation (GOFC GOLD, 2009).
Remote sensing approaches for mapping and monitoring forest degradation may be divided into two broad types: 1) direct – this method uses simply aerial photography or very high resolution spectral imagery to identify degraded areas; and 2) an automatic approach which is based on spectral differences to identify and quantify different type of forest degraded areas (Achard et al., 2008).

Studies based on direct interpretation approaches have some limitations. The temporal availability of high resolution imagery is limited which does not allow mapping degradation at temporal scales as some signature of forest degradation change quickly or at least annual mapping required (Wertz-Kanounniko., 2008). Although very expensive, the cost of high resolution imagery doesn't make it useful for degradation assessment (Souza et al., 2009, DeFries et al., 2007).

CLAS (Carnegie Landsat Analysis System) approach was developed based on the indirect method by Asner et al., (2005) and Broadbent et al., (2008) to assess forest degradation associated with selective logging using Landsat imagery. CLAS data processing steps include: i) atmospheric correction; ii) deconvolution of spectral sig-natures into sub-pixel fractional cover; iii) cloud, water, and deforestation masking; and iv) pattern recognition algorithms for forest disturbance mapping.

The major limitation of CLAS is the difficulties for atmospherically correcting Landsat imagery in the tropic regions and correcting for shade caused by partial cloud cover (Asner et al., 2005). Moreover, it is difficult to detect change with 30x30 m Landsat pixel if degradation from selective logging contains various landuses (Asner & Warner 2003).

2.3.4. Ground based methods

Field based observations are well adopted to assess the level and extend of forest degradation at small scales (Griscom *et al.* 2009), but monitoring at the regional scale is time –consuming and costly. These methods are also limited in that they are area specific and results cannot be applied anywhere (Sonneveld, 2003).

2.3.5. Integration of remote sensing and ground based methods

Integration of remote sensing and ground based approaches is a strong method to map forest change activities in detail with very high accuracy. Lambin (1999) reviewed that the integration information from the spectral, spatial and temporal domains is a necessary requirement to monitor deforestation and forest degradation. Many studies have also suggested a combination of remote sensing and ground-based survey for forest loss and degradation monitoring e.g. Asner et al. (2005), Broadbent et al. (2008), Brown and Braatz (2008), Gibbs et al. (2007), GOFC-GOLD (2010), Lambin (1999), Hansen et al. (2008), Herold et al. (2011), Saatchi (2007) and Wertz-Kanounniko (2008). The comparative analysis of the strengths and weakness among the degradation assessment methodologies and accuracy levels suggest that forest degradation assessment accuracy increases if it is supported by the ground based information (Acharya and Dangi, 2009).

A study was organized to measure forest degradation in the upper catchment of the river Tons, North India, using IRS 1D –III (23.5m), PAN (5.8m) and SRTM DEM. GPS based field survey was also included to collect information on degradation status. Finally, forest degradation was studied classifying different classes. A slope map was derived from 6 slope categories which was then correlated with the degradation map to derive slope-wise forest degradation information (Nandy *et al.*, 2011).

Linear mixture modelling has also been used to estimate selective logging in 32,520 ha area in the Amazon. A forest soil fraction image was prepared to identify logging. Soil fractions above 20% that contained from 1 to 3 contiguous pixels were considered log landings. This method is suitable, especially using high resolution imagery with ground information (Souza and Barreto, 2000).

The direct interpretation approach requires spatially explicit observations of change (i.e. deforestation layer). The data may be obtained either by sampling of geographically located points, a complete tally (wall–to–wall mapping), or a combination of the two. The approach is comprehensive and relatively simple conceptually, but data intensive to implement. The target area (i.e. forest loss) is subdivided (i.e. deforestation, degradation and responsible drivers) into spatial units such as grid cells or polygons

appropriate to the scale of land-use variation and the unit size required for sampling or complete enumeration (IPCC 2006).

Thus, in this study, a direct interpretation approach based on wall–to-wall mapping practices is developed to update the 2009-2013 year time period deforestation layer (based on automatic pixel based analysis) with ground verification to ensure the goal of vegetation modelling (to map and verify deforestation and forest degradation associated with responsible drivers). This approach is able to quantify the uncertainty in forest change mapping as it is based on verification data. The direct interpretation approach is recommended in GOFC GOLD source book (2010) and IPCC good practice guidelines (2004) to monitor forest degradation and identify drivers of deforestation and degradation with remote sensing. The availability of verification data (aerial photographs and GPS survey) makes it possible to adopt this approach for the specific time period from 2009 to 2013 year over the study area.

2.4. Soil erosion risk assessment

2.4.1. Soil degradation in the Man River basin

The level and extent of soil degradation is quite high in the Man River basin with a considerable amount of the land having become unreclaimable at the farm scale. Large scale change in land use/land cover has occurred over the past decades in the basin, but the actual effectiveness of these changes on soil erosion is difficult to quantify at the regional scale due to the complexity of soil erosion processes. The changes and improvements at the local scale can be buffered at the large scale (De Vente *et al.*, 2008). The Vindhy region (one of the largest forest regions located in the Man River basin) was historically covered with 39% dense forest in 1989, but this proportion had declined to 30% by 2005 (FSI 2009). The density of forest cover has decreased. It has been converted into open forest area as the proportion of open forest in 2009 is high at 81 % (FSI, 2009). This open forest is mostly degraded with minimal forest cover. Due to increasing population pressure in the region over the last few decades, forest areas have been drastically changed into agriculture land. Forest lands are being converted into deforested land, which is then occupied by farmers to undertake agricultural activities which in turn are increasing soil erosion risk in the river basin. High soil erosion risk on the surface, especially on the *hillslopes*, washes top soil away; this is the leading cause of soil degradation in the region.

Agriculture is the major source of livelihood of tribal populations in the region. It is promoted by the Indian government to increase agriculture production through providing agriculture subsidies and facilities like water, electricity, hybrid seeds, chemical fertilizers and pesticides (Banerjee, 2010). Government forest policy also allows farmers to extend agricultural land on the protected forest area

through land ownership licence of cultivated land. Farmers are mostly marginal and include many small farmers undertaking cultivation without soil and water conservation measures. Recently, most agricultural land converted from forest land is a permanent change in land category and the areas do not return to forest land. This permanent agricultural extension does not represent a shifting agriculture pattern as some publications suggest (GOI –UNDP-GEF 2007). Continued unsustainable cultivation reduces permanent productive capacity of the land; this forest land becomes degraded and cannot be used for any cultivation or plantation practices.

To design and implement an effective soil erosion risk management strategy for the Man river basin, the quantification of soil erosion risk in reference of historic land use land cover change scenario is required. Assessment of soil erosion risk is a challenging task due to the lack of availability of high resolution data sources and appropriate measurement techniques. Consequently, it becomes difficult to develop an effective soil erosion assessment tool for appropriate conservation and management practices in high risk areas. The information available on soil erosion has either large uncertainty or is insufficient for effective planning and conservative practice for local mangers and farmers.

The next sections review published research related to soil erosion processes and modelling technologies that provide a background to the current study. First, the application of remote sensing data for soil erosion modelling is discussed, and then soil erosion risk assessment studies including some of the popular erosion prediction models are reviewed. The specifics of the GeoWEPP model are reviewed and justification for its use in this study outlined.

2.4.2 .Satellite data and soil erosion modelling

The lack of input data for assessing soil erosion always poses a problem in developing countries. Satellite imagery can provide valuable spatial information on vegetation, terrain climate and soil parameters to improve the performance of soil erosion models (De Asis and Omasa, 2007; Zhang et al 2009). One of the most recent and comprehensive reviews of remote sensing for soil erosion assessment is made by Vrieling (2006). This review discussed the application of remote sensing in the field of erosion research by providing necessary spatial data at various scales. Several studies used remote sensing to parameterize model inputs which are explained here.

Topography is a major factor controlling water erosion. Current spatial erosion models nearly always require DEM input for the assessment of slope characteristics. Traditionally such DEMs have been

obtained from contour lines on topographic maps, or less frequently from stereo aerial photography. Recently, various options exist to extract good quality DEMs from satellite data such as LIDAR, SPOT, ASTER, synthetic aperture radar (SAR) imagery and SRTM. Many researchers have applied DEMs derived from satellite data for erosion studies (Bishop and Shroder, 2001; Barnes and Baker, 2000).

Soil properties are a significant input into models because they are involved in a large number of processes such as evapotranspiration, photosynthesis and biogeochemical cycling. Soils differ in their resistance to erosion, which is a function of a range of soil properties such as texture, structure, soil moisture, roughness, and organic matter content. Remote sensing and aerial photography techniques have been utilized in soil survey for many years. Aerial photography can be used to help identify and evaluate variation within soil mapping units (Milfred and Kiefer, 1976).

Vegetation caver: Many satellite remote sensing studies of soil erosion focus on the assessment of vegetation cover. These studies need to account for the temporal variation, and consequently image timing is highly important, although not always sufficiently highlighted variability (e.g. Cyr et al., 1995; Sharma and Singh, 1995; Jain and Goel, 2002).

Climate: TRMM observations are focused on the rain over tropical and sub-tropical regions, with swaths extending to 38°N-38°S. Recently, a few studies have focused on use of TRMM data to assess soil erosion. Vriling et al., (2008) examined 3-hourly TRMM rainfall to estimate soil erosion risk for a 100 km^2 pasture area in the Brazilian Cerrados. This study showed that TRMM data is valuable for areas where data availability is otherwise poor. Precipitation measurements from TRMM are compared with real precipitations from a rain gauge network for erosion assessment in the Himalayas at the catchment scale. Results show that TRMM data limits the small–scale erosion prediction (Christoff et al., 2009). The relative distribution of rainfall was estimated using TRMM data in the catchment basin of the MalekaWakena reservoir, Ethiopia (Bouaziz et al., 2011). Thus, remote sensing contributes to erosion assessment in many ways. Recent availability of satellite data provides new possibilities for erosion research and assists in filling current gaps. The effectiveness of most methodologies presented largely depends on site characteristics and the intended use. Many interesting techniques (models) were applied to assess soil erosion or risk. However, due to the complexity of erosion processes, regional differences, scale dependency and purpose of research, it cannot be expected that a single standardized operational erosion assessment system will be suitable for every study area.

2.4.3. Soil erosion risk assessment

Soil erosion risk is referred to as the relative risk of erosion occurring at a certain location by comparing with other locations in the region mapped (Vrieling et al., 2006). Risk assessment used in various disciplines involves identification of the risk and the measurement of the exposure to that risk. In the case of soil erosion risk assessment, it is the combination of parameters which influence the erosion processes in the landscape that provide the necessary steps to measure the intensity of the associated risk. The magnitude of erosion risk and its distribution at various locations is determined by the weights of the influential parameters and their unique combinations. Recently, many studies of soil erosion risk assessment have been undertaken around the world at the regional and local scale. A division can be made here between expert based and model based approaches.

The use of the expert based approach judgement to estimate erosion risk is an important tool (CORINE, 1992). The limitation of this approach is that the researcher does not give a clear–cut definition of the criteria according to which areas were delineated (Yassogou et al., 1998). A problem with most expert based methods is that the results are affected by the criteria defined by experts with input datasets (Knijff et al., 2000). Many researchers have therefore used modelling approaches instead.

A wide variety of model based approaches are available for assessing soil erosion risk (see Table 2.1). These prediction models are useful applications to understand the whole scenario of soil erosion process and the impact of these processes in the selected study area. Models can be sub-divided in three types; (1) Empirical or statistical/metric; (2) Conceptual; and (3) Physically based. Empirical models are a simplified representation of natural processes based on empirical observations. They are based on observations of the environment and thus are often of statistical relevance (Nearing et al., 1994). Conceptual models tend to include a general description of catchment processes, without including the specific details of process interactions, which would require detailed catchment information (Sorooshian, 1991). Physically-based models are based on the solution of fundamental physical equations describing stream flow and sediment and associated nutrient generation in a catchment. Standard equations used in such models are the equations of conservation of mass and momentum for flow and the equation of conservation of mass for sediment (e.g. Bennett, 1974).

A new method, called RUSLE _IDM coupled model, which embeds the IDM (Information Diffusion Model) into the RUSLE model was applied to reveal soil erosion risk in different scenarios in the Bohai sea region (Lifen et al 2012). Mutekanga et al (2010) tested a method for assessing change in erosion risk yield information to aid policy development and decision making for sustainable natural resources

management in the Ngenge watershed in Uganda. Historically erosion risk was evaluated in three steps using multi-temporal satellite data. First, current erosion risk was assessed by combining slope and vegetation cover during periods of high intensity rainfall. The data used for the assessment was obtained from satellite images. Erosion risk was then linked to land use and finally to the change in vegetation cover over the years 1980– 2000. This method of erosion risk mapping provides a quick and straightforward means for identifying priority areas for interventions for soil and water resource management.

An integrated method using RUSLE and GIS was adopted to determine the soil erosion risk of a forested mountainous sub-watershed in Kerala, India. GIS data layers including, rainfall erosivity (R), Soil Erodabillity (K), slope length and steepness (LS), Cover management (C) and conservation practice (P) factors were computed to determine their effects on average annual soil loss in the area (Prasanna et al., 2012) .

Models differ in terms of complexity, processes considered, and the data required for model calibration and model use. In general there is no 'best' model for all applications (Merritt et al., 2003). The most appropriate model will depend on the intended use, data requirements and the characteristics of the catchment being considered.

2.4.4. Need of physical process based model for soil erosion risk assessment at the *hillslope scale*

To undertake the proposed research a suitable soil erosion model needed to be selected to be applied to the Man River basin. The characteristics that the model needed to be appropriate for are as follows:

- The Man River basin is located in a remote area where ground data (e.g. soil, topography, vegetation and rainfall) availability is a major issue. Therefore, the choice of soil erosion model was influenced by the availability (or lack of) of datasets. Thus the model should be able to use satellite data as sufficient coverage of remote sensing data is available at spatial and temporal scale.
- Deforestation and forest degradation are strongly linked with shifting agriculture and both are major problems in the study area; hence results must help understand soil erosion /risk behaviour with different land cover at spatial and temporal scale.
- Over the past few decades, agriculture producers appear to have made improvements in tillage practices and large forest areas have been turned into the agricultural land which has changed the runoff management system and increased soil erosion risk. However, the actual effectiveness of

these changes is difficult to quantify at the regional scale due to the complexity of the soil erosion process, because improvements at the local scale can be buffered at large scale. Thus, the model should be able to work at the small scale (*hillslope* scale) .

- The model should be able to suggest spatially distributed management solutions of soil erosion risk to farmers and local mangers.

A wide range of models were explored for use in this research and these models are presented in Table 2.1, but the choise of a sutable model depends on the desired informationa and data available in the study area to run the model and map on to the objectives of the study. After careful consideration the physical processes based GeoWEPP Soil erosion model was selected. The WEPP Model has been extensively used worldwide; by several researchers in Spain (Soto and Diaz-Fierros, 1998), the UK (Brazier et al., 2000), Australia (Yu et al., 2000; Yu and Rosewell, 2001), Norway (Gronsten and Lundekvam, 2006), Brazil (Bacchi et al., 2003) and India (Pandey et al 2008, 2009). These studies have underlined the success and relevance of the model.

The GeoWEPP is designed to run using raster datasets such as DEM and land cover and soil raster files, hence it is sutable for sattelite datasets as good quiality of remote sensing data is avialble for Man River basin; appart from remote sensing data, availability of other types of information is a big issue in the region. With GeoWEPP input parameters can be prepared using remote sensing data. GeoWEPP also offers several advantages over simple empirical models. It is able to estimate the spatial and temporal distribution of net soil loss and deposition for a wide range of time periods and spatial scales (Flanagan and Nearing, 1995) and it has an enahnced technology which enables the model to simulate particle size information. The WEPP model has its own embedded climate generator (CLIGEN) (Nicks et al 1995), which produces daily estimates of precipitation, temperature, dew point, wind, and solar radiation for a single geographic point. Among the commonly used weather generator, CLIGEN is the only one that generates detailed storm parameters such as storm duration, time to peak, and intensity (Zhang and Garbrecht, 2003). A WEPP hillslope version calculates erosion along a single slope profile, or the hillslope can be divided into overland flow element (OFE) to simulate more complex hillslope soils or cropping management.

One of the requirerments of the current research is to check the response of soil erosion with historical land use/land cover change and with various land use management practices for soil conservation. GeoWEPP offers an opportunity to fulfill these requirements because the model works on the hillslope scale and is a strong tool for practical decision making to understand and manage the influence of land

use and management practices on soil. GeoWEPP also supports visualisation of soil erosion processes to aid communication of results to wider audiences.

Although several studies have been carried out using the WEPP model, further refinement and additional testing of the model is still required for wide ranging conditions. It is also evident from the literature that very limited information on application of the WEPP model using RS and GIS is available for Indian watersheds and there is none in central India. Topographical conditions, soil conditions, rainfall pattern and cultivation practices are different in India from those in other parts of the world. WEPP also has the ability to assess soil loss with different types of land cover and management practices, topography, soil and climate condition. Therefore, it is necessary to adopt a physically based model such as GeoWEPP for the study focused on the Man River basin. The detailed model structure and review of how it has been used in the research area are presented in the next section.

2.4.5. WEPP (Water Erosion Prediction Project)

The WEPP soil erosion model was developed by an interagency group of scientists working for the U.S. Department of Agriculture's Agricultural Research Service (ARS), Natural Resources Conservation Service, and Forest Service; and the U.S. Department of Interior's Bureau of Land Management (BLM) and the U.S. Geological Survey (USGS). The model has many users around the world for example, the WEPP model has been calibrated and validated using IRS-1C LISS–III satellite data for a small hilly watershed (Karso) of India. The analysis showed that the sediment yield is highly sensitive to interrill erodibility and effective hydraulic conductivity, whereas, runoff is sensitive to effective hydraulic conductivity only (Pandey et al., 2008). The WEPP model was also used as a modelling tool for the identification of critical watersheds and evaluation of best management practices for a small hilly watershed (Karso) of India.

The recent modification of the Water Erosion Prediction Project (WEPP) model has improved its applicability to hydrology and erosion modelling in forest watersheds. To generate reliable topographic and hydrologic inputs for the WEPP model, carefully selecting digital elevation models (DEMs) with appropriate resolution and accuracy is essential because topography is a major factor controlling water erosion. The WEPP (v2006.201) was applied to hydrological and erosion simulation for two small forest watersheds in northern Idaho. A total of six DEMs from the National Elevation Dataset (NED), Shuttle Radar Topography Mission (SRTM), and LIDAR at three resolutions (30 m, 10 m, and 4_m) were used to calculate topographic parameters as inputs to the WEPP model WEPP v2006.201 using the 10 m LIDAR

DEM (vs. using other DEMs). Model runs produced a total amount of, as well as, seasonal patterns of watershed discharge and sediment yield that were closest to field observations (Zhang et al 2009).

In another study, three different approaches using geographical information system (GIS) and digital evolution model (DEMs) were used and evaluated for applying the WEPP model to assess water erosion in small watersheds. Results of the analysis suggest that, given an accurate DEM and valid input data for a simple watershed, the automatic hillslope method can be used to facilitate the application of the WEPP (Cochrane and Flanagan 1999). An initial application of the WEPP model with a raster-based GIS was also conducted by Savabi et al., (1995) in a small watershed in Indiana. Cochrane and Flanagan (1999) developed an interface between WEPP (Watershed version), and Arc View GIS for small basins (0.59–29 ha), comparing the results obtained from the manual application of WEPP with those obtained using the interface, and studying the effect of DEM resolution on the results from the GIS WEPP interface. Integration of WEPP with a Geographical information System (GIS) is desirable because it facilities and improves model application. GeoWEPP is a geo-spatial erosion prediction model interfaced in ArcGIS. The limitations of WEPP, that is manual generation of input data and its application in small watershed, can be overcome by GeoWEPP.

Table 2.1.Soil erosion models.

NO	MODEL	TYPE	SCALE	INPUT	OUT PUT	References
1.	PESERA (Pan-European Soil Erosion Risk Assessment)	A process-based	Regional,	Soil ,Land cover Topography Climate	Erosion Risk	Kirkby et al., 2003
2.	WEPP	Physical	Hill slope , Catchment	Climate Management Soil ,Topography	Soil loss Sediment loss Scenario analysis	Flanagan et al., 1995 Flanagan and Nearing, 1995
3.	SWAT(Soil and Water assessment Tool)	Physical	Catchment	Topography Soil, Climate Land Use	Run off Soil erosion	Arnold et al., 1998; Srinivasan et al., 1998
4.	LISEM (LImburgSoil Erosion Model)	Physical based	Small catchment	Climate, DEM Land Use Soil Types,Road	Hydrographs and sedigraphs,Erosion and deposition maps	De Roo et al, 1996a, De Roo et al., 1996b and Jetten, 2002
5.	ANSWERS	Physical	Small	Land cover	Runoff	Beasley et al.,

	(Areal Nonpoint Source Watershed Environment Response Simulation)	based	catchment	Soil , slope , Land Use ,	and erosion, nutrients	1980 Sharma and singh 1995
6.	TOPOG	Physical based	Hills slope	High input	Water logging, erosion hazard, solute transport.	
7.	AGNPS (Agriculture Non – Point Sources Pollution Model)	Conceptual	Small catchment	High Input,	Run off volume, peak rate ,	Young et al., 1989 Rode and Fredo, 1999
8.	EMSS (Environmental Management Support System)	Conceptual	Catchment	Low Input	Runoff, sediment loads ,nitrogen loads and passports load	
9.	SWRRB (Simulator for Water Resources in Rural Basins)	Conceptual	Catchment	High input requirement	Stream,flow ,sediment ,Nutrient, and pesticide yields	Arnold and Williams, 1987
10.	SEDD (SEdiment Delivery Distributed)	Empirical	Catchment	Rainfall, soil elevation and land use.	spatial distribution of the sediment	Ferro and Porto 2000
11.	RUSLE (Revised universal soil loss equation)	Empirical	Catchment	Climate ,Soil, Topography, Cover management	Rates of rill and interrill soil erosion caused by rainfall and its associated overland flow.	Renard et al. (1997)
12.	LASCAM(large-scale conceptual catchment model)	Conceptual	Catchment	High input requirement	runoff, sediment, salt fluxes	Viney and Sivapalan, 1999
13.	PERFECT (Productivity, Erosion and Runoff, Functions to Evaluate Conservation Techniques)	Physical	Field	High input requirement	runoff, erosion, crop yield	Littleboy et al., 1989

2.5. Conclusion

This literature review provides relevant information to evaluate the effect of land use change on soil erosion for the Man River basin where land use changes extensively affect soil erosion risk. Traditional analysis of the change matrix is not sufficient to provide systematic signals of LULCC; therefore an advance change matrix technique was adopted in this study. This approach is able to compute the quantity, allocation, and dominant signals of LULCC transitions and forest activities. The combination of direct (change matrices) and indirect methods is adapted to further detailed analysis of deforestation and forest degradation associate with responsible drivers in the basin.

Physical process based soil erosion models are useful tools for understanding erosional processes and impacts in a given area. They are able to understand the soil erosion process at the hillslope scale and estimate spatial and temporal distributions of net soil loss with more accurate extrapolation to ungauged sites and have an enhanced ability to predict soil loss with different types land cover and satellite data. GeoWEPP is the most suitable model for this study because of its demonstrated capabilities as a process-based model as well as its ability to simulate events over a wide variety of spatial and temporal scales using remote sensing.

Chapter 3

Study area and data sources

3.1. Introduction

The purpose of this chapter is to present background information on the study area and outline the satellite and the spatial datasets used to support digital input for vegetation change and erosion risk modelling in the Man River basin. A combination of remote sensing and field work datasets were evaluated to establish a decadal time series of vegetation change from 1972 to the present day. All the historical imagery used to produce land cover information was acquired from Landsat sensors. Landsat imagery is freely available and suitable for monitoring temporal forest and land use change. A total of three Digital Elevation Models from different sources and resolutions were obtained and used to generate reliable topographic inputs for erosion risk modelling. Several supplementary datasets have also been assembled related to field work conducted in the River basin during study period.

3.2. Study area

3.2.1 Study area location

The Man River basin is located in the Dhar district of Madhya Pradesh state in the western part of India (Figure 3.1). It is a sub–basin of the lower Narmada River. The river basin lies between latitude 22° 9' 15" N to 22° 35' 45" and longitude 75° 0'15" E to 75° 24' 50"E and has an area of 1557 km^2.

3.2.2 Physical topography

The study area extends over three topographic divisions: the Malwa plateau in the north, the Vindyachal mountain range in the central zone and The Narmada valley in the south (Figure 3.1). The Malwa plateau, which extends about 10 km to the north of the basin, is underlain with basaltic rocks known locally as the Deccan Traps. These rocks are of low porosity and permeability and have water retention capacity only in the fractures and faults. The Vindhya mountain area extends 10 to 20 km in the centre of the basin and is made up of granite and sandstone. The Vindhyas region contributes most flow in the basin and its

topography is hilly and covered mostly with degraded forests and cultivated land; the water runoff and sediment load are both high. The Narmada valley region, extending about 15 km at the south of the basin, is underlain with granite.

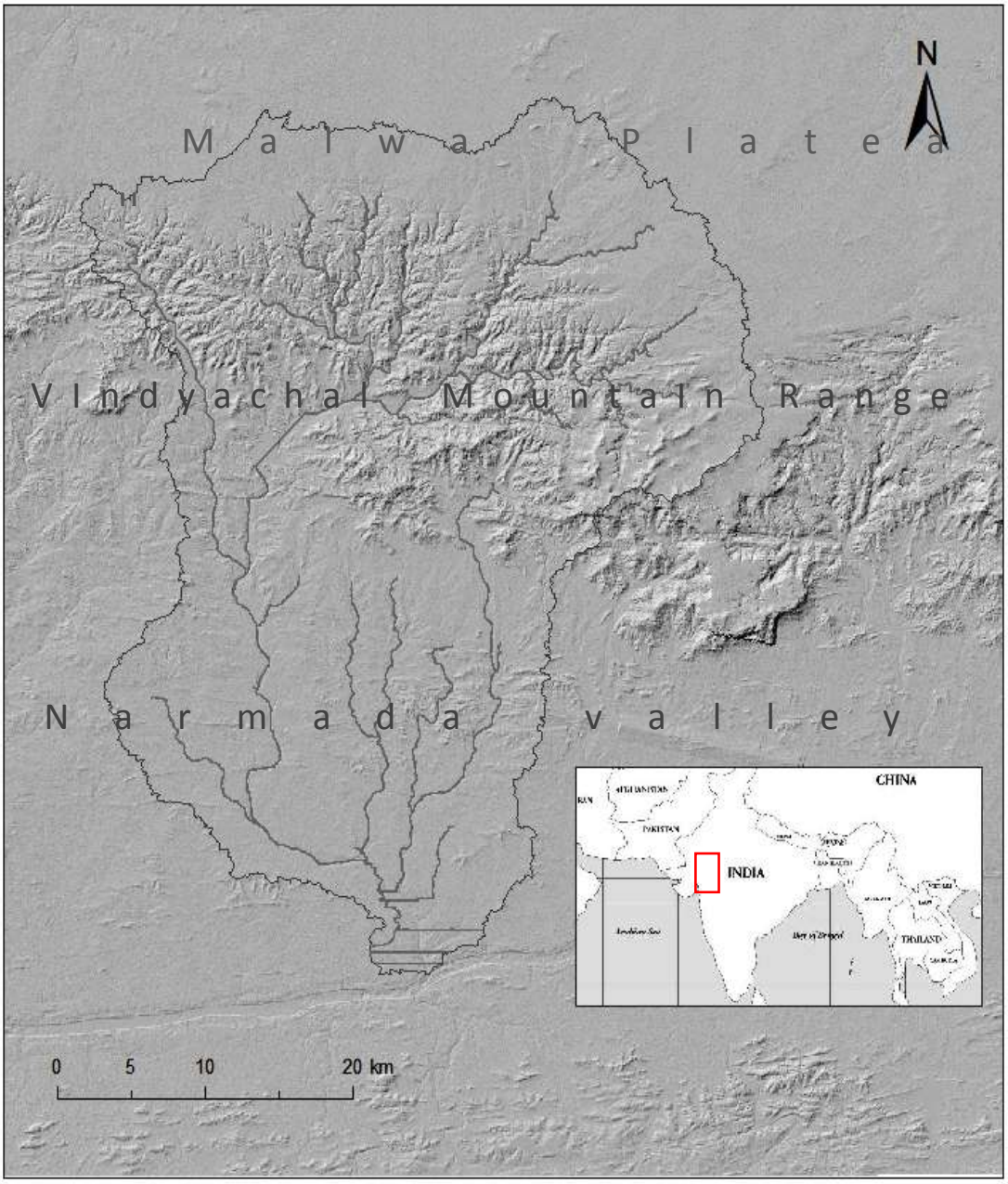

Figure 3.1.Location of Man River basin in Central India.

3.2.3 Soil

The soil is mostly rich black cotton clay in the Malwa region with some lateritic sandy loam. In the Vindhya region the soil is mostly sandy loam with some deposits of black cotton. Alluvial soils are present in the valley of the Man River just above the Man Dam at Zirabad. The Narmada valley has an equal mixture of black cotton clay and loam soils with some deposits of alluvial soils along the river valleys (Figure 3.2).

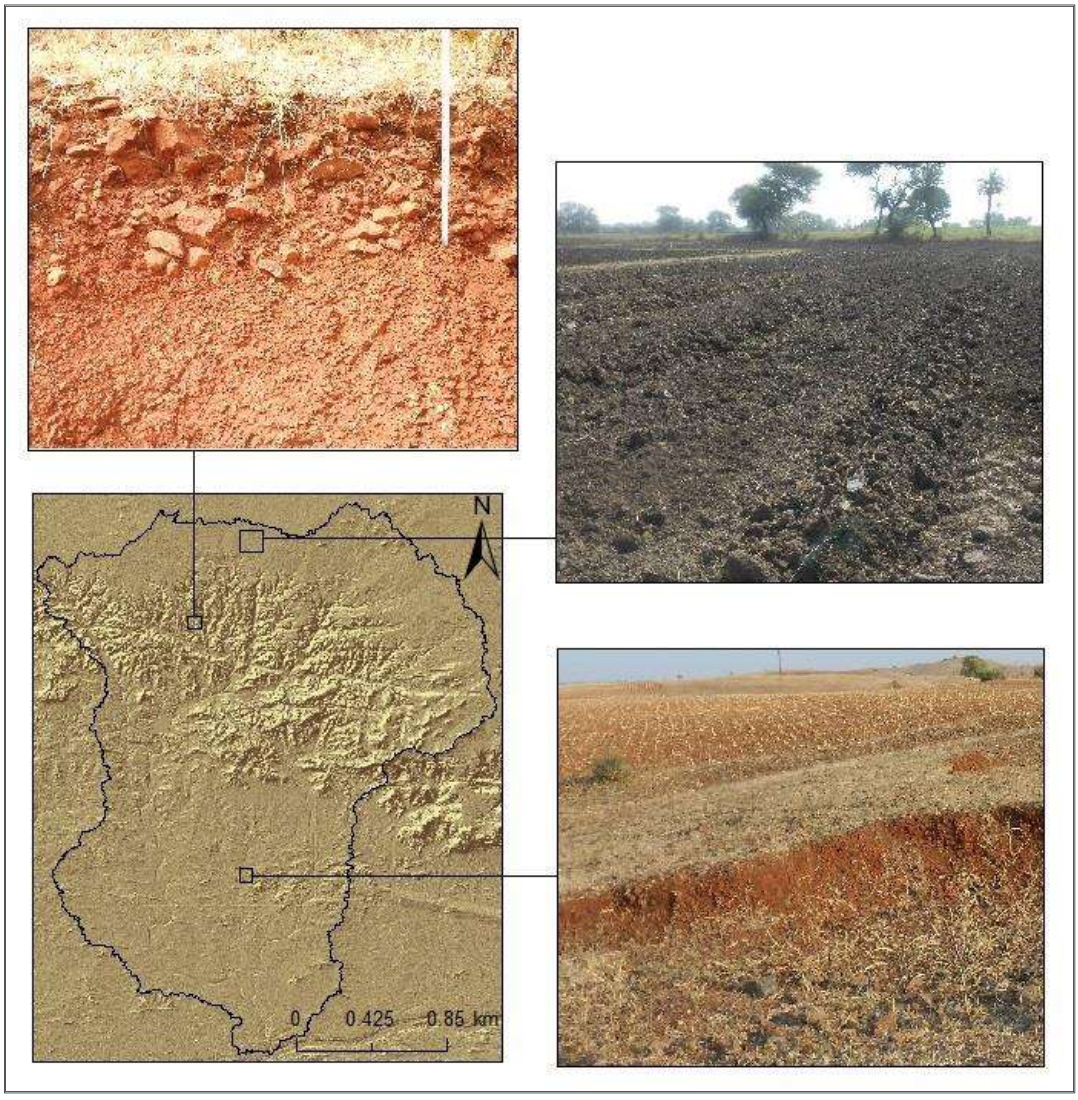

Figure: 3.2. Soil photos taken during field work from three different topographical areas of the Man River basin, Central India.

Rainfall occurs mainly in the monsoon months of mid-June to mid-September and the number of rainy days is on an average only 50. The average potential evapotranspiration rate for the area is high

at about 2100 mm. Consequently the soil moisture zone remains completely dry for about 90 days in the summer period. A perusal of the Dhar District Soil Map (Tamgadge et al, 2000) reveals that the soil depth in the Vindhyachal region of the Man basin is either very shallow or shallow, except in a thin strip along the river. The soil depth is deep in the Malwa Plateau and slightly deep in the Narmada valley areas. The available water holding capacity is either very low or low in most areas of the basin. While the organic carbon content of the soil is medium to high in the basin, the nitrogen content is low and the potassium content is medium with the overall soil quality being low in the Vindhyachal mountain region and medium to high in the Narmada valley region.

3.2.4 Climate

The whole basin has been classified on the Thornthwaite system of climate classification as a transitional ecosystem of moist semi-arid and dry sub-humid type with an index (-) 41.9 (Tamgadge et al, 2001). India's Initial National Communication (INC, 2004) to the UNFCCC notes that a decreasing trend in monsoon seasonal rainfall has been observed over east Madhya Pradesh and adjoining areas, while a significant warming trend has been observed in central India. In terms of spatial patterns of observed extreme daily maximum temperatures, it has been noted that over the central parts of India, the maximum temperatures recorded exceed 45°C. Madhya Pradesh is likely to face a mean annual temperature rise of between 2°C and 3°C by the end of the century.

3.2.5 Land use and land cover

Secondary data available with the Department of Statistics and Economics and published in the form of the annual district statistical handbooks has been relied on for a study of the land use characteristics of the study area. The data demonstrates that reserved forest constitutes 39% of the total area in the Vindhya region in 1989, but this proportion had declined to 30% in 2005. (A reserved forest is also known as a protected forest indicating a certain degree of protection. In such forest most of the activities like farming, harvesting and grazing are prohibited). Moreover the density of forest cover has decreased and the proportion of open forest in 2009 is as high as 81% (FSI, 2009). This open forest is mostly degraded with minimal forest cover or even scrubland and meadows. Due to increased population pressure and agriculture extensification in forested areas, the protected and non–protected forest lands are being converted into deforested and degraded areas which are increasing soil erosion risk in the river basin. Agriculture is a major source of income for the villagers in the basin. The majority of farmers fall in the

landless, marginal (<1 ha) or small (1 -2 ha) farmer categories. Farmers are mostly marginal and small farmers undertaking cultivation without soil and water conservation measures. Recently, most agricultural land converted from forest land is a permanent change in land category and the areas do not return to forest land. This permanent agriculture extension does not represent a shifting agriculture pattern as some publications suggest (GOI –UNDP-GEF 2007). This means than from the start of cultivation after removing the forest people will continue farming until the topsoil layer gets washed away from land surface. Continued unsustainable cultivation reduces permanent productive capacity of the land; this forest land becomes degraded and cannot be used for any cultivation or plantation practices. Government forest policy allows farmers to extend agricultural land on the protected forest area through land ownership licence of cultivated land.

The Man River basin is located in dry deciduous zones, with high precipitation and temperatures. Soil and agro-ecological conditions are thus not adequate for a long agricultural season. The landscape is highly susceptible to soil erosion and surface soil run-off, owing to its characteristically undulating terrain, fragile geological conditions, and heavy rains. In areas of intensive land use, soil erosion, forest degradation, and reduction of soil fertility in agricultural land have become increasingly evident.

3.3 Data sets

The appropriate satellite and non-satellite data sources at the necessary scale were identified for the current research. The choice of data sources was based on the spatial and temporal resolution of data and their potential to model land use/land cover change at the regional scale and erosion risk at the hillslope scale. All remote sensing datasets were available through open sources. Landsat (30m) imagery is major source of information for both modelling approaches which is used at regional scale for vegetation change modelling and at the hillslope scale for soil erosion risk assessment modelling. There is broad range of literature available on application of Landsat imagery for land use/land cover mapping and monitoring at the regional scale. These studies include land use/land cover change mapping (Manandhar et al., 2010; Teferi et al., 2013), forest change activities such as deforestation (Bürgi *et al.*, 2005), and forest degradation at the regional scale (Asner et al. 2009; Souza et al .2009). Landsat (30m) data has also been often used as an input for soil erosion assessment at the hillslope scale. For example, land cover data were derived from Landsat TM+ imagery to evaluate sediment and soil erosion using WEPP and SWAT model for basins in Oklahoma: model results were in good agreement with field measurement (White and Storm, 2010). Landsat has good availability at a range of temporal scales in the study region to map historical aspects of vegetation change, which is one of the major objectives of research. Landsat data also fulfills

the need of the current study to map vegetation change at the regional scale and estimate soil erosion risk at the hillslope scale in the river basin. Technical detail on Landsat imagery is presented in the next section.

Appropriate resolution of digital elevation models is essential to produce reliable topographic and hydrologic inputs for soil erosion assessment. Therefore, three publicly accessible DEMs for the selected watersheds in the Man River basin were acquired: Cartosat DEM at 30 m resolution, ASTER DEM at 30 m resolution and SRTM at 80 m resolution. Several studies have adopted 30m and 90 m resolution DEMs to generate topographic input for soil erosion assessments at the watershed scale which were recorded satisfactorily (Covert et al., 2005; Zhang et al., 2009; Kumar et al 2008; Tirkey et al., 2013). Similarly, IRS LISS-III imagery (23.5 m) has been adopted to generate satisfactory soil input for GeoWEPP (see section 6.6.4.3). To assess the effect of remote sensing and ground based precipitation on soil erosion estimation, which is one of the objectives of research, TRMM and IMD rainfall data were chosen to produce climate input for GeoWEPP. IMD data is the best available source of rainfall information in the region which is based on ground measurement. Field work datasets were also collected from the study area to determine the appropriate representation of ground information for both modelling approaches, such as land use land cover information by GPS, soil sample collection and crop management databases. Scientific procedure was adopted to collect field data which is explained in the next chapters which resulted in high quality field data at the fine scale. The detailed description on these data sets is explained below.

3.3.1. Satellite datasets

Six different remote sensing datasets were collected and processed over the study period to enable the extraction of spatial and temporal inputs for both modelling approaches. These included: (1) Landsat, (2) LISS-III, (3) Cartosat_1, (4) ASTER DEM, (5) SRTM DEM and (6) TRMM.

3.3.2. Landsat Time Series

Landsat is a multispectral sensor with a very long historical record and is available from the US Geological Survey (Table 3.1). Landsat data has a capability to monitor land use and land cover change, deforestation and forest degradation, water bodies and settlements (e.g. Figure 3.3). Landsat has also helped to assess damage from natural disasters such as fires, floods, and tsunamis, and subsequently, plan disaster relief and flood control programs.

Landsat multispectral scanner (MSS) at 80 m, Landsat Thematic Mapper at 30 m, and Thematic Mapper Plus at 30 m resolution are freely available over the Man river basin with comprehensive temporal coverage. Two Landsat scenes (WRS 1 Path 174 and row 44, 45) are required to cover the Man River basin. Overall, 12 cloud-free and L1T terrain corrected Landsat scenes were downloaded. These included Landsat 1 & 3 MSS scenes for 1972, 1980, Landsat 5 TM for 1989, 2001, 2009 and Landsat 8 for 2013. Landsat scenes 2001 and 1989 are orthorectified data sets.

The **Landsat Multispectral Scanner** (MSS) imagery is the only satellite record available for the historical time period over the Man River basin. MSS images consist of four spectral bands with 60 m spatial resolution. Approximate scene size is 170 km north-south by 185 km east-west (106 mi by 115 mi). Specific band designations differ from Landsat 1-3 to Landsat 4-5. The MSS sensors are line scanning devices observing the Earth perpendicular to the orbital track. The cross-track scanning is accomplished by an oscillating mirror; six lines are scanned simultaneously in each of the four spectral bands for each mirror sweep. The forward motion of the satellite provides the along-track scan line progression. MSS band 1 (Green) can be used to detect green reflectance from healthy vegetation, and band 2 (Red) is designed for detecting chlorophyll absorption in vegetation. MSS bands 3 (Near Infrared) and 4 (Near Infrared) are ideal for recording near – infrared reflectance peaks in healthy green vegetation and for detecting water – land interfaces.

The **Thematic Mapper (TM**) is an advanced, multispectral scanning; earth resources sensor designed to achieve higher image resolution, sharper spectral separation, improved geometric fidelity and greater radiometric accuracy and resolution than the MSS sensor. TM data are sensed in seven spectral bands simultaneously. **Landsat Enhanced Thematic Mapper Plus (ETM+)** images consist of eight spectral bands with a spatial resolution of 30 m for Bands 1 to 7. The resolution for Band 8 (panchromatic) is 15 m. All bands can collect one of two gain settings (high or low) for increased radiometric sensitivity and dynamic range, while Band 6 collects both high and low gain for all scenes. Approximate scene size is 170 km north-south by 183 km east-west (106 mi by 114 mi).

Landsat 8 Operational Land Imager (OLI) and Thermal Infrared Sensor (TIRS) images consist of nine spectral bands with a spatial resolution of 30 m for Bands 1 to 7 and 9. New band 1 (ultra-blue) is useful for coastal and aerosol studies. New band 9 is useful for cirrus cloud detection. The resolution for Band 8 (panchromatic) is 15 m. Landsat images are composed of different bands, each representing a

different portion of the electromagnetic spectrum. The feature and application for each band are explained here and illustrated in (Figure 3.4).

Band 1 (Blue-green): This short wavelength of light penetrates better than the other bands, and it is often the band of choice for monitoring aquatic ecosystems (mapping sediment in water, coral reef habitats, etc.). Unfortunately this is the "noisiest" of the Landsat bands since it is most susceptible to atmospheric scatter.

Band 2 (Green): This has similar qualities to band 1 but not as extreme. The band was selected because it matches the wavelength for the green we see when looking at vegetation.

Band 3 (Red) since vegetation absorbs nearly all red light (it is sometimes called the chlorophyll absorption band) this band can be useful for distinguishing between vegetation and soil and in monitoring vegetation health. **Band 4 (Near infrared):** Since water absorbs nearly all light at this wavelength water bodies appear very dark. This contrasts with bright reflectance for soil and vegetation so it is a good band for defining the water/land interface.

Band 5 (Mid-infrared): This band is very sensitive to moisture and is therefore used to monitor vegetation and soil moisture. It is also good at differentiating between clouds and snow.

Band 6 (Thermal infrared): This is a thermal band, which means it can be used to measure surface temperature. Band 6 is primarily used for geological applications but it is sometimes used to measure plant heat stress. This is also used to differentiate clouds from bright soils as clouds tend to be very cold. The resolution of band 6 (60m) is half of the other bands.

Band 7 (Mid-infrared): This band is also used for vegetation moisture, although generally band 5 is preferred for that application, as well as for soil and geology mapping.

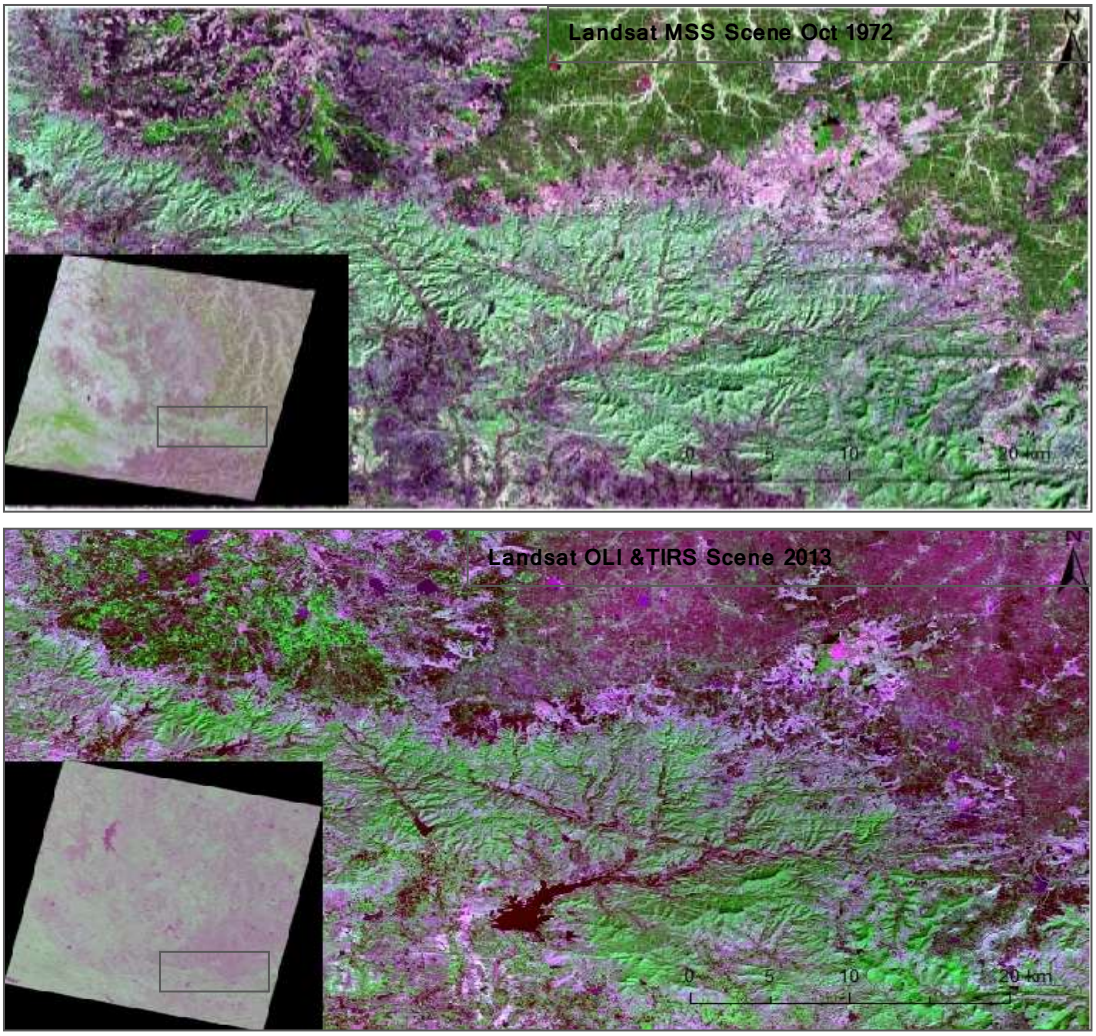

Figure 3.3: Two Landsat scenes produced by Multispectral Scanner Sensor 1972(above) and Landsat OLI & TIRS sensor 2013(below). Images reveal forest cleared and land cover change in the Man River Basin, Central India, between 1972 and 2013. Green areas represent healthy forest.

3.3.3. Linear Imaging Self-scanning Sensor (LISS) - III

The soil surveys carried out through RS methods are more convenient, quick and cost effective compared to conventional methods (Rao et al. 2005). However, mapping soil especially in hilly terrain, as exists in the Man River basin, using RS techniques is a challenge. Such mapping requires use of remote sensing, but also knowledge of the field and lab measurement relationship. Towards this end, IRS Resourcesat-1 multi-spectral, medium-

Table 1.1. General characteristics of Landsat scenes used For Study area

Landsat image	Date Acquired	Band Quality	Cloud Cover	Path	Row	Data Type	Level	Resolution (m)
Landsat 8 OLI &TIRS	Feb 2013	9	0%	147	44	MS	L1T	30
Landsat 8 OLI &TIRS	Feb 2013	9	0%	147	45	MS	L1T	30
Landsat 5 TM	Nov 2009	9	0 %	147	44	MS	L1T	30
Landsat 5 TM	Nov 2009	9	0%	147	45	MS	L1T	30
Landsat 7 ETM+	Oct 2001	9	0%	147	44	MS	Ortho	30
Landsat 7 ETM+	Oct 2001	9	0%	147	45	MS	Ortho	30
Landsat 5 TM	Dec 1998	9	0%	147	44	MS	L1T	30
Landsat 5 TM	Dec 1998	9	0%	147	45	MS	L1T	30
Landsat 5 TM	Oct 1989	9	0%	147	44	MS	Ortho	30
Landsat 5 TM	Oct 1989	9	0%	147	45	MS	Ortho	30
Landsat 3 MSS	Oct 1980	9	0%	158	45	MS	L1T	80
Landsat 3 MSS	Oct 1980	9	0%	158	44	MS	L1T	80
Landsat 1 MSS	Dec 1972	9	0%	158	44	MS	L1T	80
Landsat 1 MSS	Dec 1972	9	0%	158	45	MS	L1T	80

resolution data used in conjunction with ground and lab data offered the most potential for this research. In view of this, the present study was carried out to characterize soil texture of three selected watersheds in the Man River basin using RS data, field survey and lab testing. For this study, digital data of Indian Remote Sensing was used.

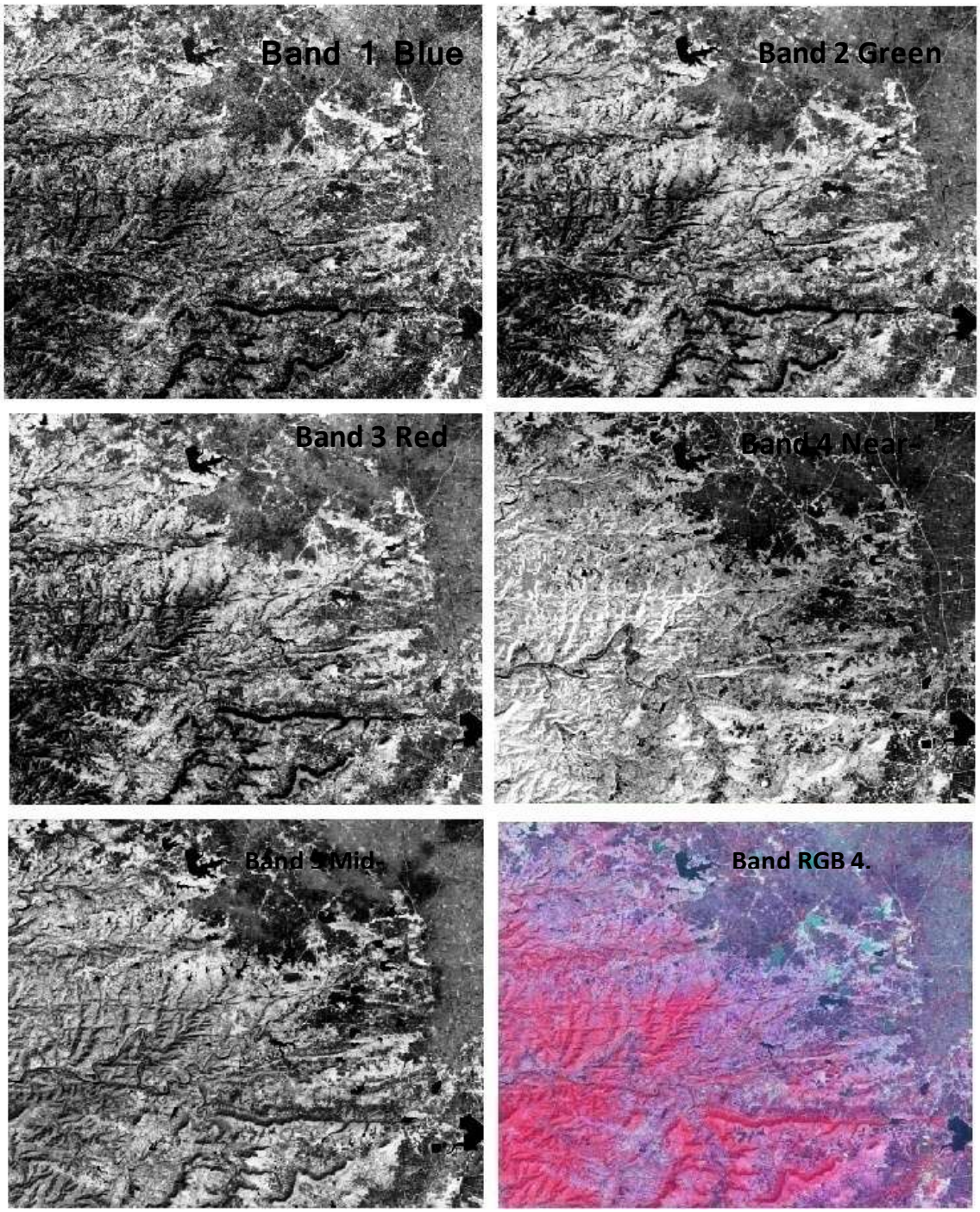

Figure 3.4: Images produced from 5 bands of Landsat 7 ETM data of Man River basin. Each image in the illustration represents reflectance values recorded in each wavelength band. False colour images are produced by colouring three bands.

Satellite Resourcesat-1 in Linear Imaging Self- scanning Sensor (LISS) - III of 18 Oct 2008 was used (Figure 3.5). LISS-III is a multi-spectral camera operating in four spectral bands, three in the visible and near infrared and one in the SWIR region. The new feature in LISS-III camera is the SWIR band (1.55 to 1.7 microns), which provides data with a spatial resolution of 23.5 m. The data products are categorized as Standard and have a system level accuracy.

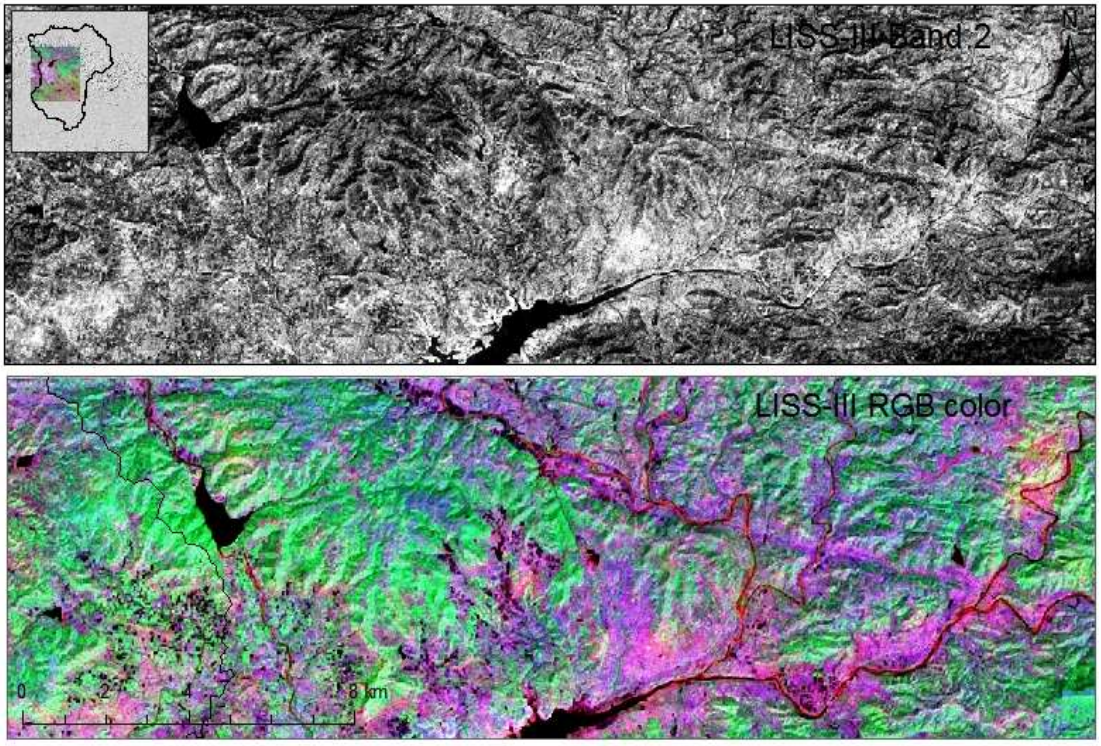

Figure 3.5: Above: LISS –III band -2, Below: RBG coloured Image of LISS –III in the Man River basin, Central India.

3.3.4. Topographical Datasets

Soil erosion modelling uses a digital elevation model (DEM) to derive the topographical characteristics of the study area. This study used three different types of DEMs to compare soil erosion outputs (Figure 3.6). These are explained below.

3.3.4.1. ASTER DEM

The ASTER Digital Elevation Model (DEM) was acquired from The Land Processes Distributed Active Archive Centre (LP DAAC); a component of NASAs Earth Observing System (EOS) Data and

Information System (EOSDIS). The ASTER Digital Elevation Model (DEM) product is generated using bands 3N (nadir-viewing) and 3B (backward-viewing) of an ASTER Level-1A image acquired by the Visible Near Infrared (VNIR) sensor. The VNIR subsystem includes two independent telescope assemblies that facilitate the generation of stereoscopic data. The Band-3 stereo pair is acquired in the spectral range of 0.78 and 0.86 microns with a base-to-height ratio of 0.6 and an intersection angle of about 27.7.

3.3.4.2. CartoDEM

The Cartosat-1 Digital Elevation Model (CartoDEM) has been developed by the Indian Space Research Organization (ISRO). It is derived from the Cartosat-1 stereo payload launched in May 2005. CartoDEM is generated using Augmented Stereo Strip Triangulation (ASST) – indigenously developed software by the Space Application Centre, ISRO. The seamless CartoDEM generation is an automatic process and makes use of limited Ground Control Points (GCPs) in long stereo strip pairs using dense feature matching, Triangulated Irregular Network (TIN) modelling and automatic long strip mosaicing. The automatic generation of the DEM has inherent problems such as water-body irregularities, hill-top distortions, plain-area sinks and residual mosaics; these are corrected in the Tile Editing (TE) system. Qualified CartoDEM tiles are formatted and archived systematically in database Dissemination System (DS). CartoDEM products are extremely useful in: contour generation; drainage network analysis; quantitative analysis of run-off and soil erosion; volume-area calculations; design of hydraulic structures; design of new road, rail and pipeline alignments; watershed planning; urban utility planning; landslide zonation; river configuration studies and flood proofing; and fly through visualization. Thus, Cartosat (30 m) DEM provides a sound scientific basis to identify spatial variability of soil erosion at the watershed scale (Kumar et al., 2008).

3.3.4.3. SRTM DEM

SRTM Digital Elevation Data (DEMs) for the study area were also acquired. The Shuttle Rader Topographic Mission (SRTM) DEM at 30 m resolution is a joint product from NASA and the National Geospatial Intelligence Agency (NGA). The CGIAR-CSI GeoPortal is able to provide SRTM 90m Digital Elevation Data for the entire world.

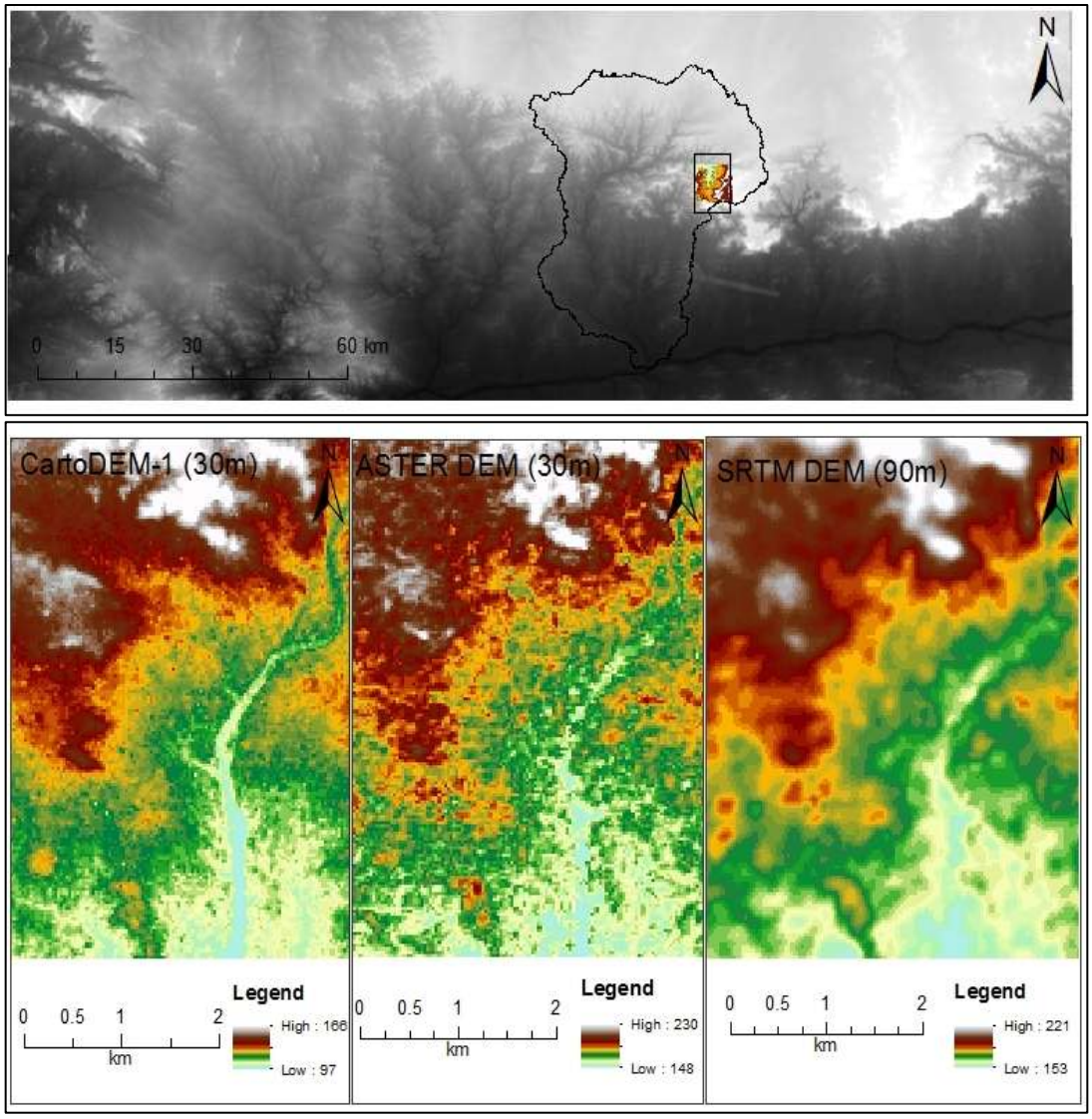

Figure 3.6: The area in the Man River basin on different DEMs shown as Elevation. (a) CartoDEM -1 features a smooth surface. River stream are clearly visible on the surface in the case of the CartoDEM while the ASTER DEM and SRTM DEM have not clear view of same feature.

3.3.5. TRMM and Other Data Precipitation Product (TRMM Product 3B43_ACC.007)

The Tropical Rainfall Measuring Mission (TRMM) is a joint project between the National Aeronautics and Space Administration (NASA) and the Japan Aerospace Exploratory Agency (JAXA) launched in November 1997 with the specific objectives of studying and monitoring the tropical rainfall (Kummerow

et al., 2000; Rozante et al., 2010). It can provide precipitation products with high temporal (3 h) and reasonably high spatial resolution (0.25_ _ 0.25_) (Figure 3.7).

The 3B43_ACC.007 data set was accessed from 1998 to present at no charge through the TRMM Online Visualization and Analysis System (TOVAS) that is created and supported by the Goddard Earth Sciences Data and Information Services Centre (GES DISC). It provides a web-based resource for accessing several other data sets, performing basic sub setting, time- and space-averaging, and output of results in plots or ASCII text. The TOVAS URL is http://disc2.nascom.nasa.gov/Giovanni/tovas/.

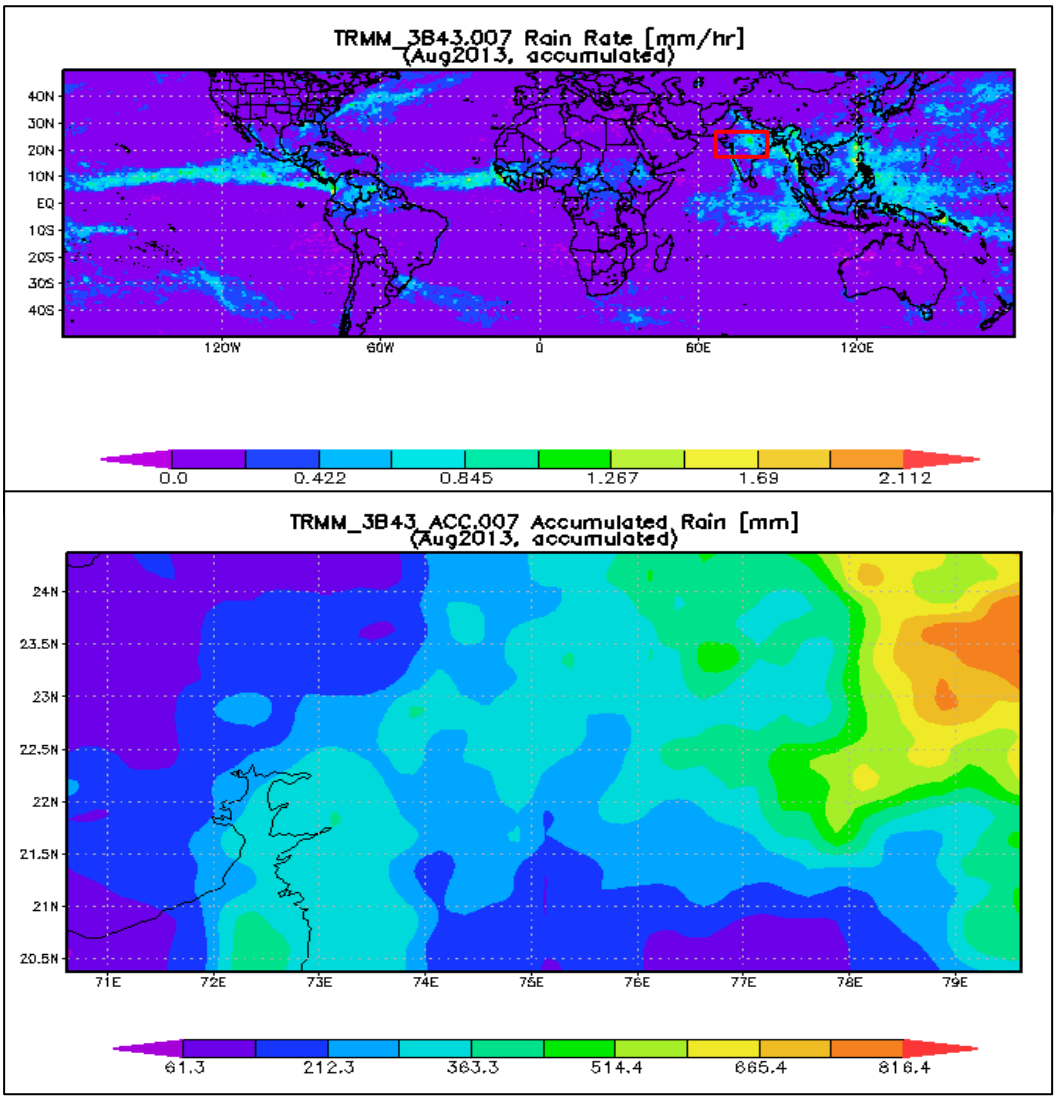

Figure 3.7: Monthly rainfall climatology images were created for August month of 2013 based on TRMM 3B43 accumulated Version 007 data. Above image shows global distribution while below image represent from Man River basin, Central India.

Figure 3.8: Top photos (A) and (B) shows photo identification of forest and agriculture land and the bottom image (C) and (D) shows GPS survey Waypoint for forest and agriculture land in aerial view images of the Man River basin, Central India.

3.4. Field work Data sets

3.4.1. GPS datasets

Two field work sessions were organized in 2010 and 2013 to validate the land cover classification map. Ground datasets were collected using a Garmin ™ Global Positioning System (GPS), as well as capturing separate pictures of each ground point using 11 megapixel digital cameras (Figure 3.8). Overall, 250 GPS plots were collected with photo verification in the study area to provide a better understanding about ground references. Google Earth TM imagery provides sufficient temporal and spatial resolution to use as a reference data for identification of forest and non-forest area and change analysis. These aerial photographs were also used for validation of the 2009 and 2013classification maps.

3.4.2. Soil datasets

To run the WEPP soil erosion model, soil parameters were obtained from field data collection and calculated by the WEPP model. In this study, soil parameters were measured based on soil samples collected from randomly selected 1 m^2 plots (i.e. 15 plots) located in the study area and Soil Resource Atlas of Dhar District. After collecting soil samples from the selected sub-watersheds in the study area and analysing them in the soil laboratory, the soil properties including soil texture, albedo, saturation level, soil depth, sand-clay-organic matter ratios, cation exchange capacity, and rockiness were entered into soil input file. The detail descriptions are presented in Section 4.5.4.

3.4.3. Climate

In the continuous mode, WEPP requires daily weather data (e.g. precipitation amount (Figure 3.9), storm duration, temperature extremes, solar radiation and wind speed/direction) for simulating runoff, erosion, residue decomposition, crop growth and other model components. These data sets were obtained from the National climate Centre (NCC), Pune, Metrological Department of India and District Land Information Department, India. Detailed description is presented in section 5.4.

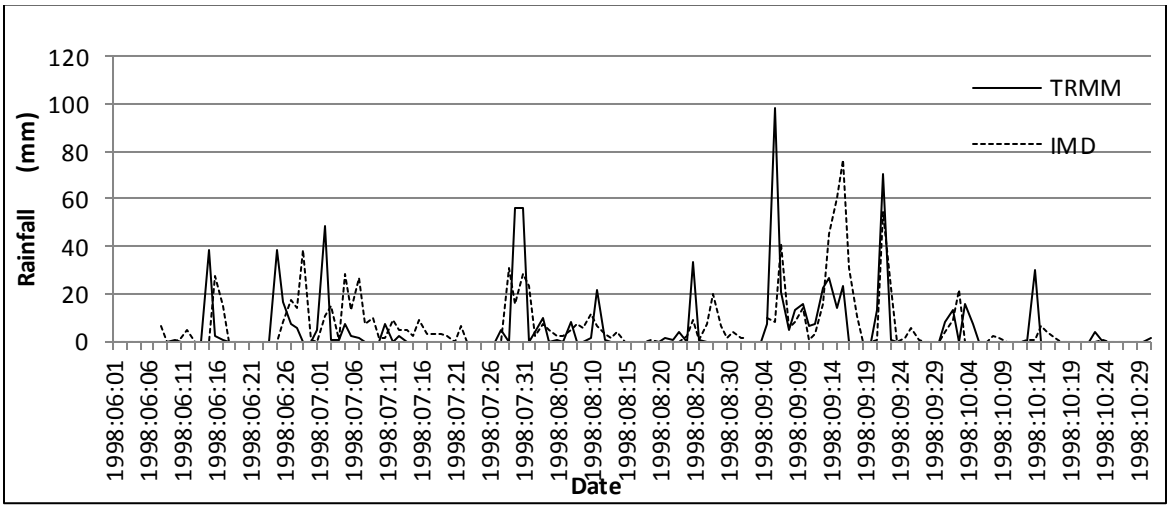

Figure 3.9: TRMM and IMD daily rainfall data comparison from Jun to Oct 1998

3.4.4. Management data sets

WEPP requires a timeline of operations (e.g. planting, tillage, harvesting) for cropland management practices. Information regarding initial land conditions, crop growth, residue decomposition and details of tillage implements are the main requirements of the model in terms of land use. These data sets were obtained from field measurement in the watershed area. The captured data included the time, location, amount and type of tillage practices performed, seeds planted and crops harvested Parameters related to the associated tillage practices described in detail in Section 5.5.

3.5. Conclusion

This chapter has explained valuable background information on the study area and outlined the satellites and ground based datasets available for the basin from 1972 to the recent time. Spatial and temporal coverage of datasets is good and have the ability to provide rapid and reliable information to map landscape dynamics and soil erosion at the regional and watershed scale. Landsat data is one of the main sources of information in the study area and a valuable resource for decision makers in such diverse fields such as agriculture, forestry, land use, water resources and natural resource exploration. The quality of verification data is also of a good standard which is based largely on google Earth™ Arial photography and field measurement GPS points. This research also developed methods of collecting detailed, timely, accurate and reliable datasets of the land cover, topography, climate and management using the remote sensing and field measurement for soil erosion modelling in the river basin. Overall, this chapter has outlined the remote sensing datasets which were combined with field work to generate better digital input for vegetation change detection at the regional scale and soil erosion risk modelling at the watershed scale in the Man river basin. The methodology employed for LUCC and WEPP modelling are outlined in Chapters 4 and 6 respectively.

Chapter - 4

Methods used for Vegetation Change Detection

4.1. Introduction

In this chapter Remote Sensing Technologies are evaluated to monitor and verify landscape change following the recommendations set out in GOFC–GOLD (2009) for identifying and quantifying the change and uncertainty. Landsat Satellite image classification, change analysis and modelling are used to identify land cover, land use change and forestry activates that are linked with the drivers of deforestation and forest degradation. Historical Landsat scenes were pre-proceed using a series of sequential operations, including image registration, geometric correction, atmospheric correction, mosaicking, sub-setting, masking and automatic change detection. First, the historical pattern of change was produced using change matrix approach 3 (IPCC guideline), specifically deforestation and its rate of change in the Man River basin from 1972 to 2013. Additionally, an independent spatial assessment of deforestation, forest degradation and responsible drivers for the period 2009-2013 was conducted to update forest loss layer using the direct interpretation approach. Finally, a robust accuracy assessment method was developed to verify thematic errors in the 2009 and 2013 maps following the GOFC–GOLD (2009) good practice guidelines as appropriate. Thus, four datasets relevant for landscape dynamics were produced including land use/land cover maps, change analysis and deforestation, degradation and driver maps with direct interpretation approach and verification assessment.

4.2. Data pre-processing

4.2.1. Image acquisition

The historical cloud free satellite images from Landsat and L1T terrain corrected data sets, which have a finer spatial resolution of 30 m, were acquired for the research from US Geological Survey. The dates selected were as follows:

- Nov 2013, Nov 2009, Dec 2001 and Oct 1989 (WRS 1 Path 147, Row 44, 45).
- Landsat 3 MSS scene for year 1980.
- Landsat 1 scene of year 1972 with a spatial resolution of 80 m (WRS 2 Path 158 Row 44, 45).
- Landsat 5 TM image for 2001 and (orthorectified).

- Landsat 1 MSS image for 1989 (orthorectified).

4.2.2. Geo-referencing

Accurate per-pixel registration of multi-temporal remote sensing data is essential for change detection analysis which is performed on a pixel-by-pixel basis; therefore any mis-registration greater than 1 pixel will provide an anomalous result for that pixel. To overcome this problem, the RMSE between any two dates should not exceed 0.5 pixels (Lunetta and Elvidge, 1998). In this study, the geometric correction of all Landsat images was carried out. Landsat images were registered with the same UTM Projection (UTM zone 46 N). The 2001 Ortho–rectified Landsat satellite image was used as the base image to more precisely geo-reference the other four scenes. The Root Mean Square Error (RMSE) between the two images was less than 0.5 pixels which is acceptable. The RMSE can be defined as the deviations between GCP and GP location as predicted by the fitted-polynomial and their actual locations. The rectified Landsat images were resampled to a 30 metre pixel size using the nearest neighbour resampling. The change of resolution was necessary in order to gain better results.

4.2.3. Radiometric correction

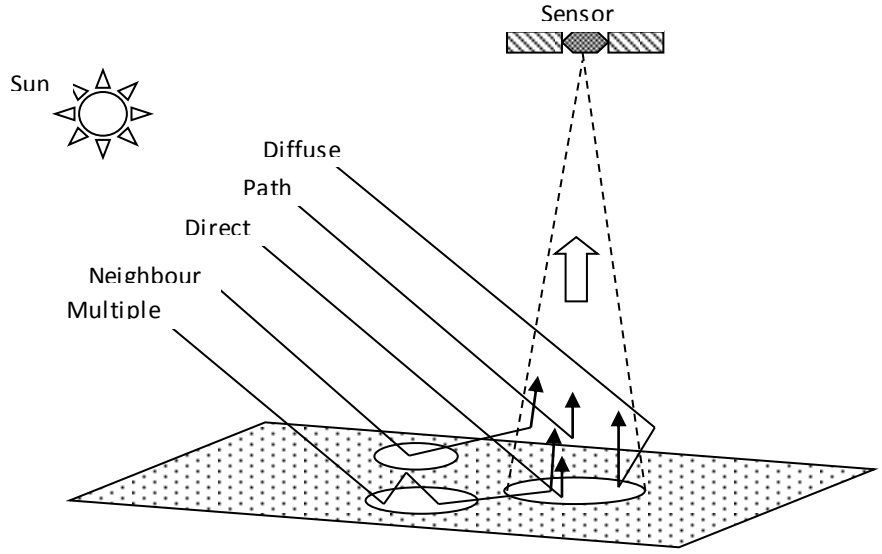

Figure 4.1: Types of radiative interaction with the atmosphere

The electromagnetic radiation signals collected by satellites in the solar spectrum are modified by scattering and absorption by gases and aerosols while travelling through the atmosphere from the Earth surface to the sensor (Figure 4.1). Scattering of radiation by the constituent gases and aerosols in the atmosphere causes degradation of the remotely sensed images. Most noticeably, the solar radiation scattered by the atmosphere towards the sensor without first reaching the ground produces a hazy appearance of the image. The amount of scattering that occurs is a function of wavelength and must be assessed and explicitly removed from each image band.

Several different atmospheric scattering or haze removal techniques have been developed for use with digital remotely sensed data. Several methods use atmospheric transmission models, derived from field data, or require specific targets to be present in the image (Rahman et al., 1994; Richter, 1990; Richter, 1996). A major limitation of these sophisticated techniques is that they require information other than digital image data (e.g., path radiance and (or) atmospheric transmission at several locations within the image area collected during satellite's overflight). These measurements are frequently unavailable or of questionable quality, which makes routine atmospheric correction of images difficult. Many applications of remote sensing have to rely on algorithms that utilize information derived from the image itself to correct for atmospheric effects, and in the current study investigation was limited to image-based correction algorithms.

The Dark Objective Subtraction (DOS) method is the simplest and most widely used image-based atmospheric correction approach for classification and change detection applications (Huguenin et al., 1997). DOS was used to correct atmospheric effects from images. This approach assumes the existence of dark objects (zero or small surface reflectance) throughout a Landsat scene and a horizontally homogeneous atmosphere. The minimum DN value in the histogram from the entire scene is attributed to the effect of the atmosphere and is subtracted from all the pixels. More sophisticated algorithms derive atmospheric optical properties from dark objects in the image, and correct the images with the derived information (Chavez et al, 1989). For instance, Ahern et al. (1977) and Gordon (1978) used clear water as the dark object to derive atmospheric optical information for radiometric normalization.

The Landsat datasets used in this study are from 1972 to 2013 for the Man River basin. The DOS correction algorithm was applied to the Landsat images using assessed 'histogram minimum values'. The reflectance from dark objects, such as a deep lake and river were measured and minimum histogram value were calculated that values were subtracted from the Landsat images for each band using ENVI 4.7

image process software. It means dark objects in the image were measured to calculate minimum histogram values which were subtracted from the image. The results obtained by applying DOS atmospheric correction were encouraging (Figure 4.2 and 4.3). The DN frequency Histogram of the spectral Bands 1, 2, 3, 4, 5 6, and 7 of the Landsat TM image is as shown in Figure (4.2 and 4.3).

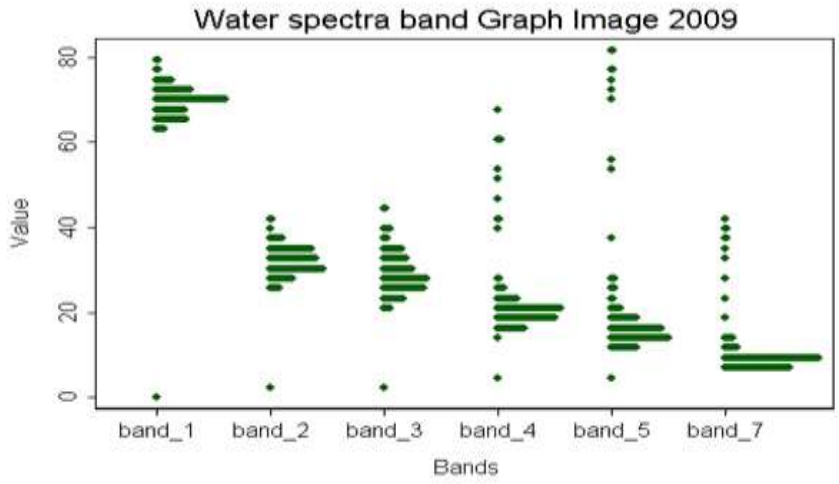

Figure 4.2: Water spectra band graph of Landsat TM image 2009

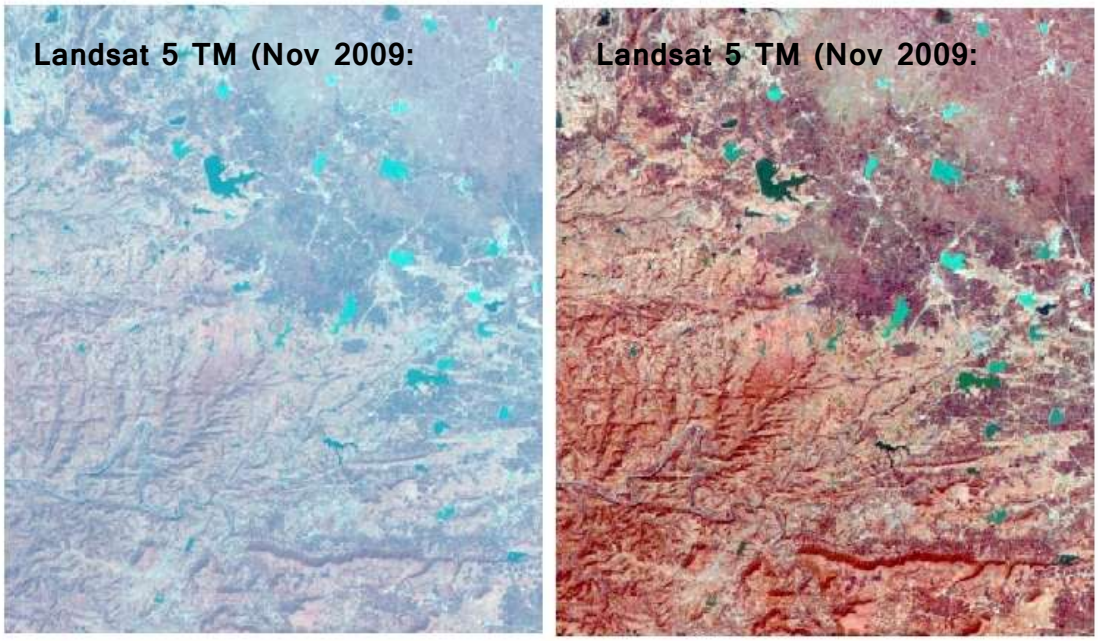

Figure 4.3: Landsat scene 2009 reported before (left) and after (right) the Dark -Object Subtraction.

4.2.4. Automatic vegetation mapping

4.2.4.1. NDVI calculation from Landsat to guide Land Cover Mapping

Normalized Difference Vegetation Index (NDVI) derived Forest/Non-Forest maps were developed to use as a guide to select land use/land cover training samples for forest/non forest mapping (Figure 4.4). NDVI was first proposed formally by Rouse (1973). The use of NDVI to measure ecological phenomena involving vegetation was presented in subsequent years by Rouse et al. (1975) and Tucker (1979). Since then, NDVI has become one of the important tools for mapping and monitoring vegetation (Running, 1990).

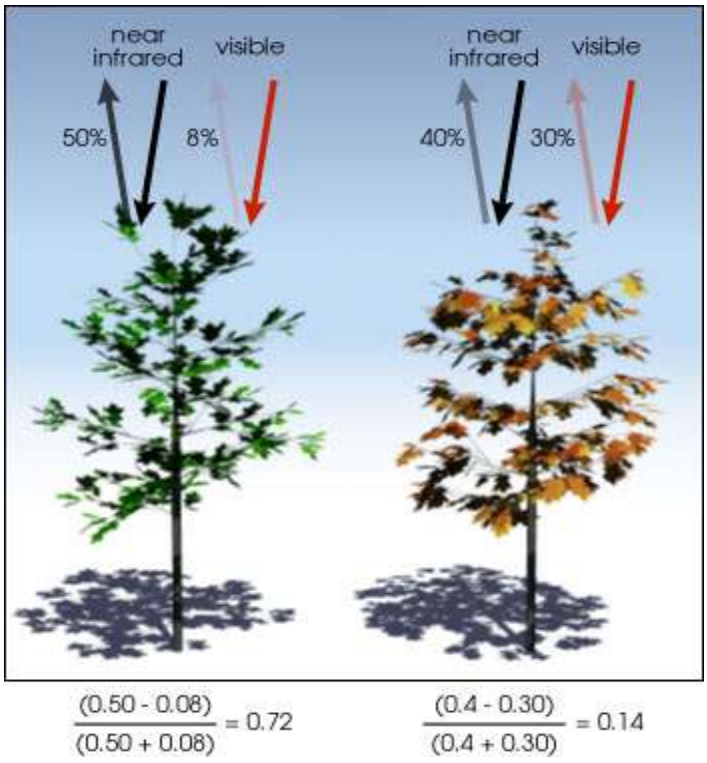

Figure 4.4: NDVI calculated from the visible and near - infrared light reflected by vegetation. Healthy vegetation (left) absorbs most of the visible light that hits it, and reflects a large portion of the near infrared light. Unhealthy or sparse vegetation (right) reflects more visible light and less near–infrared light. The numbers on the figure above are representative of actual values, but real vegetation is much more varied (Illustration by Robert Simmon).

NDVI takes advantage of the plant adaptation that causes healthy plants to reflect red light and near–infrared (NIR) light in different ways. This adaptation is a result of how plants use sunlight for

photosynthesis. The break-up of proteins that occurs during photosynthesis requires light with enough energy. Red light and more energetic light have enough energy to power photosynthesis, so it is highly absorbed as the plant thrives. Near infrared light is not energetic enough to create organic compounds, but does contain enough energy to heat the plant up, which could lead to overheating and plant death. Since the plants can't use NIR light and it could be somewhat harmful to them, they reflect it back. This means that healthy plants absorb very different amounts of red light and NIR light. Unhealthy or dead plants, however, are not performing photosynthesis, so they do not absorb as much energetic light and reflect it back. This means that unhealthy or dead plans will not have a notable difference in the amount of red and NIR light they reflect. The NDVI is calculated from these individual measurements as follows:

NDVI = (Near IR band – Red band)/ (Near IR band + Red band) ….....Equation (4.1)

Where, Red and NIR stand for the spectral reflectance measurement acquired in the red and near–infrared regions, respectively. By measuring how much visible and near–infrared light is reflected off the surface, one can gauge the "greenness" of the vegetation, to which an index value can be assigned. The values usually range between -1 and 1. For example, a value of 0.5 indicates dense vegetation, whereas values less than zero imply no vegetation. Vegetation reflects both visible light and other radiation from invisible parts of the electromagnetic spectrum in unique ways (Myneni et al., 1995). The spectral reflectance of photosynthetically active vegetation in the visible parts of the EM spectral is related to the presence of plant pigments such as Chlorophyll a and b; in the near infrared part of the spectrum, plant structure, particularly the interactions of light with leaf structure dominates the reflectance signature. NDVI is a useful measure because it has been shown to be strongly related to Leaf Area Index and to the presence and amount of photosynthetically active material (Myneni et al., 1995). In summary, the primary photosynthetic plant pigments absorb light from the blue and red parts of the EM spectrum, while near infrared light is strongly refracted by spongy mesophyll cells in leaves so that healthy vegetation provides large NDVI values and areas containing a dense cover of healthy vegetation canopy will tend to have positive values ranging from 0.3 to 0.8. By contrast areas that contain little or no vegetation, or vegetation that is not photosynthesising, will have values ranging from zero to 0.3.

Providing the raw spectral data are correctly calibrated to radiance values, the NDVI is a normalised variable that can be used to make quantitative comparison of spectral signature from different image sources, from different areas and from different time periods. Landsat images were selected to support the time series analysis in this study. Landsat imagery is moderately high resolution Earth observation data that is acquired through sensors on the NASA Landsat satellites. The satellite sensors acquire high

integrity images of the planet surface in a systematic fashion. It is useful to determine the health and type of vegetation, amount of built surfaces, success of agriculture, or apply it for a myriad other uses. Landsat imagery is acquired in a very precise manner, to better emphasize particular land cover aspects. Some of the parameters of this precision involve a scene's radiometry, providing distinct characteristics to components of the image scene.

Red chlorophyll absorption band of healthy green vegetation is one of the most important bands for vegetation discrimination. In addition, it is useful for soil boundary and geological boundary mapping. The red band may exhibit more contrast than the blue and green bands because the effect of the atmosphere is reduced. The 0.69 um cut–off represents the beginning of a spectral region from 0.68 to 0.75 um where vegetation reflectance crossovers occur that can reduce the accuracy of vegetation studies. The near infrared band is especially responsive to the amount of vegetation biomass present in a scene. It is useful for identification of vegetation types, and emphasizes soil – crop and land – water contrasts.

During the research the NDVI was calculated in the ArcGIS software for each image using Red (R) and Near Infrared band (NIR) in each image (Figure 4.5). Index values can range from -1.0 to 1.0, but vegetation values typically range between 0.1 and 0.7. Higher index values are associated with higher levels of healthy vegetation cover, whereas clouds and snow will cause index values near zero, making it appear that the vegetation is less green.

4.2.4.2.Enhanced Vegetation Index (EVI) approach

The Enhanced Vegetation Index (EVI) derived map was developed using Landsat 8 imagery and used to identify areas of non-forest within the forest mask represent potential areas of forest change (i.e. deforestation or degradation). The delineated non–forest areas were input into a GIS and used as an ancillary layer in the change mapping. The key to differentiating forest from non-forest is to link the reflectance properties of the vegetation to its structure. Several vegetation indices exist that enhance non-forest detection as described by Asner (1998), but the Enhanced Vegetation Index (EVI) as described in Huete et al. (1997), was favoured over other vegetation indices as it includes the blue reflectance. The strength of the EVI is in its ratio concept which provides a correction for soil background signals and reduces atmospheric influences, including aerosol scattering. EVI was successfully applied to separate forest – non forest areas by (Bholanath and Cort, 2015) and widely discussed in the scientific literature (Deng et al 2007).

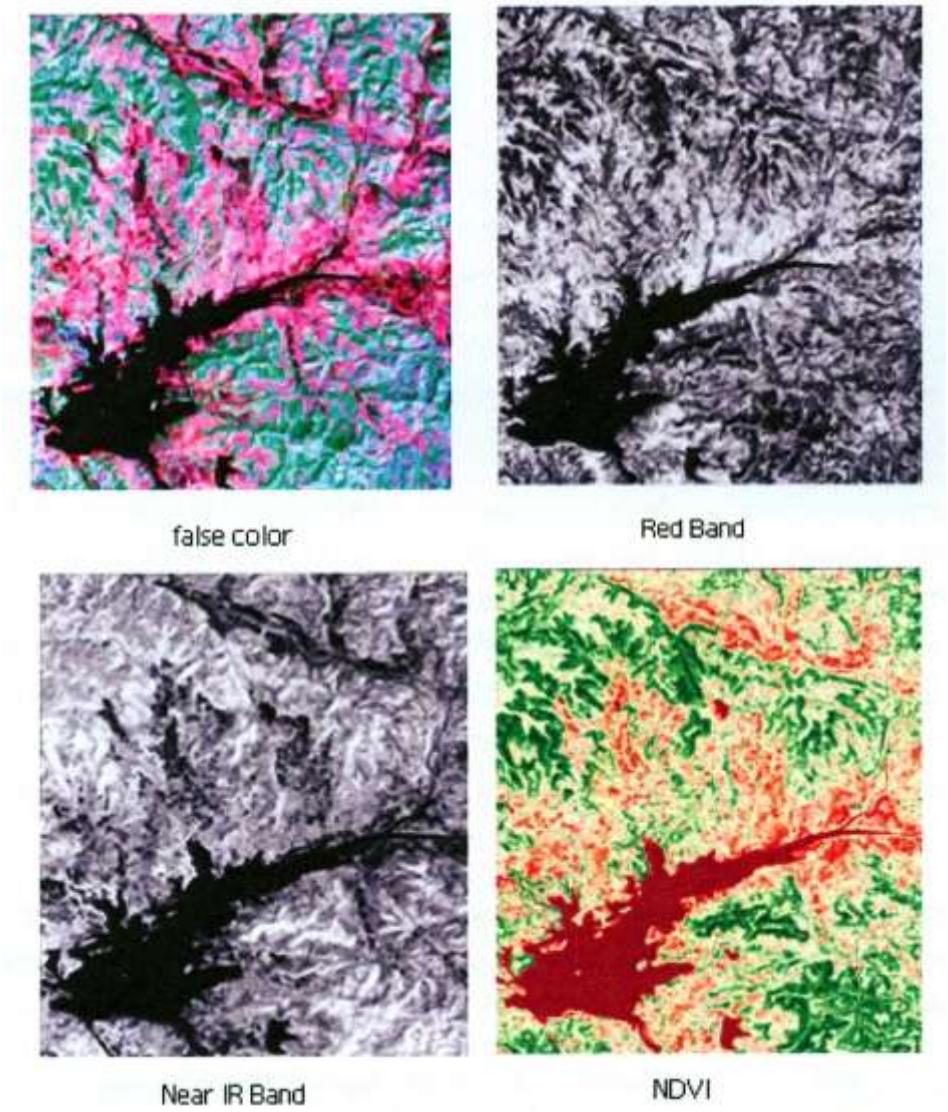

Figure 4.5: Example of an NDVI image calculation from a Landsat TM, 2009 image on an area in the Man River basin. The "False" colour composite image (upper -left). " The Red " (upper -right) and " Near Infrared (Lower -left) bands for this area each highlight different aspects of the area. Form the NDVI image (lower – right) the vegetation and non-vegetation area are easily distinguishable

The EVI is calculated using the following equation as presented and described in Huete et al., (2002).

$$EVI = \mathrm{G}\frac{pNIR - p\,RED}{p\,NIR + c_1 \times pRED - c_2 \times pBLUE + L} \quad \text{..... (Equation 4.2)}$$

Table 4.1: Landsat Red and Near IR bands summery used for NDVI analysis

Sensor	Year	Spectral band (um)	Electromagnetic Spectrum	Cloud Cover	Pixel size (meters)
Landsat 1	1972	MSS			
		Band 5:0.60-0.70	Red	0%	80
		Band 7:0.80-1.10	Near IR	0%	80
Landsat 3	1980	MSS			
		Band 5: 0.60-0.70	Red	0%	80
		Band 6: 0.70-0.80	Near IR	0%	80
Landsat 5	1989	TM			
	2009	Band 3 : 0.63-0.69	Red	0%	30
		Band 4 : 0.76-0.90	Near IR	0%	30
Landsat 7	2001	ETM+			
		Band 3:0.63-0.69	Red	0%	30
		Band 4:0.76-0.90	Near IR	0%	30
Landsat 8	2013	ETM+			
		Band 4: 0.64 – 0.67	Red	05	30
		Band 5 : 0.85 – 0.88	Near IR	0%	30

G is the gain factor, ñ are atmospherically corrected or partially atmosphere corrected (Rayleigh and ozone absorption) surface reflectance's, L is the canopy background adjustment that addresses nonlinear, differential NIR and red radiant transfer through a canopy, and C1, C2 are the coefficients of the aerosol resistance term, which uses the blue band to correct for aerosol influences in the red band. The coefficients adopted in the EVI algorithm are, L=1, C1=6, C2 = 7.5 and G = 2.5.

The EVI values range from 0 to 1 with low values indicating non-vegetative surfaces and those closer to 1 representing closed canopy forest. The same approach was successfully applied to separate forest and non-forest components for the 1990-2010 period. The method has been widely discussed in the scientific literature. Deng et.al., (2007) found that EVI was effective in vegetation monitoring, change detection, and in assessing seasonal variations of evergreen forests. Additionally, the EVI has been found to perform well in the heavy aerosol, biomass burning conditions in Brazil (Miura, et al., 1998). Miura, et al., (2001) also showed that the EVI ratio can successfully minimize residual aerosol effects resulting from the dark target-based atmospheric correction.

4.3. Determining the Land Use Land Cover Area definition

An accurate and complete set of land use/land cover class definitions were created under this assessment following IPCC categorization and guidelines. Over all, six broad categories of preliminary forest and non-forest land scheme were developed and forest land was further subdivided into three major land use class based on purpose (Dense Forest, Scrub Forest and Open Forest). The land use/land cover categories are broad enough to classify all land areas and to accommodate differences in classification systems (Figure 4.6, 4.7, 4.8 and 4.9). The name of these land categories are a mixture of land cover (e.g. Forest land, Fallow land, Water body) and land use (e.g. Agriculture, Settlements) classes. Land cover represents the features present on the land surface while land use represents the activities with which the land cover is being used. These particular categories have been selected because they are consistent with the IPCC guidelines, are relatively straightforward to apply and are a robust method for change mapping (e.g. deforestation, forest degradation and carbon loss). The definitions of each category are as follows:

Forest land: Forest category includes the area of evergreen and deciduous trees with N10% canopy cover as well as degraded forest types that have 10% of the canopy cover. This definition is similar to the forest cover definition used by the National Remote Sensing Centre, India (NRSA, 2007). Forest land is classified in three sub class include dense forest, scrub forest and open forest.

Figure 4.6: Forest land in the study region.

Agricultural land includes arable and tillage land, and agro-forestry systems where vegetation falls below the thresholds used for the forest land category, consistent with the selection of national definitions.

Figure 4.7. Agricultural land in the study region.

Fallow land: includes rangelands and pasture land that is not considered as cropland and also not included as forest land. It also includes systems with vegetation that fall below the threshold used for the forest land category. The category also includes all grassland from wild lands to recreational areas as well as agricultural and silvi-pastural systems. The area which degraded due to soil erosion and forest harvesting included in the category.

Figure 4.8: Photos of fallow land in the study region.

Water Body; includes land that is covered or saturated by water for all or part of the year (e.g. ponds) and that does not fall into the forest land, cropland, and grassland or settlements categories.

Figure 4.9: Man dam in the river basin: an example of water body structure.

Settlements; includes all developed land, including transportation infrastructure and human settlements of any size, unless they are already included under other categories. This should be consistent with the selection of national definitions.

Other land; includes bare soil, rock, and all unmanaged land areas that do not fall into any of the other five categories. It allows the total of identified land areas to match the national area, where data are available.

4.4. Mapping Land Use Land Cover

LULC maps were produced from 1972 to 2013 using Landsat time series images. All the Landsat Images that are currently used for assessment are described in Chapter 3. The Man River basin is covered by two Landsat Scenes (raw 147 path 44) and (raw 147 path 45). All the Landsat images were taken approximately at the peak of the vegetation period (winter season).

4.4.1 Building & evaluating signature sets for classification scheme

Spectral signatures were generated using the area of interest (AOI) tools in the ERDAS 2011 software that matched each spectral class from ISODATA and assigned class names for the signatures through ancillary data such as Aerial photographs, GPS points and Survey Of India maps (Scale 1:50000), as well as the interpreter's knowledge. The numbers of training samples were presented in the table no 4.2.

Table 4.2. Training samples used for classification.

Classes	2013	2009	2001	1989	1980	1972
Agriculture	28	05	07	05	06	04
Dense forest	02	02	04	02	03	02
Scrub forest	10	01	04	01	02	01
Open forest	03	01	03	02	02	01
Fellow land	09	03	14	05	02	06
Water body	01	05	03	03	03	02
Settlement	01	01	03	01	01	03
Dry river bid	03	02	03	05	02	03
Total	65	20	41	25	21	22

Spectral separability of training samples within each feature class was evaluated to assist the quality of training data. A second spectral separability including each two-feature classes was evaluated to ensure that each pixel was categorized into the land cover it most closely resembled and that no overlapping of pixel classification occurred. The evaluation of training signature was measure using the separability feature from the Evaluate menu in ERDAS Software. This option produces a report for one of several measures. During the process, users need to highlight all of land use land cover classes within the editor window before running the separability measure. The separabality tool measure yields real values between 0 and 2, where 0 indicates complete overlap between the spectral signature of two land cover classes, and 2 indicates a complete separation between the two classes. The following rules are suggested for each of the possible ranges of separability values

:

- $< x < 1.0$ (poor separability)
- $1.0 < x < 1.9$ (moderate separability)

- $1.9 < x < 2.0$ (good separability)

Poor separability ($0.0 < x$ 1.0) indicates that the two signatures are statistically very close to each other. Poor separability can be arbitrarily discarded (suggested when the separability is closer to 0), or the two signatures can be merged (suggested when the separability is closer to 1). Moderate separability ($1.0 < x$ 1.9) indicates that the two signatures are separable, to some extent. However, it is desirable to improve separability, if possible, perhaps by adding or modifying training areas which was done in the current analysis. Low signature separability is usually caused by improper combinations of image bands, and/or training sites which have large internal variability within each class.

Reference datasets such as field based GPS training points, aerial photographs for 2009, 2013 and Toposheet for historical forest land use mapping were used to identify land use /land cover areas to evaluate the classification scheme. Additionally the NDVI derived Forest/Non- Forest map was also used as a guide to select land use/land cover training sample for forest mapping (Figure 4.10). There are a number of common methods for applying spectral signatures for each class to the images; these methods vary in complexity and accuracy. Supervised classification is found to be more appropriate and less sensitive to radiometric variations (Mas, 1999). Thus, the maximum likelihood classifier (MLC) algorithm was used to perform the final classification using the spectral bands 1-5 and 7 (VIS, NIR and SWIR) in ERDAS Imagine software.

4.5. Determining Historical Change Mapping from 1972- 2013

This section describes the process which was applied for representing land use land cover areas using the broad categories defined previously (IPCC approach 2). This approach used tracking of land use changes between land use categories. The essential feature of this approach is that it provides regional scale assessments of not only the losses or gains in the area of specific land categories, but what these changes represent (i.e. changes from and to a category). This approach is more data intensive than others as it can account for all land use transitions. This means that emission and removal factors or parameters for rates of change can be taken into account.

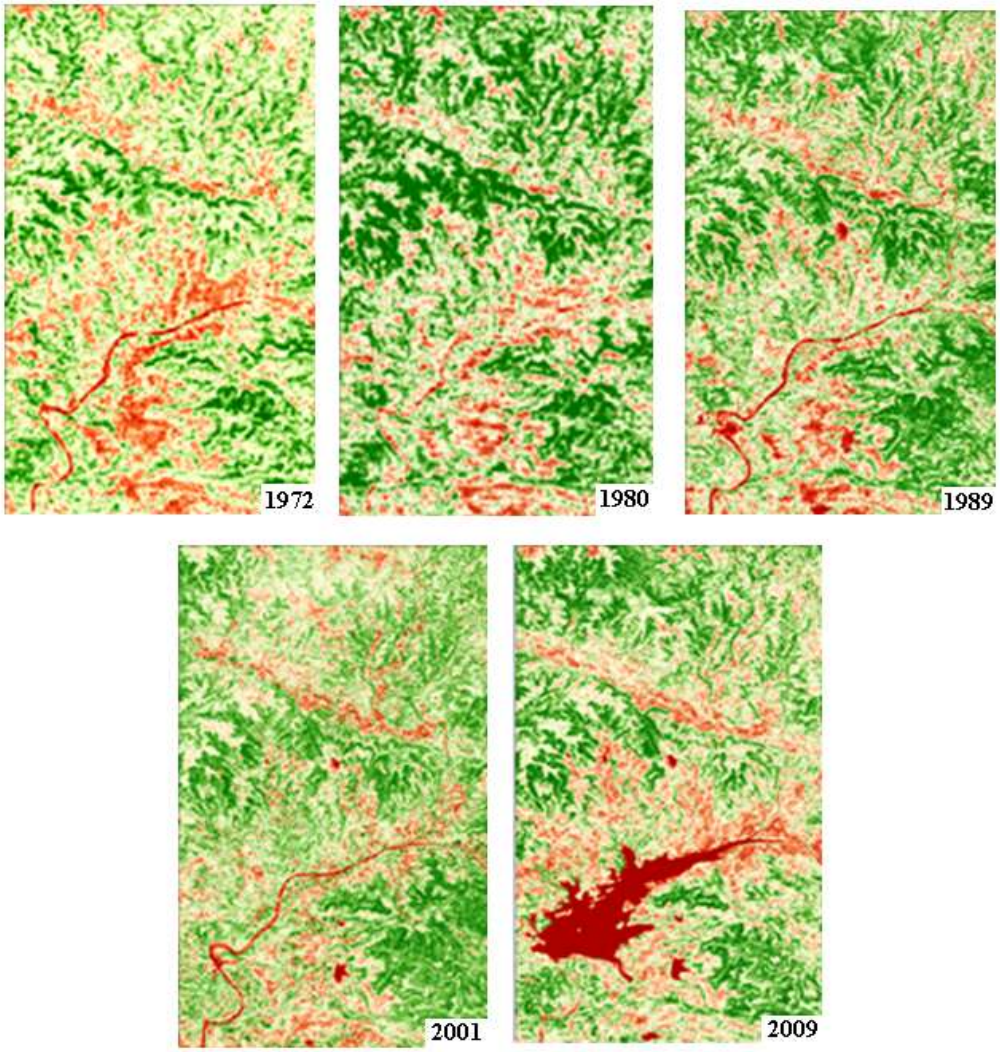

Figure 4.10: Time series NDVI images for a portion of Man River basin.

The change was produced for mapping historical change in the Man River basin for six periods:

- Mapping year 1972 -1980
- Mapping year 1980- 1989
- Mapping year 1989- 2001
- Mapping year 2001- 2009
- Mapping year 2009- 2013
- Benchmark period 1972-2013

The time period for each mapping epoch is not equal. For each temporal period of the research specifically focused on deforestation, agriculture extensification and water bodies' extension as they are major issues in the study region. Deforestation was defined as the long–term or permanent conversion of land from forest use to other non – forest uses was adopted (GOFC- GOLD, 2010). The final results of this assessment were presented as a non-spatially explicit land-use change matrix. The matrix form is a compact format for representing the areas that have come under different transitions between all possible land-use categories (Table 4.3).

Table 4.3: Land Use change matrix table example

Initial / Final	Agriculture	Forest	Fellow land	Final sum
Agriculture				
Forest				
Fellow land				
Initial sum				

4.6. Direct Interpretation Approach for mapping deforestation, forest degradation and responsible drivers

The direct interpretation method was adopted for mapping deforestation and forest degradation and associated responsible drivers over the river basin area from 2009 to 2013. The integrated wall to wall mapping approach is a direct and repeated assessment of land use land cover change from full spatial coverage. The approach extends automatic pixel based analysis by allowing land-use changes to be tracked on a spatial basis. This approach requires spatially explicit observations of land use and land use change. The data may be obtained either by geographical location points, a complete wall to wall mapping, or a combination of both. The approach is comprehensive and relatively simple conceptually, but data intensive to implement. The target area is subdivided into spatial units such as polygons appropriate to the scale of the land use variation and the unit size required. In this study, polygons were subdivided according to deforestation and forest degradation by specific drivers such as deforestation by

agriculture extension, deforestation by timber harvesting and deforestation by infrastructure development. If wall to wall mapping is used, a polygon based approach can be used equivalently to a grid approach. Observation may be from remote sensing, site visits or aerial imagery.

This method was developed to continue forest change assessment in detail to understand spatial distribution of deforestation and responsible drivers with ground verification which was not possible in previous assessment. Direct interpretation of satellite images is a recognized approach that is outlined in GOFC-GOLD (2010) and IPCC Approach 3 (2006). A forest loss layer for the period 2009- 2013 was created by identifying new change using Land cover thematic maps (generated by Landsat imagery in the current study) in ArcGIS. If areas had already recorded change in the previous year, then they were not considered with recent change year (2009-2013 epochs).

Over the deforestation layer 2009-13 in the river basin, aerial imagery and EVI were also brought into the GIS. The river basin was also divided into a series of regular 1x1 km space grids for systematic wall to wall mapping. A two stage approach for mapping forest change was used. Stage one involved delineating the forest change, while stage two involved attributing (drivers) to the delineated change.

The delineation was based on aerial imagery and EVI threshold which was manipulated as required by the operator. Aerial imagery was used to verify and delineate the deforestation and forest degradation areas which were mapped by Landsat. Manual interpretation and editing of the polygon boundary of non-forest areas from aerial imagery were performed in the GIS. As part of continual improvements, additional EVI inspections were also undertaken over the non–forest areas to further refine the delineation of deforestation and forest degradation which was delineated by aerial imagery. The EVI values range from 0 to 1 with low values indicate non–vegetation surface and those closer to 1 represent closed canopy forest. Therefore, the EVI values ranged from 0.25 to 0.35 for delineating non forest areas. This was applied uniformly in the study. It means EVI was simply used as a guide tool to improve the quality of non-forest area delineation.

For example, the deforestation polygon layer for time period 2009-13 was overlaid on aerial imagery 2013 to identify and delineated the deforestation area. EVI further used to update the potential boundary of delineation. Finally, the polygon boundary of non-forest was generated and edited in GIS. Once the polygon was delineated through the manual review of aerial imagery and EVI vectors, the driver and resultant land use class were determined by visual inspection of the Google Earth imagery. The decision tree that shows the process followed when mapping deforestation and degradation delineation is presented in Figures 4.11and 4.13 and Table 4.4.

Table 4.4: Summary of activities & drivers captured in the GIS

Activity	Driver	Criteria	Ancillary info Available	End Land Use class
Agriculture	Deforestation	Deforestation site >1 ha	Satellite imagery	Fallowland
Water bodies	Deforestation	Deforestation Site > 1	Satellite imagery	Fallowland /crop land /forest
Forestry (harvesting timber)	Deforestation	Deforestation Site > 1	Satellite imagery	Degraded forest by type
Agriculture	Deforestation	Deforestation Site > 1	Satellite imagery	Fallow land
Shifting agriculture	Degradation	Degradation Site > 1	Satellite imagery	Degraded forest by type

Degradation surrounding year 2009 -2013 sites was mapped by selecting the polygon of deforestation. Any forest that showed visual evidence of forest degradation was mapped as degradation resulting year 2009 -13 forest change. No degradation is mapped around sites from periods processing 2009-13.The visual interpretation method has the advantage over a remote sensing method as it allows for context to be included in the decision-making process. The method used to delineate the main drivers of deforestation and degradation is described in detail below. The following description and examples provide a summary of the main characteristics of each driver in the Man River basin.

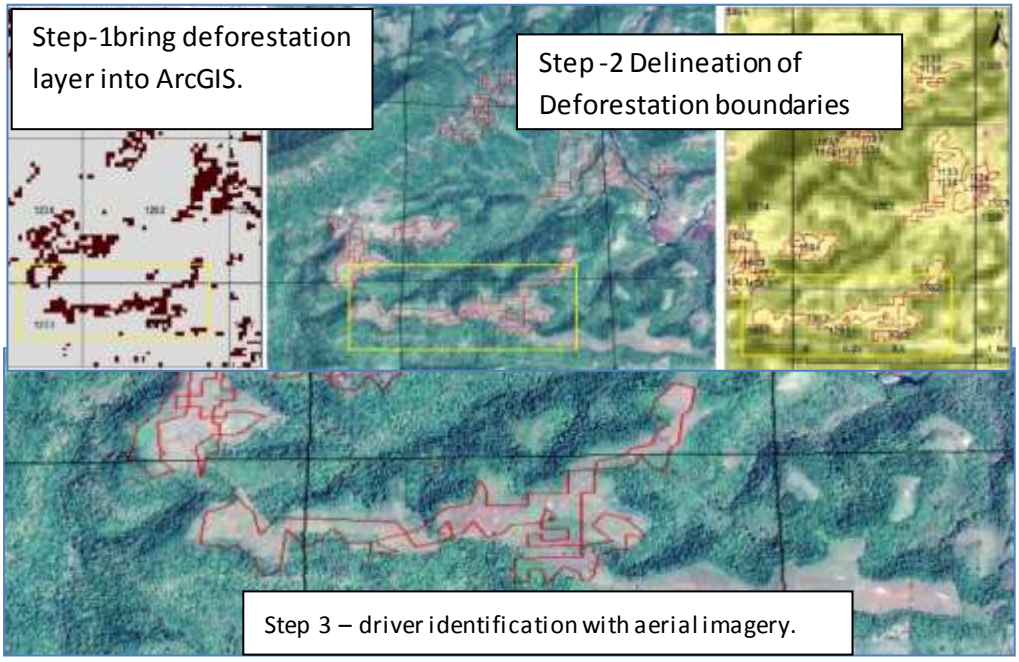

Figure 4.11: Decision steps for deforestation and forest degradation mapping associate with drivers.

4.7. Minimum Mapping Unit

The choice of an MMU that is appropriate for the classification is an important consideration because it can have important implications for area estimation and accuracy (Knight and Lunetta, 2003). For example, using large sizes of MMU will lead to a reduction in the actual representation of small sizes of land use areas (Saura, 2002). However, producing classification with small sizes of MMU is a challenge for users (He et al, 2011). However, the effect of minimum mapping unit will vary according to resolution of satellite imagery and classification procedure. GOGC GOLD guidelines (2009) suggest some useful recommendations for use of MMU for fine, medium and coarse resolution imagery (table 8.2). In the current study, 30m X 30m MMU was used to produce time series land use and change maps. The objective was to produce much more precise classification maps which are able to provide much more information about small patches. This land use land cover information can also be used for soil erosion modelling at hillslope scale to provide appropriate land use representation as large size MMU (e.g. 1ha MMU) doesn't count small size of land cover areas which has significant effect on soil erosion modelling when it used as an input for soil erosion modelling. Landsat (30m) data also allows adopting 30mX30m MMU for classification.

Table 4.5. Utility of optical sensors at multiple resolutions for deforestation monitoring.

Sensor & resolution	Examples of current sensors	Minimum mapping unit	Utility for Monitoring
Coarse (250-1000m)	SPOT-VGT(1998-)Terra-MODIS(2000-) Envisat-MERIS(2004 -)	~ 100 ha ~ 10-20 ha	Consistent pan-tropical annual monitoring to identify large clearings and locate "hotspots" for further analysis with mid resolution
Medium (10 -60 m)	Landsat TM or ETM+, Terra-ASTER IRS AWiFs or LISS III CBERS HRCCD DMC SPOT HRV	0.5 - 5 ha	Primary tool to map deforestation and estimate area change
Fine (<5 m)	IKONOS QuickBird Aerial photos	< 0.1 ha	Validation of results from coarser resolution analysis, and training of algorithms

Source: GOFC –GOLD Source book, 2010.

Secondly, one (1) ha MMU was adopted to continue and update 2009-13 year deforestation mapping produced by automatic pixel based approach. The purpose was to map drivers of deforestation and forest degradation with ground verification during 2009-13 in the study area which is not sufficiently mapped by automatic pixel based approach. The one ha MMU provided sufficient coverage to identify and map drivers of deforestation and forest degradation as well as estimation of deforestation and forest

degradation with 1 ha MMU. One ha Minimum Mapping Unit is also recommended in GOFC GOLD guideline (2009) for Landsat based imagery to estimate drivers of forest change (table 4.5). Also, adopting two different MMU provides an opportunity to examine the effect of MMU of land use change estimation.

4.8. Identification of change drivers in the Man River basin

This section gives an overview of the major drivers of deforestation and forest degradation which were mapped through remote sensing in the Man River basin**.**

4.7.1 Agricultural extensification

Agriculture is the main driver of deforestation and forest degradation. It is also the backbone of livelihoods and economies of local communities in the Man River basin. Since the 1970s, the human population has increased by 15-20% which has created a huge pressure on agriculture activities. Government policies are used to grant land rights in forestlands, protect farmers from exploitation by traders; supply modern inputs at a subsidised price and ban import of high value crops have encouraged agricultural extensification by local people in the basin. Extensive agriculture has occurred in mountain regions, especially on hillslopes and tops of hills in the last decade. This change is a major cause of deforestation and forest degradation in river basins.

In this research, agriculture intensification has been differentiated by the effect on the land surface as responsible drives for deforestation and degradation. First, this category includes arable and tillage land. Cropland is identified as permanent fields mainly cotton, soybean wheat grain and also mix agriculture land. Forest areas converted to agriculture are generally found adjacent to existing established farmland, in proximity to settlements and around the Malwa Plateau in the upper areas of the river basin and valley areas where soil layer is quite thick. These areas of change take the form of large, regular shapes, greater than 1 ha blocks. Each block has its own distinctive spectral signature. Google Earth aerial images were used to help identify these agriculture areas.

Second, permanent agriculture land that was traditionally used for shifting cultivation is located mostly on tops of the hills and in some flat valley bottoms where conditions are favourable. They are often presented in the landscape as a mosaic of forest and small-scale cultivation land cover types. Agriculture is

primarily rain-fed and is the major source of income in this area. The majority of farmers fall in the landless, marginal (2.5 acres) or small (2 .5 -5 acres) farmer categories. Farmers living within 5 km of the forest are mostly marginal and small do not use soil and land conservation measures. In the past, forest land that was cut, was used for agriculture then left fallow to return to regenerating forest. In this way subsistence agriculture is characterised by a disordered patchwork of forest clearings on hill slopes and flat valley bottoms. However, in recent times the cultivation has not resulted in land being left fallow and returning to forest land cover. Soil depths on hill slope are very thin and once soil is washed away due to unsustainable land management practices, traditional cultivation activates and enhances soil erosion. The area thus converts into areas not suitable for forest plantation (Figure 4.14). The result is net deforestation rather than forest degradation as shifting or swidden cultivation systems are normally regarded as classifications of degraded forest land cover types. In the context of soil erosion, the important factor is the resultant land cover type which is agriculture.

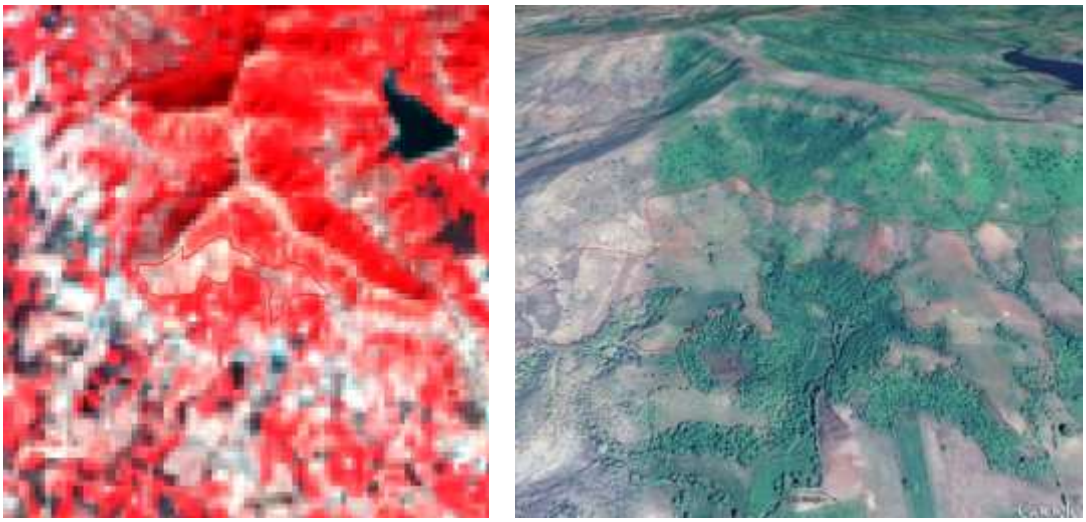

Figure 4.12: Shifting cultivation as detected from Landsat and aerial Image

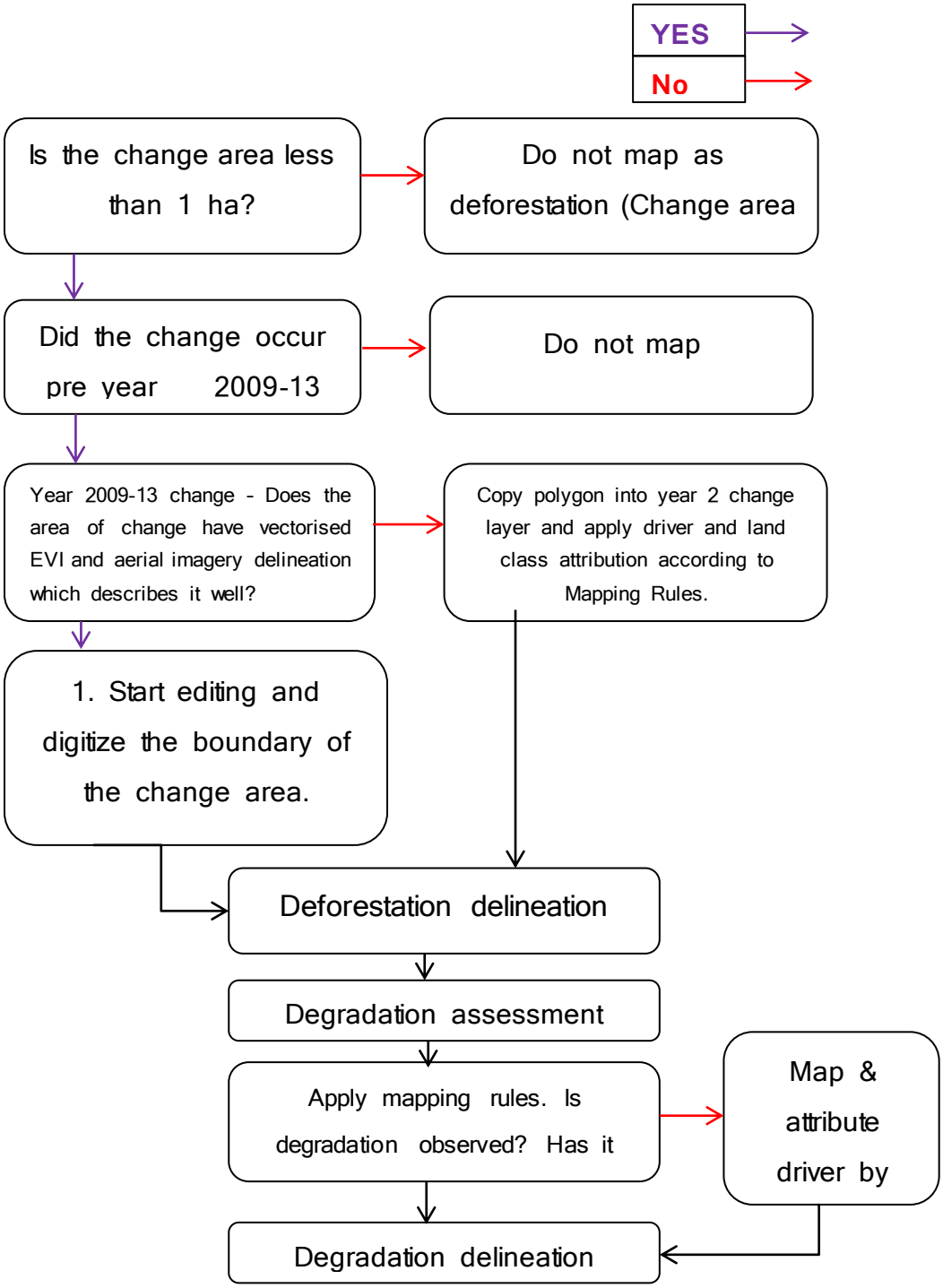

Figure 4.13: Change Mapping decision Tree

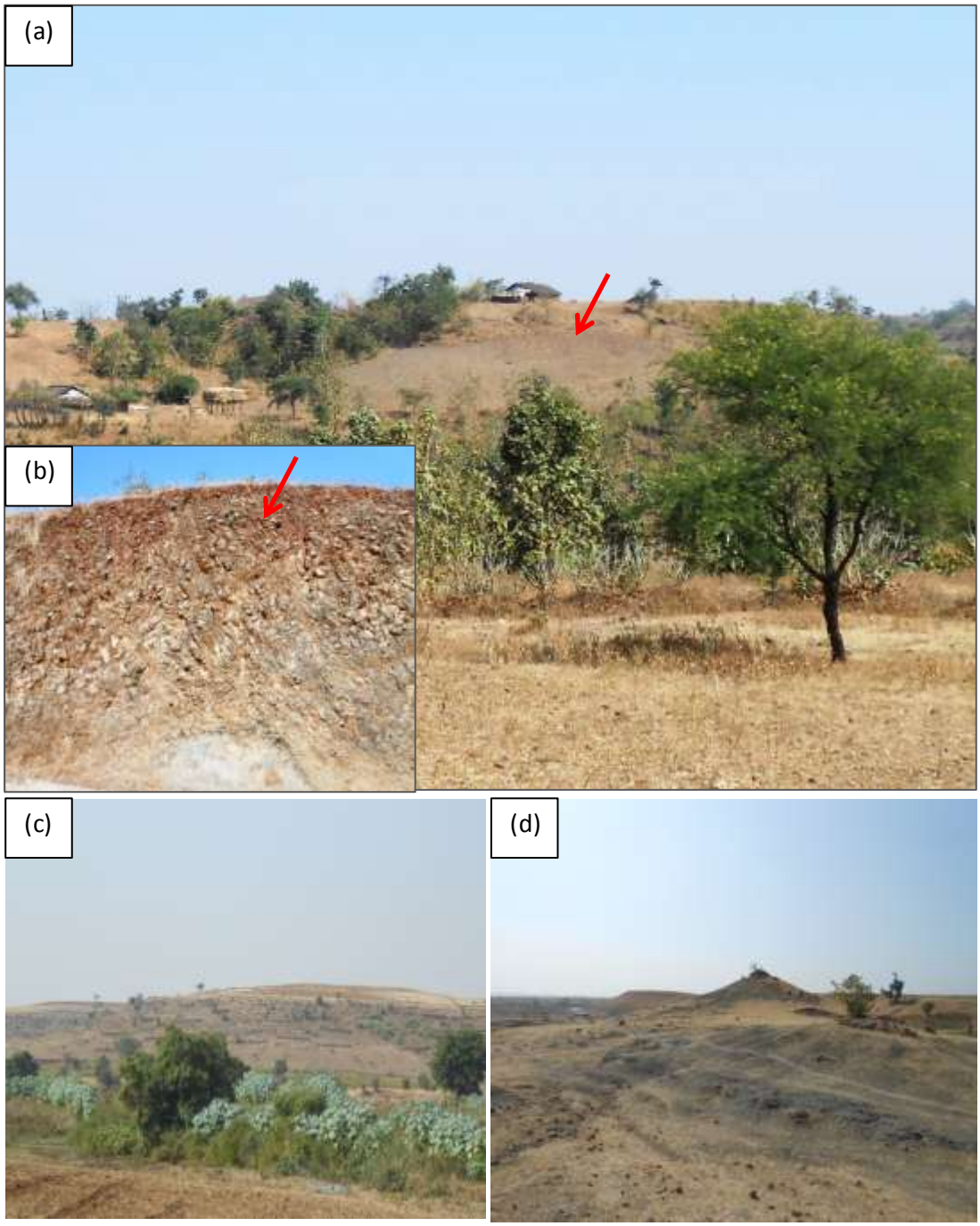

Figure 4.14: Photos are showing (a) shifting agriculture on hillslope and (b) very thin soil depths. (c) and (d) show two further examples in the region.

The extent of these areas was mapped by delineating the extent of the activity. Over time the coverage of these areas may extend or contract. The extent of any regeneration still remains to be quantified in the field. A single polygon around the spatial extent of the visibly impacted area is created. The polygon includes a patchwork of degraded forest areas and land under permanent cropping (Figure 4.13).

4.8.2. Water bodies

Water bodies are easily detectable drivers in the Landsat imagery and aerial photograph. Areas of water body responsible for deforestation were identified using Landsat and Google earth images by digitizing a single polygon around the spatial extent of the change in area from forest to water body (Figure 4.15).

Figure 4.15: Water bodies as detected from Landsat and aerial Image.

4.8.3. Forest Harvest

Forestry activities within the basin area are characterised by both legal and illegal harvesting activities. It is possible to recognize areas of clear-cut forest and areas of illegal harvesting which may result in severe forest degradation. There are also areas of planned selective logging. The most noticeable land cover change results from clear cutting which allows forest to be replaced by cultivation and grassland land cover types. The extent of selective forest harvesting is difficult to estimate and has a higher level of uncertainty associated with it. Small–scale forest harvesting is identifiable from Google Earth imagery.

In mapping forest harvest, the best method is to define the extent of areas that appear to have been harvested due to canopy gaps and spectral differences within or nearby harvested areas. These areas are delineated as single polygons around the spatial extend of the impacted area; a land use class of fallow land by the forest type is assigned (Figure 4.16).

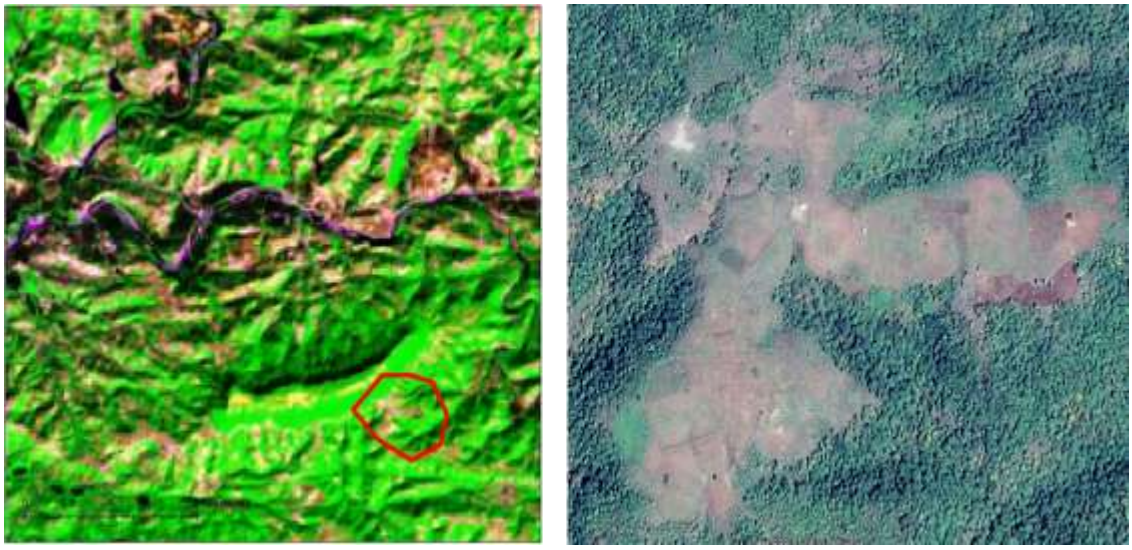

Figure 4.16: Forest harvest as detected from Landsat and aerial Image

4.9. Mapping land cover using the direct interpretation approach for all three watersheds in the Man River basin.

The direct interpretation approach (described in section 4.6) was also applied to produce land use/land cover maps for 2009 in the all three watersheds in the Man River basin. These three watersheds were selected for soil erosion modelling. The purpose of this experiment was to prepare two sets of LULC maps for GeoWEPP inputs using two different mapping approaches to identify the effect of different LULC mapping approaches on land use area estimate and its effect on soil erosion estimate. First, LULC maps for all three watersheds were prepared which was based on the automatic pixel based approach (30mX30m MMU) described in section 4.4, then secondly, a set of LULC maps for all three watersheds were produced using the direct interpretation approach (1ha MMU). This experiment was useful to identify how Landsat (30m) data for the same time period was mapped using different approaches and how the MMU would produce different LULC statics which may produce different estimates if soil erosion if used as an input into soil erosion models. The comparative analysis of outcomes of both mapping approach for three watersheds are explained in Section 5.3.3.

4.10. Verifying Land Use and Land Cover and Change Mapping

The land use/land cover maps were validated for the period 2009-2013. The purpose of the accuracy assessment is to identify and quantify the thematic error of forest, non-forest and deforestation mapping. The validation approach derives a statistically robust and quantitative assessment of the uncertainties associated with the forest and non-forest area and change area estimates following GOFC GOLD good practice guidelines as appropriate. This verification process uses three principle steps for a statistically rigorous validation: sampling design, response design, and analysis design (Stehman and Czaplewski, 1998) (Figs. 4.17 and 4.18).

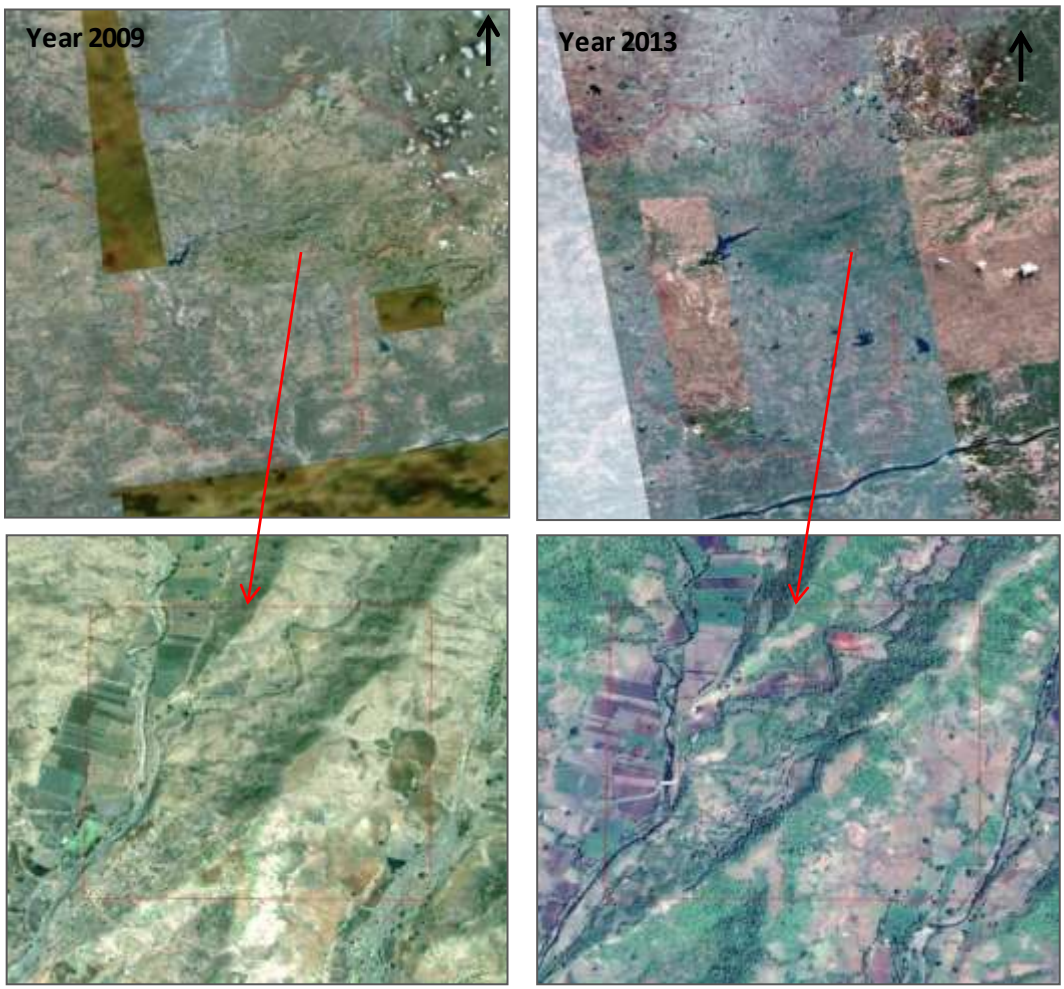

Figure 4.17: Verification aerial image for year 2009 and 2013 and examples highlighted in red box.

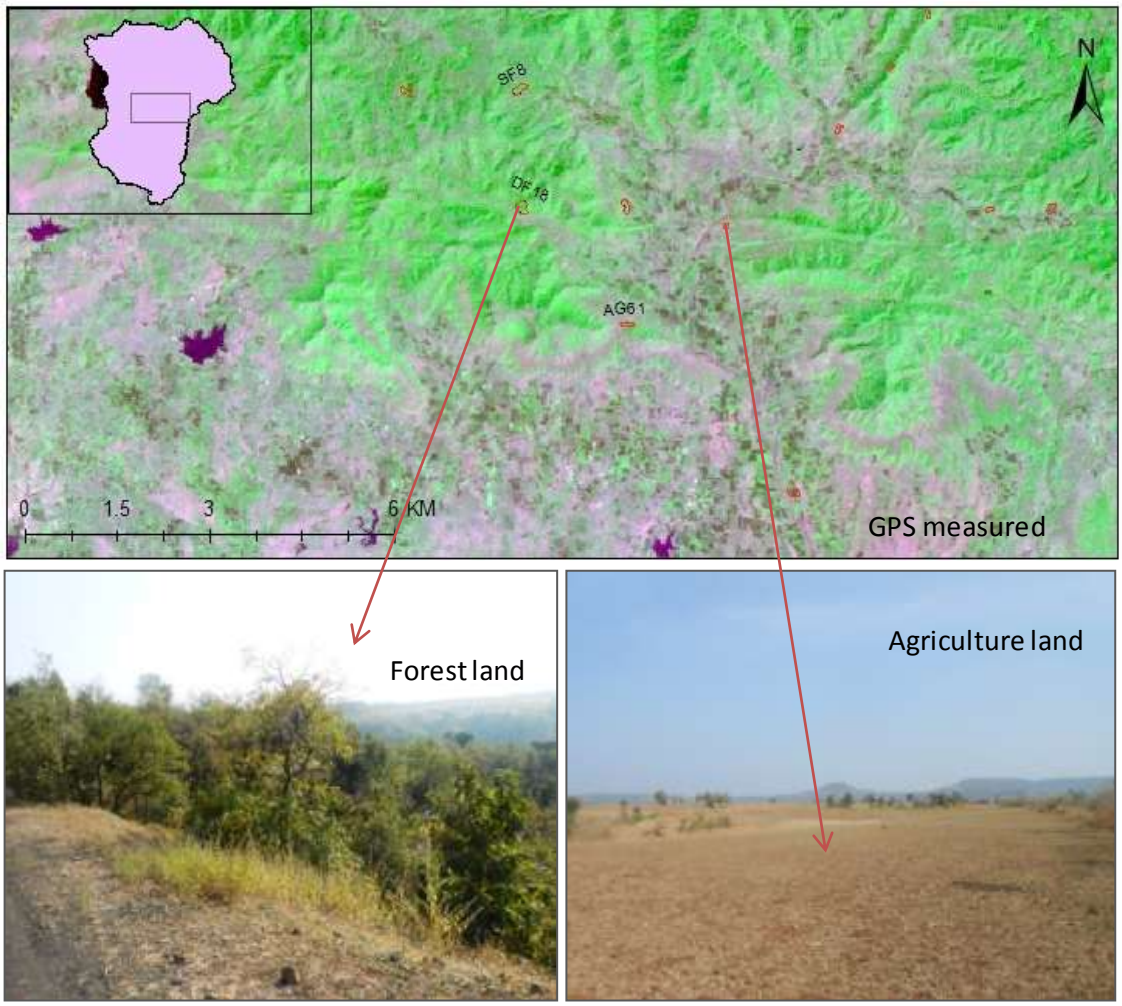

Figure 4.18: an example of GPS measured plots with photo verification used in accuracy assessment.

4.10.1. Response Design

Response design is one of the principle steps for robust accuracy assessment of either land cover or land cover change. The response design consists of the protocols used to determine the reference or ground condition label (or labels) and the definition of agreement for comparing the map label(s) to the reference label(s). Reference information should come from data of higher quality, i.e. ground observations or higher-resolution satellite data. Consistency and compatibility in thematic definitions and interpretation is required to compare reference and map data (GOFC GOLD, 2009). To assess how well the Landsat based forest and non-forest map compared with the ground, field measured GPS plots and good quality

available Google Earth ™ imagery were used for year 2009 and 2013 (Figure

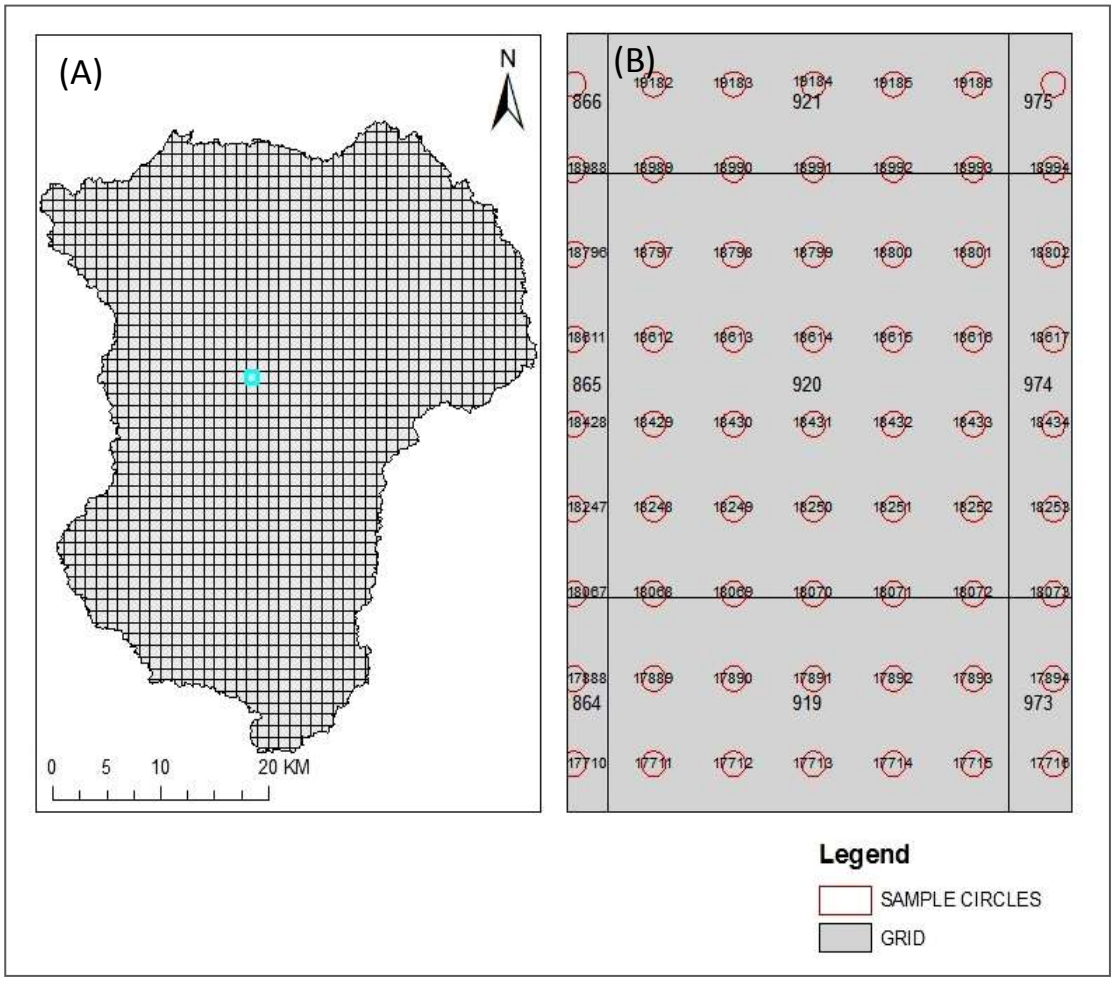

Figure 4.19: A grid of 1km by 1 km in size was created with the centroids within the boundary of river basin and (B) a systematic 25 circulars within each grid square were created .

4.17). Google Earth ™ imagery provides sufficient temporal and spatial resolution to use as a reference data for identification of forest and non-forest area and change analysis. GPS plots (250) were also collected with photo verification in the field area to provide better understating about ground references (Figure 4.18).

4.10.2. Sampling Design

The sample design is the protocol by which the reference data are selected (Stehman and Czaplewski, 1998). According to assessment objectives, an appropriate sample design includes specification of the sample frame, size, sample locations and the reference assessment units: all were established following GOFC – GOLD (2010) recommendations. A sampling frame is defined as the 'materials or devices,

which delimit, identify, and allow access to the elements of the target population' (Sa¨rndal et al. 1992, p. 9). A sampling frame that is most appropriate for large-area land cover validation depends on the nature of each land cover class and whether the class is discrete or extensive. As the area of Man River basin is mostly covered by agriculture, forest, fallow land and water bodies, it is efficient to adopt a stratification framework than use simple random or systematic sampling.

A two stage sampling strategy with stratification of the primary units was used to assess the accuracy of land cover and change mapping (Figure 4.19, 4.20, and 4.21). There are several reasons for the popularity of stratified random sampling, including the following (Cochran, 1977; Lehtonen and Pahkinen, 1996): (i) stratification can enhance the precision of estimates if each stratum is homogeneous; (ii) stratification provides unbiased estimates of parameters not only for the whole population, but also for each stratum; (iii) stratification can guarantee representation of small subpopulations in the sample if desired. A circular sampling area of less than one hectare in size as a Minimum Mapping Unit (MMU) was selected according to landscape characteristics, feature of the mapping process and location (Stehman and Czaplewski 1998, Zhu et al. 2000).

To develop systematic sampling design, these steps were followed in ArcGIS:

- A square grid of 1 km by 1 km in size (1578 grids) was created within the spatial extent of the Man River Basin.
- Grid squares were stratified in ArcGIS according to criteria of land use/land cover, percentage and 100 squares were randomly selected for assessment (Figure 4.20).
- Four strata were selected according to land use classes named agriculture land, forest land, fellow land (dry river bed and settlement) and water bodies (Table 4.6).
- Within each grid square, a systematic sample of points spaced at regular 140 meter intervals was created, yielding 25 points in each sample square.
- These points were then buffered to create a circular sampling area of < 1 hectare in size corresponding to the minimum mapping unit.
- Each of the grid squares was assigned an ID according to its centre point location, and each of the sampling circles has an ID according to its respective centre point location. In total 4500 hectare sampling areas are available for accuracy assessment.
- The land cover class is determined for the each sample area.

Table 4.6: Area represented by each stratum

Stratum	Area 2009 (%)	Area 2013 (%)	Total no of grids 2009-13	Random selected grid for 2009	Random Selected grid for 2013	Sample area cover 2009(%)	Sample area cover 2013(%)
Agriculture	48	58	816	52	58	6.3	7
Forest	32	29	556	31	28	5	5
Fellow land	15.8	9.9	174	13	10	7.4	5.7
Water bodies	2	2.4	26	2	03	7.6	11.5
Others	1	1	6	0	01	0	16.
Total	100	100	1578	101	100	6.4	6.3

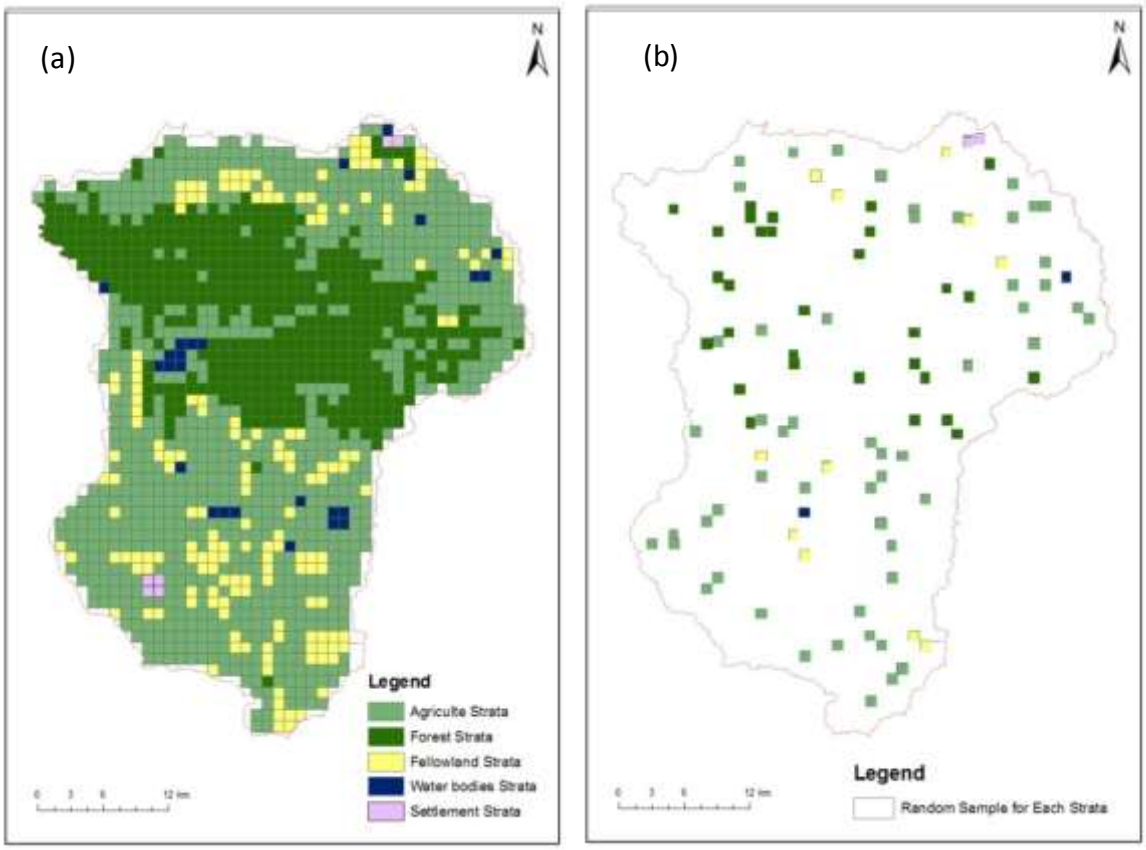

Figure 4.20: Strata according to Land cover 2013 (a) and random sampling for each stratum (b).

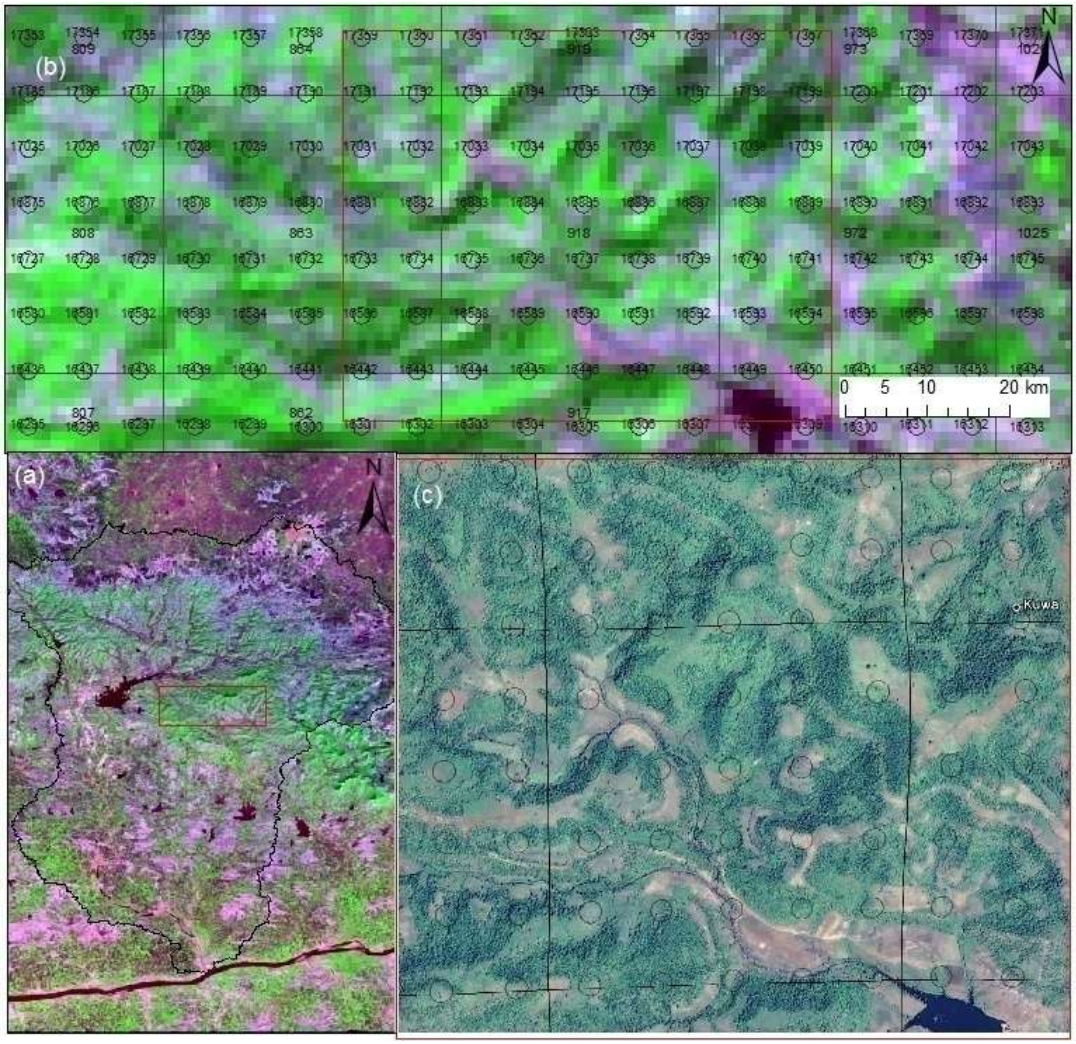

Figure 4.21: Systematic circle sampling showing on a false colour 30 m resolution Landsat image and same area on Google Earth™ aerial photography.

4.10.3. Accuracy and area estimation for classification change analysis

The objective of this section is to adopt a simple analysis and estimation strategy for using the information obtained for map accuracy assessment to estimate area of a land cover and land change, and construct confidence intervals that reflect the uncertainty of the area estimates obtained. An analysis has been presented that makes full use of the map and accuracy assessment data by: 1) estimating accuracy (e.g., user's, producers, and overall accuracies); 2) estimating area of land change using the accuracy assessment sample data to adjust area for map classification error; and 3) estimating standard errors or confidence intervals for the error-adjusted area estimates.

Two sections are presented here, in the first section; the key information and equations needed to produce a complete and rigorous report of accuracy of a land change map and estimation of an area are explained. In the second section, the calculation is presented that makes full use of accuracy data for estimating area and associated confidence interval.

4.10.3.1. Equation for estimating accuracy and area of change

Validated samples of assessment units (e.g. circles, pixels) by simple random, stratified random or systematic sampling are recorded in a table called a confusion or error matrix as shown in Table 4.7. This matrix was used to quantify the quality of mapping, uncertainty and change area estimation. In the error matrix table, map categories (i = 1, 2… q) are represented by rows and the reference categories (j = 1, 2… q) by columns. This matrix table is widely used and was revised by Card, (1982), Foody (2002), Story and Congalton (1986), and Van Oort (2007). The basic principle described here requires map categories and reference categories by row and columns. This approach is reviewed and clearly presented by Olofsson et al, (2013).

Table 4.5 illustrates the common practice of reporting the error matrix in terms of sample counts. A more informative presentation of the error matrix is in terms of the unbiased estimator of the proportion of area in cell i, j of the error matrix:

$$\hat{p} = w_i \frac{n_{ij}}{n_i} \quad \text{.....Equation (4.3)}$$

Where the total area of the map is A_{tot}, the mapped area of category i is $A_{m,i}$ (subscript m denotes "mapped"), and the proportion of the area mapped as category i is $W_i = A_{m,i} \div A_{tot}$. The error matrix in terms of estimated area proportions is shown in Table 4.7. An advantage of the presentation given in Table 4.6 is that accuracy and area estimates can be computed directly from the error matrix. Because of classification error, the mapped area proportions given by $A_{m,i} \div A_{tot}$ are usually biased when the objective is to estimate the true proportion of area of category $i$as determined from the reference classification. Instead of obtaining the area directly from the map classification, an area estimator can be based on the reference classification of each sample unit. The area proportions for each reference-defined category j are estimated from the column totals ($\hat{p}_{\cdot j}$) in Table 4.8. An unbiased estimator of the total area (based on the reference classification) of category j is then:

$\widehat{A_J} = A_{tot} \times \hat{p}_j$……Equation (4.4)

Eq. (4.4) can be re-expressed in an expanded alternate form that more clearly reveals the estimator as a stratified estimator:

$\hat{A}_j = A_{tot} \sum_i w_i \frac{n_{ij}}{n_i}$……Equation (4.4a)

This stratified estimator can be viewed as an "error-adjusted" estimator of area because it includes the area of map omission error of category j and leaves out the area of map commission error. The estimated standard error of the estimated area proportion is (Cochran, 1977).

$S(\hat{p}_j) = \sqrt{\sum_{i=j}^{q} w_i^2 \frac{\frac{n_{ij}}{n_i}\left(1-\frac{n_{ij}}{n_i}\right)}{n_i - 1}}$……Equation (4.5)

The standard error of the error-adjusted estimated area is;

$S(\widehat{A_j}) = A_{tot} \times S(\hat{p}_j)$ …… Equation (4.6)

An approximate 95% confidence interval for A_j is;

$A_j = 2 \times S(\hat{A}_j)$ ……Equation (4.7)

Where the margin of error is defined as the z-score (z is a percentile from the standard normal distribution) multiplied by the standard error (i.e., the ± part of the confidence interval), and the value of the z-score depends on the confidence level (for 95% confidence, z = 1.96 which is approximated here to 2 for simplicity of presentation).

Table 4.7: Error matrix of sample counts n_{ij}. Map categories are the rows while the reference categories are the columns.

Class	**1**	**2**	**…**	**q**	**Total**
1	n_{11}	n_{12}	…	n_{1q}	$n_{1.}$
2	n_{21}	n_{22}	…	n_{2q}	$n_{2.}$
⋮	⋮	⋮	⋱	⋮	⋮
q	n_{q1}	n_{q2}	…	$n_{q\,q}$	$n_{q.}$
Total	$n_{.1}$	$n_{.1}$	…	$n_{.q}$	n

Table 4.8: Error matrix of estimation area proportions, p_{ij} (Eq.4.3). Map categories are the rows while the reference categories are the columns.

Class	**1**	**2**	**…**	**Q**	**Total**
1	$\hat{p}_{11}$	$\hat{p}_{12}$	…	$\hat{p}_{1q}$	$\hat{p}_{1\cdot}$
2	$\hat{p}_{21}$	$\hat{P}_{22}$	…	$\hat{p}_{2q}$	$\hat{p}_{2\cdot}$
⋮	⋮	⋮	⋱	⋮	⋮
q	$\hat{p}_{q1}$	$\hat{p}_{q2}$	…	$\hat{p}_{qq}$	$\hat{p}_{q\cdot}$
Total	$\hat{p}_{\cdot 1}$	$\hat{p}_{\cdot 2}$	…	$\hat{p}_{\cdot q}$	1

Eqs. (4.3)–(4.7) are applicable to simple random, systematic, or stratified random sampling. These estimators are the usual stratified estimators if stratified random sampling is implemented. If applied to simple random or systematic sampling, the estimators are post stratified estimators in which the strata are incorporated via the estimator instead of via the sample selection as is the case for a stratified design (Card, 1982, Cochran, 1977 and Sarndal et al., 1992). Although the area of estimated change is based on the reference classification of the sampling units, the map is still an important component of the area estimation approach because of the role of (w_i) in the area estimator and the importance of the stratification defined by the map classification when the strata are used in the sampling design or used in a post-stratified area estimator. The standard error formula (Eq. 4.5) for the post stratified estimator is an approximation if the sampling design is systematic. This approximation is usually expected to overestimate the true standard error because, for each stratum, the formula applied is based on simple random sampling, and the simple random approximation typically overestimates the standard error if the sampling design is systematic (Wolter, 2007).

Although the primary focus of the research is estimating the area of land change, I briefly review the estimation of accuracy for stratified random sampling. User's accuracy requires data only from within a given stratum so it can be computed directly from the sample counts. But overall and producer's accuracies should not be estimated directly from the error matrix of sample counts (Table 4.7) because the sample units from different strata require different estimation weights; thus the error matrix should be accompanied by information describing the sampling design used for accuracy assessment. The known area proportions of the map classes (w_i) must be incorporated in the stratified estimators of overall and producer's accuracies to account for different sampling intensities in different strata. Once the error matrix

area proportions are estimated (Eq. 4.3), user's ($\widehat{U}_i$) and producer's ($\widehat{P}_j$) accuracy for any category and overall map accuracy ($\widehat{O}$) can be estimated directly from this estimated error matrix (Table 4.8). The estimators are:

$\widehat{U}_i = \frac{\hat{p}_{ii}}{\hat{p}_i}$ ……..Equation (4.8)

$\widehat{P}_j = \frac{\hat{p}_{jj}}{\hat{p}_j}$ …….. Equation (4.9)

$\widehat{O} = \sum_{j=1}^{q} \hat{p}_{jj}$ ……Equation (4.10)

The estimators shown in Eqs. 4.8–4.10 are viewed as post stratified estimators if the sampling design is simple random or systematic.

4.10.3.2. Process for accuracy and area estimation

In this section, the computations for the stratified estimator of the proportion of land change area and the estimated 95% confidence interval for change area using the equations presented previously. Classification maps derived from Landsat 2009 and 2013 were analysed to map deforestation. The validated 1595 regular circles within each sample grid square using a stratified random sample were recorded in a database and used to generate a cross tabulation between reference data and the maps (Table 4.9). The accuracy of this map was assessed using equal area segmentations.

Table 4.9: Error matrix of sample counts (n_{ij}) constricted from the accuracy assessment samples. Class DF is deforestation, and classes FO and NF are forest and non- forest respectively.

Class	**DF**	**FO**	**NF**	**Total**	**Map area(ha)**	**W_i**
DF	242	6	39	287	25108	0.218
FO	38	381	23	442	24919	0.216
NF	2	0	1593	1595	65102.6	0.565
Total	282	387	1655	2324	115130.7	1

Table 4.10: Estimated error matrix on table (4.7) with cell entries expressed as the estimated proportion of area. Accuracy measures are presented with a 95% confidence interval. Class DF is deforestation, and classes FO and NF are forest and non- forest respectively. Map categories are the rows while the reference categories are the columns.

Class	**DF**	**FO**	**NF**	**Total**	**User's**	**Producer's**	**Overall**
DF	0.1172	0.0029	0.0188	0.139	0.8432	0.8268	0.9392
FO	0.0238	0.2387	0.0144	0.277	0.8619	0.9879	
NF	0.0007	0	0.5832	0.584	0.9987	0.9459	
Total	0.141	0.2416	0.6165	1			

The first step in the analysis of deforestation quality is to calculate (p_{ij}), the estimated proportion of area in cell i,j of the error matrix (Equation 4.3) and to construct the error matrix of these estimated proportion (Table 4.10). Since the category of interest is column "DF" (deforestation), the estimate proportion of deforestation based on the reference classification is:

$$\hat{p} = w_i \frac{n_{ij}}{n_i} = 0.218\frac{242}{287} + 0.216\frac{38}{442} + 0.565\frac{2}{1595} = 0.20309 \ldots\ldots\ldots\ldots\ldots \text{ Equation (4.11)}$$

A stratified estimator of the area of deforestation (A_1) can now be obtained using Equation (4.4):

$$\hat{A}_j = A_{tot} \times \hat{p}_j = 115130.26 \times 0.20309 = 23382.6ha \ldots\ldots\ldots\ldots\ldots\ldots \text{ Equation (4.12)}$$

The mapped area of deforestation in this case is 25,108 ha whereas the stratified error – adjusted area estimate of deforestation is bit smaller; 23382.6ha. The reasons for this discrepancy can be deduced from the error matrix (Table 4.7).

The error matrix indicates that almost 14% of the proportion of area of deforestation is omitted from the map (the estimated area proportions omitted from the deforestation class were 0.023 and 0.007, column "DF", table 3), so the error – adjusted estimate of the area of deforestation adds this omitted deforested area to the mapped area of deforestation. Here, the omission error associated with a few sample units of deforestation has an influence on the estimated area of deforestation. For example, each sample unit of omission error from the forest stratum (FO) contributes $A_{tot} * W_2 * P_{21} = 115130 * 0.277 * 1/442 = 72.15$

ha of deforestation and each sample unit of omission error from the non-forest stratum (NF) contributes an estimated 42.15 ha of deforestation to the error-adjusted total. The sensitivity of the area estimate to the omission of a few sample units of deforestation is captured by the relatively large standard error of the estimated area. To compute the confidence intervals for the area of deforestation, we first calculate the standard error of ^p·1 using Eq. (4.5):

$$S(\hat{p}_{.1}) = \sqrt{\sum_{i=j}^{q} w_i^2 \frac{\frac{n_{ij}}{n_i}\left(1 - \frac{n_{ij}}{n_i}\right)}{n_i - 1}} =$$

$$\left(0.139^2 \frac{\frac{242}{287}\left(1-\frac{242}{287}\right)}{286} + 0.277^2 \frac{\frac{38}{442}\left(1-\frac{38}{442}\right)}{441} + 0.584^2 \frac{\frac{2}{1595}\left(1-\frac{2}{1595}\right)}{1594} =\right.$$

$$\left. 0.004782 \right) \text{.....Equation (4.13)}$$

The standard error of the adjusted area estimate is;

$$S(\hat{A}_1) = A_{tot} \times S(\hat{p}_1) = 115130.26 \times 0.004782 = 550.5ha$$

.....Equation (4.14)

This gives a final land change area estimate with a margin of error (at approximate 95% confidence interval) of;

$$\hat{A}_1 \pm 2 \times S[\hat{A}_j] = 23382 \pm 550\ ha.$$

.....Equation (4.15)

The confidence interval quantifies the uncertainty associated with the sample-based estimate of the area of deforestation. Taking this uncertainty into account, the true area of deforestation could be as low as 22832 ha or as high as 23932ha at the 95% level of confidence. Note that even though the confidence interval for the area of deforestation is wide, it does not include the value for the map area of deforestation which is 25108ha, highlighting the need to adjust the area obtained from pixel counting by taking into account the information contained in the error matrix.

Estimates of accuracy for this change map, based on the stratified random accuracy assessment sampling design, can be obtained by applying Eqs. (4.8)– (4.10) to the estimated error matrix in Table 4:

$\widehat{U}_1 = \hat{p}_{11} \div \sum_{i=1}^{3} \hat{p}_{1j} = 0.117 \div 0.139 = 0843$

……Equation (4.16)

$\hat{P}_1 = \hat{p}_{11} \div \sum_{i=1}^{3} \hat{p}_{1j} = 0.117 \div 0.142 = 0.831$

……Equation (4.17)

$\hat{O} = \sum_{i=1}^{3} \hat{p}_{jj} = 0.117 + 0.2387 += 0.5832 = 0.939$

……Equation (4.18)

The effect of incorrectly ignoring the stratified design when estimating accuracy is illustrated by computing the estimates directly from the error matrix of sample counts (Table 3). Overall accuracy based on the error matrix in Table 3 is (242 + 381 + 1593) ÷ 2324 = 0.95, which in this analysis does not deviate far from the estimate of 0.93, obtained using the stratified estimator. Similarly, the stratified estimator of producer's accuracy (Eq. 4.9) of deforestation yields an estimate of 0.82 which is close from the sample count estimate of 242 ÷ 287 = 0.84.

4.11. Summary

This chapter has outlined the methodology for estimating land use land cover change in the Man River Basin. The range of techniques utilised are outlined along with a critique of research that has previously used similar methods. Chapter 5 now presents the results from this element of the research.

Chapter -5

Vegetation change detection modelling: Results

5.1 Introduction

In this chapter the results are organised in four sections. First, the accuracy of 2009 and 2013 forest-non forest classification was assessed using Google Earth ™ imagery, field work data and Landsat imagery. Secondly, the information obtained from an accuracy assessment of the Landsat-based mapping was used to estimate deforestation area and construct confidence intervals that reflect the uncertainty of the area estimates obtained. Thirdly, a landscape change matrix analysis is presented based on the interpretation of a time series of Landsat imagery. Finally, the results from the GIS–based forest change mapping (polygon mapped) for the time epoch 2009-2013 are summarised. This includes area estimations of deforestation and forest degradation associate with responsible drivers.

5.2 Classification and change detection accuracy

The accuracy and forest area estimation calculations are presented using error matrix analysis and area estimation proportion.

5.2.1. Quality of classification

The error matrices are summarized in Table 5.1 for 2009 and 2013. The overall correspondence between the map and reference data are a good measure for 2009 and 2013; 94.03 % and 92.8 % respectively. User's and producer's accuracies of individual classes range from 75 % to 99 %. This is a very high figure, as good as one would expect from an automated classification of multispectral remotely sensed data and is almost certainly explained by careful selection and on–screen digitizing of training data. In the accuracy assessment all the reference data used for the validation were of high quality and there were no missing samples due to cloud or cloud shadow.

In 2013 83 samples (14.1%) and in 2009 71 (7.7%) sample areas that were mapped as forest were found to be agriculture and fallow land. These estimates are not suitable for change analysis and indicate that

further analysis is necessary because areas of deforestation are being missed; it is important to understand why this is happing. Further analysis demonstrated that 12 samples in 2013 and 6 samples in 2009 were mapped as non–forest and were found to be forest covered. The reason behind the majority of these incorrect classifications is likely to be the presence of trees and woodland surrounding agricultural fields in some parts of the study area.

Table 5.1: Error matrices (in terms of sample counts) for the 2009 and 2013 LULC. Map categories are rows while the reference categories are columns.

2013	**Forest**	**Agriculture**	**Fellow land**	**Other**	**Total**	**W_i**	**User's**	**Producer's**	**Over-all**
Forest	505	11	1	0	517	0.28	97.7	85.9	92.81
Agriculture	79	1544	46	1	1670	0.58	92.5	97.5	
Fallow land	2	28	164	0	194	0.1	84.5	74.9	
Other	2	0	8	85	95	0.03	89.5	98.8	
Total	**588**	**1583**	**219**	**86**	**2476**	**1**			
2009									
Forest	667	6	0	0	673	0.32	99.1	90.4	94.02
Agriculture	63	1377	52	0	1492	0.49	92.3	98.4	
Fallow land	8	17	210	1	237	0.16	88.6	79.8	
Other	0	0	1	74	75	0.03	98.7	98.7	
Total	**738**	**1400**	**263**	**75**	**2476**	**1**			

The high number of fallow land (46 (21%) in 2013 and 52 (11.8%) in 2009) were classified wrongly as agricultural land use and similarly 1.7 % of those classified as agriculture were found to be fallow land.

5.2.2. Quality of deforestation assessment and error adjusted area estimation of deforestation.

The results of the area estimation of deforestation are summarised step-by-step in this section, starting with the deforestation of 25,108 ha mapped from Landsat imagery. The accuracy assessment based on a stratified estimator revealed that the change map had an overall accuracy of 95% and a user's accuracy of deforestation of 84%. However, the producer's accuracy of 85.8 % for deforestation served as a warning that omission error associated with the deforestation class was problematic.

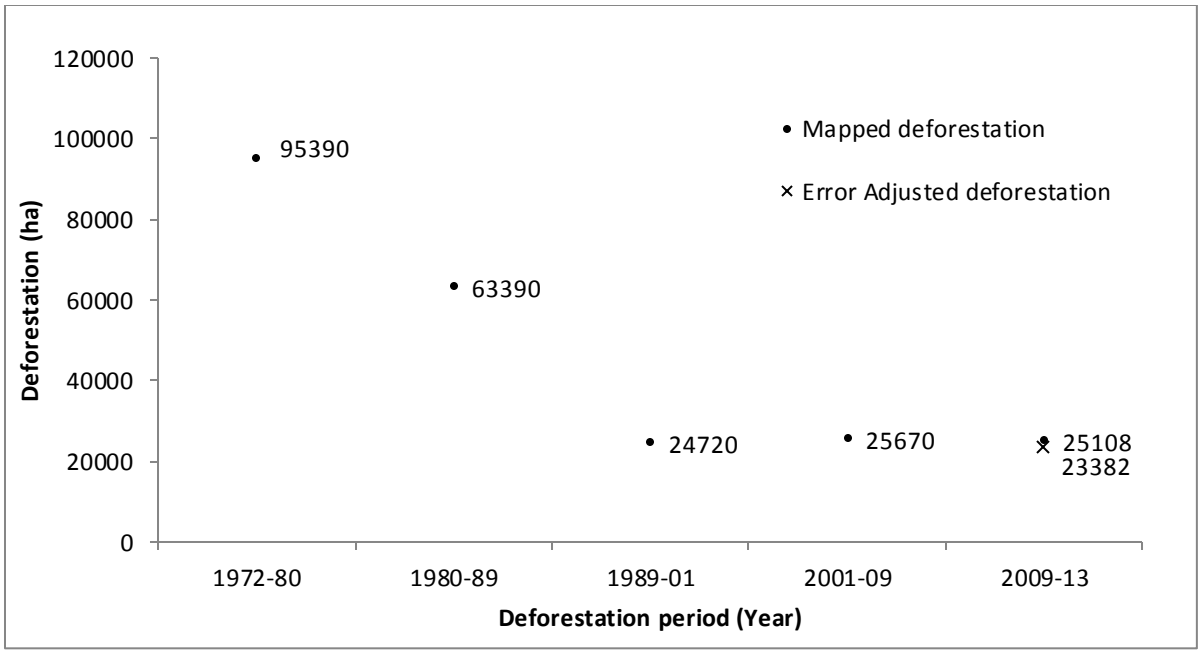

Figure 5.1: Mapped deforestation areas and error- adjusted estimated areas.

Moreover, a naive assessment of the producer's accuracy, based upon sample counts, would suggest that the classification was highly accurate (appearing as 95% but actually 85%) and would not indicate a potential concern. Using a simple set of equations and the information in the error matrix, an error-adjusted estimate of the area of deforestation was obtained (± 95% confidence interval) of 23382 ± 550 ha (Figure 5.1 and Table 5.2). The area of deforestation obtained with the stratified estimator confirms the need to adjust the mapped area of deforestation obtained from pixel counting to account for the error of omission.

Table 5.2: the resulting error matrix for the first change map (2009-2013) together with the mapped and adjusted areas and the 95% confidence intervals.

Study area	Mapped deforestation	Adjusted	Margin of error (95%CI)	± 95 % CI
Man River basin	25108	23382.6	± 550	2.3 (%)

In this analysis the mapped area of deforestation is slightly underestimated, it is outside the 95% confidence interval obtained using the error-adjusted area estimator. Using the mapped area of 25108 ha could have a substantial effect on applications that use this area as an input compared to the results based on using the estimated adjusted area of 23382 ± 550 ha. Due to the relatively larger area of deforestation

(>21%), omission error only has a small impact on the final area estimates. As a result, the confidence interval for the deforestation estimates is small (>2%).

5.3. Historical change in the Man River basin

This section describes the change detection analysis based on a transition matrix of the Landsat based classified maps and extract systematic transitions. Traditional analysis of the change matrix is not sufficient to provide systematic signals of LULC change. Therefore, the detail of the change matrix to compute the quantity, allocation, and dominant signals of land use and land cover (LULC) transitions were analysed over the 41 year time period of the study for the Man River basin.

The transition matrix from 1972 to 2013 LULC maps is shown in Table 5.4. The vertical column indicates the year of the initial land cover image. The duration of the period of change extends to the image from the final year, as shown in the horizontal row. The diagonal of the table indicates unchanged land area units between initial and final year (in bold font). The traditional transition matrix would have had only the bold digits without the last column and the last row, while this extended transitional matrix includes the last column indicating gross loss by category and the last row indicating gross gain by category in the landscape during the 41-year accounted period.

Table 5.3: Summary of Landsat classification area statistics and relative change from 1972 to 2013

	1972		**1980**		**1989**		**2001**		**2009**		**2013**		**1972-2013 Relative change**	
Classes	Area (00ha)	%	Area (00ha)	%	Area (00ha)	%	Area (00ha)	%	Area (00ha)	%	Area (00ha)	%	%	Area (00ha)
Agriculture	363.0	23.3	293.6	18.9	603.0	38.7	621.2	39.9	759.1	48.7	910.3	58.5	35.1	546.6
Forest	982.9	63.1	945.7	60.7	580.8	37.3	540.6	34.7	500.5	32.1	441.7	28.4	-34.8	-542
Fallowland	222.4	14.3	309.8	19.9	346.2	22.2	372.7	23.9	247.3	15.8	154.3	9.9	-4.4	68.5
Water	2.8	0.2	4.8	0.3	4.4	0.3	11.4	0.7	32.5	2	38.8	2.5	2.3	35.8
Other	5.9	0.4	2.8	0.2	18.5	1.2	18.8	1.2	17.3	1.11	11.8	0.8	0.4	6.2
Total	1557.4	100	1557.4	100	1557.4	100	1557.4	100	1557.4	100	1557.4	100	0.0	

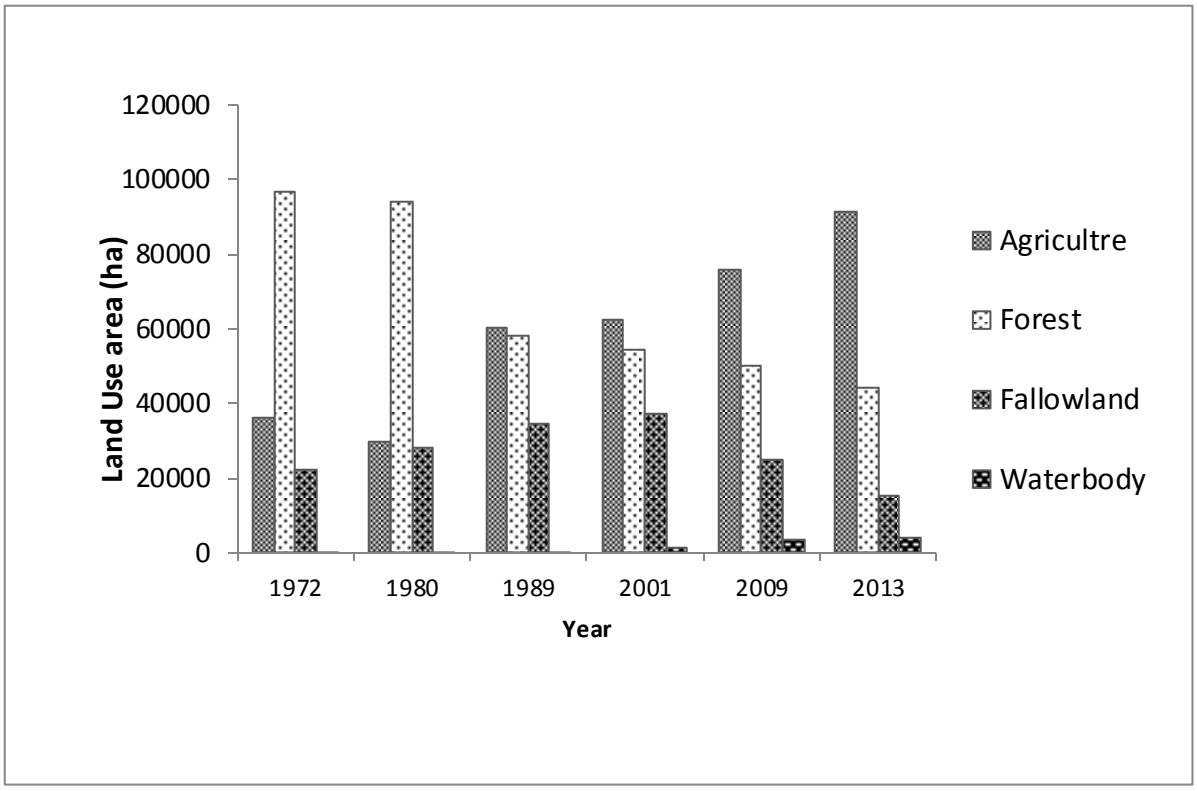

Figure 5.2: Land use and land cover change in the study area over four decades.

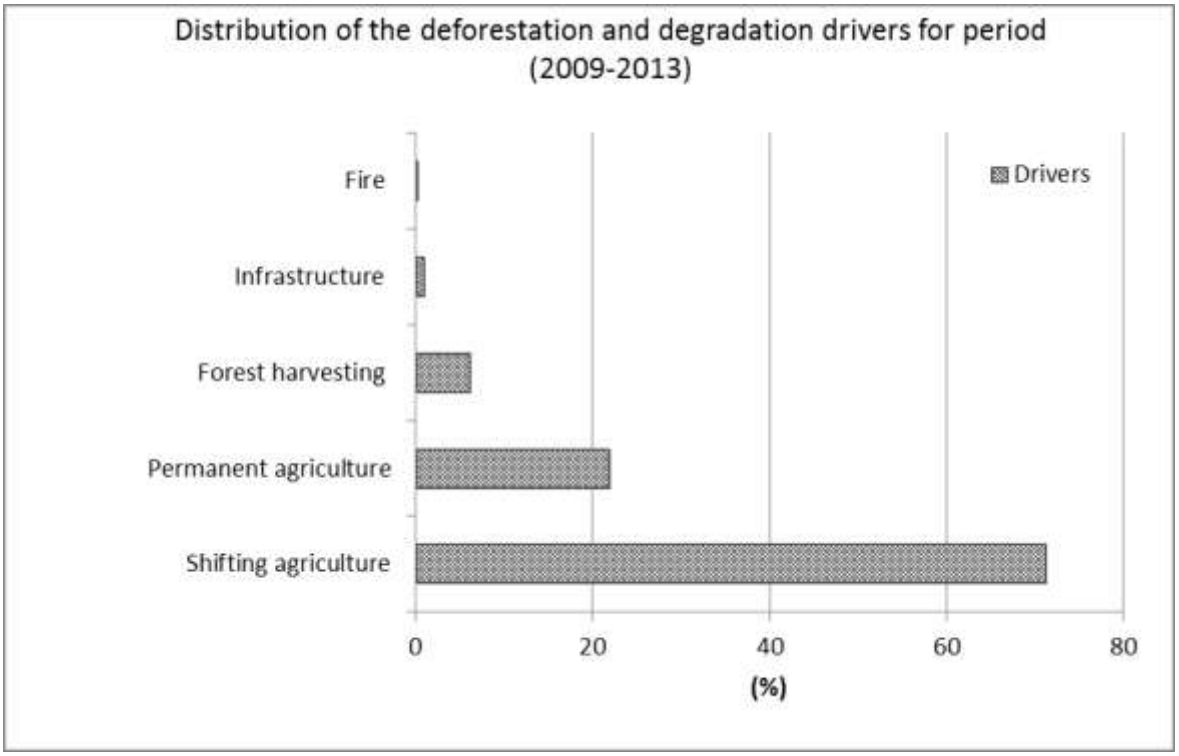

Figure 5.3: Distribution of the deforestation and degradation drivers for period (2009-2013).

5.3.1 Grass gain, grass loss and persistence

The cross tabulation matrix (Table 5.4) depicts the proportion of each land use/land cover class that made a transition from one category to another for each of the study periods. During the 41 year period, forest and agriculture land were the major proportions compared to other land use categories. The largest LULC category in 1972 was forest (60%) followed by agriculture (23%) and fallow land (14%) (Figure 5.2). A dramatic change has taken place and by 2013 the forest and agriculture categories have almost been exchanged. Now, agriculture land use is the largest category (58%) followed by forest land (28%), fallow land (10%) and water bodies (2.5%). Forest areas experienced the highest loss (40%) recorded which is mostly captured by extension of agriculture land (31%) and fallow land (7%) from 1972 to 2013. Agriculture land has the highest gain (41%) which is extended on forest areas (31%) and fallow land (9.7%) (Fig. 5.3 and 5.4).

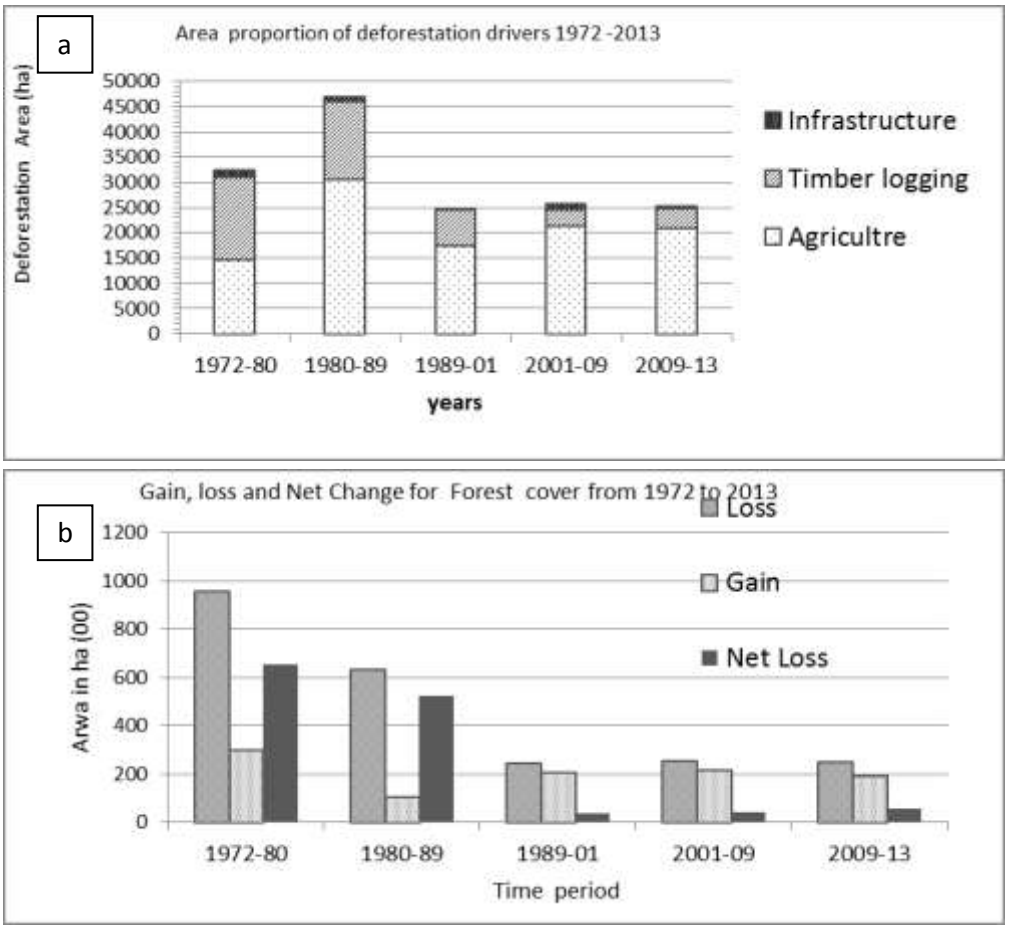

Figure 5.4: a) Area proportion of deforestation drivers 1972 – 2013. b) Gain, loss and net change for forest cover (2009-2013).

Table 5.4: Matrices of land cover and changes (00 ha) from 1972 to 2013

		2013					
	Class	**AG**	**DF**	**FL**	**WB**	**OT**	**TOTAL**
	AG	**270.7**	70.0	10.2	8.0	2.1	361.0
	DF	486.7	**345.0**	110.0	20.1	5.7	967.5
1972	**FL**	151.0	26.2	**33.0**	7.7	3.2	221.1
	WB	1.0	0.3	0.0	**0.5**	0.0	1.8
	OT	1.0	0.9	0.5	2.7	**0.8**	6.0
	TOTAL	911.1	442.3	154.2	38.9	12.5	1557.4
				2013			
	CLASS	**AG**	**DF**	**FL**	**WB**	**OT**	**TOTAL**
	AG	**547.6**	164.9	38.4	5.7	2.5	759.1
	DF	210.0	**249.7**	38.4	1.8	0.8	500.8
2009	**FL**	143.4	22.0	**73.6**	4.3	4.2	247.4
	WB	4.5	2.5	0.6	**24.8**	0.1	32.6
	OT	5.3	2.6	3.1	2.4	**4.1**	17.5
	TOTAL	910.8	441.7	154.2	39.0	11.7	1557.4
				2009			
	CLASS	**AG**	**DF**	**FL**	**WB**	**OT**	**TOTAL**
	AG	**408.3**	132.8	67.1	8.8	4.3	621.3
	DF	213.5	**284.6**	32.9	7.7	2.6	541.2
2001	**FL**	134.3	82.8	**143.7**	6.3	5.6	372.8
	WB	0.8	0.1	0.9	**8.4**	1.3	11.5
	OT	2.1	0.4	2.9	1.3	**3.8**	10.5
	TOTAL	759.1	500.8	247.4	32.6	17.5	1557.4
				2001			
	CLASS	**AG**	**DF**	**FL**	**WB**	**OT**	**TOTAL**
	AG	**326.0**	146.0	126.8	2.1	2.2	603.0
	DF	176.2	**333.7**	69.5	0.6	0.9	580.9
1989	**FL**	114.5	59.0	**169.8**	0.6	2.5	346.3
	WB	1.4	0.6	1.5	**4.6**	0.2	8.3
	OT	3.3	1.9	5.2	3.7	**4.7**	18.8
	1980-	621.3	541.2	372.8	11.5	10.5	1557.4
				1989			
	Class	**AG**	**DF**	**FL**	**WB**	**OT**	**total**
	AG	**143.3**	73.2	74.8	1.6	1.6	294.3
	DF	306.8	**471.9**	154.2	3.1	6.2	942.2
1980	**FL**	137.1	34.3	**109.0**	1.6	4.7	286.6
	WB	14.0	0.0	0.0	**3.1**	0.0	17.1
	OT	14.0	3.1	7.8	0.0	**6.2**	31.1
	Total	615.2	582.5	345.7	9.3	18.7	1557.4
				1980			
	Class	**AG**	**DF**	**FL**	**WB**	**OT**	**TOTAL**
	AG	**99.**7	208.7	43.6	1.6	6.2	361.3
	DF	148.0	**644.8**	163.5	1.6	10.9	967.1
1972	**FL**	46.7	87.2	**74.8**	1.6	10.9	221.2
	WB	0.0	1.6	0.0	**0.0**	0.0	3.1
	OT	0.0	1.6	1.6	0.0	**1.6**	4.7
	Total	294.3	943.8	283.4	4.7	31.1	1557.4

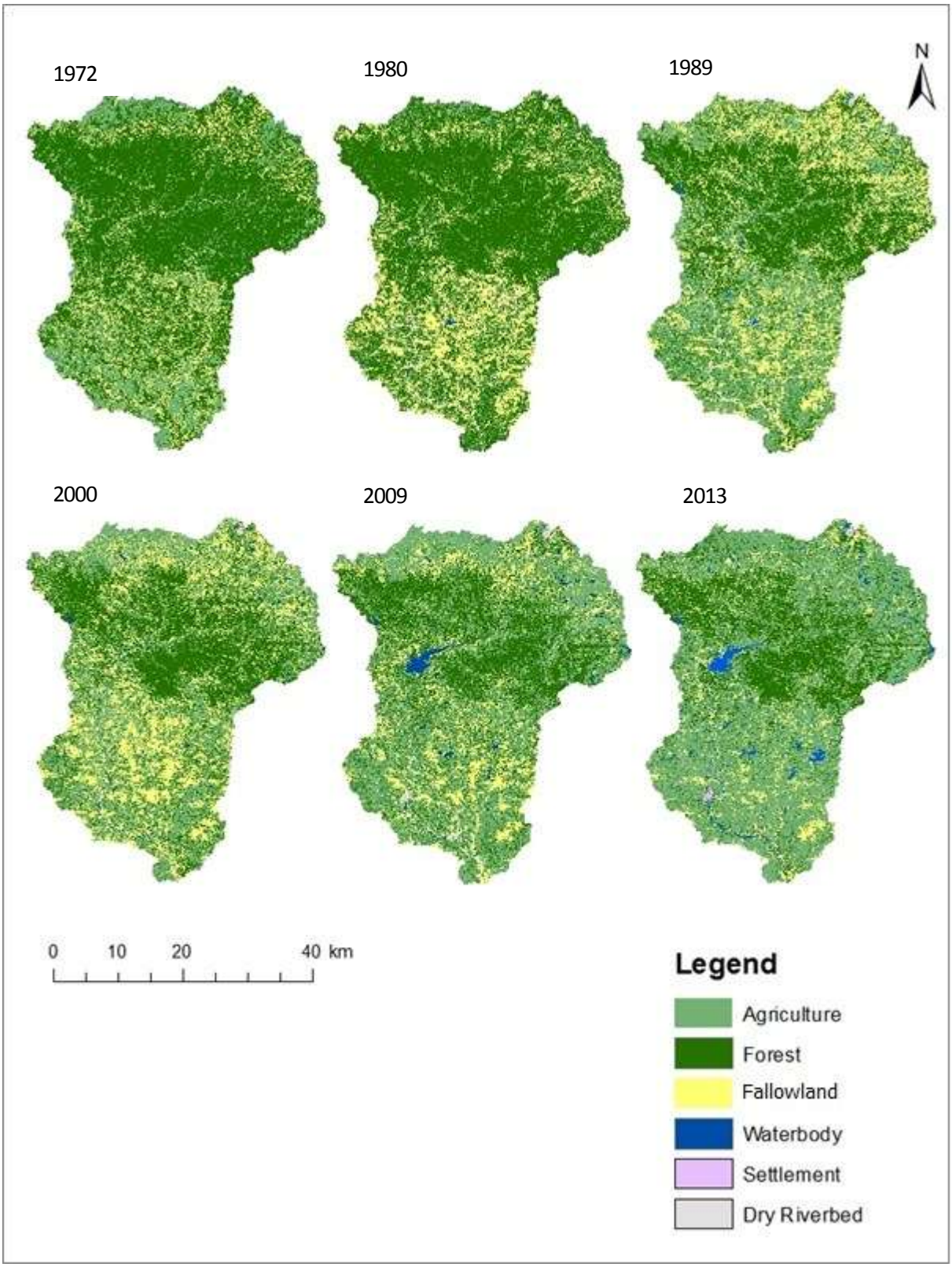

Figure 5.5: Maps show vegetation change in the Man River basin from 1972 to 2013.

The overall gain in the last four decades is highest for agriculture land followed by fallow land (7.7%), forest (6.2%) and water bodies (2.5%) (Figure 5.4). Agriculture areas increased by approximately 39900 ha, while water bodies and fallow land increased by 2978 ha and 2702 ha respectively. The area under agriculture land witnessed a constant increase over the four decades (excluding 1972-1980) and the greatest increase occurred between 1980 and 2013. Loss is highest from forest land (40%), followed by fallow land (12%). The analysis indicates that the total area converted from forest to non–forest between 1972 and 2013 was 46,357 ha. Hence, agriculture has the highest area of gain and loss, however gain is much higher in comparison to loss in this category while for forest land has the second highest area of gain-loss with greater loss than gain. There are substantial exchanges of area between agriculture and forest land and also between fallow land and agriculture land (Table 5.4).

As persistence dominates most landscapes, it is important that statistical methods account for persistence when examining LUCC (Pontius et al., 2004). The percentage of landscape that remained unchanged is 52%, 47%, 53%, 54% and 57%, respectively during the period 1972-1980, 1980-1989, 1989-2001, 2001-2009 and 2009-2013. Forest, agriculture, and fallow land accounted for 22%, 17% and 2.1% of the persistence of the landscape in the respective period. The difference between the total change and net change is the amount of swap change. Swap land change dynamics accounted for 41%, 29%, 43%, 35% and 32% of total landscape change for periods 1972-1980, 1980-1989, 1989-2001, and 2009-2013, respectively.

While the sum of gross gain and gross loss indicates the total change, the difference between the gross gain and gross loss for a category is the net change for the given category. Agriculture and forest land are the most dynamic category in terms of total change as shown in (Table 5.5). Agriculture land exhibits highest net change (35%) compared to other categories and it is followed by forest land (-33.7%) and fallow land (4.4%) during 1972-2013 (Figure 5.4).

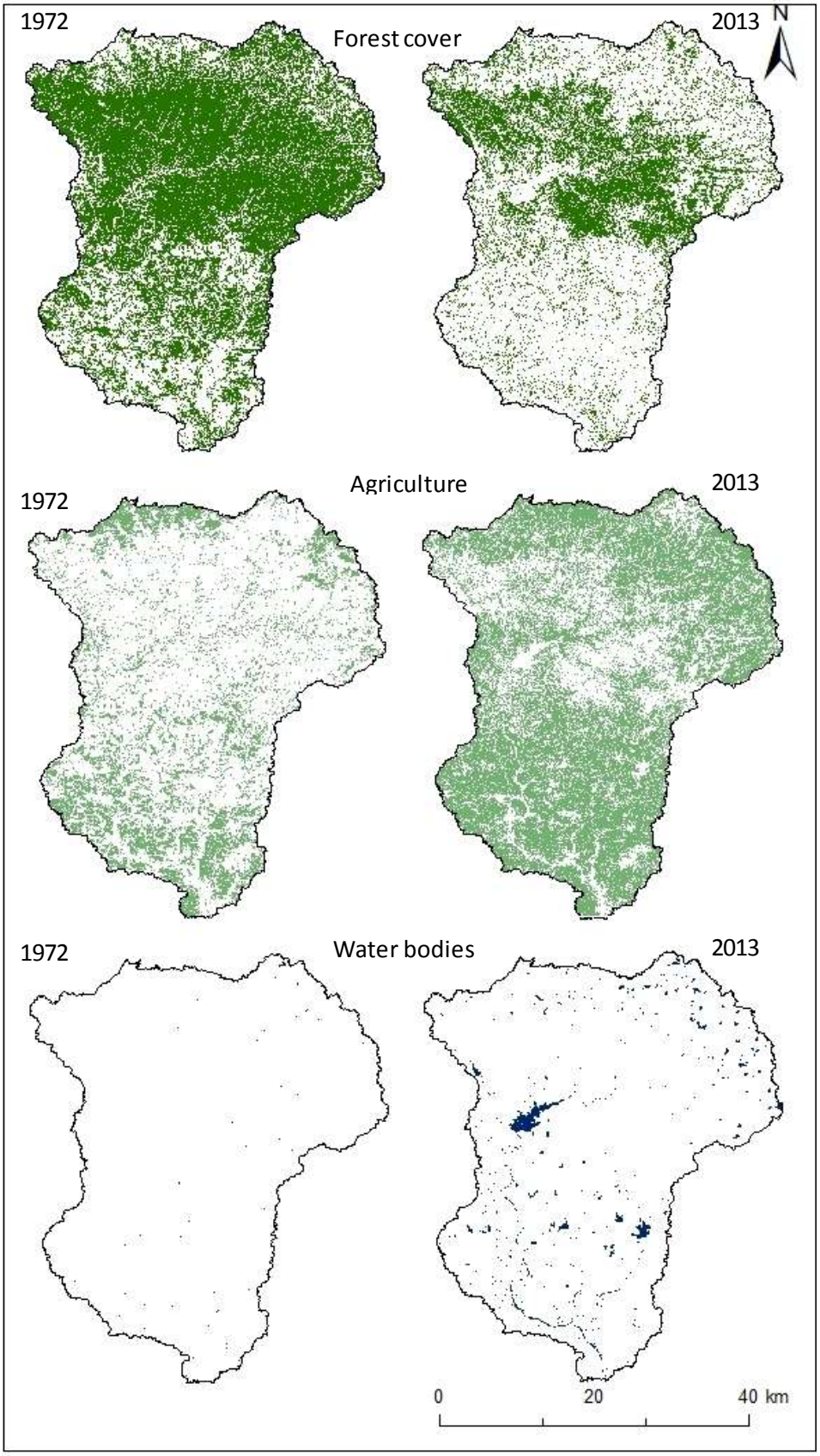

Figure 5.6: Land use land cover in 1972 and 2009 based on Landsat imagery analysis.

Table 5.5: Budget of landscape persistence and components of change in terms of percent of study area from 1972 to 2013.

(In %)		1972-2013				
Land Cover	**Persistence**	**Loss**	**Gain**	**Total Change**	**Swap**	**Absolute value of net Change**
Agriculture	17.4	5.8	41.1	46.9	11.6	35.3
Forest	22.2	40.0	6.2	46.2	79.9	-33.7
Fallow land	2.1	12.1	7.7	19.8	24.2	-4.4
Water bodies	0.0	0.2	2.5	2.7	0.4	2.3
other	0.4	0.3	0.8	1.1	0.6	0.5
Total	**42.1**	**58.3**	**58.3**	**58.3**	**20.2**	**38.1**
		2009-13				
Land Cover	**Persistence**	**Loss**	**Gain**	**Total Change**	**Swap**	**Absolute change of net Change**
Agriculture	35.2	13.6	23.3	36.9	27.2	9.7
Forest	16.0	16.1	12.3	28.5	32.2	-3.8
Fallow land	4.7	11.2	5.2	16.3	22.3	-6.0
Water bodies	1.6	0.5	0.9	1.4	1.0	0.4
other	0.3	0.9	0.5	1.4	1.7	-0.4
Total	**57.8**	**42.2**	**42.2**	**42.2**	**32.1**	**10.1**
		20012009				
Land Cover	**Persistence**	**Loss**	**Gain**	**Total Change**	**Swap**	**Absolute value of net Change**
Agriculture	26.2	13.7	22.5	36.2	27.4	8.8
Forest	18.3	16.5	13.9	30.3	33.0	-2.6
Fallow land	9.2	14.7	6.7	21.4	29.4	-8.0
Water bodies	0.1	0.2	1.7	1.9	0.4	1.5
other	0.2	0.5	0.9	1.4	1.0	0.4
Total	**54.0**	**45.6**	**45.6**	**45.6**	**34.9**	**10.7**
		1989-2001				
Land Cover	**Persistence**	**Loss**	**Gain**	**Total Change**	**Swap**	**Absolute value of net Change**
Agriculture	20.9	17.8	19.0	36.8	35.6	1.2
Forest	21.4	15.9	13.3	29.2	31.7	-2.6
Fallow land	10.9	11.3	13.0	24.3	22.6	1.7
Water bodies	0.3	0.2	0.4	0.6	0.4	0.2
other	0.3	0.9	0.4	1.3	1.8	-0.5
Total	**53.9**	**46.1**	**46.1**	**46.1**	**43**	**3.1**
		1980-1989				
Land Cover	**Persistence**	**Loss**	**Gain**	**Total Change**	**Swap**	**Absolute value of net Change**
Agriculture	9.2	9.7	30.3	40.0	19.5	20.6
Forest	30.3	30.3	7.0	37.3	60.5	-23.2
Fallow land	7.0	11.2	15.3	26.5	22.5	4.0
Water bodies	0.2	0.9	0.4	1.3	1.8	-0.5
other	0.4	1.6	0.8	2.4	3.2	-0.8
Total	**47.0**	**53.7**	**53.7**	**53.7**	**29.1**	**24.6**
		1972-80				
Land Cover	**Persistence**	**Loss**	**Gain**	**Total Change**	**Swap**	**Absolute value of net Change**
Agriculture	6.4	16.7	12.5	29.2	33.5	-4.3
Forest	41.4	20.7	19.2	39.9	41.4	-1.5
Fallow land	4.8	9.3	13.3	22.7	18.7	4.0
Water bodies	0.0	0.2	0.3	0.4	0.3	0.1
other	0.0	0.2	1.8	2.0	0.5	1.6
Total	**52.7**	**47.2**	**47.2**	**47.2**	**41.5**	**5.7**

5.3.2 Deforestation and forest degradation associated with responsible drivers with GIS mapping (Integrated approach).

The results summarised in this section are for the time epoch 2009-2013 based on GIS mapping for deforestation and degradation associate with responsible drivers in the study area. The drivers are summarised in Table 5.6.

Table 5.6: Drivers of deforestation and forest degradation in the Man River basin from 2009 to 2013.

Drivers	Deforestation (ha)	Degradation (ha)	(%)
Shifting agriculture	5418	5418	71.12
Permanent agriculture	1660	--	21.8
Forest harvesting	462	---	6.06
Infrastructure development	72	--	0.94
Fire	6	---	0.08
Total	**7617**	**5418**	**100**

5.3.2.1 Comparative analysis of deforestation outcomes from different mapping approaches for the Man River basin.

The areas of deforestation mapped by this assessment are smaller than the areas mapped by automatic change detection due to more precise delineation of the change boundary by GIS mapping and because the minimum mapping unit for deforestation as 1 ha (Figure 5.7, 5.11 and 5.12). This means that the forest loss areas smaller than one hectare are not recorded in the integrated approach. The total area of deforestation is estimated at 7,617 ha over the 4 year time period. This figure is 17,491 ha less than the area estimated by the change matrix approach (automatic pixel based approach) and 15,765 ha less than the area estimated by verification analysis. The pattern of deforestation sites was small, irregular and scattered on the fringes of the forest areas. The spatial pattern of deforestation was closely related to the extension of agriculture on hill slopes (Figure 5.7). The conversation of the forest area started from the most accessible areas (i.e. low gradient hill slopes or at top of the hills) either by expansion of traditional shifting agriculture or illegal forest harvesting. Deforestation is mostly found in the upland region of the river basin which in theory has legal protection because forest land is held in government ownership. For this reason, the causes of forest encroachment are often linked with illegal cutting and the extension of agriculture land.

Table 5.7. Estimated deforestation areas using three different approaches.

Approach	Deforestation area (ha)	Minimum Mapping Unit	Sources
Landsat based automatic supervised classification	25108	30X30 m pixel	Landsat image, Vegetation index, field work data, aerial imagery
Error estimated area using accuracy data	23382.6+ 550		Used accuracy data based on field work and aerial imagery
GIS based wall to wall mapping	7615.19	1 ha	Polygon delineation of Landsat classification map using vegetation index and aerial imagery.

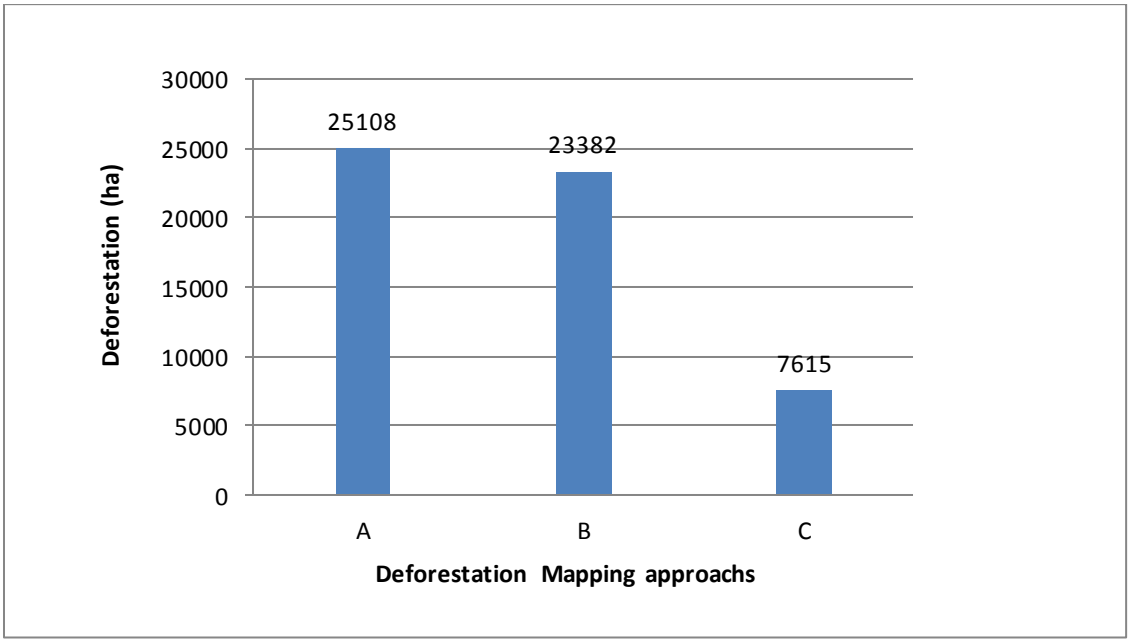

Figure 5.7 effects of land use land cover and change mapping approaches on deforestation results for time period 2009 -13. (A): Automatic pixel based approach (30X30m MMU); (B) error adjusted deforestation and (C) Integrated wall to wall mapping approach (1ha MMU).

5.3.2.2 Drivers of deforestation and forest degradation.

The forest change was assessed by drivers of change. Agriculture is identified as a leading contributor to deforestation (7082.6 ha / 92.9 %) in the basin over the last four years followed by forest harvesting (462.7 ha) and infrastructure development (71.5 ha). The distribution pattern shows that areas of deforestation associated with shifting and permanent agriculture are located mostly in the mountain region in small clusters (1-5 ha).

The area of degradation mapped is large (5,418 ha). The main cause of degradation is shifting agriculture which accounts for 71.1% of all degradation mapped. It is extremely difficult to map shifting agriculture related degradation from medium resolution optical satellite imagery like Landsat TM and ETM+. The integration approach which is based on automatic pixel analysis using Landsat imagery, aerial imagery and vegetation index such as NDVI and EVI allows proper assessment of degradation area, degradation boundary and a detailed knowledge of the processes behind degradation (Figure 5.11).

5.3.3. Comparative analysis of LULC from different mapping approaches for three watersheds.

The results of LULC maps using two different approaches and MMU for three watersheds (Loni , Salkanpur and Mograba watersheds) are presented in this section. Changing the MMU and mapping approaches have a big influence on the land use areas (see figures 5.8, 5.9 and 5.10). Agricultural area increased significantly in all three watersheds similarly when MMU was increased from 30mX30m to 1 ha. While forest land was mapped much higher with 30mX30m compare to 1 ha MMU. The detailed analysis of effect of MMU and mapping approach on soil erosion is presented in section 7.3.5.

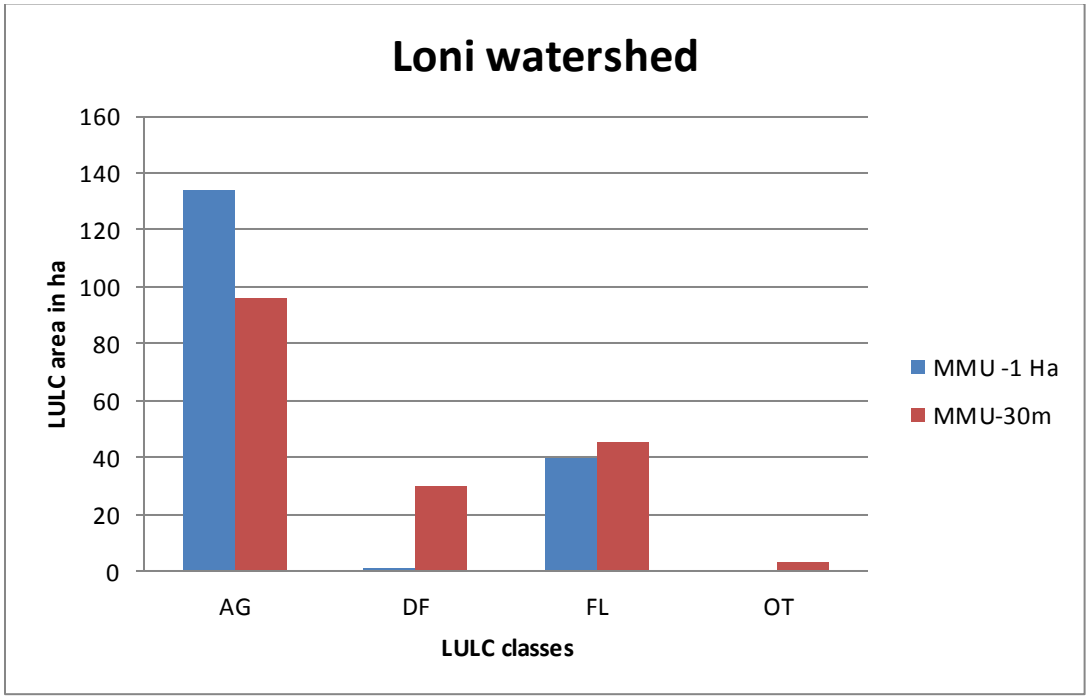

Figure 5.8 Effect of different mapping approaches on LULC in the Loni Watershed.

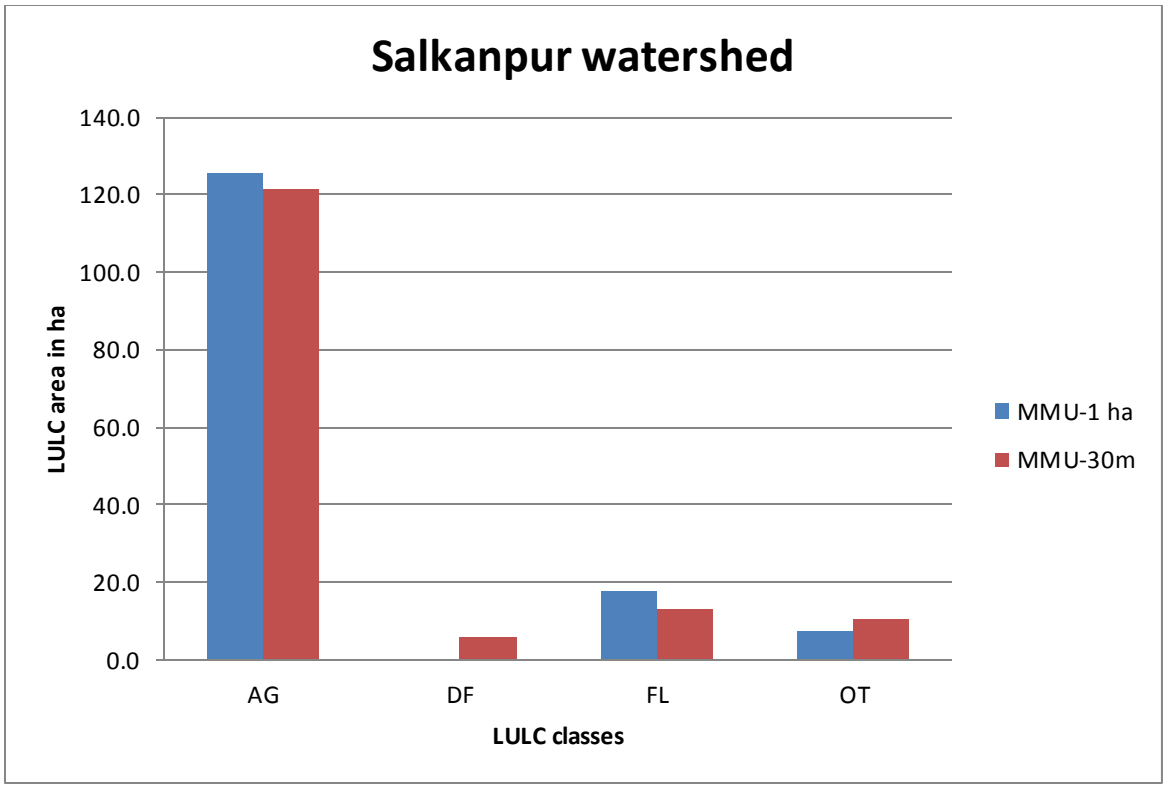

Figure 5.9. Effect of different mapping approaches on LULC in the Salkanpur watershed.

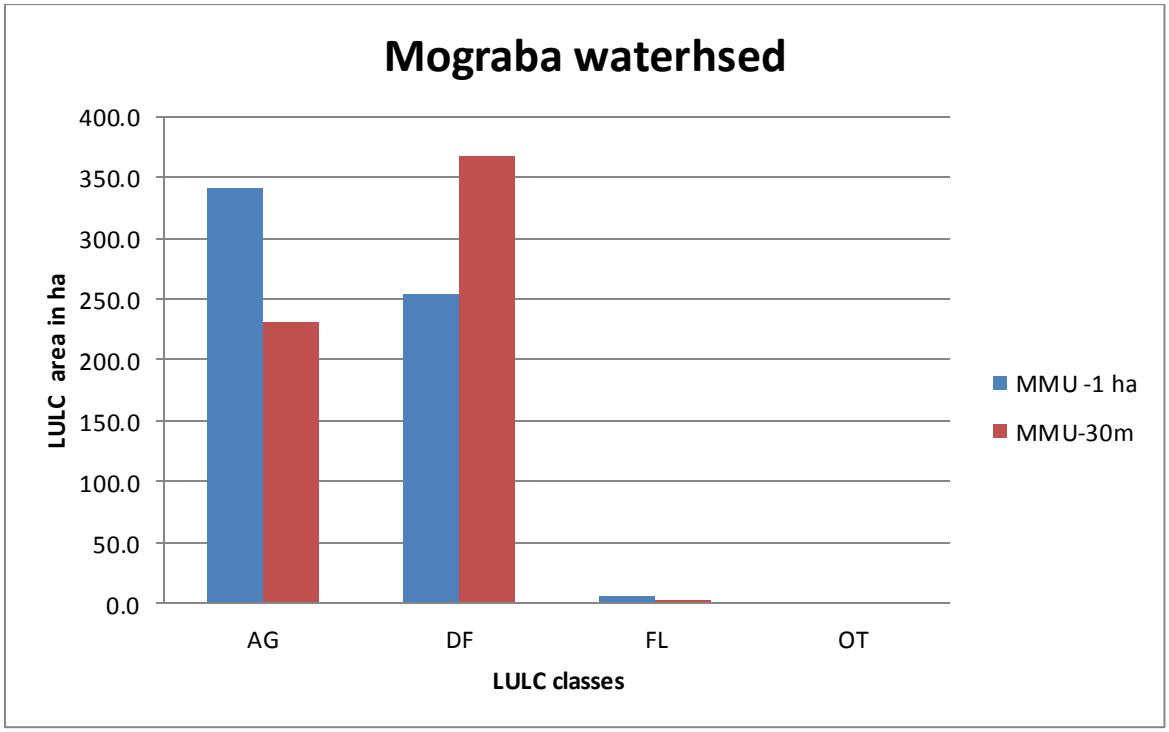

Figure 5.10. Effect of different mapping approaches on LULC in the Mograba Watershed.

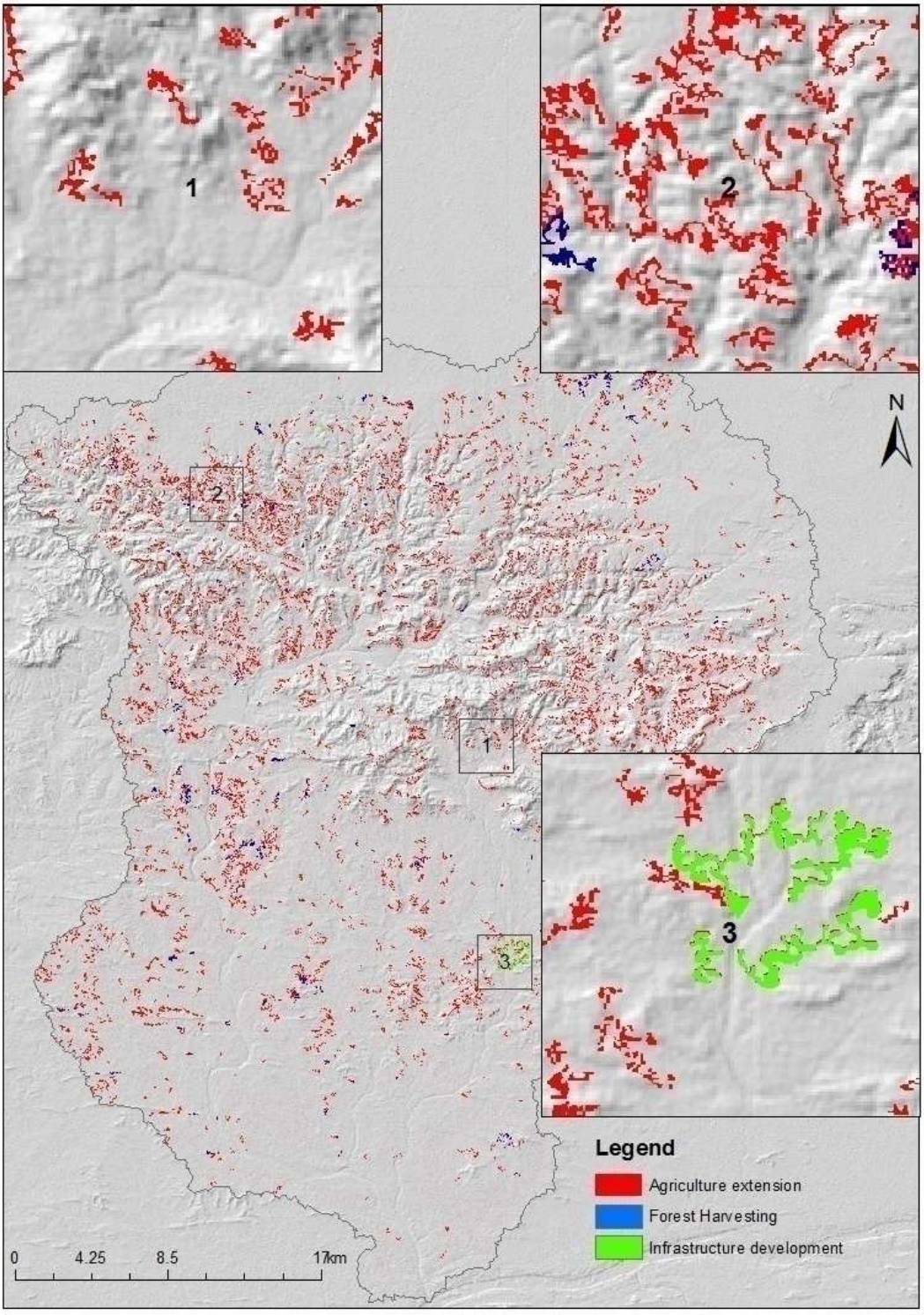

Figure 5.11: Mapped deforestation and forest degradation associated with responsible drivers using the GIS based direct interpretation approach (2009-2013).

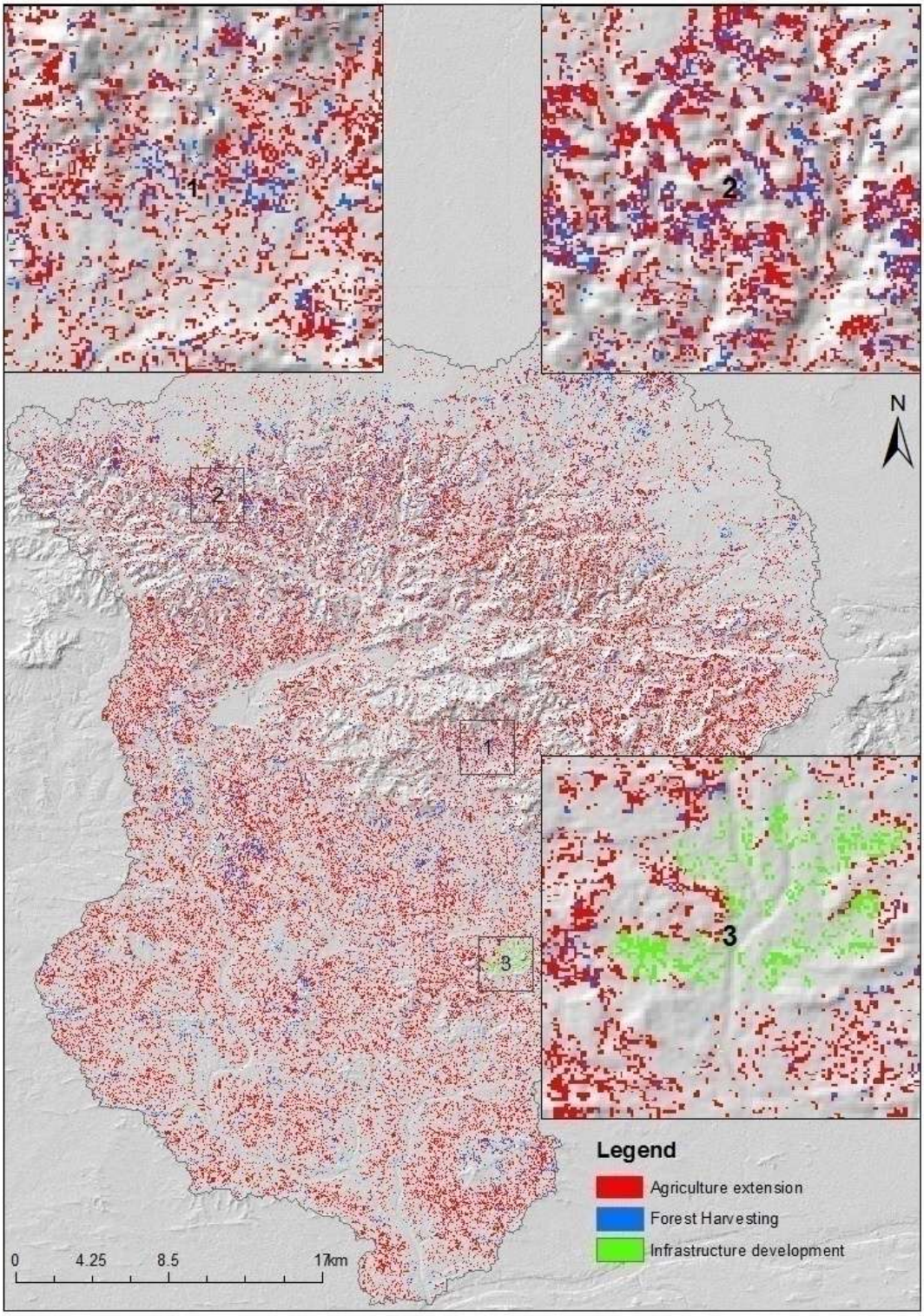

Figure 5.12: Mapped deforestation area using automatic change detection analysis (2009-2013).

Figure 5.13: Characteristics of land degradation in the study region.

5.4.**Summary and conclusion**

The results demonstrate that Landsat classifications can be used to produce accurate landscape change maps and statics. Historical and current pattern and trends of land use change in the Man River basin were evaluated by: (1) quantitatively assessing the quality of the land use change mapping for 2009 -2013 based largely on interpretation of Landsat imagery., Google Earth™ and field based GPS survey datasets. It was found that the prevalence statistic is a good measure of overall correspondence between the map and reference data; (2) further, accuracy data were presented which were used to estimate the quality of deforestation assessment and error adjusted area estimation of deforestation. The mapped area of deforestation in this case was 25,108 ha whereas the stratified error-adjusted area estimate of deforestation was about 23,382 + 550 ha; (3) analysing the change detection based on a transition matrix approach over the 41 year time period was undertaken to extract systematic transactions of land use. The major finding of transaction matrix analysis was that agriculture and forest land were the most dynamic category in terms of total change. It was also found that agriculture expansion was a significant driver for forest loss in the study region; (4) In addition, the results from the GIS – based deforestation and forest degradation associated with responsible drivers for 2009- 2013 were presented which estimated forest cover area in a more accurate way than using automatic change analysis and demonstrated that agricultural expansion and forest harvesting were major causes for deforestation and forest degradation in the Man River basin. The results quantify the land cover change patterns and responsible drivers for change in the study area and demonstrate the potential of multi-temporal Landsat time series data to provide an accurate, budget friendly means to map changes in landscape dynamics over time. The detailed discussion of implications from these results is presented in Chapter 8.

Chapter - 6

Assessment of soil erosion risk at the hillslope scale using the GeoWEPP model: Methodology

---

6.1 Introduction

The purpose of this chapter is to present a detailed description of the study sites, data collection, manipulation and preparation of data to undertake soil erosion risk assessment modelling. The research was carried out with the specific objective to calibrate and evaluate the geo-spatial interface of the WEPP (Water Erosion Prediction Project) model (GeoWEPP) for estimation of soil erosion risk in the sub-tropics by selecting watersheds located in the Man River basin, Central India. WEPP was developed as a physically based model so that it could be applied to a wide range of topographies, vegetation change scenarios, climates and soil conditions. This study implemented WEPP to simulate soil loss in several scenarios derived from both ground and satellite based precipitation, DEMs and vegetation change.

6.2 Outline of WEPP

The WEPP model predicts runoff and erosion on a simple hillslope or in a watershed (including hillslopes combined with channels and impoundment elements) for agriculture, forestry and a range of management scenarios (Flanagan et al., 1995). The GeoWEPP model (GeoWEPP ArcGIS 9.2-9.3; Renschler, 2003) combines the WEPP (v2012.8) model (Flanagan et al., 1995) with Topography Parameterization software (TOPAZ) (Garbrecht and Martz, 1997) within the ArcGIS 9.1 and 10.1 GIS program (ESRI, 2000) to predict runoff and erosion at the hillslope and watershed scale.

WEPP was designed to predict erosion on agricultural, forest and rangeland based on a simple hillslope profile (Flanagan et al. 1995). WEPP was developed to replace the empirically-based Universal Soil Loss Equation with a user-friendly simulation model that could be readily modified to nearly any type of watershed at any location (Laflen et al. 1997). WEPP was further developed to model whole watersheds by combining hillslopes with channels and impoundment elements (Flanagan et al. 1995). WEPP can currently simulate erosion from both hillslopes and watersheds.

In 2000, the USDA Forest Service developed FS WEPP, a suite of internet-based interfaces to the WEPP model specific to forests and forest management such as roads and timber harvest (Elliot et al. 1999a). In

2003, ERMiT (Erosion Risk Management Tool), an internet-based probabilistic erosion prediction model was developed based on WEPP technology to help determine the risk of erosion in forests, rangeland and chaparral after fire (Robichaud and Elliot 2003). Further development of the WEPP model continues in order to allow the WEPP hillslope parameterization to be based on digital data sources and for digital outputs to be viewed and analysed in a GIS environment; such changes are included in the GeoWEPP model (Renschler, 2003).

Figure 6.1 demonstrates how research using WEPP was operationalised. The WEPP model requires daily climate data, including rainfall amount and duration. A relatively simple technology was needed to accompany WEPP to provide daily climate input data. A separate climate generator, CLIGEN, was adopted to generate the climate files required by the WEPP program (Nicks et al., 1995). CLIGEN version 4.2 was used to produce daily, monthly, and annual precipitation amounts, extremes and storm events using the Tropical Rainfall Measurement Mission (TRMM). Ground based measurements were also available from the Indian Metrological Department (IMD) rainfall data sets. The ability of CLIGEN was evaluated to generate satisfactory precipitation statistics outside of the central U.S. by comparing the CLIGEN–generated and observed rainfall amounts and to assess further the impact of satellite and ground based precipitation on WEPP runoff and erosion prediction in the Man River basin.

To generate reliable topographic and hydrologic inputs for the WEPP model, digital elevation models (DEMs) were carefully selected with the appropriate resolution and accuracy because topography is a major factor controlling water erosion. A total of three DEMs from the Indian Space Research Organization (cartosat-1), The Land Processes Distributed Active Archive Centre (LP DAAC) a component of NASAs Earth Observing System (EOS) Data and Information System (EOSDIS) (ASTER), and the Shuttle Radar Topography Mission (SRTM) at a resolution of 30m, 30m, and 90m, respectively were obtained and used to calculate topographic parameters as inputs for the WEPP model.

Vegetation is one of the key factors affecting soil erosion. WEPP is a useful tool for understanding erosional processes and impacts in a given area. The effects of vegetation on soil erosion were quantified using classified Landsat images from long term historical datasets. The study determined the

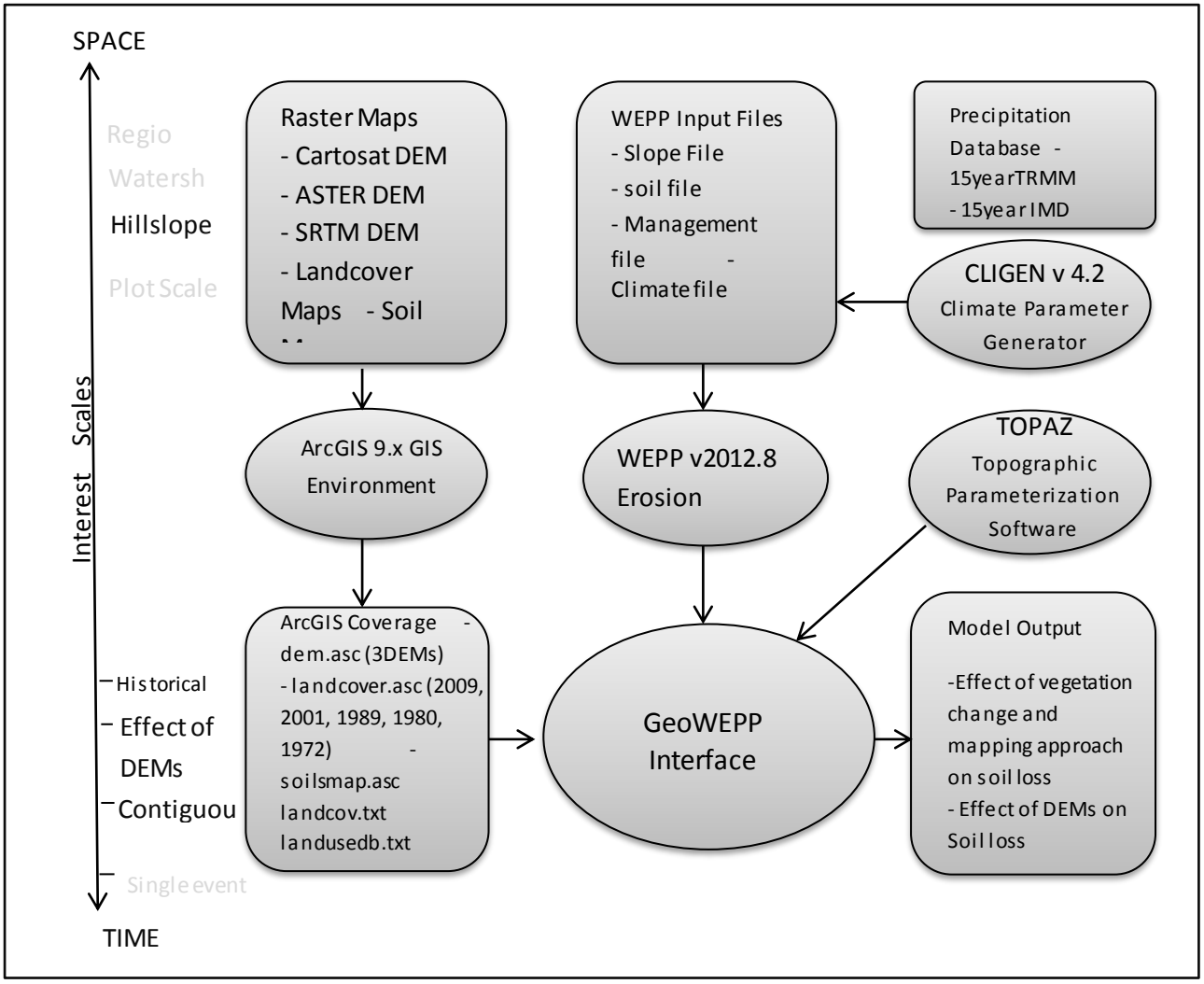

Figure 6. 1: Flow diagram showing the process of undertaking the soil erosion risk modelling with GeoWEPP, including the major software components in the WEPP GIS based interface.

susceptibility of the landscape to erosion and estimated runoff and sediment yields at the hillslope scale and assessed erosion susceptibility under multi vegetation scenarios (land use /land cover 2009, 2001, 1989, 1980 and 1972).

6.3. Model Structure: Water Erosion Prediction Project (WEPP)

WEPP is founded on the fundamentals of hydrology, erosion mechanics, plant growth, and open channel hydraulics (Flanagan et al., 1995). The model has both a hillslope and a watershed version and can be

used to model spatial and temporal distributions of net soil loss and sediment deposition along a hillslope or across a watershed on an event or a continuous time basis (Flanagan and Nearing, 1995). The model has several components that determine the response of soil to the eroding agent; water. These components include weather generation, winter processes, irrigation, infiltration, overland flow hydraulics, water balance, plant growth, residue decomposition, soil parameters, hillslope erosion and deposition, watershed channel hydrology and erosion processes, and the watershed impoundment component. These components are essential to simulate the mechanisms driving detachment, entrainment, transport, and deposition of sediment at both the field- and watershed-scale. This section gives a brief description about these components.

Simulated **climate** for use in the WEPP model is normally generated using the CLIGEN model, which is a computer program run separately from the WEPP erosion model. The algorithms in CLIGEN are based on the climate generators developed for the Erosion–Productivity Impact Calculator (EPIC) model (Williams et al., 1984) and the Simulator for Water Resources in Rural Basins (SWRRB) model (Arnold and Williams, 1989). A second–order Markov chain generates the occurrence of precipitation on each day. Inputs to the Markov chain include the probability of a wet day following a wet day, P (W/W), and the probability of a wet day following a dry day, P (W/D). The precipitation amount on each wet day is stochastically generated as a skewed normal distribution.

Winter processes modelled in WEPP include soil frost and thaw development, snowfall, and snow melting. Simple heat flow theory is used with the daily information on temperatures, solar radiation, residue cover, plant cover and snow cover to determine the flow of heat into or out of the soil, and then the subsequent changes to frost and thaw depths. Solar radiation, air temperature, and wind drive the snow melting process.

The **irrigation** component of WEPP allows simulation of both stationary sprinkler and furrow irrigation systems. The sprinkler irrigation component accommodates solid set, side-roll, and hand-move systems, while the furrow component can simulate uniform inflow, surge, and cutback flows. Spatial variations in application rate and depth within a sprinkler irrigation area are assumed to be negligible, and a sprinkler event is simulated as a rainfall event of uniform intensity. The scheduling options available for both sprinkler and furrow irrigation are depletion level and fixed-date. Depletion-level scheduling determines the date and amount of irrigation based upon the available soil moisture depletion. Fixed-date scheduling uses predetermined irrigation dates and amounts. The user may also use a combination of the two scheduling methods.

The **hydrology** component of WEPP computes infiltration, runoff, soil evaporation, plant transpiration, soil water percolation, and plant and residue interception of rainfall, depression storage, and soil profile drainage by subsurface tiles. Infiltration is calculated using a modified Green and Ampt infiltration equation. Runoff is computed using the kinematic wave equations or an approximation to the kinematic wave solutions obtained for a range of rainfall intensity distributions, hydraulic roughness, and infiltration parameter values. The water balance routines are a modification of the SWRRB water balance (Williams et al., 1985).

The impacts of tillage on various soil properties and model parameters are computed within the soils component of the WEPP model. Tillage activity during a simulation acts to decrease the soil bulk density, increases the soil porosity, changes soil roughness and ridge height, destroys rills, increases infiltration parameters, and changes erodibility parameters. Consolidation due to time and rainfall after tillage is also simulated.

The **plant growth component** for croplands calculates above and below ground biomass production for both annual and perennial crops in cropland situations and for rangeland plant communities in rangeland situations. Work is underway by the USDA Forest Service to incorporate plant growth routines applicable for forested conditions. The plant growth routines in WEPP are based upon an EPIC (Williams et al., 1989) model approach, which predicts potential growth based upon daily heat unit accumulation. Actual plant growth is then decreased if water or temperature stresses exist. Several different types of management options for cropland and rangeland plants can be simulated. Plant residue decomposition for croplands is based upon a "decomposition day" approach, which is similar to the growing degree day approach used in many plant growth models. Each residue type has an optimal rate for decomposition, and environmental factors of temperature and moisture act to reduce the rate from its optimum value. The WEPP model tracks the type and amounts of residue from the previous three crop harvests. The model also allows several types of residue management, including residue removal, shredding, burning, and contact herbicide application.

For rangelands the plant growth component simulates the aggregate above and below ground biomass production for the entire plant community. The plant growth routines in WEPP are based on the ERHYM-II (White, 1987) and SPUR models (Wight and Skiles, 1987). Plant growth for rangelands is based on a potential growth curve. Actual plant growth is initiated in the spring when temperature is above a

threshold and is a function of water stress. Decomposition of surface litter is based on temperature and precipitation. Root biomass decomposition is based on temperature and soil water content.

The impacts of soil roughness, residue cover, and living plant cover on runoff rates, flow shear stress and flow sediment transport capacity are computed in the hydraulics of the overland flow section of the WEPP model. Rougher surfaces, fields with more residue cover, and closely spaced crops tend to increase the soil surface resistance to flow, which in turn decreases runoff rates, decreases flow shear stress acting on the soil, and decreases sediment transport capacity of the flow.

In addition to the model components used in hillslope applications, the watershed simulations use three more components: channel hydrology and hydraulics, channel erosion and impoundments. The channel hydrology component computes infiltration, soil evaporation, transpiration, soil water percolation, rainfall interception, and depression storage and soil drainage in the same way as the hillslope hydrology component. Excess rainfall is then combined with runoff from upstream elements: hillslopes, channels or impoundments. Transmission losses are computed using a modified form of the Green-Ampt infiltration formula. Runoff peaks are then computed using either the CREAMS peak computation method (Knisel, 1980), i.e. an empirical formula that is a function of the volume of runoff, the contributing area and its slope, and the time of concentration, or a modified form of the rational formula as used in the EPIC model (Sharpley and Williams, 1990).

The channel erosion component predicts detachment and deposition in channels in a similar manner to rills on a hillslope. Detachment occurs if the shear stress is greater than a critical value and if the incoming sediment load from upstream and lateral channels, impoundments and/or hillslopes is less than the transport capacity of the channel. If the sediment load is greater than the transport capacity, deposition is predicted to occur. The particle size distribution of the sediment leaving the channel and an enrichment ratio are also calculated. An enrichment ratio is also computed for the entire watershed.

Downslope damage by detached sediment can be minimized by the use of impoundments. Typical impoundments include terraces, farm ponds, and check dams. Impoundments form small pond areas which reduce the flow velocity, thus decreasing the sediment carrying capacity and allowing sediment to settle out of suspension. Impoundments can significantly impact sediment yield by trapping as much as 90% to 100% of incoming sediment, dependent upon particle size, impoundment size, and inflow and outflow rates (Haan et al., 1994).

The impoundment routines in WEPP route runoff and sediment through an impoundment determining the total amount of runoff leaving the structure, the amount of sediment deposited in the structure and the amount and size of sediment leaving the structure. Since impoundments are one of the best methods to limit off-site damages from water erosion, the impoundment routines are crucial to the usefulness of WEPP.

6.4. The Geospatial Modelling for Soil Erosion (GEMSE) interface (GeoWEPP)

6.4.1 GeoWEPP

GeoWEPP is a geo-spatial erosion prediction model that was developed in collaboration with Purdue University, the Agriculture Research Service, and the USDA National Soil Erosion Research Laboratory (Renschler 2002). GeoWEPP was developed to allow WEPP hillslope parameterization to be based on digital data sources such as digital elevation models (DEMs), land cover, and soil maps and the digital outputs to be viewed and analysed in a GIS environment for practical assessment purpose and decision support at a particular location (Renschler 2003). The major components of GeoWEPP are explained in more detail below.

6.4.2 TOPAZ

GeoWEPP uses TOPAZ to parameterize topographic data from DEMs to create hillslope profiles called sub-catchments for each watershed. TOPAZ delineates a channel network from the DEM based on the steepest downslope path from each raster cell (pixel) from the 8 cells surrounding it (Garbrecht and Martz 1997). Adjustments can be made to the detail of the channel network by changing values of Mean Source Channel Length (MSCL) and Critical Source Area (CSA). The MSCL is the shortest length that any channel is allowed to be. The CSA defines the minimum drainage area below which a permanent channel forms (Garbrecht and Martz 1997). Setting these to low values increases the density of channels, which is useful when defining small watersheds. From the defined channel network, the user specifies the exact watershed outlet and TOPAZ generates the sub-catchments that make up the watershed. Each sub-catchment represents the direct contributing area for each side of the drainage (Garbrecht and Martz 1997) and has homogeneous slope and aspect (Renschler 2002).

6.4.3 WEPP

Once the sub-catchments have been delineated by TOPAZ, GeoWEPP accesses the WEPP model. WEPP requires four input files that describe the slope, soil, climate, and management to simulate hillslope erosion (Flanagan and Livingston 1995). The inputs to these files are described below.

Slope: WEPP requires information about hillslope geometry in order to calculate erosion rates. The slope file includes slope gradient, shape, width and orientation along its length to create a slope profile. GeoWEPP uses the sub-catchment profiles generated by TOPAZ from the user-specified watershed and allows the user to assign a single soil and management to each sub-catchment. In the standard WEPP model, each slope can be divided into a maximum of ten overland flow elements (OFEs). An OFE is a hillslope section of a desired length that can be assigned individual soil and management parameters in order to create a more realistic representation of the spatial variability within each hillslope (Flanagan and Livingston 1995). Currently, the use of OFEs is not compatible with the digital outputs generated by GeoWEPP and can't be used. Therefore, GeoWEPP users can represent spatial variability between sub-catchments, but not within them.

The WEPP model uses a stochastic weather generation model called CLIGEN, which generates site-specific files with daily values of precipitation, temperature, solar radiation, and wind speed based on historical data from a database of over 2600 climate stations located across the United States (USDA ARS and USFS 2003). The user can request a climate for a specific location and length of time. Customized climate files can be generated by using the Rock:Clime application in FS WEPP (Elliot et al. 2002). Rock:Clime was developed to account for the spatial climate variability in mountain environments (Elliot et al. 1999a). Rock:Clime uses the same weather station database as CLIGEN and includes a number of stations located in remote, mountainous regions. Rock:Clime also allows users to adjust the inputs of monthly average precipitation and temperature values to known values for the site, or access climates from a database generated by PRISM (Parameter-elevation Regressions on Independent Slopes Model) (Elliot and Hall 2000). The PRISM model estimates precipitation and temperature based on orographic effects generated from DEMs with 5- min lat- long grid spacing (Daly et al. 1994). The final climate file is then added to the WEPP climate database to be used in model simulations.

Accurate soil property values are essential for erosion prediction. Critical parameters in the soil file are hydraulic conductivity, rill erodibility and interrill erodibility (Laflen et al. 1997). These values can be measured in the field or calculated by the WEPP model based on inputs of soil texture and structure.

The management file dictates the amount of ground cover based on vegetation growth and mortality throughout the simulation period. For this study the input files were created specifically to each study site based on measured and WEPP default values of soil erodibility parameters, percent ground cover and observed climate. Percent of ground cover was recorded inthe plant/management files according to the field observations. Most of the plant specific parameters were used in the study from WEPP default values. The detailed information on management file generation was explained in Section 6.6.5 and Table 6.6.

6.4.4 ArcGIS

The GeoWEPP program runs as a project in ArcGIS. The final watershed outputs are generated in ArcGIS as grid layers of soil loss as a percentage of the tolerable soil loss (TSL) (defined by the user). The grid layer highlights areas that generate soil loss values greater than, or less than the TSL. Values greater than the TSL indicate areas where management precautions should be taken. True values of runoff and sediment loss for each pixel are generated in text files that can also be imported to ArcGIS for viewing. In addition to the grid outputs, GeoWEPP generates text files summarizing average annual rainfall and number of storms, total runoff, soil loss and sediment yield for each sub-catchment and the entire watershed.

6.5. Study Sites

Three small watersheds in the Man River basin were selected to estimate soil erosion risk with long term vegetation change (Figure 6.2). These three watersheds belong to three different geographical areas within the Man basin. The Mogrba watershed extends between 75°18’55”E to 75°21’41”E longitude and 22°23’12” N to 22°25’52”N latitude. The total area of the watershed is 603.3 ha. Minimum and maximum altitudes of the basin are 443 and 665 m, respectively, while the average height is approximately 544 m above sea level. The soils contained 39 % sand clay loam, 32 % clay loam and 27 % silt clay loam. The watershed contains slopes from 0 to 40 degrees. The land cover distribution is agriculture, forest and fallow land, 38.2%, 60.0% and 0.6% respectively. Clearance of the forest on the slopes and replacement with annual crops is one of the major characterises in the watershed. Mean annual temperature is 24.5^{0}C and the mean rainfall is 1085 mm. In the last four decades, there has been substantial vegetation change in the study area: agriculture has increased to 36.9 % and forest area has decreased to 22.2 %.

The Loni watershed is located in south part of Man River basin (75^0.14 E, 22^0.22 N). The 175 ha site contains slopes with angles ranging from 2.24 to 14.66 degrees. The elevation ranges from 116 to 145 meters. The soil is composed of 71.4 % clay and 28.6 % loam. The watershed is characterised by high population pressure because the major part of the rural population is dependent on agriculture activities. The agriculture activities of the rural population are resulting in soil erosion in the all three watersheds.

The Salkanpur watershed is located in the Malwa plateau (north part of the Man River basin). The watershed lies between 75^O.38 E and 22^O.52 N. The watershed has a total area of 150.9 ha and is composed of 0.9 to 12.6 degree slopes. The elevation ranges from 487 to 518 m. The soils of the watershed are 83 % clay and 17 % clay loam. Agriculture is the primary source of livelihood for the population in watershed.

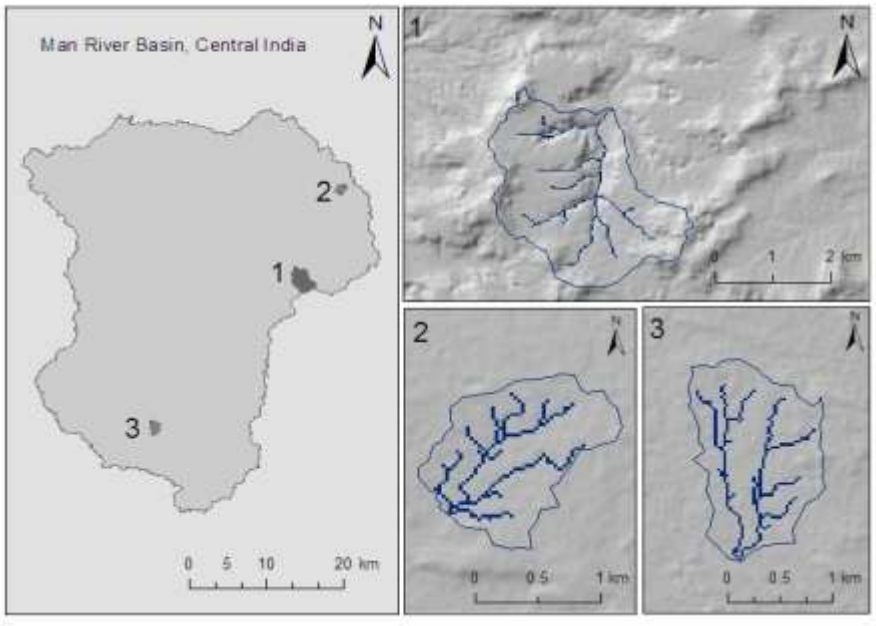

Figure 6.2.Locations of the three selected watershed in the Man River basin, Central India; (1.) Mograba watershed, 2) Salkanpur watershed, and 3) Loni watershed.

6.6. Input datasets preparation and processing

This section is organized as follows: firstly the input data used for WEPP simulations will be discussed, and secondly, the field measurement conducted at the study area will be presented.

Table 6.1. GeoWEPP input parameters estimated from different source.

GeoWEPP input data	Source	Data type
Soil raster	LISS-III	Raster ASCII
Soil texture	Soil survey	Text file
Soil depth	Soil survey and laboratory measurement	Text file
Organic matter	Soil survey and laboratory measurement	Text file
Albedo	WEPP user summary	
Initial Saturation level	Calculated by WEPP	
Baseline inter – rill erodibility	Calculated by WEPP	
Baseline rill erodibility	Calculated by WEPP	
Baseline critical shear	Calculated by WEPP	
Effective hydraulic conductivity	Calculated by WEPP	
Land use /land cover	Landsat Imagery	Raster ASCII
Management	Filed work and suggested by WEPP	Text file
Topography	DEM (Cartoset , ASTER and SRTM)	Raster ASCII
Climate	TRMM satellite and rain gauge data	Text file

6.6.1. Climate (CLIGRN parameter generation with TRMM 3B43 V7 and Ground based rainfall

CLIGEN version 4.2 was used to produce daily, monthly, and annual precipitation amounts, extremes, and storms using TRMM and Indian Metrological Department (IMD) rainfall data sets. CLIGEN was also used to assess the impact of satellite and ground based precipitation on WEPP runoff and erosion predictions. TRMM 3B43 V7 (Version 7) daily precipitation datasets were available for a period of 15 years (1998 - 2012) and were compared with ground based daily precipitation datasets for the same time period to produce TRMM 15 year and IMD 15 year CLIGEN files to be used in WEPP model runs. IMD data comprised an hourly precipitation measurement that incorporated data from study by Deshpande et al (2012). To further evaluate the impact of climate data on model predictions long term precipitation for a 40 year period from 1983 to 2013 based on IMD and Dhar District Land Information Department daily rainfall data was used to develop a CLIGEN file. Figure 6.3 and Table 6.2 compare the precipitation constructed from 15 years of TRMM data, 15 years of IMD data and 40 years of IMD data.

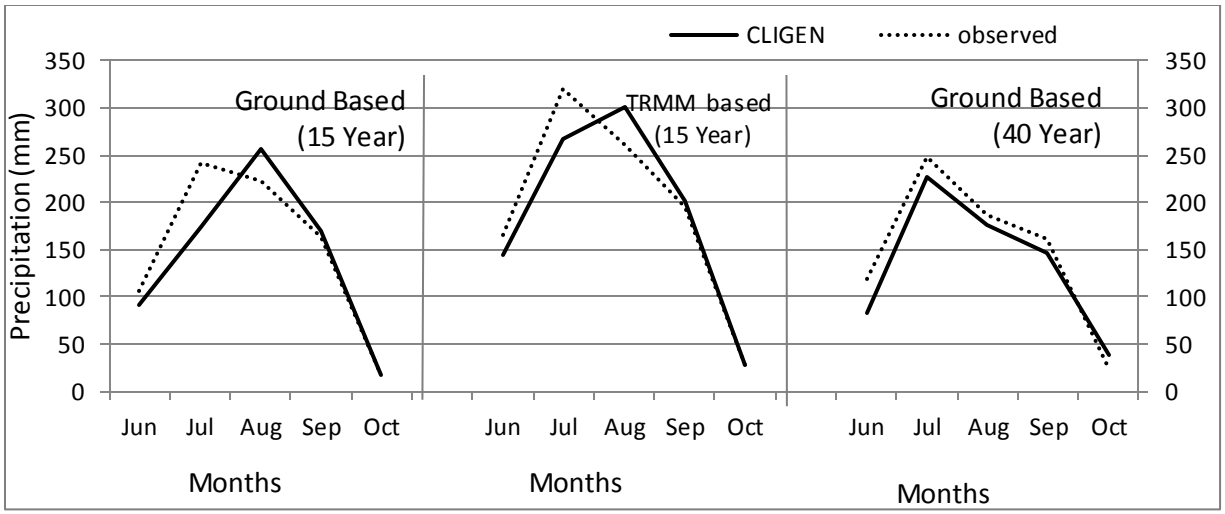

Figure 6.3: Monthly comparisons of 15 years TRMM, 15 years ground based and 40 years ground based rainfall data to CLIGEN results for 15 years and 40 years simulated data.

6.6.2 Topographic parameter generation

WEPP also utilizes topographic information for constructing the drainage network domain to correctly estimate the conveyance of runoff as well as sediment yield and soil loss. A total of three Digital Elevation Models (DEMs) from three sources at different resolutions were evaluated for their ability to delineate the channel network, determine the sub-catchment in each watershed and generate the hillslope information for WEPP modelling. Three DEMs were acquired from: i) the Indian Space Research Organization (cartosat-1 at 30m); ii) The Land Processes Distributed Active Archive Centre (LP DAAC) which is a component of NASAs Earth Observing System (EOS) Data and Information System (EOSDIS) (ASTER at 30m); and iii) the Shuttle Radar Topography Mission (SRTM) DEM at 90 m resolution which is a joint product from NASA and the National Geospatial Intelligence Agency (NGA). The ASTER DEM was updated with the filter sinks tools in ArcGIS to remove small imperfections in the data.

Table 6.2: Monthly comparisons of 15 years TRMM, 15 years ground based and 40 years ground based rainfall data to CLIGEN results for 15 years and 40 years simulated data. All data are in mm.

Month	15YrIMD		15yrTRMM		40yrIMD	
	Observed Mean	CLIGEN Mean	Observed Mean	CLIGEN Mean	Observed Mean	CLIGEN Mean
Jan	0.2	5.95	2.43	2.78	1.37	2.94
Feb	0.653	0.70	5.26	6.2	0.58	0.37
Mar	1.85	5.01	4.87	6.4	2.49	1.63
Apr	0.81	0.06	2.07	8.6	1.62	0.87
May	4.97	4.69	14.99	9.4	6.71	6.10
Jun	106.14	91.13	165.83	143.2	119.07	82.12
Jul	240.58	173.56	319.19	266.14	247.83	226.40
Aug	221.77	255.44	261.64	301.49	186.66	176.40
Sep	162.32	170.24	195.17	201.91	160.38	147.14
Oct	17.01	16.51	27.74	27.98	24.44	38.30
Nov	8.041	5.24	16.32	6.9	15.16	17.66
Dec	0.574	2.49	1.35	8.1	3.04	2.13
Total	764.98	731.03	1016.86	989.54	769.36	702.14

A step by step process for preparation of topographic datasets for GeoWEPP inputs in ArcGIS 9.3 software was followed with all three DEMs. The resolution of all three DEMs was set at 14.25 m and all the cells line up with each other. All raster files were in the same UTM zone (43 N) and converted into ASCII and text files. The following procedure was used to prepare inputs:

(1) The DEM was loaded in the ArcGIS 9.3 software.

(2) Then it was processed for the correct projection. GeoWEPP requires raster DEM to be projected into UTMs. The UTM Zone 43 was determined for study area and transformed into the DEM with output cell size 14.25 (m) using ArcGIS tool → Data management tools → Projection and Transformations → Raster.

(3) GeoWEPP primarily works with small watersheds. The DEM size should be a little larger than needed. While not required, this helps to reduce the processing time needed to convert DEM to ASCII and in many of the other GeoWEPP process. To reduce DEM size, the 'Clip Tool' located in the Data Management Tools → Raster portion of the Arctoolbox was used.

(4) Once the DEM was in the correct projection and size for GeoWEPP, the DEM raster grid was converted into an ASCII raster file using the Raster to ASCII Conversion Tool in the ArcGIS 9.3.

The topographic inputs for both hillslope profiles and channels were derived from each of the three DEMs for each watershed through the TOPAZ application in GeoWEPP. TOPAZ uses a breaching filling operation for removal of depressions and pits and the D8 algorithm (using the deterministic eight-neighbour method to simulate flow across a land surface) for determining the drainage direction (USDA, 2008). The critical source area (CSA) was set to 3 ha for Loni watershed, 2 ha for Salkanpur watershed and the minimum source channel length (MSCL) and to 100 for both watersheds in TOPAZ to make the derived channel networks and watershed structure.

6.6.3. Landuse/Land cover file generation

Landsat satellite imageries (at 30-m spatial resolution) were acquired and processed to determine the historical spatial distribution and coverage of the various land use/land cover classes in the study area for the years 2009, 2001, 1989, 1980 and 1972. The land use/land cover TIFF images for the study area derived by Landsat satellite were prepared in ArcGIS using a 30m sampling grid for GeoWEPP inputs. All the raster data files were converted into ASCII files and stored in the GRID format as with the DEMs, but with the additional steps:

(1) The Landuse classification layer projected with UTM Zone 43 N was added into ArcMap.

(2) The classification layer was clipped to match the same extent as the projected DEM. This helps to reduce the amount of storage needed for the land use layer and also processing time. The **Extract by Mask tool** allows to do this **.**The tool is located in: Spatial Analysis Tools → Extraction (Figure 6.4).

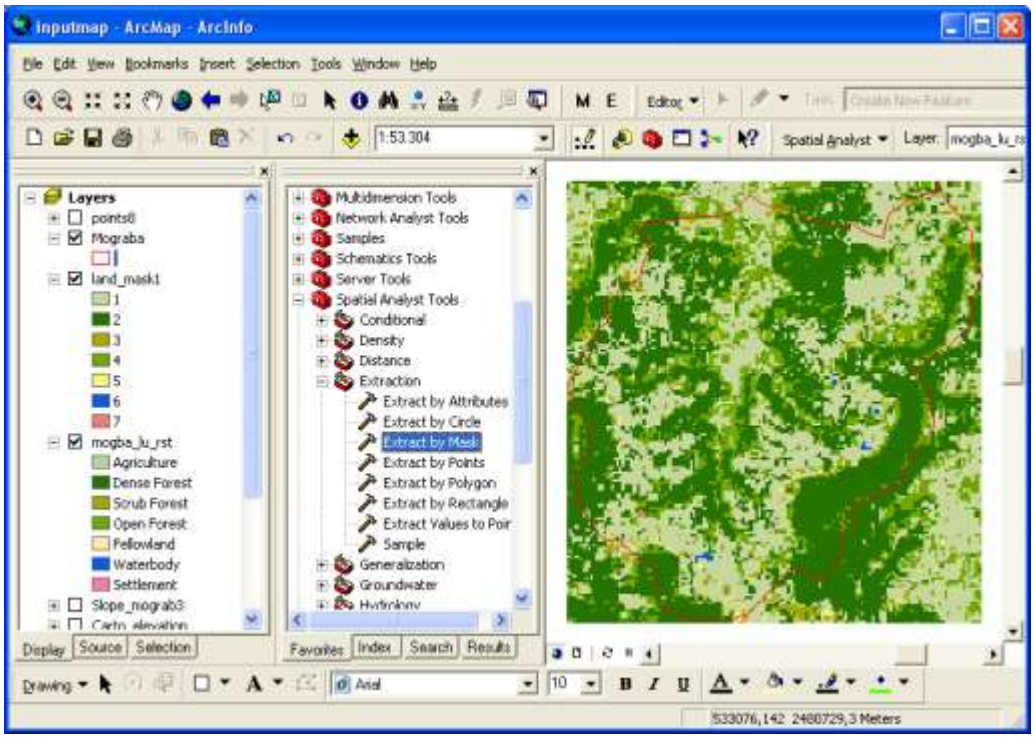

Figure 6.4: Resulting clipped land use/land cover layer.

(3) GeoWEPP requires two text files to link the GIS. One of these files links the raster cell values with a description. For the land use layer, the file called **landcov.txt** stores a list of cell values along with its corresponding description, for example "1 agriculture"; in this way the value 1 is given the description "agriculture". The creation of these files is explained in section (4.5.6.2) but the creation process is started here by exporting the land use layer's attribute table.

(3a) the attribute Table for the newly created land use layer was opened. This may be done by right –clicking on the layer's name and selecting open Attribute Table from the popup menu (Figure 6.5). The value column of the attribute table contains the values that were stored in each of the raster cells. This value will be used to create the landcov.txt file.

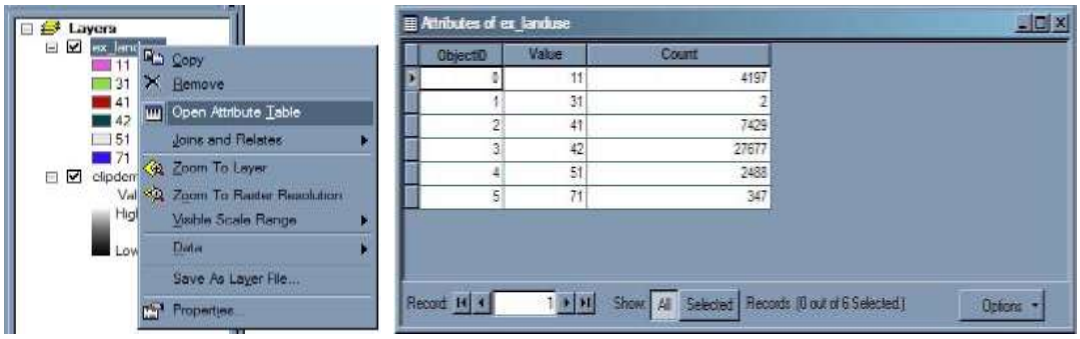

Figure 6.5 a) Right-click popup menu; b) Clipped land use layer attribute table.

(3b) all the records in the **Attribute Table Option** menu were exported to save as a text file using the following steps:

Select Export from menu → open the Export Data window → make sure "All records" appears in the box next to export → use Text File as the save as Type . The landcov.txt file is created but not yet ready for GeoWEPP run (Figure 6.6).

(4) The clipped land use layer was converted to an ASCII raster file and saved with an appropriate file name such as **landuse.asc** using the **Raster to ASCII tool.**

The pre-processing stage for land use was then complete. The same processing was repeated with each year image.

6.6.4 Soil Input Generation

WEPP requires two inputs to characterise soil, first the WEPP soil file which was prepared from field measurements (soil texture, soil depth and organic matter) in the three selected watersheds but supplemented by values calculated by WEPP itself (such as interrill erodibility, rill erodibility, critical shear and effective hydraulic conductivity). The Green-Ampt effective hydraulic conductivity equation was used to estimate hydraulic conductivity based on rainfall amount, surface cover, and runoff (Alberts et al 1995). Rill and Interrill erodibility values were determined depending on the sediment delivery equation in WEPP Model v2012.8.

Secondly, GeoWEPP needs soil textural raster file which was developed by integrating multispectral LISS –III satellite data. The Dhar District Soil Atlas also provides soil information for the study region which could have been used for WEPP inputs, but the quality of this soil data is very poor (see Figure 6.6). For instance, the soil maps in the Atlas were developed by Tamgadge et al., (2001) at the regional scale (1:1000000), which may cause large uncertainty in the model outputs when used at the hillslope scale. Thus, an integrated sub-approach was developed to produce fine scale soil textural maps for WEPP input using field sample collection, laboratory measurement and remote sensing. Soil textural class maps were generated for all three selected watersheds in the Man River basin using LISS –III multispectral image. These image – based maps were updated with soil samples collected in the field.

6.6.4.1. Soil sample collection

Required soil properties (i.e. soil texture, soil depth and organic matter) were assessed through the collection of soil samples which were then analysed in the laboratory. Soil samples were collected from the surface floor (subplot 2, 3, and 4) and underlying soil layers (subplot 2). The entire surface floor layer

was sampled from a known area after measuring the thickness at the north, south, east, and west edges of a sampling frame of a known area. Once the upper floor had been removed, soils were sampled volumetrically by collecting cores from two depths: 0 to 10.16 cm and 10.16 to 20.32 cm. Soil samples were collected within the annular plot along soil sampling lines adjacent to subplots 2, 3, and 4 (Figure 6.7 and 6.8). The soil sampling sites were spaced at 3.04 m intervals alternating on opposite sides of soil sampling site.

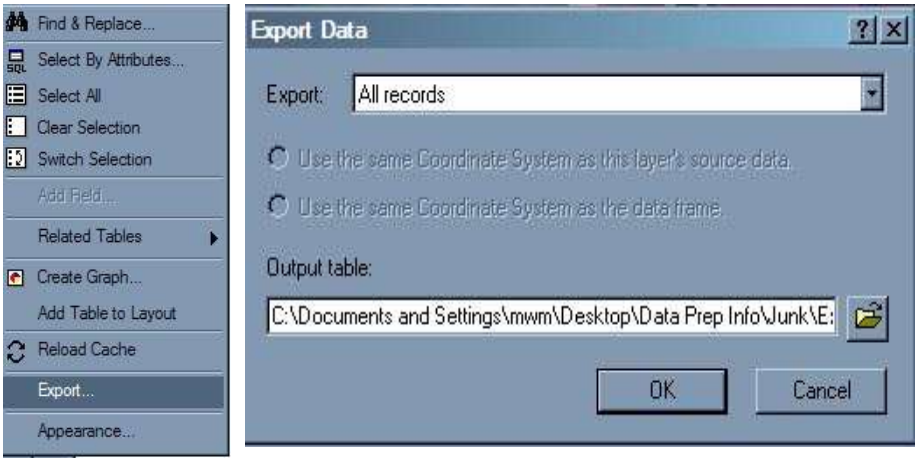

Figure 6.6. a) Attribute Table Option menu; b) Export Data window.

Table 6.3; Soil Properties in the watersheds measured in the field and tested in the laboratory.

Watershed Name	Sample No.	Latitude	Longitude	Texture	Sand (%)	Silt (%)	Clay (%)	ORG %	Depth (Inch)
Mograba	1	22.396	75.328	Clay loam	33.33	32.0	34.6	0.45	20
	2	22.409	75.323	Silty Clay loam	9.78	56.4	33.7	0.56	7
	3	22.402	75.342	Clay	17.75	66.8	15.3	0.23	19
	4	22.399	75.341	Clay loam	31.57	33.4	35	0.56	13
	5	22.410	75.340	sandy clay loam	62	9	29	0.44	17
	6	22.413	75.337	Clay	20.18	17.8	62.0	0.3	65
Loni	7	22.227	75.142	Silty loam	22.71	63.6	13.6	0.44	6
	8	22.220	75.146	Clay loam	35.93	28.8	35.2	0.39	12
	9	22.226	75.144	Clay loam	33.77	28.2	37.9	0.5	4
	10	22.219	75.147	Loamy sand	81.77	11.8	6.38	0.51	2
	11	22.217	75.143	Clay	21.7	17.2	61.0	0.54	9
	12	22.215	75.143	Clay	14.87	12.4	72.6	0.46	36
SalkanPura	13	22.512	75.373	Clay	10.08	16.6	73.2	0.44	10
	14	22.300	75.379	Clay	12.7	9.8	77.5	0.48	12
	15	22.508	75.375	Clay loam	34.57	35.8	29.5	0.39	8

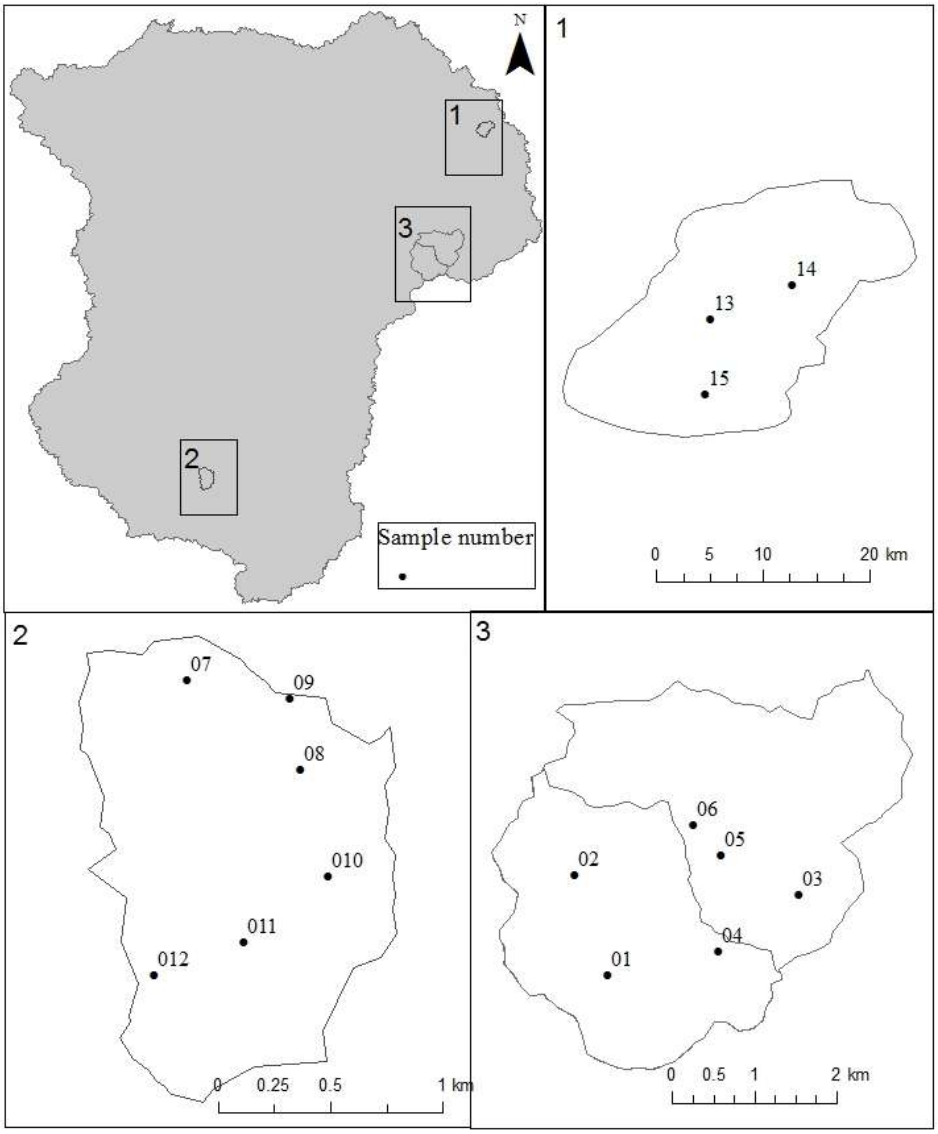

Figure 6.7: Location of soil samples collected from three different watersheds in the Man River basin, India.

6.6.4.2. Generation of the soil file for WEPP

Accurate representation of soil property values in WEPP is essential for estimating soil erosion. In WEPP, critical parameters in the soil file are the soil texture, albedo, saturation level, hydraulic conductivity, rill erodibility and interrill erodibility, and critical shear. These parameters are obtained from data collection or calculated by the WEPP model. In this study, soil parameters were measured based on soil samples collected from randomly selected 1 m2 plots (i.e. 15 plots) located in the study area (Table 6.3) and Soil Resource Atlas of Dhar District. After collecting soil samples from the selected sub-watersheds in the study area and analyzing them in the laboratory, some of the soil properties including soil texture, albedo, saturation level, soil depth, sand-clay-organic matter ratios, cation exchange capacity, and rockiness were entered into WEPP soil input file. The values of the other properties such as rill and interrill erodibility, critical shear, and hydraulic conductivity were calculated by the WEPP model itself based on input information.

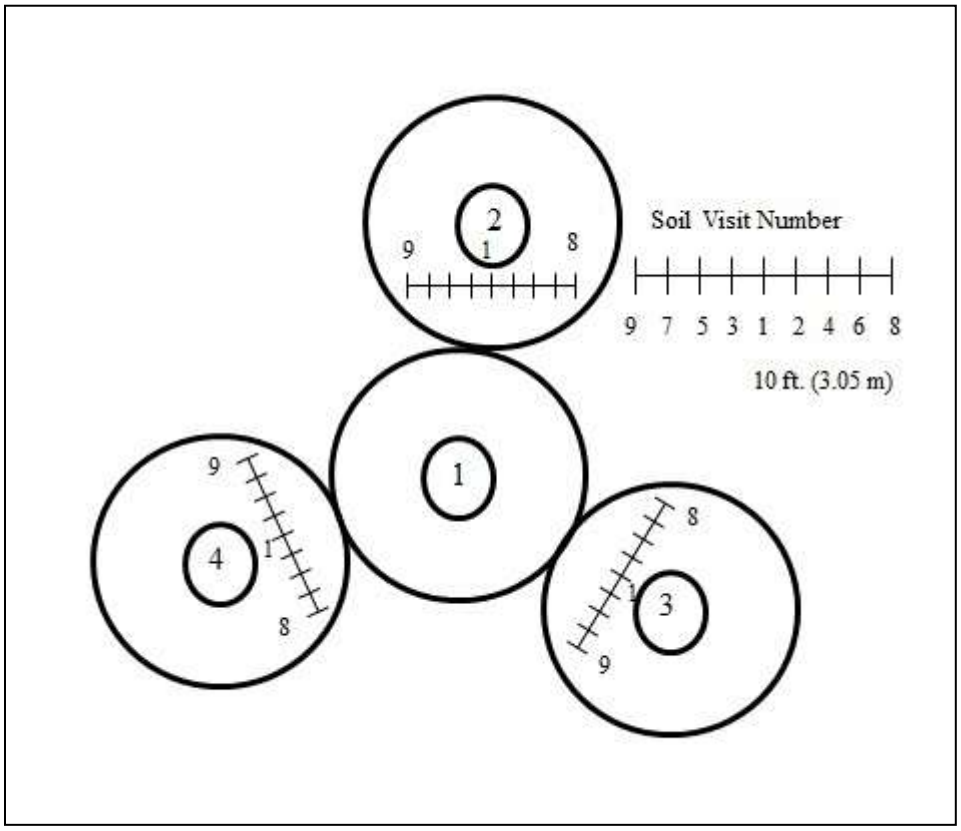

Figure 6.8: Location of soil sampling sites.

6.6.4.3. Preparing the soil raster with LISS-III

Remote sensing is an efficient, fast and economically sustainable way to detect spatial difference in soil within field. It offers the potential for identifying fine-scale spatial patterns in soil properties across a field and optimizing soil sampling strategies to quantify these patterns (Mulla et al., 2000). Several soil properties, namely, surface condition, particle size, organic matter, soil colour, moisture content, iron and iron oxide content and mineralogy have been found to affect their spectral behaviour (Dwivedi. 2001). Soil texture significantly influences the reflectance pattern; fine textures generally show greater reflectance than coarse textures (Horvath et al., 1984). Multispectral airborne (green, red, near infrared and thermal) and satellite (SPOT and Landsat TM) data were used to derive soil textural class maps for 350 ha in Maricopa, Arizona. These maps were compared to soil textural analysis results from samples in the top 30 cm of the soil profile at approximate grid spacing of 120 m. Results suggest that it is possible to map areas of soil textural class with reasonable accuracy using spectral classification procedures on a field- by –field basis (Barnes and Baker, 2000).

Table 6.4. Characteristics of LISS-III imagery, sensor system and acquisition dates.

Sensor	Spatial Resolution	Acquisition Data	Bands No	Wavelength (μm)
LISS- III	30 m	23 Oct 2008	VIS	0.52-0.59
			VIS	0.62-0.68
			NIR	0.77-0.86
			SWIR	1.55-1.7

In the current study, the soil maps for all three watersheds were derived from multispectral imagery (LISS III) at 23.5 m resolution from Indian Remote Sensing product with integrating ground based soil samples (described in 5.4.2). Characteristics of LISS-III imagery, sensor system and acquisition dates are summarized in Table 6.4 and section 3.3.2.

Digital processing was carried out in ArcGIS. The maximum likelihood classifier was used to undertake unsupervised classification of soil for all three watersheds. Unsupervised classification determined the division of the soil classes based on different soil features. It means unsupervised classification works as a tool to identify areas of a soil that have similar spectral properties. The resulting classes were then assigned to a soil class of clay and clay loam etc. based on soil texture samples which were collected from each class sites. For example, soil textures were classified into two classes for Loni Watershed, using LISS-III data, then six soil samples were collected for both class areas for laboratory analyses. These samples were tested in the laboratory for soil texture analysis. Finally, each soil textural class was identified and named according to soil texture results obtained such as clay and loamy. These soil texture maps were produced at a fine resolution (30 m) which is much better than the available soil texture maps from the District Soil Atlas (Tamgadge et al, 2001) (see Figure 6.9). Soil class maps were also verified visually using aerial imagery to satisfy that each soil class is classified properly. The classified soil raster map, which has the same cell size at the Cartosat -1 DEM, was used to proceed for GeoWEPP inputs.

6.6.4.4. Preparing soil data inputs

The soil raster layer was loaded in ArcGIS. The soil layer was in the same projection system as Cartosat -1 DEM.

(1) Following the same steps as used in the land use section the soil layers are clipped using the Extract by Mask tool.

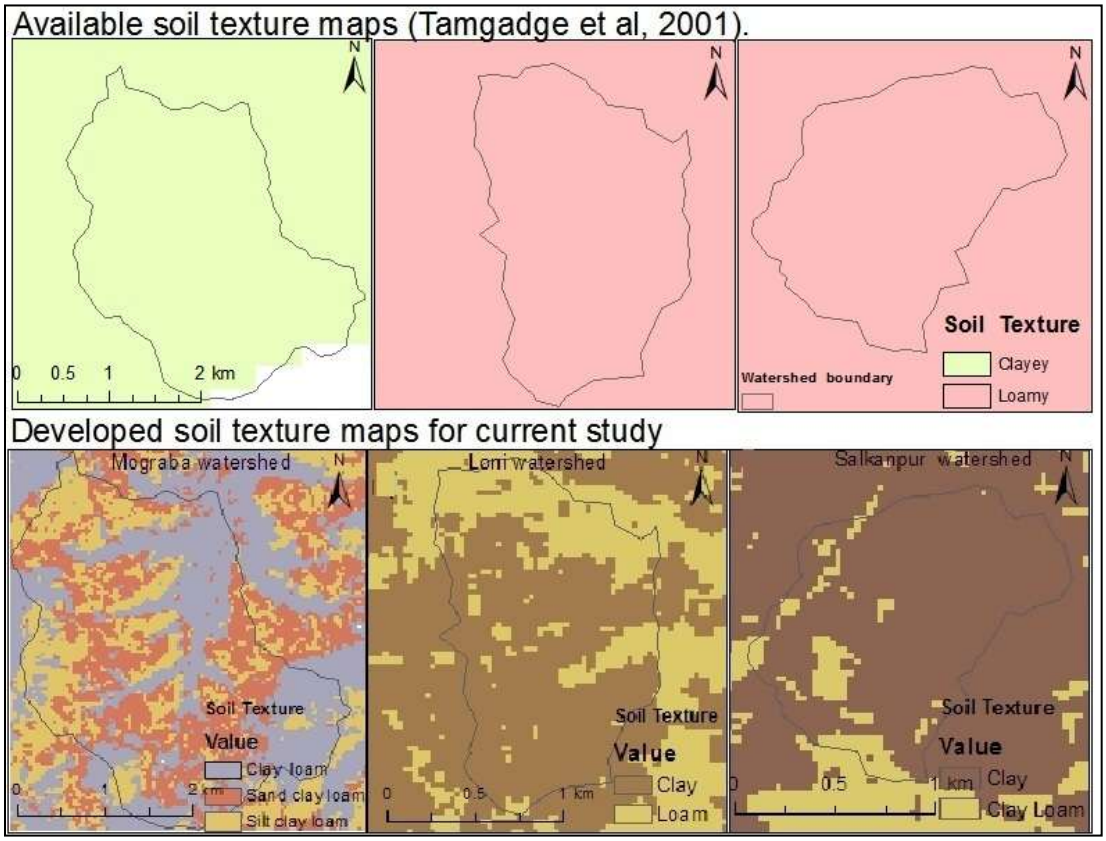

Figure: 6.9: Available poor quality soil texture maps for study sites (above) and developed fine resolution maps for current study (below).

(2) As with the land use file, GeoWEPP uses two text files to link the soil GIS data with the WEPP soil parameter files. For this, the attribute table for newly clipped soil raster layer was exported to a text file and saved as soilmap.txt.

(3) The clipped soil raster layer then needs to be converted to an ASCII raster file. This process was completed using the Raster to ASCII tool.

Still, there are few more necessary steps to prepare the GIS data for GeoWEPP run which are explained in the next section.

6.6.5. Management file generation

Field studies have shown that the amount of surface cover has a dominant role in controlling runoff and erosion (Dissmeyer and Foster, 1981; Robichaud and Brown, 2002). The WEPP model predicts surface cover every day after accounting for biomass accumulation from senescence (leaf fall) and loss through

decomposition. It means that the amount of land cover is indicated in the management file based on growth and mortality parameters. In this study, the necessary management file data (i.e. the amount of vegetation, duff, litter, and woody debris) were obtained by field measurements and from WEPP default values which were entered into the model. The management file was then generated for different land use types (i.e. agriculture land, dense forest, scrub forest, and fallow land,) for each watershed for every year of simulation. During this process, WEPP generates interrill cover data for each year using growth parameters, soil data, and climate data.

The timeline of operation (planting, tillage, harvesting) for cropland management practices was also needed to run the WEPP model. Information regarding initial land condition, crop growth, residue decomposition and details of tillage implements were prepared from field work and suggested values by the WEPP Model. Parameters for crops were adopted from (Ascough et al., 1995 and Williams et al., 1989). The captured data included the time, location, amount and type of tillage practices performed, seeds planted and crops harvested. Initial conditions for all land uses and associated management practices are provided in Tables 6.5, 6.6 and 6. 7.

Table 6.5: Crop rotation timeline for study area.

Date	Operation
2 Jan 11	Irrigation _III
17 Jan11	Irrigation _IV
25 Mar11	Harvesting
15 April11	Burning
20 April 11	Tillage _I
5 May11	Tillage _II
15 May11	Tillage _III
15 Jun11	Planting
10 Oct11	Harvesting
12 Oct11	Tillage _I
17 Oct11	Tillage _II
17 Oct11	Planting
18 Oct11	Rill making
2 Nov11	Irrigation _I
17 Nov11	Irrigation _II

Table 6.6: Initial conditions for major land uses on 1st January (1st day of the simulation period)

Parameter	Unit	AG	FO	FL	Comments
Initial Plant	-	AG	Forest	FL	
Bulk Density	-	0	1.1	1.1	
Initial Canopy Cover	%	100	90	20	
Days Since Last Tillage	days	44	2000	2000	
Days Since Last Harvest	days	45	2000	2000	
Initial Frost Depth	-	0	0	0	
Initial Interrill Cover	%	22	100	0	
Initial Residue Cropping System	-	Annual	Perennial	Fallow	
Cumulative Rainfall	-	0	1000	19.69	
Initial Ridge Height	Inch	1.5	10	0.7874	
Initial Rill Cover	%	78	100	0	
Initial Ridge Roughness	Inch	0.5	10	0.7874	
Rill Spacing	inch	8	0	0	MODEL WILL SET
Rill Width Type	-	permanent	permanent	Temporary	
Initial Snow Depth	-	0	0	0	
Initial Depth of Thaw	-	0	0	0	
Depth of Secondary Tillage Layer	Inch	6	10	3.937	
Depth of Primary Tillage Layer	Inch	6	20	7.874	
Initial Rill Width	Inch	28	0	0	
Initial Total Dead Root Mass	-	0	0.4	0	
Initial Submerged Residue Mass	-	0	0.4	0	

Note: AG – Agriculture, FO- Forest, FL- Fellow land.

Table 6.7: Crops Parameters

Input Variables	Unit.	Soybean	Winter Wheat	Cotton	comments
Biomass Energy Ratio	kg /MJ	25	30	17.5	Williams et al(1989
Growing degree days to emergence	day	60	60	90	Estimated
Growing degree days for season	day	1150	1700	2200	Estimated
In-row plant spacing	cm	2.5	0.5	10	Observed
Plant stem diameter at maturity	cm	0.95	0.64	1.3	Suggested by WEPP
Height of Postharvest Standing Residue; Cutting height.	cm	15.2	15.2	90	Observed
Harvest Index (dry yield/live biomass	%	31	42	0.5	Williams et al 1989
Base Daily air temperature	°C	20	16	16	Observed
Optimal temperature for plant growth	°C	25	15.0	27.5	Observed
Maximum temperature to stop perennial growth	°C	0	0	0	Estimated
Critical freezing temperature for perennial	°C	0	0	0	Estimated
Radiation extinction coefficient		0.45	0.65	0.65	Ascough et al1995
Canopy cover coefficient.		14	5.20	5.89	Williams *et al*. (1989)
Canopy height coefficient.		3.0	3.00	3.5	Ascough *et al*. (1995)
Maximum canopy height	cm	100	91	106	Observed
Maximum leaf area index		5	5.00	6.0	Williams *et al*. (1989)
Maximum root depth	cm	100	30	120	Observed
Root to shoot ratio	%	25	25	25	Observed
Maximum root mass for a perennial		0	0	0	Ascough *et al*. (1995)
% of growing season when LAI begins decline	%	90	80	85	Ascough *et al*. 1995
Period over which senescence occurs	days	14	14	30	Estimated
Percent of canopy after senescence	%	10	100	25	Ascough *et al*. 1995
Percent of biomass after senescence	%	10	100	10	Ascough *et al*. 1995
Flat residue cover Coefficient	Sq. m/kg	7.20	5.40	3.0	Ascough *et al*. (1995)
Standing to flat residue adjustment factor	%	99	99	99	Ascough *et al*. 1995
Above ground decomposition coefficient		0.013	0.0085	0.010	Ascough *et al*. (1995)
Below ground decomposition coefficient		0.013	0.0085	0.0065	Ascough *et al*. (1995)
Fragile (F) or non-fragile (N) residue		F	N	F	Ascough *et al*. 1995
Plant specific drought tolerance		25	25	25	Ascough *et al*. 1995
Biomass below which grazing not allowed	kg/sq. m	0	0	0	Ascough *et al*. (1995)

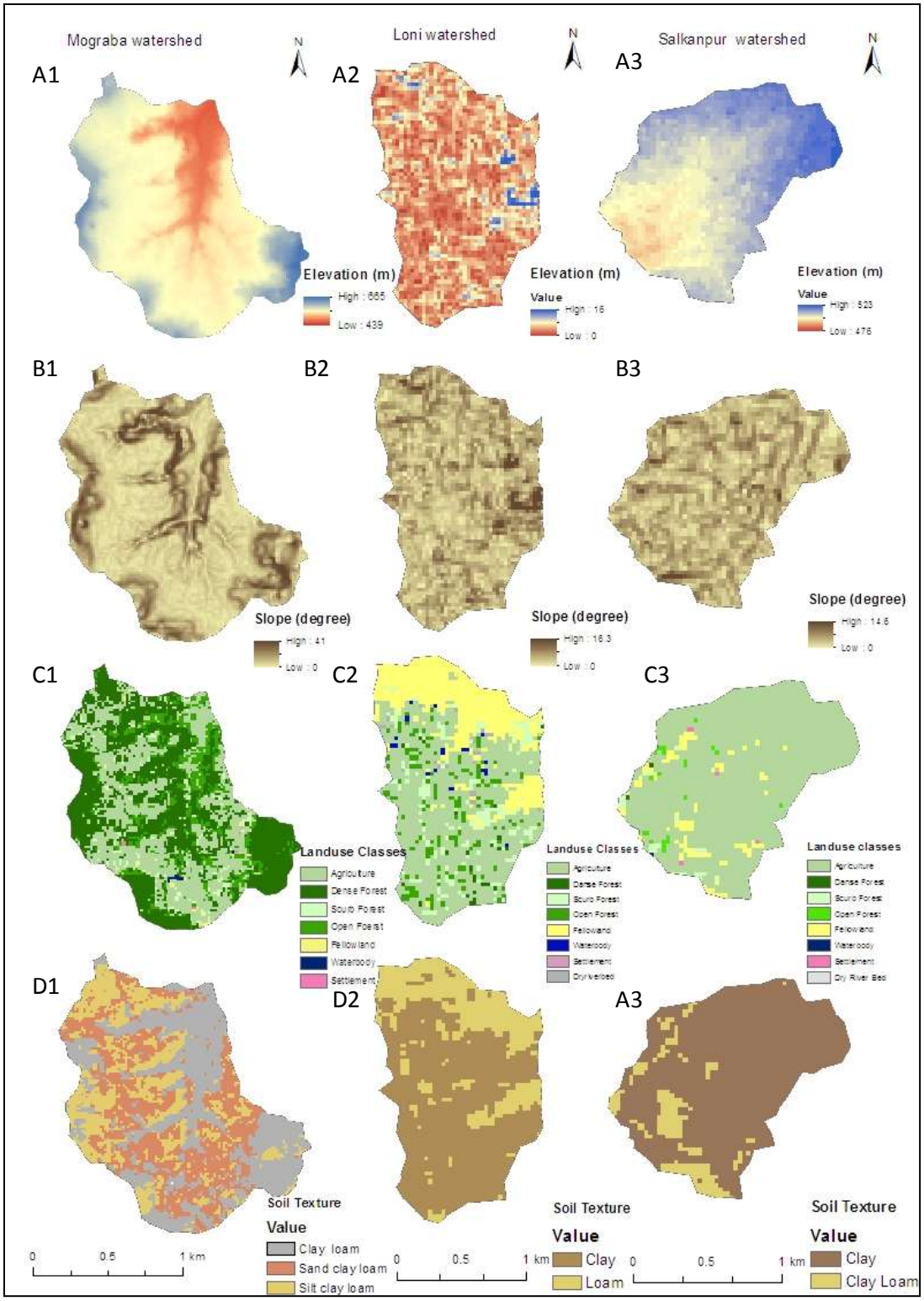

Figure 6.10: The upper row show maps of the study areas DEM (A1, A2 A3), the second row shows slope in the study areas (B1,B2,B3), the third row shows land use land cover (C1,C2, C3) and the bottom row soil texture (D1, D2 ,D3).

In the previous section, the land use and soil text files were created that would be used to connect the GIS data with the WEPP Parameter files (Figure 6.10) but still these files are not ready to connect with GIS data. This section explains how these files work and how to create them for GeoWEPP use.

6.6.5.1. The Landuse Text Files

Landuse layer uses two text files ("landcover.txt" and "landuseedb.txt") along with the raster ASCII file. These two files were created separately for the Mograba watershed using the Landuse Coding System below (Table 6.8) and assigned the same WEPP management files to each description.

Table 6.8: Landuse/land covers coding system

Code	Description
1	Agriculture
2	Dense forest
3	Scrub Forest
4	Open Forest
5	Fellow land
6	Water body
7	Settlement

6.6.5.2. **Creating the Landcover.txt file**

The idea of the landcov.txt file is to provide a number and description. The number is the value found in the land use raster layer and the description is the land use class that describes what the raster cell

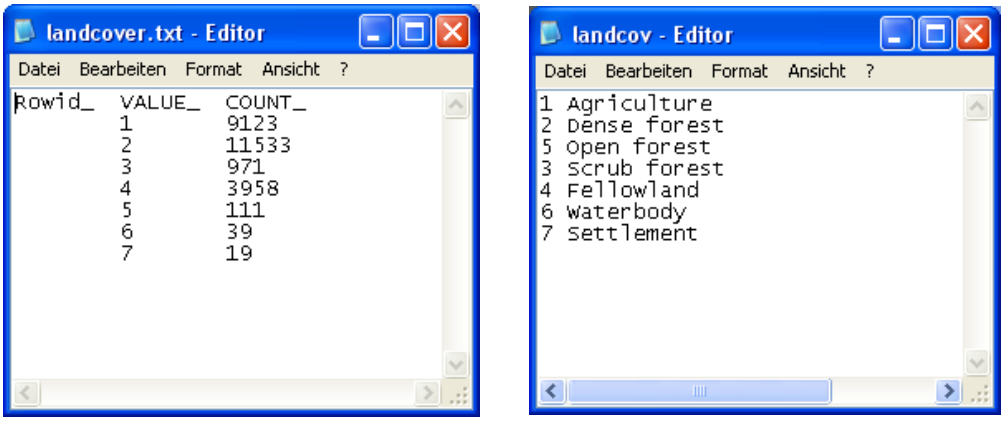

Figure 6.11. a) Exported landuse layer attribute table; b) the final landcov.txt file.

value represents. The landcover.txt file was created by editing the exported attribute table of the raster land use layer (Figure 6.11). The exported raster attribute table maintained the "value" column. This is the value found in each raster cell.

First, everything was removed from the text file then the code numbers and land use classes' description were manually entered. After finishing this, the file was saved at appropriate location. Figure 6.11 shows the exported raster attributes table and the results of this editing process.

GeoWEPP only "reads" numbers for the different cells of the land use layer. To pass on what the user "reads" to the WEPP/TOPAZ Translator, the landcov.txt is referenced to determine what the WEPP/TOPAZ Translator should display in the GIS Land use column. For example, the dark green colour in the land use raster image is for Dense Forest, but GeoWEPP only "reads" 2. WEPP/TOPAZ Translator would "look up" the number 2 in the landcov.txt and would then display Dense Forest in its GIS Land use column.

6.6.5.3 Creating the Landusedb.txt File

The land use description has been linked with the raster cell values. This description needs to be linked with the WEPP parameter file. This linkage was done through the landusedb.txt file (Figure 6.12);

(1) First, the recently created landcov.txt file was opened as it is and saved as a landusedb.txt file.

(2) Next, all the number codes were removed from this file leaved only the description. After each description, a vertical line ("I") was entered.

(3) Now, WEPP parameter paths were added. The easiest way to determine the path for the WEPP parameter file is to use WEPP itself. The following procedure was adopted to determine the WEPP path for a management file.

I) Open any hillslope in WEPP.

II) Select the management layer of the hillslope.

III) Right click on the management layer and choose import from the popup menu.

IV) Navigate to the management file needed desire using the **Select a Management file;** window. The displayed hierarchy is the path we need to enter into the landusedb.txt file.

For example, there is a description "Agriculture" in the study area landcov.txt file. The WEPP parameter file, to associate with this description is "Mograbaagriculture.rot". Using the method above, the exact location of this WEPP file is determined and entered into landusedb.txt file like this;

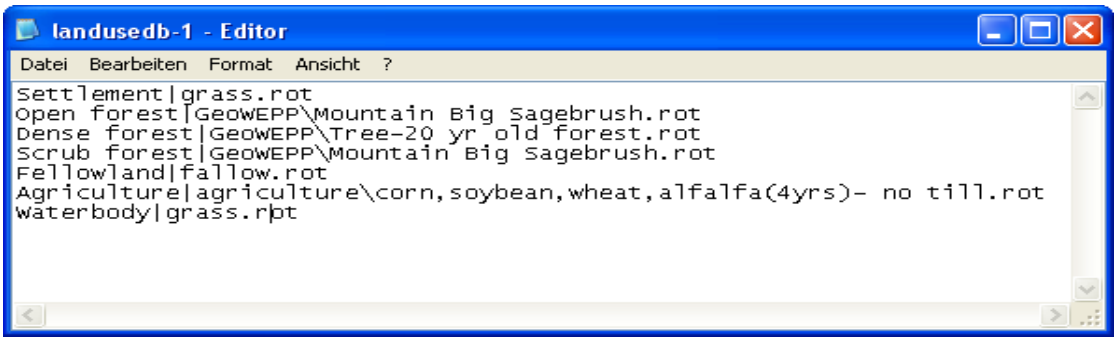

Figure 6.12. The landusedb.txt based on the landcov.txt file.

"Agriculture| Forest/Distributed WEPP management /agriculture. Rot ''

Figure 6.13 shows how the landcov.txt and landusdb.txt files work together. GeoWEPP references the landusedb.txt file to file the Agriculture description. Once it has found this correctly, it reads the path of the WEPP parameter file and enters it into the WEPP Management column of the Translator. The GIS data was now linked to the WEPP Parameter file.

6.6.5.4 The soil Text files

The soil layer also uses two text files – soilsmap.txt and soilsdb.txt – to create a bridge between the GIS raster data and the WEPP soil parameter files (.sol files). The process for creating these files was similar to the creation process discussed above; the relationship between these files and how they are used in GeoWEPP is the same as those texts.

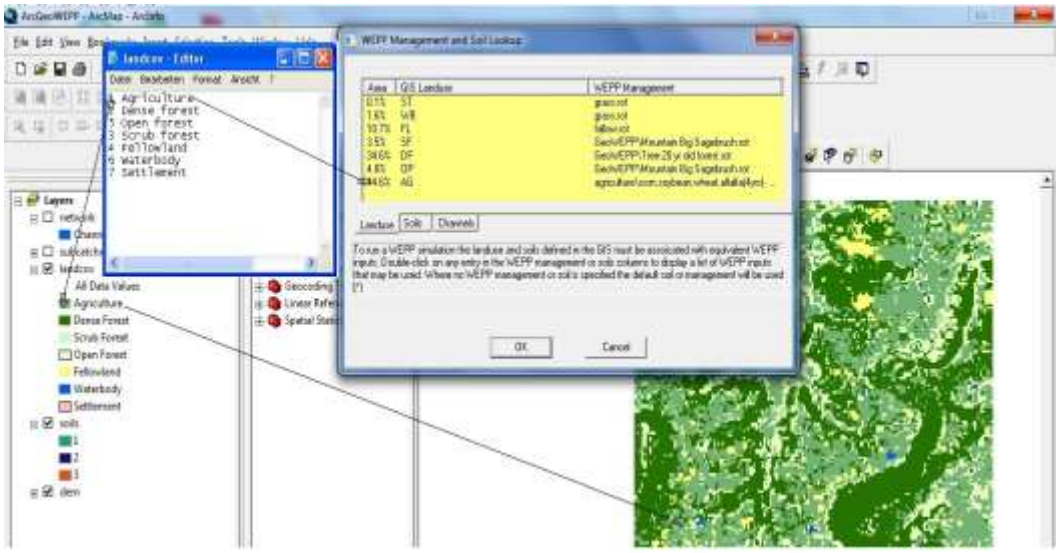

Figure 6.13. Linkage between GeoWEPP, landuse text files and WEPP: a) GeoWEPP with legend descriptions; b) landcov.txt; c) WEPP/TOPAZ Translator.

6.7. Running GeoWEPP

The model used in this study works with the combination of two independent software products as discussed previously; WEPP Model Version 2008.907 and ArcGIS 9.1 and 10.1. These two software packages were linked via GeoWEPP for ArcGIS 9.x; an ArcView project that is one of the interfaces through which the WEPP model can be used. The GeoWEPP package for ArcGIS 9.x (available for free download at: http://www.geog.buffalo.edu/~rensch/geowepp/arc_index.html) includes two tools the Topographic Parameterization tool (TOPAZ) and TopWEPP software products developed by the United States Department of Agriculture-Agricultural Research Service (USDA-ARS). This section provides a step by step process for each of the GeoWEPP tools and how they work which were used in this simulation. It also explains all the steps in the simulation process including terminology.

(1) **Loading ASCII data**: First, GeoWEPP software was started and a project folder named "MOGRABA_15YGRND_CRTO09" created to store all the necessary files to run GeoWEPP.The next step was to load the GIS data to be used in GeoWEPP. The GIS dataset files below (Table 6.9) were loaded step by step in GeoWEPP:

Table 6.9: GIS datasets used for GeoWEPP simulation

Layer	GIS file
DEM	Dem.asc
Landuse	landcov.asc, landcov.txt, landusedb.txt
Soil	soilsmap.asc, soilsmap.txt, soilsdb.txt
Topo Image	Topo.tiff
UTM	utmzone.txt

(2) Once these files have been loaded, GeoWEPP converts the ASCII grid data into raster layers. Now, GeoWEPP has completed the loading process.

(3) **Modifying the Network and Creating the Watershed**: watersheds were examined to determine how well it matched the actual watershed shape using Channel Network Delineation tool in ArcGeoWEPP. Modifications to the MSCL, CSA (critical source area) and watershed outlet location were made in TOPAZ to generate the best fit watershed for study area with Watershed

Outlet Point tool. TOPAZ (Topographic Parameterization) mapped the topographic evolution, drainage identification, watershed segmentation and sub-catchment parameterization of watershed. This analysis was based on the application of the deterministic eight-neighbour (D8) method, the slope-of-steepest descent routing concept, and the critical source area (CSA) concept to simulate flow across the land surface represented by a raster (grid) digital elevation model (Garbrecht and Martz, 1997). Hillslopes and their slope profiles were explicitly defined and prepared for further characterization by TopWEPP.

(4) Now, the watershed areas have been generated and proceed for first WEPP simulation using Accept Watershed Delineation tool in ArcGeoWEPP.

(5) Then, the management and soil WEPP files were reviewed in the WEPP Management and Soil Lookup window. This window allows the GIS Land use and GIS Soil information to be compared with the corresponding WEPP management and soil data files to insure that they are assign properly.
(6) Once this was done, the WEPP/TOPAZ Translator window provides a last chance to change any of the parameters for the run.

GeoWEPP uses watershed and flow path methods to run the model simulation for watershed. The Watershed Method takes each hillslope in the sub-catchment, determines a representative profile for the hillslope and assigns one soil and one landuse to the hillslope. For each hillslope, GeoWEPP determines what the dominate soil or landuse is for that hillslope and assigns it to the profile. Once this is done, the WEPP simulation runs on each hillslope and the results are compiled.

The Flow path Method concentrates on each flow path within the sub-catchment. Unlike the Watershed Method, the slope used for the simulation is the slope for the flow path itself; there is no representative profile. Also, this method keeps the diversity and spatial distribution of the soil and land use layers. Each section of the flow path is assigned the soil and land use found in that section, thus a flow path can have a number of different soils and land uses in the simulation. When the simulation is complete, the results are compiled. The translation of land cover and soil types to hillslopes are done by TopWEPP, which uses grid-based information stored in the raster layers of land cover and soil type. The TopWEPP program executed the model runs using climate file and produced estimates of annual soil loss and deposition on the hillslope, sediment yield delivered from each hillslope, absolute soil loss and absolute sediment.

For this study, the flow path method was used because the watershed method only uses one soil and one management for each hillslope, thus the spatial variability in the study area is lost for these parameters. The flow path method retains the diversity of study area. The flow path method shows which portions of a particular hillslope are the main contributors to this problem rather than watershed method which shows *hillslopes* are the problem areas in the study site. Results are presented in Chapter 7.

Table 6.10: Modifications in model input parameters for different simulations.

Land caver /land use	**Topography**	**Precipitation**	**Scenarios No**
Vegetation change effect on soil erosion			
Landuse2009	Cartosat DEM	40yrIMD	01
Landuse2001	Cartosat DEM	40yrIMD	02
Landuse1989	Cartosat DEM	40yrIMD	03
Landuse1980	Cartosat DEM	40yrIMD	04
Landuse1972	Cartosat DEM	40yrIMD	05
Topographic effect on soil erosion			
Landuse2009	Cartosat DEM	40yrIMD	06
Landuse2009	ASTER DEM	40yrIMD	07
Landuse2009	Fill ASTER DEM	40yrIMD	08
Landuse2009	SRTM dem	40yrIMD	09
Rainfall effect on soil erosion			
Landuse2009	Cartosat DEM	15yrTRMM	10
Landuse2009	Cartosat DEM	15yrIMD	11
Landuse2009	Cartosat DEM	40yrIMD	12
Land cover mapping approach effect on soil erosion			
Land use 2009 maps (Automatic pixel based approach)	Cartosat DEM	40yrIMD	13
Land use 2009 maps (Direct integrated approach)	Cartosat DEM	40yrIMD	14

Chapter – 7

Assessment of soil erosion risk at the hillslope scale using the GeoWEPP model: Results

---

7.1. Introduction

The chapter is organised as follows. The first section discusses results for the runoff simulated under the different scenarios. In the second section, soil loss for the different scenarios such as the effects of land cover change, filed management setting, DEM resolution, rainfall and the effect of different land use land cover mapping approaches on soil loss is discussed. Finally, the estimated average annual soil loss for the study watersheds was grouped into different risk classes based on the minimum and maximum values. The spatial distribution of each class is then presented. Finally, limitations of the GeoWEPP model are discussed for the current application.

7.2. Runoff

Average annual runoff for Mograba, Loni and Salknapur watershed under scenario 1 (Table 7.1) are 9.80, 2.06 and 3.02 mm^3yr^{-1} respectively. The maximum predicted mean annual runoff is 21.1 mm^3y^{-1} for the Mograba watershed (under scenario 4) and the minimum runoff predicted is 1.05 mm^3y^{-1} (also in scenario 4). Estimated runoff varies in time and space depending on the individual slope profile, soil type, and land use/land cover of each hillslope. Moreover, even though the amount of runoff predicted is not substantially different, there is some variation in runoff patterns with vegetation change scenarios, DEMs resolution and satellite and ground based rainfall data. A summary of the average annual runoff with various scenarios and effects of land use/land cover types on runoff for selected watersheds in the Man River basin are shown in Table 7.1 and Figure 7.1.

Table: 7.1 Variation in runoff and mean annual soil loss for the all scenarios

Watershed		Mograba		Loni		Salkanpur	
	Scenario no	Mean annual runoff (mm^3yr^{-1})	Mean annual Soil loss $T.ha^{-1}$	Mean annual runoff ($mm^3.yr^{-1}$)	Mean annual Soil loss $T.ha^{-1}$	Mean annual runoff (mm^3yr^{-1})	Mean annual Soil loss $T.ha^{-1}$
Vegetation Change	01	9.80	35.1	2.06	12.6	3.02	15.6
	02	3.00	43.7	1.09	13.2	1.7	15.9
	03	2.32	34.4	3.56	12.4	0.9	11.5
	04	21.17	21.1	1.05	10.1	1.29	8.5
	05	21.07	21	2.67	12.4	1.12	7.8
Effect of DEMs	06	9.8	35.1	2.06	12.6	3.12	15.6
	07	10.17	41.7	1.09	17.7	2.64	27.5
	08	8.75	40.2	0.91	14.1	2.79	20.4
	09	11.6	31.1	1.25	4.2	7.69	7.7
Effect of rainfall	10	9.12	49.5	2.13	13.2	3.23	15
	11	9.8	33	2.3	12.1	3.02	14.8
	12	9.8	35.1	2.06	12.6	3.12	15.6

7.2.1. Effect of Land use/land cover on runoff

As described in Table 7.1 runoff varies with land use /land cover types in scenario 1 within the selected watersheds. The highest predicted mean annual runoff (0.65 mm^3yr^{-1}) occurs in agriculture land in the Salkanpur watershed. Forest land has the second highest runoff (0.48 mm^3yr^{-1}) in the Mograba watershed, while the lowest runoff (0.003 mm^3yr^{-1}) was recorded in the forest area within the Loni watershed. Although the annual average runoff values are different between scenario 5 (land use /land cover 1972) and 1 (land use/land cover 2009) in all three watershed, there is a 60.6 % increase in annual mean runoff under scenario 1 compared to scenario 5. This translates to a 34.91 % increase when it comes to soil loss (Table 7.1), highlighting the effect that land use change has had on the watersheds. The highest increase in runoff (78.87 %) was recorded within the Mograba watershed. These differences cannot be solely attributed to land use/land cover because other factors such as soil type and individual plot slope profile also play important roles in runoff generation.

7.2.2. Effects of DEM resolution and source on runoff

The effect of topographic resolution and source was assessed with scenario 6, 7, 8 and 9 for Mograba, Loni and Salkanpur watersheds as described in Table 7.1. The mean annual runoff for the Mograba and Salkanpur watersheds was higher (11.6 and 7.69 mm^3yr^{-1} respectively) with SRTM DEMs than the other

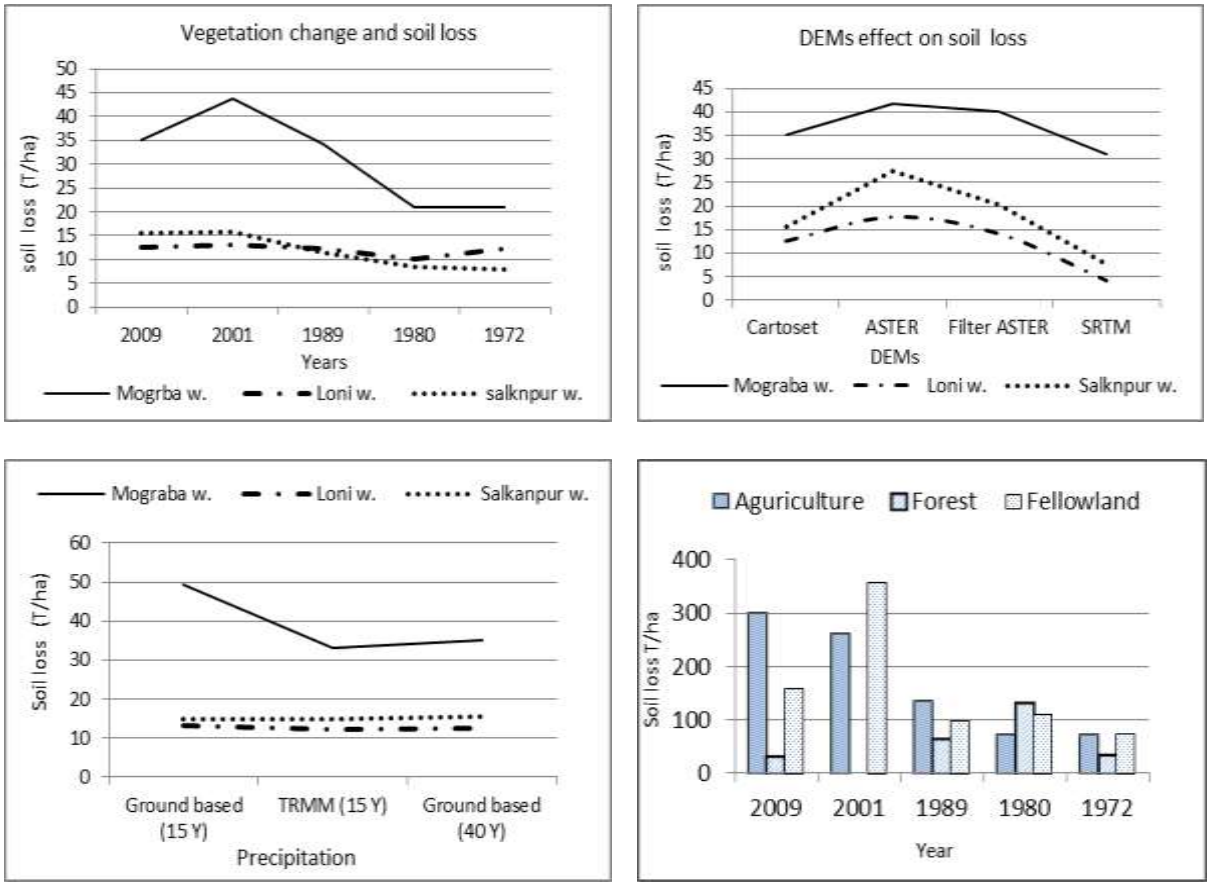

Figure: 7.1. (A) WEPP simulated annual hillslope soil loss with long term vegetation change scenario; (B) simulated soil loss with different DEMs; (C) Esimated soil loss with three diffrent set of precipitation and; (D) mean annual soil loss rate in each land cover.

three DEMs (Figure 7.1). There was not much difference in predicted runoff between the 30-m Cartoset, 30-m ASTER and 30-m filter ASTER DEMs in the Mograba and Salkanpur watersheds. The 90-m SRTM DEMs generated 1.25 (mm^3yr^{-1}) runoff, followed by the 30-m ASTER and filter ASTER DEMs for Loni watershed and the higher mean annual runoff 2.06 mm^3yr^{-1} was estimated with 30-m Cartoset DEMs.

7.2.3. Ground based and TRMM based rainfall effect on runoff

The mean annual runoff for all three rainfall scenarios is similar, but TRMM based runoff is slightly less than IMD based runoff because the hourly rainfall rate with TRMM data is lower than that estimated using IMD data.

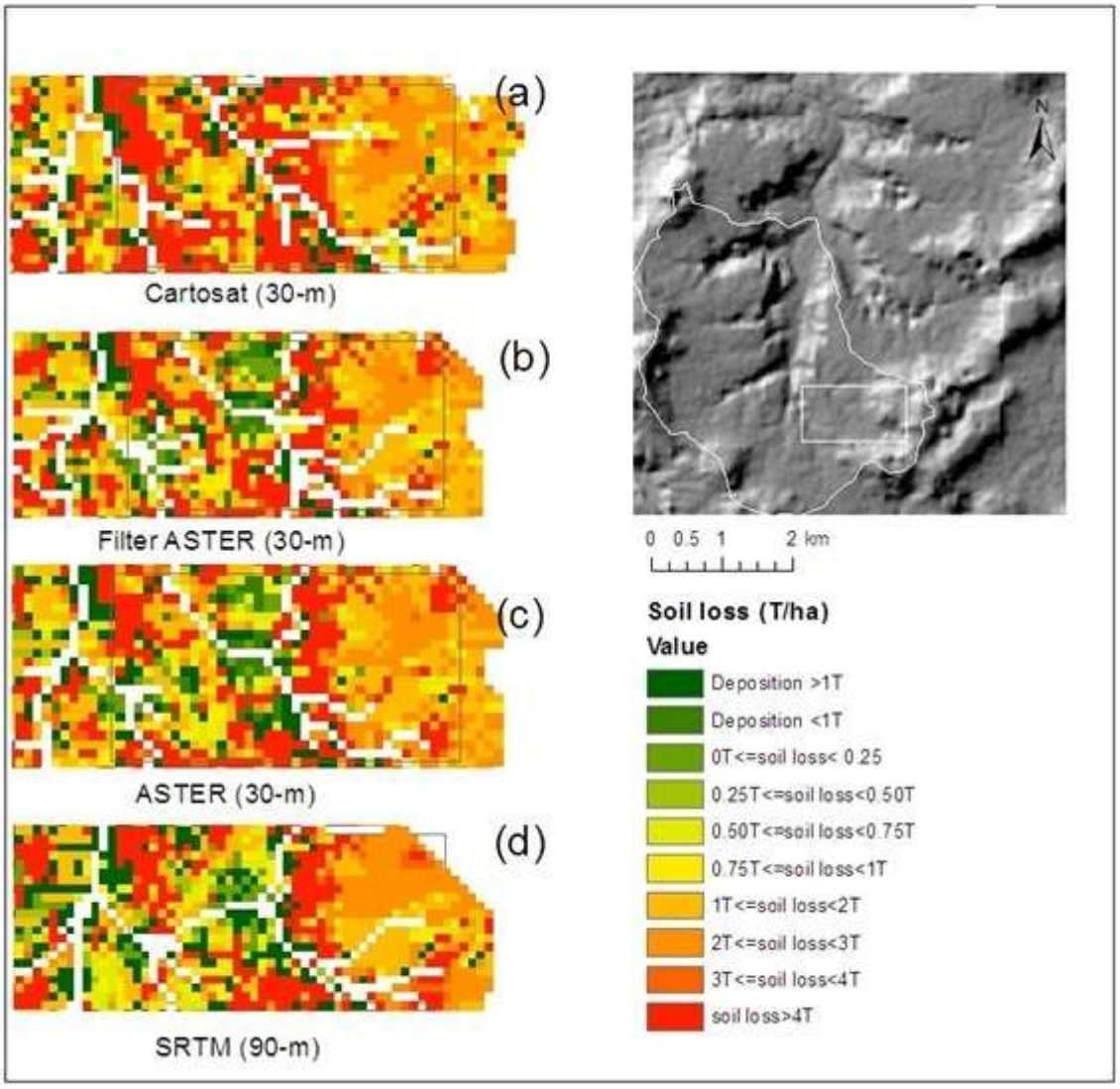

Figure 7.2. Effects of DEM resolution and source on soil erosion modelling.

7.2.4 Effect of land/use land cover mapping approach on runoff estimation

In this section, the outcomes of two different LULC mapping approaches (as GeoWEPP inputs) on runoff estimates were examined. LULC was mapped for all three watersheds using two different mapping approaches outlined in Chapter 4 and used as a model input to understand the effect on runoff and soil erosion (see Table 7.2). The mean annual runoff was higher for all three watersheds using the integrated wall to wall mapping approach compared to using the automatic pixel based approach.

The highest runoff difference was recorded in the Mograba watershed. The mean annual runoff increased by 9.8 mm to 48.7 mm^3yr^{-1}, by 2.06 mm to 6.07 mm^3yr^{-1} and by 2.3 mm to 4.05 $mm3.yr^{-1}$ respectively in the Mograba, Loni and Salkanpur watershed when LULC maps using integrated wall to wall mapping approach were used. The Mograba watershed experienced very large differences in runoff prediction with integrated wall to wall mapping approach. The comparative analysis results based on the two model outputs confirmed that LULC mapping approaches have had an impact on estimated surface runoff in the all three watersheds in the Man River basin.

Table 7.2. Effect of land use land cover mapping approach on estimated soil erosion

Mapping approach	**Minimum Mapping Unit**	**Watershed**	**Runoff Volume $mm^3.yr^{-1}$**	**Mean soil loss $T.ha^{-1}$**	**Total Soil loss $T.\ y^{-1}$**
Automatic pixel based approach	30mX30m	Mograba	9.8	35.1	21209.9
Integrated wall to wall mapping	1ha	Mograba	48.7	36.50	23157.9
Automatic pixel based approach	30mX30m	Loni	2.06	12.6	2217.3
Integrated wall to wall mapping	1ha	Loni	6.07	11.52	2132.7
Automatic pixel based approach	30mX30m	Salkanpur	2.3	15.67	2365.6
Integrated wall to wall mapping	1ha	Salkanpur	4.05	20.2	3091.8

7.3. Soil Loss

Average annual soil loss for the Mograba, Loni and Salkanpur watersheds under scenario 1 is 21209.9, 2217.3 and 2365.6 T, respectively; approximately 35.1, 12.6 and 15.6 $T.h^{-1}yr^{-1}$. The highest soil loss rate is 807 T ha^{-1}, predicted for an agriculture area in the Salkanpur watershed. The lowest soil loss rate is 2.1 Ty^{-1}, predicted to occur in forest land cover. Soil loss is generally highest in areas with agriculture and fallow land (Figure. 7.1). The soil loss trend with different land use/land covers is not similar. Soil erosion was most responsive with agriculture and fallow land and less active in forest area. The soil loss trend with long-term vegetation change scenario is similar among all three watersheds. Soil loss is much lower for the land cover in 1972 than recent estimates of land cover (2009). Results demonstrate that average annual soil loss has increased over the last four decades. WEPP simulated hydrological and erosion results using different sources and resolutions which generated varied topographic and hydrologic attributes, which in turn led to significantly different simulated erosion.

Table: 7.3. Effect of different land use/land cover types on runoff and soil loss.

Scenarios		**Mograba**		**Loni**		**Salkanpur**	
	Land use/ land cover	Average runoff (mm^3y^{-1})	Average soil loss ($T.ha^{-1}.y^{-1}$)	Average runoff ($mm^3 yr^{-1}$)	Average Soil loss ($T.h^{-1}y^{-1}$)	Average runoff ($mm^3 yr^{-1}$)	Average soil loss ($T.h^{-1}y^{-1}$)
Scenarios 1 (Year 2009)	Agriculture	0.434	87.67	0.472	9.3	0.659	807.2
	Forest	0.488	64.80	0.003	2.1	---	---
	Fallow land	---	---	0.085	26.37	0.006	291.3
	Other	---	---	---	---	0.036	10
Scenarios 2 (year 2001)	Agriculture	0.207	86.43	0.431	9.70	0.759	691.7
	Forest	0.604	4.05	0.002	5.1	0.007	7.5
	Fallow land	0.100	272.8	0.128	23.9	0.064	773.4
	Other	---	---	---	---	0.011	9.1
Scenarios 3 (Year 1989)	Agriculture	0.159	60.81	0.506	8.12	0.273	340.9
	Forest	0.546	1.7	0.002	5.7	0.111	187.9
	Fallow land	0.336	151.31	0.032	24.23	0.253	2470.1
	Other	---	---	---	---	---	---
Scenarios 4 (Year 1980)	Agriculture	0.096	120.3	0.118	2.69	0.126	97.1
	Forest	0.855	17.95	0.175	2.8	0.307	374.5
	Fallow land	0.011	31.25	0.173	27	0.050	276.6
	Other	---	---	---	---	0.004	4.1
Scenarios 5 (year 1972)	Agriculture	0.088	123.19	0.373	4.55	0.112	88.1
	Forest	9.898	36.32	0.052	3.35	0.263	69.5
	Fallow land	0.006	3.2	0.085	44.49	0.135	2596.1

Note: Presented figures of runoff and soil loss in the table are based on the watershed method. The watershed method takes each hillslope in the sub-catchment, determines a representative profile for the hillslope and assigns one soil and one land use to the hillslope. The method does not keep the diversity and spatial distribution of the soil and landuse layers.

7.3.1. Land use/land cover effect on soil loss

The average rates of soil loss in agricultural, forest and fallow land plots for all three watersheds are 301.39, 33.05 and 158.83 Tha^{-1}, respectively. Table 7.3 shows these differences, as well as the effects of long term land use/land cover on soil loss.

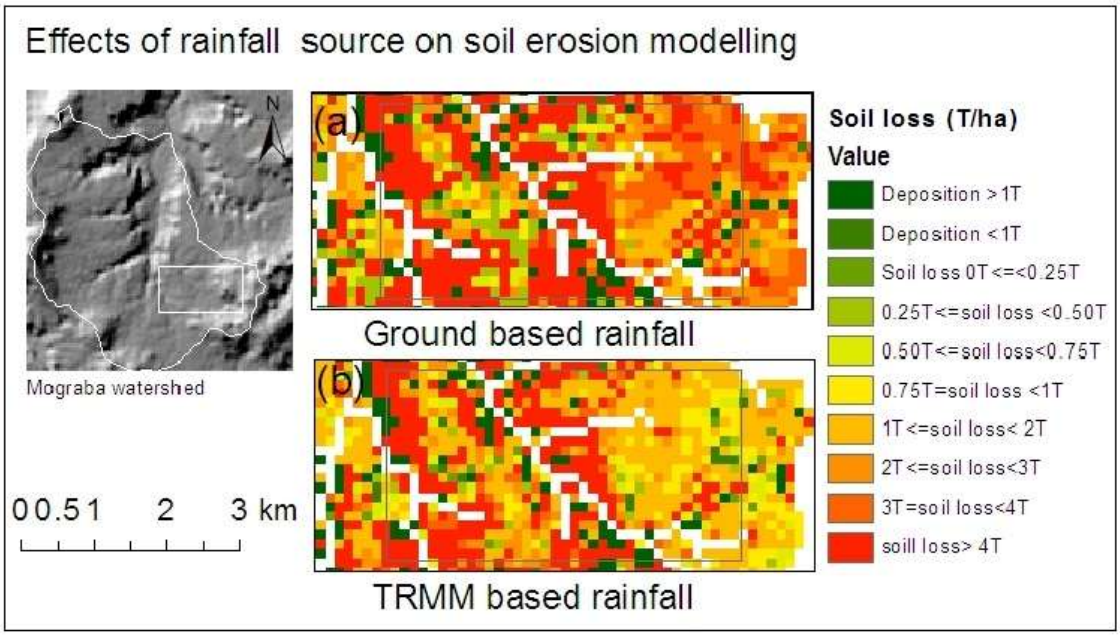

Figure: 7.3. Effects of rainfall source on soil erosion modelling.

7.3.2. Land use and/land cover change and soil loss

As shown in Table 7.1 and Figure 7.1 the effect of long-term land use/land cover change on soil loss is comparable. Results show that the average annual soil loss is lower in 1972, but since then an increasing trend of rate of soil loss is recorded similarly in all three watersheds in light of recent land use /land cover

scenarios. The average annual soil loss rates for Mograba, Loni and Salkanpur in 1972 are 12716.4 T, 2178.2 T and 1192.1 T respectively, while those under the present land cover are 21209.9 T, 2217.3 T and 2365.6 T respectively. Hence soil loss increased by 40%, 1.7% and 49.6 % respectively. The highest soil loss was recorded under the 2001 land use/land cover for all three watersheds.

The land use/land cover change statics for all three watersheds illustrate the dramatic decrease in scrub forest, dense forest and open forest and the equally dramatic increase in agricultural land. The forest land in Mograba, Loni and Salkanpur watershed decreased 22.2 %, 5.5% and 56.5 % respectively whilst the area of agriculture increased 36.9 %, 0.2 % and 61.4 % respectively over the last four decades.

The analysed changes in soil erosion rate and land use from 1972 to 2009 highlight the relationship between soil erosion and land use. Table 7.3 shows that from 1972 to 2009, the average soil loss rate changed as the vegetation scenario changed with each land use type. Soil erosion rate in agricultural land increased in the Loni and Salkanpur watersheds which contain mostly agriculture, but it decreased slightly in the Mograba watershed. Agricultural land caused more soil erosion due to its increased area (32.8 %) in the period in all three watersheds. The erosion rate in the forest land changed from a low erosion rate to a high one in the Mograba watershed. It was 36.3 $T.ha^{-1}y^{-1}$ in 1972 and 87.6 $T.ha^{-1}y^{-1}$ in 2009. The average soil erosion rate in forested areas is lower than other land uses/ land covers. The largest increase in soil erosion occurred where forestland was converted to fallow land and agricultural land.

Results for fallow land demonstrated similar trends to those in forestland in the Mograba watershed, but the erosion rate decreased in the Loni and Salkanpur watersheds with fallow land. Thus, statistical results show different land use types have a greater impact on soil erosion. Changing forest to agricultural land promoted soil erosion increasing to as high 288.3 Tha^{-1}, while modifying forest land to fallow land produced an increase in average annual soil erosion amount of 125.8 Tha^{-1}.

7.3.3. DEM's effect on soil loss

The different DEMs resulted in slightly different watershed areas and considerably different numbers of hillslopes and channels as show in Table 7.4 The average annual soil loss rate for the Mograba, Loni and Salkanpur watershed using the Carotset DEMs is 35.1, 12.6 and 15.6 $T.ha^{-1}$ respectively. The average slope in the Mograba watershed increased from 6.88 to 7.04 degrees when the resolution was the upgraded from SRTM 90 –m to Cartosat 30-m. Likewise, a similar trend was found in the Loni and

Salkunpur watersheds where average slope increased 1.15 degrees and 1.23 degrees respectively as DEM resolution was increased. However, even when holding the resolution constant, DEMs from different sources produced varied slope statics in all three watersheds. For the 30-m DEMs, the ASTER DEM had the highest average slope, followed by the filter ASTER and the Cartosat DEM. The Cartosat DEM had a smaller average slope and the lowest standard deviation compared with the ASTER DEM and the filter ASTER DEM.

Table: 7.4: Slope statistics for Watersheds [a]

	Mograba				**Loni**				**Salknpur**			
	Carto DEM	ASTER	Filtr ASTER	SRTM	CartoDEM	ASTER	Filter ASTER	SRTM	Carto DEM	ASTER	Filter ASTER	SRTM
Average slope	7.04	8.5	8.3	6.8	2.5	4.57	3.64	1.35	2.67	4.4	3.52	1.44
Standard deviation	5.98	7.3	7.42	5.8	1.76	2.97	2.9	1.1	1.91	2.81	2.71	1.08
Minimum slope	2.85	2.93	2.77	2.2	0.98	2.49	0.93	0.7	0.98	2.1	0.96	0.6
Maximum slope	40.3	37.2	37.2	26.7	13.9	26.5	26.5	6	12.6	22.3	18.9	5.68
erosion t/ha/yr	35.1	41.7	40.2	31.8	12.6	17.7	14.1	4.2	15.6	27.5	20.4	7.75

[a] ArcGIS 10 was used to compute slopes from DEMs.

The soil erosion rate estimated with 30 m Catrtosat and 90 –m SRTM DEMs was found to be comparable to similar studies carried out in this region (Tamgadge et al., 2001). This study was carried out to produce soil erosion maps at the regional scale by the National Bureau of Soil Survey and Land Use Planning (NBSS & LUP), India using the USLE soil erosion model.

Table 7.5: GeoWEPP determined watershed configuration and WEPP simulated watershed discharge and erosion for the study watersheds

Watershed	**DEMs**	**Area (ha)**	**No of Hillslopes**	**No of channels**	**Discharge Volume (m^3)**	**Erosion ($T.ha^{-1}y^{-1}$)**
Mograba	Cartosat 30 m	603.3	288	121	13123176.8	35.15
	ASTER 30 m	603.3	199	82	9883589.4	41.75
	Fill ASTER 30	588.3	268	118	13727169.4	40.28
	SRTM 90 m	604.8	236	114	10489360	31.84
Loni	Cartosat 30 m	177.54	33	13	2212727.4	12.67
	ASTER 30 m	149.03	46	18	2265652.3	17.77
	Fill ASTER 30	143.3	48	19	2460598.1	14.14
	SRTM 90 m	135.43	34	15	2912721.7	4.24
Salkanpur	Cartosat 30 m	152.62	96	39	6382735.2	15.67
	ASTER 30 m	166.06	78	31	5408587.9	27.56
	Fill Aster 30 m	166.6	77	31	5329310	20.47
	SRTM 90 m	140.6	116	48	5408587.9	7.75

7.3.4. Ground based and TRMM based rainfall effect on soil loss

Estimated hillslope soil loss rate in all three study watersheds under the TRMM based rainfall datasets is predicted to be less than in the IMD based rainfall datasets (Table 7.1 and Figure 7.1, 7.3). The annual average hillslope soil loss rate for the Mograba, Loni and Salkanpur watersheds is 33.0, 12.1 and 14.8 Tha^{-1} respectively under 15 year TRMM based rainfall datasets; this is 33.5%, 8.3% and 12% less than reported under 15 year ground based rainfall respectively.

There may be several reasons for this difference as follows: i) The TRMM rainfall intensities are too low to generate surface runoff compared with the ground based rainfall. ii) The number of wet days is higher in TRMM rainfall with a consequence that there is a lower rain rate which in turn produced less runoff and soil erosion than ground based rainfall. iii) The pattern of effect of ground and remote sensing rainfall data on soil erosion in the Loni and Salkanpur watershed is quite similar, rather than in the Mograba watershed.

7.3.5 Effect of land use land cover mapping approach on soil loss and uncertainty analysis of soil erosion

The uncertainty in the land use/land cover maps in all three watersheds and evolution of uncertainty in the modelled erosion rates are addressed in this section. The outcomes of soil erosion rate with both land use/land cover mapping approach has a significant impact on modelled soil erosion rates. As shown in Table 7.2, the effect of both LULC mapping approach (as a GeoWEPP input) on soil loss is comparable. Results show that the average annual soil loss is higher with the integrated wall to wall mapping approach (1 ha MMU) in the Mograba and Salkanpur watersheds compared to the updated automatic pixel based approach (30X30m). However the opposite trend was found in the Loni watershed. The results are presented here for each watershed explaining how both mapping approaches produce different land covers which then effect soil erosion in the study areas.

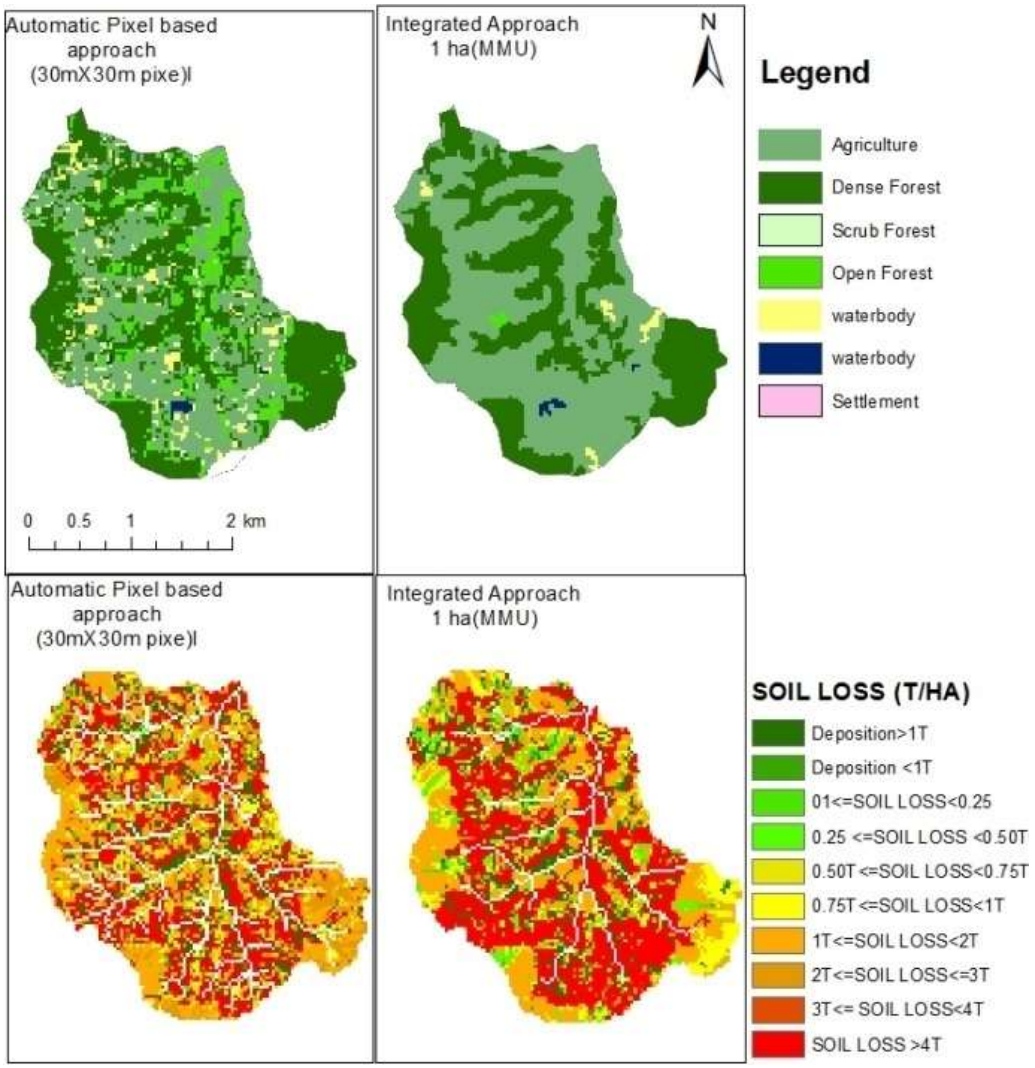

Figure 7.4 Effects of two different LULC mapping approaches on soil erosion in the Mograba Watershed. The upper images are land cover maps produced by two different mapping approaches. Their effect on soil loss is shown in the two images below.

Mograba Watershed: The average annual soil loss in the Mograba watershed was 36.5 T/ha with the integrated approach, while the pixel based approach predicted 35.1 T/ha. The mean 1.4 T/ha annual average soil loss increased when land cover maps were updated using the integrated approach (1 ha MMU). The large difference in the land use and land cover areas with both mapping approaches may be one of the significant causes for differences in estimated soil erosion. Agricultural land increased (111 ha) while forest land decreased (123 ha) in the Mograba watershed when automatic pixel based approach was updated using the integrated (1 ha MMU Approach).

Salkanpur Watershed: The average annual soil loss also increased in the Salkanpur watershed from 15.6 to 20.2 T/ha when land use input data for GeoWEPP was upgraded using the integrated mapping

approach. As show in Figure 7.5 fallow land area increased from 12.8 ha to 17.8 ha when the land cover map was updated using the integrated approach. The increase in fallow land is one of the factors responsible for increased soil erosion in the study area. There are two likely causes for this. First, forest area plays a significant role inprotecting soil from erosion which was mapped at 6 ha using the automatic pixel based approach, butforest area decreased to 0 ha when it was mapped using the integrated approach and fed into the soil erosion modeling. Secondly, agriculture land increased by 4 ha when the land cover map was updated using the integrated approach, which also promoted soil erosion.

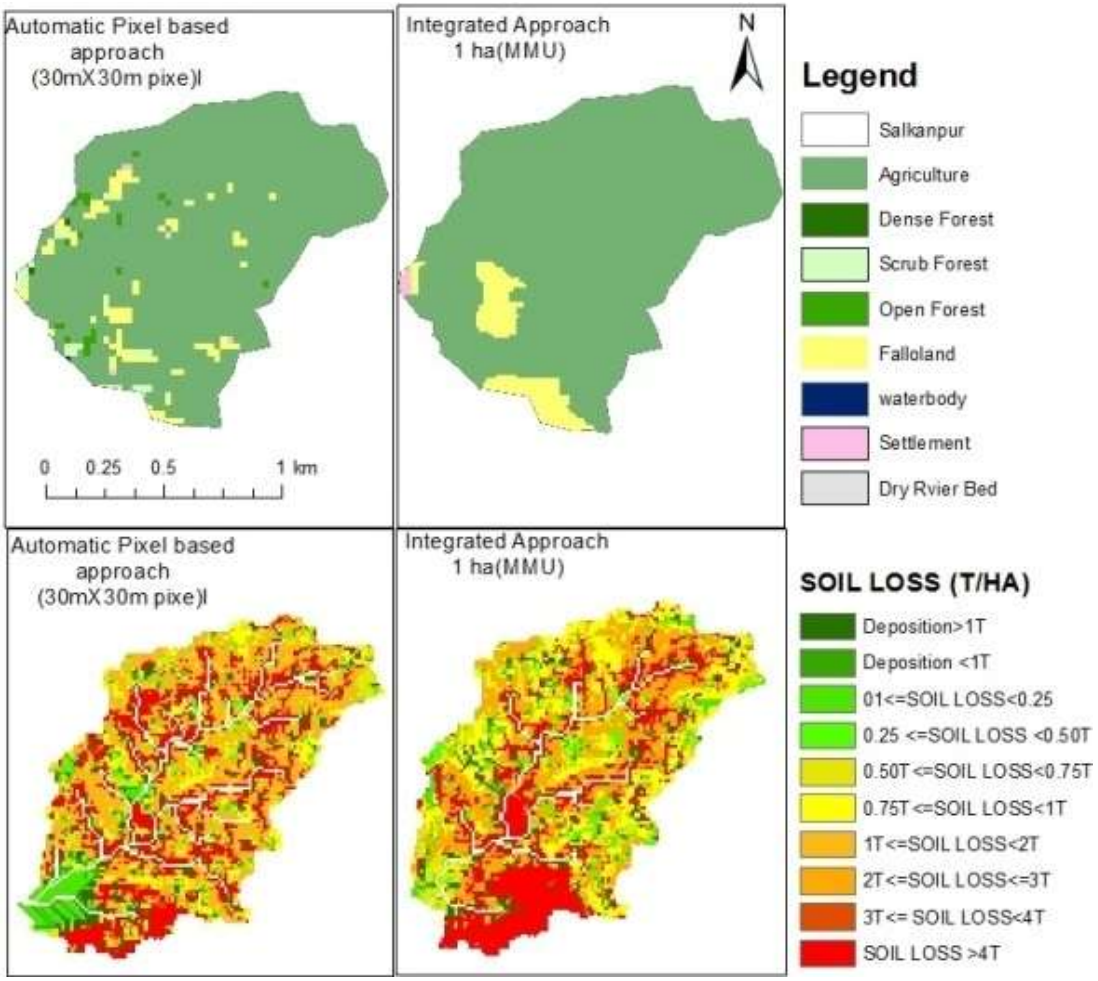

Figure 7.5 Effects of two different LULC mapping approaches on soil erosion in the Salkanpur Watershed.

Loni Watershed: The average annual soil loss decreased (by 1.1 T/ha) in the Loni watershed when land use input produced by the integrated approach was applied. The comparative analysis of land use/land cover of both mapping approaches for the Loni watershed shows that agricultural land increased by 22 %, while forest land decreased by 16 % when land cover was mapped by the integrated approach; the

different estimates have a significant effect on runoff as shown in Table 7.2, but only a very small effect on the predicted soil erosion. Results also demonstrate that average annual soil loss in the Loni watershed is lower compared to the other two watersheds in the Man basin. The average annual soil loss in the Loni watershed is 12.6 T/ha while it is 35 and 15.6 T/ha in the Mograba and Salkanpur watershed respectively. Thus soil erosion is less active in this watershed compared, which means that land use inputs provided by two different approaches do not make a large difference in soil loss variability in the watershed.

The estimated annual average soil erosion using the integrated wall to wall mapping (as a land use land cover input for GeoWEPP) for all three watersheds in the basin is relatively high (22.7 $T.ha^{-1}$) compared to reported values obtained with the pixel based approach (21 $T.ha^{-1}$). The estimate produced in this study is higher than estimated by Tamgadge et al., (2001) (5-10 $T.ha^{-1}$) using the Universal Soil Loss Equation Model, but similar to that estimated by Sing et al., (1992) (21 $T.ha^{-1}yr^{1}$).

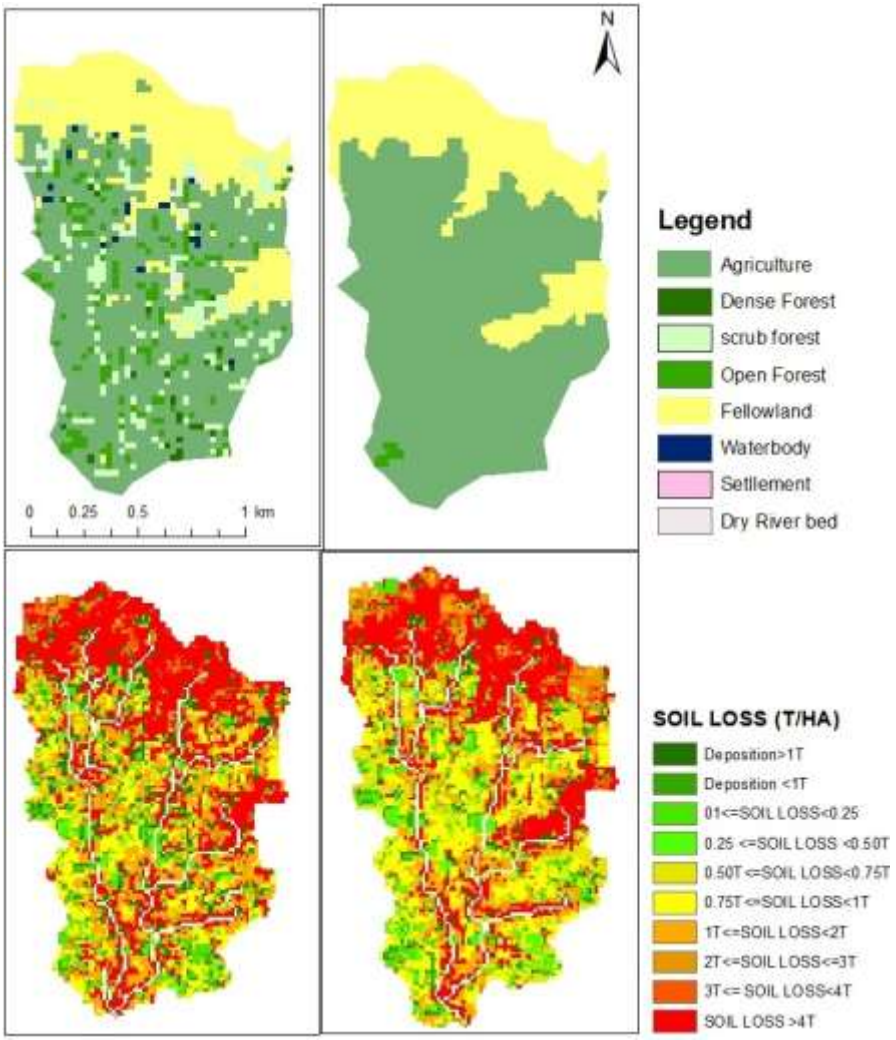

Figure 7.6 Effects of two different LULC mapping approaches on soil erosion in the Loni Watershed.

This example shows that the choice of Minimum Mapping Unit for preparing land use land cover maps as an input for GeoWEPP model has a significant effect on runoff and soil loss estimation in the study area. Land use land cover classification maps using the integrated wall to wall mapping approach with one hectare Minimum Mapping Unit omitted a large number of small areas (30mX30m pixels) of forest, scrub and open forest in the watersheds which has a significant impact on runoff and soil loss. These omitted forest cover areas accumulated to make a small amount of differences (1-5 $Tha^{-1}yr^{1}$) in soil erosion estimation when it is used as input information for the soil erosion model in all three watersheds.

A larger impact was seen on the amount of runoff, which increased from 9.8 $mm^{3}yr^{1}$ to 48.7 $mm^{3}yr^{1}$ in the Mograba watershed when land use/land cover classification maps (using the integrated wall to wall mapping approach) was used as an input for GeoWEPP. Differnces in estimated runoff were smaller in the other two watersheds. The Mograba watershed is located in a hilly region which has a very high slope area. This may be a significant attribute for increasing runoff in the watershed, but dense forest cover on the hillslopes plays an important role in protecting the surface from soil erosion.

7.4. Soil erosion risk assessment

It is important to understand the estimated soil loss as an indicator of erosion risk for prioritizing and programming conservation interventions. Therefore, the soil erosion outputs were translated into risk categories that can be used by local formers and policy makers. The assessed average annual soil loss of the study watersheds was grouped into different risk classes based on the minimum and maximum values of soil loss (Low 0-1 Tha^{-1}, Moderate 1-4 Tha^{-1} and High more than 4 Tha^{-1}) to assess erosion risk in the study areas. The spatial distribution of each class is presented in Figure 7.4. Historical erosion risk from year 1972 to 2009 was assessed by combining vegetation cover for all three watersheds as shown in Table 7.5.

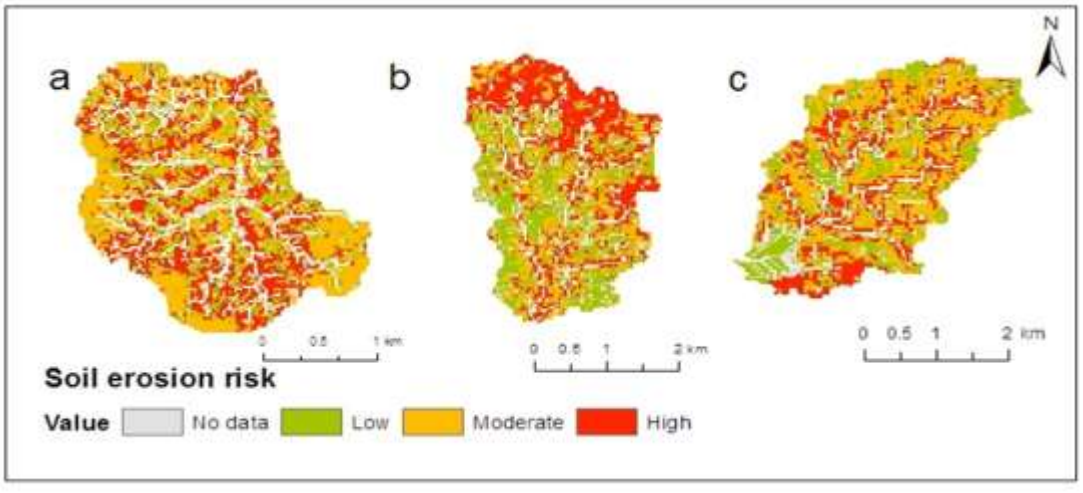

Figure: 7.7: Soil erosion risk maps for (a) Mograba, (b) Loni , and Salkunpur watersheds.

Soil erosion risk trends are different in each selected watershed. In the Mograba watershed, high and low erosion risk areas have increased 5.86% and 5.98%, respectively in last four decades. At the same time the moderate soil erosion risk area decreased by 14.82%. These results can be correlated with vegetation change which shows a 63.9% increase in agricultural land, which in turn indicates that the area at risk of high erosion has increased over the years. Most of the moderate erosion risk area is under forest land and has decreased; there has been a 22.2% reduction in forest land between year 1972 and 2009.

Soil erosion risk areas mapped in the Loni watershed are 33 % high, 26.5 % moderate and 27% low erosion risk with land cove/land use from 2009. Recently, moderate and high erosion risk areas were estimated as 4% lower in year 1972. Increased fallow land and decreased forest area play a significant role in producing high erosion risk in the upper parts of the Loni watershed.

The assessed erosion risk areas are 25.71%, 39.8% and 25.5% for low, moderate and high erosion risk respectively in the Salknpur watershed. The high erosion risk area was 46.4 ha in 1972, but it was recorded as highest (65.2 ha) in 1989. The moderate erosion risk noted a continuous increasing trend. It was 22.1, 34.1, 52.3 and 60.3 ha in year 1972, 1989, 2001 and 2009, respectively. In total there was a 25.5 % increase in the area experiencing moderate erosion risk. The low erosion risk area decreased 14.4 % over the last four decades. The increased 61.3 % of agricultural land and 48.9 % loss of forest has a strong relationship with erosion risk in the Salknpur watershed.

Table 7.6: Soil erosion severity zones with area covered.

Erosion risk grade	**2009**		**2001**		**1989**		**1980**		**1972**	
	Area (ha)	%	Area (ha)	%	Area (ha)	%	Area (ha)	%	Area (ha)	%
					Mograba watershed					
Low	98.64	16.33	88.5	14.67	87.12	14.42	44.2	7.33	62.5	10.35
Moderate	146	24.18	231	38.25	249.6	41.34	218.7	36.21	235.5	39
High	287.1	47.54	214	35.55	203	33.62	297.5	49.26	252	41.86
					Loni Watershed					
Low	48.86	27.87	44.2	25.24	60.76	34.66	35.1	20.02	67.3	38.39
Moderate	46.45	26.5	43.1	24.61	41.14	23.74	50.3	28.73	39.16	22.34
High	57.91	33.03	66.3	37.87	55.62	31.73	66.7	38.07	50.54	28.83
					SalknpurWaterhed					
Low	38.94	25.71	33.5	22.13	28.6	18.93	41.9	27.71	61.9	40.12
Moderate	60.3	39.84	52.3	34.59	34.13	22.53	39.23	25.9	22.1	14.37
High	38.5	25.43	49.4	32.63	65.22	43.06	49.79	32.87	46.4	30.07

7.5. Privatization of soil erosion risk areas

Soil erosion risk categories are discussed for prioritization and programming conservation interventions.

7.5.1. Areas of high soil erosion risk

A large percentage of land is recorded in the high erosion risk category in all three watersheds. This category covers 47.5%, 33% and 25.4% (287 ha, 57.9 ha and 38.5 ha) areas respectively in the Mograba, Loni and Salkanpur watersheds (Table 7.6).

In the Mograba watershed, agriculture is the dominant land use system in the high erosion risk areas. This watershed is characterised by steep slopes. Soil texture quality is also poor in high erosion risk areas (sand -62%). Similarly, in the Salkanpur watershed, most areas of high erosion risk are extended in the agricultural land with steep slopes. These environmental conditions have the potential for production of high surface runoff and massive soil loss in the watersheds. Therefore, soil conservation and management options should be devised to protect soil from the impact of heavy monsoon rainfall, increasing surface roughness to reduce the velocity of runoff and soil erosion and improving the quality of soil. Agronomic and mechanical soil conservation measures are potential land management options that could be used to reduce the high soil erosion risk in these watersheds. Particularly, the development of agro-forestry systems in agricultural land use to reduce the effects of heavy rainfall and maintain soil fertility, construction of check dams and planting of vegetation to protect gully areas and terracing and contour ploughing on areas of steeply sloping cultivated land are recommended in the Mograba and Salkanpur watersheds.

In the Loni watershed, most areas of high erosion risk are extended in the fallow land category in the upper part of the watershed (Figure 7.7). Poor soil texture (loamy sand) and thin soil depths (2-6 inches) provide an ideal environment for high erosion risk in this particular zone. High risk areas are also characterised by steep slopes. Therefore, intensive soil conservation and management are a necessary requirement for these high erosion risk areas. Planting of grasses and shrubs on steep slopes and areas of thin soil cover, construction of hillside ditches for storm water diversion, terracing, contour ploughing and agro-forestry systems are suggested to reduce the high soil erosion risk in the Loni watershed.

7.5.2. Areas of moderate soil erosion risk

The total area that falls under moderate soil erosion risk category is 24 %, 26.5%, and 39.8% (146 ha, 46.4 ha, and 60.3 ha) respectively in the Mograba, Loni and Salkanpur watersheds.

Moderately vulnerable areas of soil erosion risk are found in the forest land cover category in the Mograba watershed which is characterised by isolated hills with very steep slopes. However, forest land is the major land cover in this risk area which has a generally low erosion rate but with very steep slopes and poor soil texture quality which contributes to produce very high runoff and moderate soil erosion in these areas. Managers need to carefully evaluate harvesting impacts, site preparation disturbances, amount of trees removed, and fire factors to manage soil erosion in the forest land. Improving vegetation cover through afforestation, construction of stone bunds and check dams would be some of the recommended soil erosion conservation measures in the Mograba watershed.

In the Loni and Salkanpur watershed, agriculture is the dominant land use system in the moderate soil erosion risk areas. Topographically, these areas are characterized by average slopes of 2.5 degrees and relatively low drainage density. Black rich soil (clay) also helps protect soils from heavy rainfall. However, the cultivated land is the major land use system which maintains a soil erosion rate between 1-4 Tha^{-1}. A combination of mechanical and agronomic land management strategies such as grass strips, contour ploughing and agro-forestry would be suitable for these areas to reduce soil erosion, preserve the fertility of the soil and maximize the productivity level of the watershed.

7.5.1. Areas of low soil erosion risk

Only 16.3 % (98 ha) are categorized as low erosion risk in the Mograba watershed and 27.8% (48.8 ha) and 25.7 % (38.9 ha) respectively in the Loni and Salkanpur watersheds with soil erosion rates between 0-1 $Tha^{-1.}$ Farming is the major land use system in this soil erosion risk category in all three watersheds. Land management practices such as agro-forestry would be suggested to maximize the productivity level in the low risk areas. The predicted soil erosion rate using the GeoWEPP interface is found to be similar to other studies carried out in this region that calculated soil erosion using the universal soil loss equation (USLE) (Tamgadge et al., 2001).

The spatial pattern of classified soil erosion risk zones indicates that the areas with high erosion risk are located in the agriculture land, while the areas with low erosion risk are in the forest land of the study area. The spatial pattern of annual average soil erosion risk map shows a strong spatial correlation with land cover. It indicates that the agriculture activities in the watershed appear to play a significant role in producing high soil erosion risk. Therefore, it is the agriculture land cover areas that need to be studied in more detail if soil erosion is to be reduced in future. The area of dense forest shows a lower level of erosion risk suggesting that forest land can effectively increase the vegetation coverage and help control soil erosion.

7.5. Conclusion

Soil erosion prediction by simulation models is a useful approach for studying the vulnerability of landscapes to erosion and assessing the effectiveness and feasibility of different aspects of land use/land cover, landscape dynamics and the impact of resolution and sources of data. A quantitative assessment of runoff and soil loss for the Mograba, Loni and Salknpur watersheds located in the Man River basin was made using the GeoWEPP soil erosion model that uses rainfall, soil, land use and topographic datasets. The research study developed a realistic estimate of the expected runoff and soil loss with detailed information on the physical relationship of vegetation, topography, climate and soil. The results show that runoff fluxes and soil loss vary with land use/land cover, long term land use/land cover change, DEM resolution and ground and satellite based rainfall data. In the present land use/land cover, the high runoff areas were dominated by agricultural land with an average runoff of 0.521 mm^3y^{-1} for all three watersheds. The highest runoff for different DEMs was also found in agricultural land, with an average 0.532 mm^3y^{-1} generated by the filtered ASTER DEM. Long–term land use/land cover change affected runoff considerably. Average runoff reported was 4.99, 1.93, 2.26, 1.57 and 1.57 mm^3y^{-1} for 2009, 2001, 1980, 1989 and 1972, respectively. The ground based rainfall produced slightly higher runoff (5.11 mm^3y^{-1}) than TRMM based rainfall (4.74 $mm^3y)^{-1}$.

The output of soil loss had similar trends to those in runoff. The average annual soil loss for all three watersheds with long–term vegetation change scenarios was 21.1, 24.26, 19.43, 13.23 and 13.73 Tha^{-1}, respectively. The highest soil loss rates occurred in agricultural and fallow land areas, while the lowest rates were observed in forested areas. In the study area, increased agriculture land in last four decades is one of the significant causes that has increased the rate of soil erosion. The higher soil loss was recorded using the 30-m ASTER DEM. The Cartoset and SRTM DEMs produced 21.1 and 14.33 Tha^{-1} of soil loss respectively, similar to previously published research. The 15 year ground based rainfall data generated 5.94 Tha^{-1} soil loss, more than 15 year TRMM based rainfall datasets.

The generation of soil erosion risk maps assists the visualization of the erosion process at a range of spatial and temporal scales in the study area. The spatial pattern of erosion risk indicates that areas with forest cover have minimum rates of soil erosion, while areas with extensive human intervention such as agriculture and fallow land have high estimated rates of soil erosion. The estimated amount of soil loss and its spatial distribution can provide a basis for comprehensive management and sustainable land use for the watershed. The areas with high levels of soil erosion warrant special priority for the effective conservation and management in the study area.

Thus, a simulation model like GeoWEPP is a useful approach for assessing spatially distributed soil erosion patterns and assisting practical decision making for land use and land cover management practices. The GeoWEPP approach allowed a straight forward model setup to undertake modelling for large and more complex watershed simulations, by utilising digital elevation data and other land use /land cover and soil GIS data layers that can be automatically processed to create the watershed structure and slope inputs. Other geospatial data can provide soil and land use information. The community of international users of geospatial WEPP applications is continuously increasing because GeoWEPP enables them to use their own data formats and standards that are different from the U.S.

Although GeoWEPP is easy to setup and run for particular types of users (e.g., foresters, ranchers, and farmers in the tropical region like Man River basin), further work is needed to be able to customize the applications for users with more specific scenario building capabilities. For instance ;inking the desktop GeoWEPP and the web-based WEPP GIS could allow users to more easily prepare data inputs on a server, download the input datasets locally, and then use GeoWEPP to further customize the scenario input data to run the core WEPP model on a desktop.

Chapter – 8

Modelling the impact of land use land cover change on soil erosion risk using remote sensing: Discussion and conclusion

---

8.1. Introduction

Various techniques for mapping and verifying vegetation change based on remote sensing and GIS have been developed which have enhanced the efficiency of such techniques (Teferi et al. 2013; Berberoglu and Akin, 2009; Lu et al., 2004). The scientific literature continues to highlight the key difficulties associated with mapping, reporting and verifying land use/land cover change accurately and identifying mechanism responsible for this change (Manandhar et al., 2010; Wertz-Kanounnikoff, 2008). Any approach that uses satellite imagery to map land use/land cover change should provide detailed information on the intensity of the LULC transactions, drivers of change, and estimate error (uncertainty analysis) (Olofsson et al., 2013). In addition, many studies demonstrate difficulties in mapping accurate delineation of forest change and forest degradation areas, especially in terms of understanding mechanisms which are responsible for this change. The current study developed an integrated approach to overcome these issues to undertake reliable change mapping and estimate uncertainty. Further, the land use information was linked through the GeoWEPP model, within the RS and GIS environment, to explore relationships between soil erosion risk and LULC distribution and change pattern. In this chapter I discuss the reliability and consistency of the approach taken and outline future recommendations on following points:

1. Accuracy assessment of LULC and area estimation of deforestation area using uncertainty analysis.
2. Understanding land use and land cover dynamics and the associated change drivers.
3. Modelling the impact of land use/land cover on soil erosion risk using GeoWEPP.

8.2. Accuracy assessment of LULC and area estimation of deforestation area using uncertainty analysis

The confusion matrix used in accuracy assessment provides information on the magnitude of the classification errors that allows an adjustment to be made in the area estimator. This method enhances the

use of the accuracy assessment data and leads to better estimates of deforestation area, accuracy and the uncertainty associated with these estimates. The quality of land use/land cover mapping based on Landsat imagery is of a good standard. The prevalence statistic is a good measure of overall correspondence between the map and reference data.

The method used for accuracy assessment in the study followed the recommendations set out in the GOFC- GOLD guidelines to help identify and quantify uncertainty in the LULC and deforestation area estimation in the study basin over the period 2009 to 2013. Overall, 2324 samples were measured, which covers 6.3% of the total study area. This is a good sample size which covers a sufficient area for validation. The number of samples and area covered is in line with existing published research. Random samples were selected according to land use/land cover classes which provided proper area representation for each land cover class. The sample size less than one hectare (30mX30m)was found satisfactory to identify map and reference quality, but it is suggested that increased size of sample circle (around one hectare) would enhance the quality of accuracy assessment. The analysis of rechecking of some samples that were incorrectly allocated indicated that the presence of trees along boundaries of fields resulted in areas of agriculture being mistakenly classified as forest by Landsat 30 meter imagery. The small size of agricultural fields along tree lines created confusion for land cover classification and it was not possible to map these precisely using 30 m spectral pixels (Figure 8.1). A high number of pixels were classified as fallow land (around 2%) although more detailed investigation found agricultural land present in some of these pixels. It is important to understand the incorrect classification of fallow land (as agricultural land) because agricultural extensification is one of the major issues in the region, but also a high percentage error with the fallow land class directly impacts on the land surface change mapping. After rechecking these samples it was found that most agricultural land areas were cropless (bare) and located on the hill areas, resulting in the classification as fallow land in the Landsat classification. The reason behind this error is that all Landsat scenes used in this study were captured during the winter period and cultivation during this season depends on irrigation facilities. Farmers sustain these agricultural lands without planting crops due to a lack of sufficient irrigation facilities which produces confusion for automatic classification of Landsat imagery and hence there are identified as fallow land. These examples suggest that use of Landsat imagery should be at a specific scale (resolution) for land cover/land use mapping as it can be mapped (capability) with 30 meter Landsat. Results from this study suggest that a one hectare minimum mapping unit for land cover mapping should be used with Landsat Imagery. GOFC-GOLD (2010) and IPCC (2006) also recommended this unit in good practice guidelines.

Despite the availability of statistical methods to improve estimation of area of forest loss through the accuracy assessment, the automatic pixel based approach continues to be widely used (Manandhar et al., 2010; Yuan et al., 2005: Manandhar et al., 2010; Teferi et al., 2013). Most land use/land cover change studies end with accuracy analysis. The result of this is that the full potential of using accuracy data for area estimation is not being utilized as well as it could be (Olofsson et al 2013). This problem of not using accuracy data to area estimation to its full potential is very common and well known in remote sensing. In this study, the information obtained from map accuracy assessment of the years 2009 and 2013 was fully utilised to estimate deforestation and construct confidence intervals that reflect the uncertainty of the deforestation area obtained. The results highlight that the accuracy assessment of land cover classification does more than indicate the error in classification map; it provides statistical analysis to sample data to correct the measurement error based on automatic pixel analysis and to decrease the standard error of the estimated area. The results also demonstrate that the effect of the uncertainty on deforestation area estimation is quite small (2.3%).

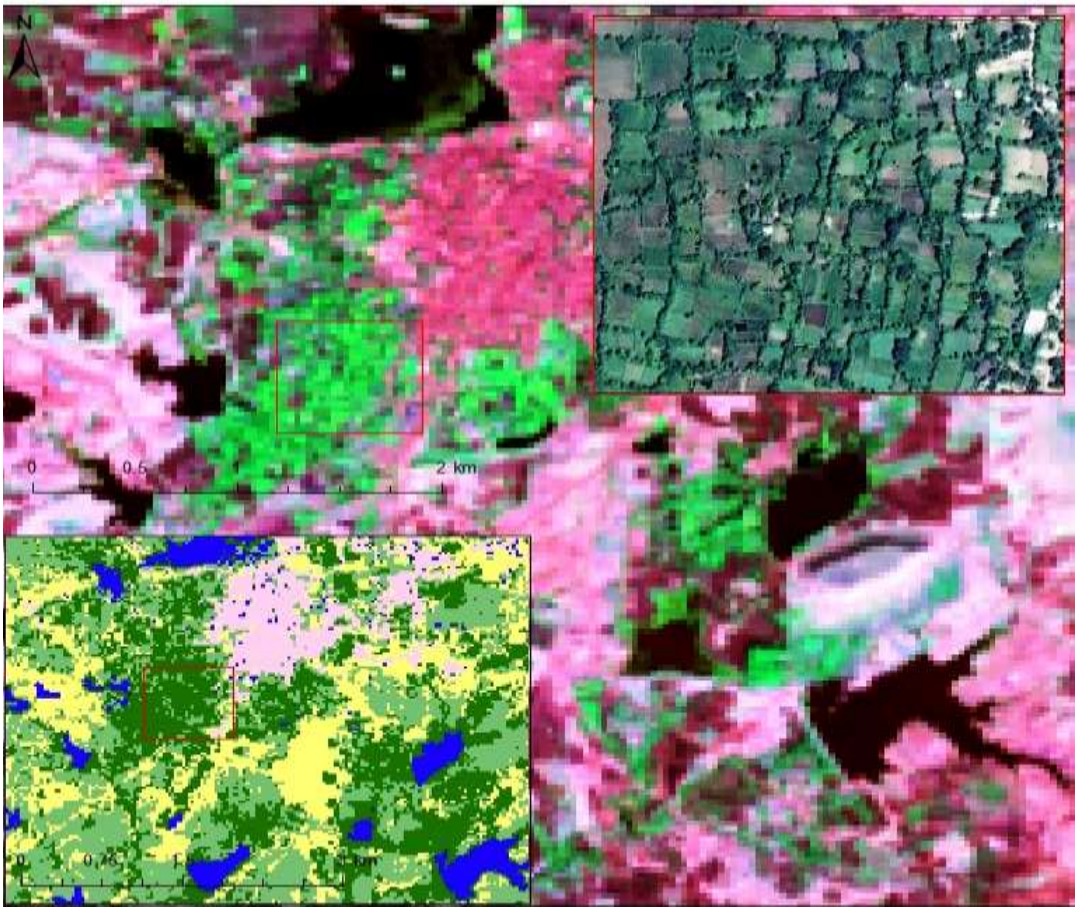

Figure 8.1: The inset aerial photograph shows that the presence of trees along the boundaries of fields results in areas of agriculture being mistakenly classified as forest when using Landsat 30 m data in the study area.

8.3. Understanding land use and land cover dynamics and the associated drivers of change.

This study has highlighted that the integrated use of remote sensing and GIS technology, combined with ground information through advance change matrix analysis, improved quantification of the statistical modelling, which therefore improved understanding of the process of LULC change in detail. The change matrix approach allowed the tracking of land-use changes between categories and was helpful to understand historical patterns and processes of landscape change, as well as the current distribution of land uses.

Analysis of historical landscape change using the transition matrix approach allowed a detailed analysis of the nature and drivers of land use/land cover change. The historical analysis of the change matrix indicated that the Man River basin has undergone significant land use alterations since 1972. Over the last four decades, forest and agriculture areas were found to be the most dynamic land use /land cover categories. During the last four decades, around 54200 ha (33.7 %) of forest area has decreased due to agriculture extension, forest harvesting and infrastructure development. The area under agricultural land increased by 35.3 % (54660 ha) due to deforestation activities, through vegetated land being converted into agriculture. About 58% of the basin area experienced transition from one category to a different category of land use/land cover over the 41 year time period. Of the 58% area of change, about 38 % of the changed area was a net change, while 20% was a swap change. Swap change analysis highlighted the importance of the swapping component methods of land use /land cover changes that other studies may miss.

Forest land tends to be the type of land use with the highest loss (40%) and agriculture land tends to have the highest gain (40%). Water bodies account for 2.7% of total change and 2.3% net change; water bodies thus increased 3580 ha in the basin. Overall, the transition matrix analysis has enabled an understanding of the major transitions of LULC categories, which in turn has provided insights into the nature and process of landscape transitions. The modelling approach also allowed improved understanding of the processes of LULCC for identifying driving factors for further in depth analysis.

Deforestation is one of the most serious issues in the study area and is strongly related to agricultural expansion and forest harvesting. Also, accuracy assessment results highlight uncertainty in the automatic image classification method of deforestation area estimation. Thus, mapping of the deforestation and forest degradation and identifying the responsible driver was the subject of further analysis to better understand the processes leading to change in the Man River basin. Therefore, the choice of direct

interpretation approach (wall-to-wall) was the appropriate step for mapping forest activities in detail. The technique of GIS-based direct interpretation (wall-to-wall) performed well to map forest loss. The approach helped to quantify the status of deforestation and forest degradation (with associated drivers) in the Man River basin from 2009 -2013 based on Landsat thematic maps and Google earth ™ imagery. The spatial pattern of deforestation in the study area is strongly related to the expansion of agricultural land. The deforestation in the study area is caused mainly by forest harvesting (462 ha) and extension of agricultural land on an individual farm basis (7078 ha). The development of dams and water ponds for irrigation and fishing (72 ha) also have an effect on deforestation. Forest degradation is also seen in the basin. Total forest degradation area during 2009-2013 is estimated 5418 ha which is derived from agriculture expansion.

Integrated wall–to–wall mapping based on Landsat imagery analysis, Vegetation Index (EVI and NDVI) and aerial imagery helps to generate deeper, more precise and location specific data for deforestation associated with responsible drivers: a key goal of this research. Enhanced Vegetation Index (EVI) and Normalized Difference Vegetation Index (NDVI) allow better delineation of deforestation and forest degradation areas and Google aerial imagery helps to identify associated drivers. The reliable assessment of forest change and accurate measurement of areas were not possible from Landsat-based automatic classification due to the (30m) resolution of imagery and the nature and scale of forestry activates.

This approach is also recommended in IPCC (2006) guidelines for land use/land cover mapping and performed more reliably compared to recent published research (e.g. Manandhar et al., 2010; Margono et al., 2012; Knorn et al., 2011; Olofsson et al., 2011). The integrated approach produced a new set of maps quantifying the deforestation and forest degradation associated with responsible drivers and estimated the uncertainty in forest mapping. Three different methods were used in this study to map forest loss using Landsat imagery and supporting datasets for time period 2009 -2013 which produced three different results. A discussion on these three different outputs raised an interesting and challenging question among the research community that is how the choice of Minimum Mapping Unit, use of polygon delineation to map forest loss area and use of accuracy data for forest loss area estimation can all affect the quantification of forest loss area. The results of the current study provide some valuable suggestions for development of a land use/land cover mapping approach according to user's requirements and utility of available satellite data. This study used two different Minimum Mapping Units to classify forest cover change which produced different estimates of forest loss. Using one hectare minimum mapping units is much more reliable and consistent in terms of accurate forest loss area estimation according to the definition of forest cover area in Indian region. Results also demonstrated that the choice of minimum

mapping unit less than a one hectare (30mX30m) was also found to be an appropriate decision in terms of accurate estimation of soil loss using forest cover area. Forest cover classification using one hectare minimum mapping unit omits a large amount of small forest cover areas which have less than one hectare. These omitted forest cover areas accumulated to produce large errors in soil erosion estimation when it was used as an input parameter for soil erosion model. This example suggests that the choice of appropriate minimum mapping unit should depend on requirement of land use/land cover change assessment and capability or utility of pixel resolutions of optical sensor. GOFC – GOLD (2010) source book suggests the ideal utility of optical sensors at multiple resolutions for deforestation monitoring.

Global Forest Change maps based on Landsat 30 meter resolution datasets developed by Hansen et al. (2013) are freely available on the Google Earth Engine to use for various environmental studies such as climate change and soil erosion (http://earthenginepartners.appspot.com/science-2013-global-forest). Forest loss and gain maps from 2000 to 2012 were developed to understand human and naturally induced forest changes and how these changes affect other natural and societal systems. Unfortunately, it was found that GFC measurement produced large amounts of error in the estimation of forest loss area when it was compared with the estimation by the current study in the Man River basin area. GFC mapped forest loss area is one thousand times less than the area mapped by the current study (Figure 8.2). GFC forest lost mapping showed that forest loss in the Man River basin during the 12 year time period from 2000 to 2012 was 2.93 ha, while GIS based wall-to-all mapping based on ground reference data estimated 7615.19 ha forest loss in similar areas during the 4 year time period from 2009 to 2013. GFC maps were not validated in this region as maps produced during the current research were verified following GOFC – GOLD guidelines. Thus, the current approach applied in Central India raisees a big question about the quality and use of GFC data for various environmental purposes. The results of the current study were also compared with another study carried out in India at the national level using inventory LULC datasets along with the LULC datasets developed from the Advanced Wide-Field Sensor (AWiFS) of Resourcesat-1 to construct LULC at 5 arc minute resolution during 1880–2010 (Tian et al, 2014). The trend of deforestation is found to be similar in both studies, which indicated that deforestation has reached an alarming stage in recent years in the region (Figure 8.3 and 8.4). The comparison of both studies raisees an interesting and challenging question among the research community; the need for more detailed studies to understand the driving factors of change and produce accurate estimates of change through an integrated approach as developed in the current research. The study on deforestation and forest degradation associated with responsible drivers in India at large spatial scales using satellite data is not done sufficiently. The current integrated approach developed in this thesis provides an opportunity to apply this technique more widely in other parts of India. The current research also recommends that

methods for deforestation and forest degradation mapping are developed in reference to predicted climate change for the Indian region.

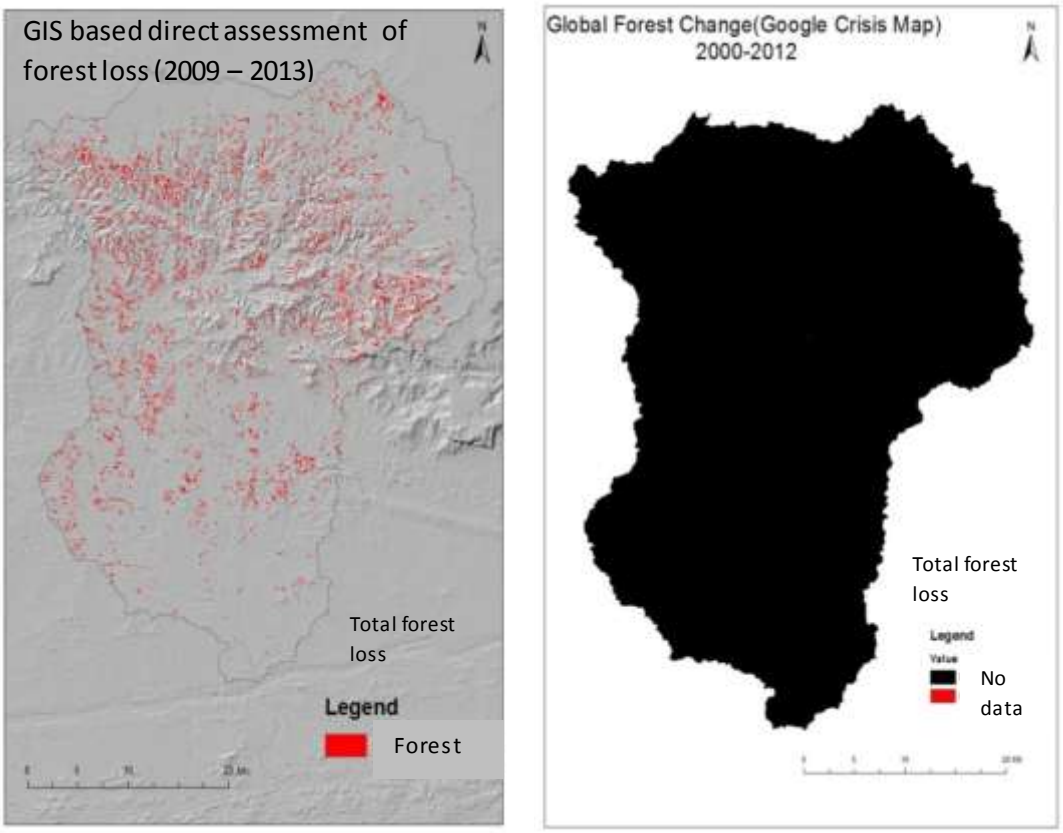

Figure 8.2: Forest loss estimation by GIS based direct assessment approach and the Global Forest Change project.

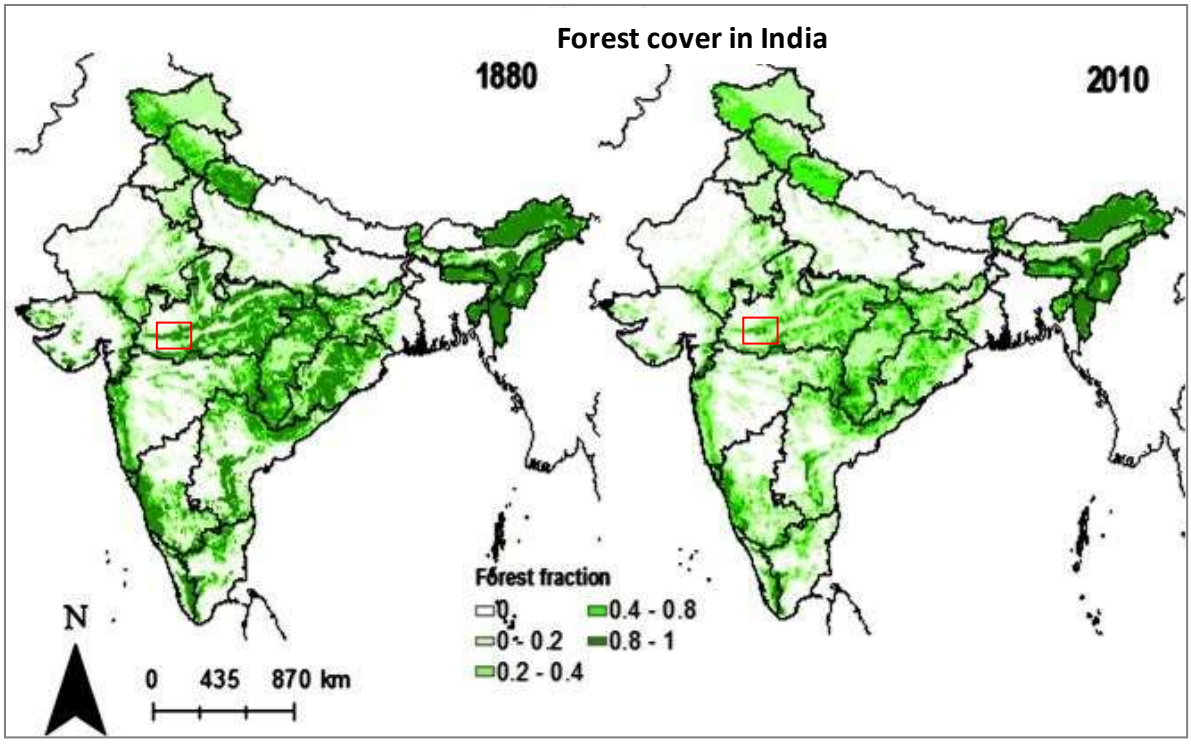

Figure 8.3: Red colour box shows forest loss in Man River basin, Central India (source: Tian et al; 2014).

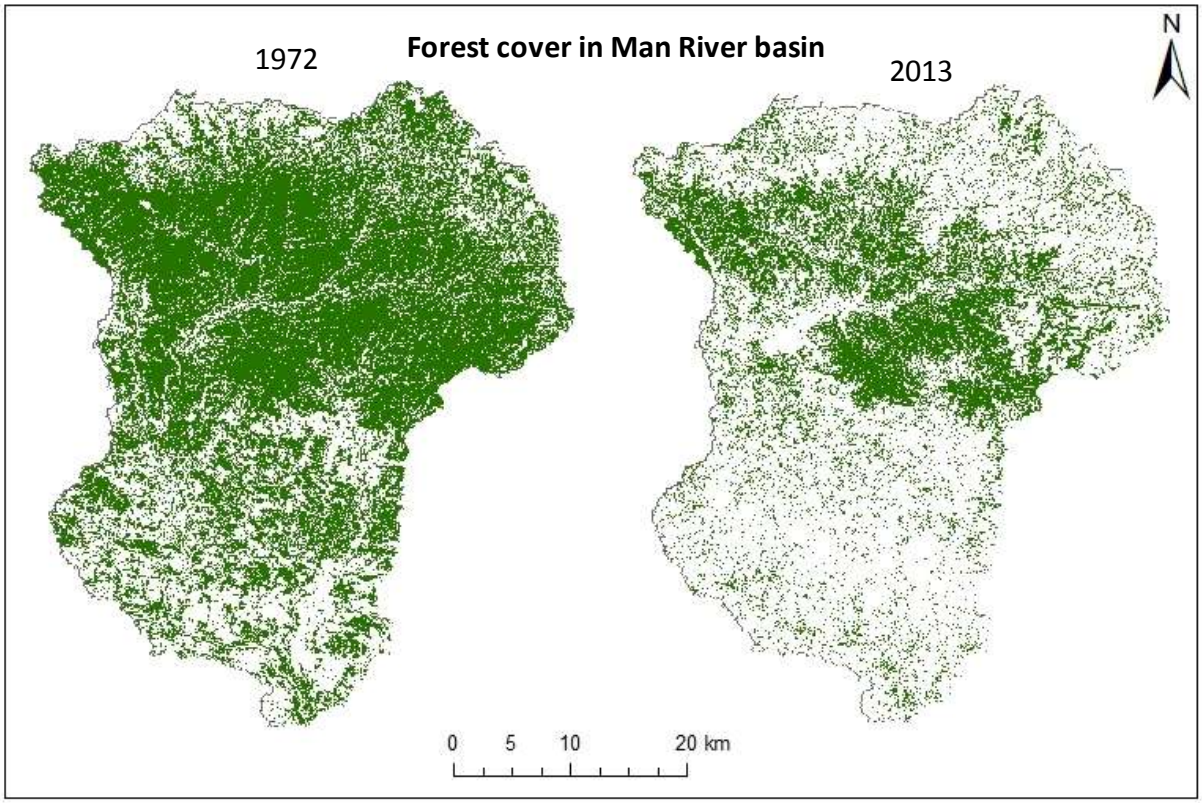

Figure 8.4: Forest loss in Man River basin between 1972 to 2013.

8.4. Modelling the impact of land use/land cover on soil erosion risk using GeoWEPP

To understand how land cover change leads to soil erosion risk in the study basin GeoWEPP was applied in selected watersheds. This approach used the GeoWEPP spatial interface and led to a greater understanding of dynamics of vegetation and soil erosion risk, along with the interaction between the model and remote sensing and digital mapping. The key findings can be grouped into the following themes:

- Impact of land use / land cover input variable on soil erosion risk;
- Reliability of satellite datasets (TRMM rainfall, DEMs and Landsat) for soil erosion risk mapping;
- Different LULC mapping approach and soil erosion;
- Environmental concerns and opportunities for further study.

8.4.1. Soil erosion and land use/land cover

GeoWEPP software performed well to enable the research objectives of the study to be met. The research demonstrated that the local human activities such as agricultural extension and forest harvesting were the main causes of the land use changes during the last 41 years which has led to changes in the soil erosion risk. Some parts of the selected watersheds experienced an increase in permanent agriculture; mostly in areas of steep terrain which are predominantly affected by deforestation and associated forest degradation. However, the overall effect of land cover change over the period 1972–2013 has affected the watershed negatively by increasing soil erosion risk.

The main reason for the increase in the soil erosion potential of the watershed over the study period is attributed to the reduction of forest, increase in fallow land on steeper slopes, and increased cultivation practices in more erosion-prone soils. Results also showed that the forest area was the most effective barrier to soil loss, while the transition of other LULC to agriculture was most detrimental. Since agriculture and fallow land are the two dominant land use categories, implementation of best agricultural practices, tillage operation, and development of forest cover in fallow land are suggested to help reduce soil erosion potential of the watersheds and similarly throughout the Man River basin. Results also indicated that the spatial position of land use/land cover parcels with respect to terrain and associated soil properties is equally important in the soil erosion assessment processes and should be considered as a key factor for proper implementation of soil conservation practices in the study site. Agricultural area also needs to be studied in more detail in terms of soil erosion to reduce soil loss in this particular land use.

The outputs from the current integrated approach are also useful for an on-going conservation project established by the United Nation Development Program (UNDP) in the Madhya Pradesh State. The UNDP program, in conjunction with the Department of Forest, Government of Madhya Pradesh, is implementing practices to reverse the process of land degradation, improve ecosystem integrity services and functions, and improve human livelihoods in the area (GOI –UNDP-GEF 2007). This work could be supported using recent research techniques which are able to provide spatial information about deforestation and forest degradation in term of soil loss behaviour.

8.4.2. Soil erosion risk and remote sensing

The integrated approach applied during the research combined satellite data, digital mapping and ground information, which in turn enabled parameters to be generated for application of GeoWEPP and allowed the spatial distribution of soil erosion risk in the selected watersheds of the Man River basin to be produced. Four parameters within the GeoWEPP model were derived from different satellite data and land use mapping sources; DEMs from a range of source data (Cartosat_1, ASTER and SRTM), Landsat, LISS-III and TRMM all were used to examine the capability of remote sensing data for soil erosion risk modelling.

The different DEMs resulted in slightly different watershed areas and considerable different estimates of numbers of hillslopes and channels in all three watersheds. Overall Cartoset and SRTM DEMs produced the most accurate estimate of soil loss compared to the ASTER DEM, which produced similar estimates of soil erosion to previously published research in the area (Tamgadge et al., 2001). Cartosat and SRTM generated suitable numbers of channels, slopes and areas which were not produced using ASTER-30m data due to poor data quality. This experiment thus makes a strong recommendation that the quality of the DEM should be evaluated before using the DEM data in soil erosion modelling. It is also concluded that future availability of cheap, high resolution and good quality DEMs through advanced satellites applying airborne laser technology will improve soil erosion assessment quality.

The analysis of erosion prediction and the slope statics revealed that DEMs that generated steeper average slopes resulted in higher soil erosion in all three watersheds. This output followed the general principal that steeper slopes have greater potential to erode. For example, ASTER and filter ASTER DEMs had the highest and second highest average slopes respectively compared to the other DEMs. Using these DEMs produced the highest and second highest erosion rate respectively in all three watersheds. The 90-m

SRTM DEMs simulated substantially less soil loss rate than other DEMs in all three watersheds as it had the lowest average slope. Thus, the study of DEM resolution and sources made a unique contribution to the estimating of spatially distributed soil erosion risk at watershed scale.

One of the objectives of soil erosion modelling in this research was achieved by qualitatively comparing TRMM rainfall estimates with Ground based rainfall for 15 years (1998–2013). TRMM rainfall data has good to use as a rainfall parameter for soil erosion risk mapping in study area. The study highlights that the effect of both types of data on soil erosion risk was quite similar. TRMM rainfall data was very useful and should be use if ground rainfalls are not available. Results also highlight that the soil loss and runoff performance with both datasets was not much different in plain areas compare to hill areas. This output indicates that topographic factors are significant with TRMM rainfall datasets. However, TRMM rainfall is a good option for soil erosion risk assessment for remote areas where regular rainfall measurement facility is not available.

8.4.3. Effect of different LULC mapping approaches on soil erosion

The outcomes of two different LULC mapping approaches in three selected watersheds of the Man River basin provide some valuable suggestions for development of a LULC mapping approach according to modelling requirements and the capability of satellite data. The current study uses two different mapping approach (i.e. 30mX30m MMU automatic pixel based approach and 1 ha MMU based wall–to-wall mapping approach) for three watersheds to classify LULC and fed this information into a soil erosion model which produced different LULC estimates and soil erosion rates. The automatic pixel based approach (30mX30m MMU) was found to be an appropriate approach in terms of accurate estimation of soil loss because estimated soil erosion rates were similar to previous estimates in the region (Tamgadge et al., 2001). Land cover classification using the integrated wall-to-wall mapping approach (one ha MMU) omitted a large amount of small land use areas which were less than one hectare. These omitted small areas contributed to make a significant amount of difference in soil erosion estimation when it was used as an input parameter for the soil erosion model. However, the integrated approach is also much more reliable and consistent in terms of accurate forest loss area estimation at the regional scale.

8.4.4. Comparison with previous soil erosion studies

Estimated soil loss results from the current study in the Man River basin were compared with other studies in the central India, as well as in other parts of the world. The purpose of this comparison was to

check the capability of the GeoWEPP technique for soil loss estimation in the Man River basin. The average annual soil erosion estimated in the Man River Basin was 5-10 $Tha^{-1}y^{-1}$ for the Dhar District, according to the District Soil Erosion Atlas developed by the National Bureau of Soil Survey and Land Use Planning using the Universal Soil Loss Equation. This estimate is less than that estimated in the current research using the GeoWEPP model; 21 $Tha^{-1}y^{-1}$. Previously published research by Sing et al., (1992) developed a countrywide map of Indian soil erosion rates based on 21 observed and 64 estimated soil loss data points spread over different land resource regions of' the country. These estimates were superimposed on topographic maps and erosion rate lines drawn. Soil loss data from various research stations, watersheds, and sedimentation of reservoirs were also used. Soil losses for a number of places were estimated using the Universal Soil Loss Equation. The estimated annual erosion rate was 20 $Tha^{-1}y^{-1}$. This figure is similar to the soil erosion estimated in the current research which suggested average annual soil loss of 21.6 $T.ha^{-1}y^{-1}$in all three watersheds.

Boardman (2006) discussed the status and current challenges with soil erosion approaches and suggested some overarching issues that are not answered sufficiently well by current soil erosion modelling. The capability and limitation of current modelling approaches suitable for the Man River basin within Boardman's framework were examined to assess the status of my approach in terms of present day soil erosion science. The GeoWEPP soil erosion modelling emerged positively from this examination. However, there is also a need to validate soil erosion results which can be undertaken using high resolution satellite data. However this can be costly and not always within economic budgets available to validate models at small scale areas. The validation exercise needs to test monthly soil loss and runoff during the rainy session. The 30 meter raster input datasets for land use land cover, topography and soil are useful to run the model, but high resolution imagery will definitely enhance the quality of runoff and soil loss estimation.

Different satellite data sources and spatial resolutions have different data quality and applicability which affected GeoWEPP performance. The evaluation of these data is necessary before they are used for modelling, which was undertaken in this research using Landsat data to produce land cover information. However, such analysis is not routinely carried out. The uncertainty regarding input data sets may introduce larger uncertainties in soil erosion risk estimates. Estimation of soil erosion risk using remote sensing in small watershed is often difficult to process and subject to strong uncertainty analysis. Validation of soil erosion risk class at ground level using quality data will be more appropriate. The GeoWEPP model has limitations to work with small watersheds. In this way, further research is needed to develop a large scale application for GeoWEPP to study at regional scale.

8.4.5. Concerns for the environment and food security

The research results highlight that human activities have caused significant alterations in the land use and land cover change including large amounts of forest loss (40%), forest degradation and agricultural expansion (41%) in the Man River basin during the period 1972 -2013. In the last four decades, the area of agricultural land has increased by 52,600 ha while the area of forest lost was 54,200 ha and this appears to have resulted in an average rate of soil erosion of 21 $Tha^{-1}y^{-1}$ in the basin. In 1972 the rate of soil erosion was 13.7 $Tha^{-1}y^{-1}$ and this has increased to a rate 21 $Tha^{-1}y^{-1}$ which is significantly greater than the average rate of soil erosion of 2.2 tons/acre/year observed in India (Sudhakar et al., 2013; Singh at al., 1992). These figures are of concern in terms of environmental degradation, climate change and food security, both for the present situation and for the future. In addition, the last four decades (1970-2010) have seen a significant growth of population (by 25.53 %) in the study region, most of whom are dependent on subsistence agriculture (Dhar District Census 2011). It is expected that the population will continue to increase for the coming decades. This reflects estimates of population growth for India which predicts 1.69 billion people by 2050, with an average density of 500 people per square kilometre (INED, 2013).

A high population growth rate, deforestation, soil erosion risk and food security are strongly interrelated and continue to increase at an alarming rate in the region. Figures 8.5 to 8.7 were captured in and around the region which signals a clear message of concern for environment degradation and food security. Figure 8.5 shows severe land degradation resulting from deforestation and agricultural expansion in the Man River basin. Thousands of hectares of forests have been removed in the past few decades; much of it has turned into very sensitive degraded land with a high risk of soil erosion.

Figure 8.5: Land degradation in the study area.

For land managers, this is a difficult process to reverse because of the lack of topsoil. Figure 8.6 shows hail storms and unseasonal heavy rain which occurred in 2014 for the first time in the region and caused devastating damage to crops leaving the farmers in a pitiable condition and thrown into crippling debt. Besides crop damage, the unseasonal excessive rains along with hailstorms and lightning also caused losses to human lives. Hundreds of cattle perished and thousands of houses were damaged. It is estimated that more than 20 lakh farmers in the Madhya Pradesh state were badly affected by this single event. Figure 8.7 shows poor tribal children also captured in the study area; it is estimated that 48.6 % of the population live Below the Poverty Line (BPL) and are totally dependent on farming activities for their livelihood.

These images serve to remind us that one of the biggest concerns in India is how to increase food production to feed an increasing population and at the same time attempting to avoid disastrous environmental degradation. It is desirable to increase food production by agricultural expansion, but it is also important to recognise the conservation of forests and other natural vegetation. Unfortunately, it is not possible as the level of forest cover in the Man River basin is now 28.44 % which does not meet the

criteria of a minimum of 33% forest cover in the plains and 66% in the mountain areas that were set by the National Forest Policy of India in 1988. This policy anticipated the problem of soil erosion and ecosystem degradation that we see in the Man River Basin today (Joshi et al., 2011). Further, deforestation for agricultural expansion will most likely result in serious ecosystem degradation from soil erosion and loss of soil carbon in the form of CO^2 emissions.

Another way to address the food production issue is by intensive agriculture management practices (e.g. more application of fertilizer, improved irrigation facilities, and increasing cropping intensity) on existing cropland. Mapping and monitoring of land use change and soil erosion risk on a regular basis also seems necessary. Previously, Mishra (2002) reported that population growth has significant effects on each indicator of agricultural intensification. However, greater fertilizer inputs may result in nutrient transport from croplands to water-bodies, thereby causing eutrophication. Further, agricultural intensification may substantially alter regional climate, water resources, and biogeochemical cycles (Ren et al., 2012; Tian et al., 2012b).

Figure 8.6: Hailstorm and unseasonal heavy rain, Source: The Hindu News March 2014.

Figure 8.7: Poor tribal children whom families totally dependent on farming activities for livelihood and mostly lives below the poverty line.

8.5. **Summary**

In summary, findings confirm that the Man River basin is seriously threatened by loss of natural vegetation such as forest loss driven by agricultural expansion and forest harvesting which has accelerated soil erosion. More specifically, the rate of deforestation and soil erosion risk has reached an alarming rate compared to other parts of India. This is a serious problem because land degradation can have a significant effect on climate change and food security. Findings also confirm that the Man River basin has the appropriate availability of remote sensing data and this study demonstrates that is possible to generate accurate maps of vegetation change and soil erosion risk. This study indicates that it is feasible to apply the GeoWEPP model to evaluate the effect of land use on soil erosion at the watershed scale in areas like the Man River basin where detailed land management data are not easily sourced. Overall, in the Man River Basin there is an urgent requirement for land surface management through effective forest and soil conservation practices.

Chapter – 9

Conclusion

9.1. Introduction

In central India, the Man River basin is facing serious environmental degradation problems including deforestation and soil erosion risk caused by rapacious exploitation and irrational utilization of natural resources. There is a need for a comprehensive methodology to assess and visualize environmental degradation to support sustainable management and attempt to halt further degradation. To understand these problems it is necessary to collect and analyse information on the physical relationships between vegetation, soil and land management. This is complicated when there is a lack of ground data and appropriate modelling techniques. The current study offers an integrated approach which allows a clear understanding of the factors that drive land use cover change and enable assessment of the impact of land use change on soil erosion risk in the Man River basin without incurring a large cost. The approach is partly based on remote sensing data which provides a valuable solution for remote poorly mapped areas where there is a lack of data for parameterising soil erosion models. This study used freely available Landsat time-series imagery from 1972 to the present day for vegetation change modelling and LISS–III, TRMM, Cartosat, ASTER and SRTM satellite imagery for capturing topographic, soil and rainfall information to understand the effect of vegetation change on soil erosion risk. The study also integrated ground-based information with remote sensing to make the approach more robust, reliable and consistent.

9.2. Overview of research objectives and findings

(1) To establish a decadal time series of ortho-rectified Landsat images from 1972 to the present day and further satellite datasets to support erosion modelling.

The study demonstrated that Landsat satellite imagery had an appropriate availability with good quality images from 1972 onwards and with a spatial resolution appropriate to enable patterns and processes of landscape change to be mapped accurately. The study also established a range of satellite data to map the topography, vegetation and soil information for the Man River basin. It includes 30 meter Cartosat and ASTER DEMs, 90 meter SRTM DEM, TRMM and LISS –III.

(2) **To analyse four decades of vegetation changes in order to identify major drivers of landscape change in the Man River basin.**

The study developed an improved technique for vegetation change mapping under the GOFC – GOLD (2009) and IPCC (2006) guidelines and successfully achieved the research goal. The application of remote sensing and field-based information were used to estimate four decades of vegetation change with an advanced change-matrix approach to understand the land use change transactions in detail. The integrated approach improves quantification, statistical modelling and therefore provides an improved understanding of the process and drivers of land use/land cover change. The study also developed a further direct interpretation approach to study deforestation and forest degradation and associated responsible drivers. The quality of change analysis was assessed using data derived from Google Earth™ aerial imagery and field measured GPS waypoints.

(3) To test the sensitivity of the GeoWEPP model to different parameterizations.

The findings show that the sensitivity of GeoWEPP was tested thoroughly using different land use/land cover and satellite data parameters. GeoWEPP is a useful tool to successfully simulate the spatial distribution of soil erosion in response to LULC change and satellite-based rainfall and DEM data. The findings demonstrated that changes in LULC have a significant effect on the estimated levels of soil erosion. It was estimated that declining natural vegetation cover such as forest, scrub forest, fallow land and intensive agricultural extension especially on hillslopes over the last four decades has resulted in an apparent increase in soil loss of 7.37 $Tha^{-1}y^{-1}$. An extensive increase in topsoil removal suggests soil nutrient losses, downstream sedimentation and scarcity of soil water availability, which will translate into reduced crop yields and loss of income to the smallholders and farmers in the study area. This research also implies that satellite datasets and digital mapping for land use/land cover, soil, topography and rainfall provide promising tools that can be used to map soil erosion for developing countries and in remote areas where data availability is not normally sufficient to run process based soil erosion models.

(4) To produce a soil erosion risk map to provide information for effective soil erosion conservation in the Man River basin.

The approach using GeoWEPP, remote sensing and GIS allowed a clear understanding of the soil erosion risk in selected watersheds of the Man River basin which represent the whole study area. GeoWEPP is a

process based model which has the ability to model the behaviour of soil erosion risk linking with different types of land use and cultivation practices. It provides the managers with the information on areas with high soil erosion risk potential. Therefore, watershed managers can locate the problematic areas in a watershed and implement the necessary mitigation to minimize or prevent soil erosion risk**.** GeoWEPP also estimated soil erosion risk with historical vegetation change scenarios. This provides insights into the likely trends of soil erosion risk over a period of four decades. This approach is not only useful for soil erosion risk in term of vegetation change scenarios, but also provides detailed information on soil erosion risk related to topography. Soil erosion risk varies with particular land use or land management practices and responds differently with topography. This approach has the capability to explore the connectivity of soil erosion risk with slope and land use. It helps to estimate the soil erosion risk on hillslopes where forest cover was removed for farming activates. Detailed information on soil erosion risk at a spatial scale that can be linked with vegetation change and land use practices is useful for policy makers and farmers to develop a decision making tools for effective conservation and management plans. Thus, overall this modelling approach has achieved its research objectives.

9.3. Limitations and recommendations for further research

The research conducted in this study has led to some useful outputs on vegetation change detection and soil erosion risk modelling with remote sensing; however it has also uncovered many areas that need additional study. The purpose of this section is therefore to identify and discuss the limitations of the current approach and need for further research.

9.3.1. Vegetation change detection modelling

- The major limitation of this study is the unavailability of historical ground data in the region to validate aspects of the vegetation change analysis. The research focused on the development of spatial and temporal LULC change patterns at 30 meter resolution by integrating Landsat time series imagery, current field-based data and aerial photography from 1972 – 2013. Due to the limited availability of historical ground datasets, current vegetation change results may not have correctly estimated fluctuations in LULC changes over historical time periods. A more accurate estimation of vegetation change and soil erosion modelling would be possible if more comprehensive and accurate data for historical time periods were available.
- Errors in classification and image registration are very common limitations when considering the accuracy of change detection analysis with Landsat imagery. In the current study, a large number

of areas of agriculture were classified incorrectly as fallow land due to the timing of satellite data acquisition with respect to agricultural practices. Similarly, several times Landsat 30 meter image classified eroded areas (or river bed or rock covered areas) as a settlement land use. Such erroneous classifications are usually due to similar spectral values for both land surfaces, for instance house roofs are constructed with cement in the study region. These omission and commission errors significantly affect the accuracy of change detection analysis. As described above, a considerable amount of agriculture land was included erroneously as a commission error into the fallow land class which emphasizes the importance of the timing of satellite data acquisition. The ideal date for satellite image acquisition should be autumn at a time when the agriculture fields are completely green or covered by green crops. However, this criterion is difficult to meet in the study region due to the use of flexible cropping systems which depend on irrigation. Therefore, it is difficult to complete a comprehensive data acquisition strategy that will account for all aspects of land cover mapping for change detection.

- Assessment of the driving factors of deforestation through remote sensing techniques is limited and it is difficult to identify all possible factors that drive deforestation from remote sensing alone. For example, in the Man River basin, the scattered pattern of timber harvesting is one of the common livelihood practices and a significant cause of deforestation which is difficult to identify and map using Landsat and aerial photographs. Similarly, soil erosion on hillsides is one of the significant drivers for deforestation and forest degradation, which is also difficult to map using remote sensing data. These problems limit the study and it is recommended that further field-based research would help to validate the remote sensing results and help identify all possible drivers of forest change.
- Remote sensing data contains several types of error, caution must be taken when they are using for modelling approaches. Miss-interpretation during data evaluation and pre-processing may cause large uncertainty in the results. Calibration of satellite data using ground data is suggested if the data will be used for modelling. The uncertainty analysis regarding data sources may introduce large uncertainties in vegetation change assessment and soil erosion risk estimation. Great attention should be paid to the evaluation and pre-processing of satellite data, such as geometric correction and atmospheric correction, interpolation and registration.

9.3.2. Soil erosion risk assessment modelling

- Soil erosion risk assessment modelling estimated the effect of a range of vegetation, topographic and precipitation scenarios on soil loss, but results were not validated quantitatively in the field.

Validation of soil erosion risk class at ground level is problematic due to the lack of available high quality data.

- The GeoWEPP model has a limitation of being designed to work with relatively small watersheds. GeoWEPP works well for conservation and management practices at the small watershed scale, but at present is not suitable for regional planning. In this way, further research is needed to develop a large-scale application of GeoWEPP to study soil erosion at regional scales. Similarly, vegetation change detection modelling was applied to the whole basin area to map the land cover change, but the effects of land cover on soil erosion risk were examined only in three selected watersheds in the river basin. This is another major limitation of the current research and suggests further testing of the soil erosion model which has ability to work at the basin scale such as PESERA (Pan European Soil Erosion Risk Assessment) and RUSLE (Revised Universal Soil Lose Equation).
- GeoWEPP has the capability to simulate a wide range of watershed conditions including precipitation, impoundments, irrigation, tile drainage and others. Increases in global air temperature cause a rise in the moisture holding capacity of the atmosphere at a rate about 7% per 1 k (Mullan et al., 2012). The technical report of the IPCC (2008) on climate change and water highlights that one of the most direct impacts of climate change could be an increase in heavy precipitation (IPCC, 2008). Increased temperature, precipitation frequency and intensities influence the physical and chemical properties of soil which in turn affect infiltration and soil erosion process and will lead to a greater rate of soil loss. The implementation of rainfall sensitivity and frequency on soil erosion risk in terms of climate change offers a challenging opportunity to conduct future research in the basin area.
- The integrated approach and outputs described in this study are valuable for enhancing the capability of current modelling techniques for measuring land degradation, especially in countries such as India where ground data are sparse and land degradation and resulting soil erosion is a serious issue.
- It is also noted that the modelling approach for vegetation change detection and soil erosion risk estimation at the annual time scale do not provide adequate information to develop ground scale decision support tools for integrating different land management practices. Therefore, it is suggested that actual conservation projects should be developed with farmer participation to plan for site specific and appropriate land management activities.

9.4. Conclusion

The current study successfully demonstrated that the Man River basin is passing through a period of large scale vegetation change caused by excessive utilization of natural resources and population pressure which has accelerated soil erosion risk in the region. The current approach using remote sensing and GIS has allowed a clear understanding of the factors that drive land use/land cover change to be developed and enabled the impact of this change on soil erosion risk in the river basin to be assessed. The use of remote sensing allowed the spatial distribution of soil erosion risk to be mapped in detail for remote areas and provided valuable solutions to emerge from the data that was available in the study region. However, remote sensing data needs to be used carefully to account for possible errors and biases; uncertainty analysis is helpful to quantify the error in data and results. It is also helpful to improve the quality of results. The findings show that the GeoWEPP model is a useful tool to simulate the spatial-temporal pattern of soil erosion risk in response to LULC change and satellite data source variability in the selected watershed of Man River basin studied, indicating that it offers a useful decision making tool for watershed management and planning in data scare regions such as the Man River basin. The findings also demonstrate that changes in land use and land cover have a significant impact on the soil erosion risk. It was estimated that removing natural vegetation cover such as forest and extensive agriculture expansion have accelerate soil erosion risk by 7 $Tha^{-1}y^{-1}$ since 1972. This significant increase in topsoil removal and natural vegetation loss suggests soil nutrient losses, scarcity of soil water availability and increasing temperature which translate into reduced crop production, climate change and food security in the study region. Thus, sustainable management practices for watersheds and appropriate modelling tools are required to protect the land from the negative impact of soil erosion and vegetation change.

References

Achard, F., Grassi G, Herold, M., Teobaldelli, M., and Mollicone D., 2008. Use of satellite remote sensing in LULUCF sector. Background paper at the IPCC Expert Meeting to consider the current IPCC guidance on estimating emissions and removals of greenhouse gases from land uses such as agriculture and forestry. GTOS GOFC-GOLD Report n. 33. Available at: http://www.fao.org/gtos/gofc-gold/series.html.

Acharya, K.P. and Dangi R.B., 2009. Case studies on measuring and assessing forest degradation, Forest degradation in Nepal: Review of data and methods, Forestry Department, Food and Agriculture Organization of the United Nations. http://www.forestrynepal.org/publications/reports/4719 .

Ahern, F. J., Goodenough, D. G., Jar., S. C, Rao, V.R., and Rochon, G., 1977. Use of clear lake as standard reflectors for atmospheric measurements. In Proc.11th Int.Symp.on Remote Sensing Environment., Ann Arbo MI, pp.731-755.

Alberts, E.E., Nearing, M.A., Weltz, M.A. Risse, L.M., Pierson, F.B., and Simanton, J.R., 1995. Soil component. USDA-Water Erosion Prediction Project: Hillslope Profile and Watershed Model Documentation, 7.1-7.47. NSERL Report No. 10.

Alo, C.A., and Pontius, Jr., R.G., 2008. Identifying systematic land-cover transitions using remote sensing and GIS: the fate of forests inside and outside protected areas of Southwestern Ghana. Environ. Plann. B Plann. Des., 35: 280–295.

Arnold, J.G., Srinivasan, R., Muttiah, R.S. and Williams, J.R., 1998. Large area hydrologic modelling and assessment part I: model development. Journal of the American Water Resources Association, 34: 73–89.

Arnold, J.G., and Williams, J.R., 1987. Validation of SWRRB: Simulator for water resources in rural basins. J. Water Resource Planning Manage. ASCE, 113(2): 243-256.

Ascough II, J. C., C. Baffaut, M. A. Nearing, and D. C. Flanagan. 1995. Watershed model channel hydrology and erosion processes. In USDA Water Erosion Prediction Project: Hillslope Profile and Watershed Model Documentation, Ch. 13. D. C. Flanagan and M. A. Nearing, eds. NSERL Rep. 10, USDA-ARS National Soil Erosion Research Laboratory, West Lafayette, IN.

Asner, G.P. and Warner, A.S. 2003. Canopy shadow in IKONOS satellite observations of tropical forests and savannas. Remote Sensing of Environment 87:521-533

Asner, G.P., Knapp, D.E., Broadbent, E.N., Oliveira, P.J.C., Keller, M. and Silva, J. N. 2005.Selective logging in the Brazilian Amazon. Science 310 (5747): 480-483.

Asner, G.P., 1998. Biophysical and Biochemical Sources of Variability in Canopy Reflectance, Remote Sensing of Environment, 64: 234-253.

Asner, G.P., Knapp, D. E., Balaji, A. and Páez-Acosta, G. 2009. Automated mapping of tropical deforestation and forest degradation: CLASlite. Journal of Applied Remote Sensing, 3:033543

Bacchi, O.O.S., Reichardt, K., and Sparovek, G., 2003. Sediment spatial distribution evaluated by three methods and its relation to some soil properties. Soil Tillage Res. 69: 117–125.

Bakker, M.M., Govers, G., and Kosmas, C., 2005. Soil erosion as a driver of land-use change. Agriculture, Ecosystems and Environment, 105(3): 467–481.

Barnes, E.M., and Baker, M.G. 2000. Multispectral data for mapping soil texture possibilities and limitations. Applied engineering and agriculture, 16 (6): 731-741.

Banerjee, R., 2010. Neither water nor governance: Study report of water governance in the Man River Basin, Published by Society for Promotion of Wastelands development under a Sir Dorabji Tata Trust supported Water Governance Project.

Beasley, D.B., Huggins, L.F., and Monke, E.J., 1980. ANSWERS: a model for watershed planning Transactions of the ASAE, 23(4): 938–944.

Bennett, J.P., 1974. Concepts of mathematical modelling of sediment yield. Water Resources Research, 10: 485–492.

Berberoglu, S., and Akin, A., 2009. Assessing different remote sensing techniques to detect land use/cover changes in the eastern Mediterranean. International Journal of Applied Earth Observation and Geoinformation, 11: 46–53.

Bini, C., Gemignani, S., and Zilocchi L., 2006. Effects of different land use on soil erosion in the pre-alpine fringe (North-East Italy): ion budget and sediment yield. Sci Total Environ., 369(1–3): 433–446.

Bishop, M.P., and Shroder, Jr., J.F., 2001. Remote sensing and geomorphometric assessment of topographic complexity and erosion dynamics in the Nanga Parbat massif. In: Khan, M.A., Treloar, P.J.,

Searle, M.P., Jan, M.Q. (Eds.), Tectonics of the Nanga Parbat Syntaxis and the Western Himalaya, Special Publication, vol. 170. Geological Society, London, UK, pp. 181– 200.

Bouaziz, M., Leidig, M., and Gloaguen, R., 2011. Optimal parameter selection for qualitative regional erosion risk monitoring: A remote sensing study of SE Ethiopia. Geoscience Frontiers, 2(2): 237-245.

Boardman, J., 2006. Soil erosion science: Reflections on the limitations of current approaches. Catena, 68: 73 – 86.

Brazier, R.E., Beven, K.J., Freer, J., and Rowan, J.S., 2000. Equifinality and uncertainty in physically based soil erosion models: application of the GLUE methodology to WEPP the Water Erosion Prediction Project, for sites in the UK and USA. Earth Surf. Process. Landforms, 25: 825–845.

Braimoh, A.K.., 2006. Random and systematic land-cover transitions in northern Ghana. Agriculture Ecosystem Environment,. 113,: 254–263.

Broadbent, E.N., Asner, G.P., Peña-Claros, M., Palace, M., and Soriano, M., 2008. Spatial partitioning of biomass and diversity in a lowland Bolivian forest: linking field and remote sensing measurements. Forest Ecology and Management, 255: 2602-2616.

Brown, S., and Braatz, B., 2008. Methods for estimating CO2 emissions from deforestation and forest degradation. Chapter 5 In: GOFC-GOLD. Reducing greenhouse gas emissions from deforestation and degradation in developing countries: a sourcebook of methods and procedures for monitoring, measuring and reporting. GOFC-GOLD Report version COP 13-2. GOFC-GOLD Project Office, Natural Resources Canada, Alberta, Canada.

Bürgi M, Hersperger AM, Schneeberger N (2005) Driving forces of landscape change: current and new directions. Landscape Ecology, 19, 857–68.

Card, D.H., 1982. Using map categories marginal frequencies to improve estimates of thematic map accuracy. Photogrammetric Engineering and Remote Sensing, 49 (12): 431- 439.

Chavez, P.S., 1989. Radiometric calibration of Landsat Thematic Mapper multispectral image. Photogramm. Eng. remote sensing, 55:1285-294.

Cochran, W. G., 1977. Sampling Techniques. 3rd Edition, John Wiley & Sons, New York.

Christoff, A., Stéphane, B., and Richard, G., 2009. Geoscience and Remote Sensing Symposium. IEEE International, 978-1-4244-3395.

Cochrane, T.A., and Flanagan, D.C., 1999. Assessing water erosion in small watersheds using WEPP with GIS and digital elevation models. J. Soil Water Cons. 54 (4): 678–685.

CORINE, 1992. Soil Erosion Risk and Important Land Resources in the Southern Regions of the European Community. EUR 13233, Luxembourg.

Covert, S.A., Robichaud, P.R., Elliot, W.J., and Link, T.E., 2005. Evolution of runoff prediction from WEPP-based erosion model for Harvested and burned forest watersheds. Trans. ASAE .48 (3): 1091-1100.

Currit, N., 2005. Development of remotely sensed, historical land cover change database for Rural Chihuahua, Mexico. International Journal of Applied Earth Observation and Geoinformation, 7: 232 247.

Cyr, L., Bonn, F., and Pesant, A., 1995. Vegetation indices derived from remote sensing for an estimation of soil protection against water erosion. Ecological Modelling, 79 (1–3): 277– 285.

Czaplcwski, R.L., 1992. Misclassification bias in areal estimates, Photogrammetric Engineering b Remote Sensing, 58:189-192.

Daly, C., Neilson, R.P., and Phillips. D.L., 1994. A statistical-topographic model for mapping climatological precipitation over mountainous terrain. Journal of Applied Meteorology 33(2): 140-158.

De Fries, R., Achard, F., Brown, S., Herold, M., Murdiyarso, D., Schlamadinger, B. and Souza Jr. C., 2007. Earth observations for estimating greenhouse gas emissions from deforestation in developing countries. Environmental Science and Policy 10 (4): 385-394.

De Vente, J., Poesen, J., Verstraeten, G., Rompaey, A.V., Govers, G., 2008. Spatially distributed modelling of soil erosion and sediment yield at regional scales in Spain. Global and Planetary Change, 60, 393–415.

De Roo , A.P.J., Wesseling C.G., Ritsema, C.J., 1996a. , LISEM: a single event physically-based hydrologic and soil erosion model for drainage basins: I. Theory, input and output Hydrol. Process, 10, 1107–1117.

De Roo,A.P.J., Offermans, R.J.E ., Cremers, N.H.D.T., 1996b. LISEM: A single event physically-based hydrologic and soil erosion model for drainage basins: II. Sensitivity analysis, validation and application Hydrol.Process. 10, 1119–1126.

Deshpande, N., Kulkarni, A., and Kumar, K., 2012.Characteristic features of hourly rainfall in India. International Journal of Climatology, 32: 1730_1744.

Deng, F., Su, G., and Liu, C., 2007. Seasonal variation of MODIS vegetation indices and their statistical relationship with climate over the sub-tropic evergreen forest in Zhejiang, China.IEEE Geoscience and Remote Sensing Letters, 4(2), 236–240.

Del, M. L. T., Aide, T. M., Scatena, F.N., 1998. The effect of land use on soil erosion in the Guadiana watershed in Puerto Rico.Caribbean Journal of Science, 34(3-4): 298–307.

Douglas, D. H., 1986. Experiments to Locate Ridges and Channels to Create a New Type of Digital Elevation Models.Cartographica, 23(4):29-61

Dhar District Census, 2011.http://www.census2011.co.in/district.php.

Dwivedi, R.S., 2001. Soil resources mapping: A remote sensing perspective. Remote sensing Review, 20: 89-122.

Eiumnoh, A., 2001. Tools for identification, assessment, and monitoring of land degradation. In Response to Land Degradation, Bridges EM, Hannam ID, Oldeman LR, Penning de Vries FWT, Scherr SJ, Sombatpanit S (eds). Science Publishers, Inc: Enfield, NH,pp. 249–260.

Elliot, W.J., D.E. Hall, and D.L. Scheele. 1999a. FS WEPP: Forest Service Interfaces for the Water Erosion Prediction Project Computer Model. Available at: http://forest.moscowfsl.wsu.edu/fswepp/docs/fsweppdoc.html. Accessed 8 October2002.

Elliot W.J. and Hall D.E., 2000. Rock: Clime Beta CD Version Rocky Mountain Research Station Stochastic Weather Generator Technical Documentation. Available at: http://forest.moscowfsl.wsu.edu/fswepp/docs/0007RockClimCD.html. Accessed 9 September 2003.

Elliot, W.J., Hall D.E., and Scheele D.L., 2002. Disturbed WEPP: WEPP interface for Disturbed Forest and Range Runoff, Erosion and Sediment Delivery. Available at: http://fsweb.moscow.rmrs.fs.fed.us/fswepp/docs/distweppdoc.html. Accessed 9 September 2003. Elliot,

W.J., Hall, D.E., 1997. Water Erosion Prediction Project (WEPP) Forest Applications.Gen. Tech. Rep. INT-GTR-365, USDA For. Serv., Rocky Mt. Res. Stn., Ogden, UT, 11 pp.

Fairfield, J., and Leymarie, P., 1991. Drainage Networks from Grid Digital Elevation Models. Water Resources Research, 30(6):1681-1692.

Ferro, V., and Porto, P., 2000. Sediment delivery distributed (SEDD) model ASCE, Journal of Hydraulic Engineering, 5 (4): 411–422.

Flanagan, D.C., Ascough II, J.C., Nicks, A.D., Nearing, M.A., and Laflen, J.M., 1995. Overview of the WEPP erosion prediction model Chap. 1 ,in: D.C. Flanagan, M.A. Nearing (Eds.), USDA Water Erosion Prediction Project: Hillslope Profile and Watershed Model Documentation, USDA-ARS NSERL Rep. 10, USDA-ARS, West Lafayette, IN.

Flanagan, D.C., Livingston, S.J., (Eds.), 1995. USDA-Water Erosion Prediction Project User Summary. NSERL Rep. No. 11, Natl. Soil Erosion Res. Lab., USDA ARS, West Lafayette, IN, 139 pp.

Flanagan,D.C., and Nearing, M.A., 1995. USDA - Water erosion prediction project: Hillslope profile and watershed model documentation. National Soil Erosion Research Laboratory Report No. 10.West Lafayette, Indiana.

Foody, G.M., 2002.Status of land cover classification accuracy assessment, Remote Sensing of Environment, 80:185-201.

FSI, 2009, Forest Survey of India report on "Indian state of forest report" http://www.moef.nic.in/downloads/public-information/ISFR2009Presentation_short.pdf.

Fu, B. J., Meng,Q. H., and Qiu, Y., 2004. Effects of land use on soil erosion and nitrogen loss in the hilly area of the Loess Plateau, China. Land Degradation and Development, 15(1): 87–96.

Gao, J., and Liu, Y. S., 2008. Mapping of land degradation from space: a comparative study of Landsat ETM + and ASTER data. International Journal of Remote Sensing, 29, 4029–4043.

Garbrecht, J., and Martz, L.W., 1997. TOPAZ: An Automated Digital Landscape Analysis Tool for Topographic Evaluation, Drainage Identification, Watershed Segmentation and Sub catchment Parameterization: Overview. US Department of Agriculture, Agricultural Research Service, Durant, Oklahoma (ARS-NAWQL 95-1).

Gibbs, H. K., Brown, S., Foley, J. A., and Niles, J. O., 2007. Monitoring and estimating tropical forest carbon stocks: making REDD and reality Environmental Research Letters 2:045023.

GOFC-GOLD. 2008. Reducing greenhouse gas emissions from deforestation and degradation in developing countries: a sourcebook of methods and procedures for monitoring, measuring and reporting, GOFC-GOLD Report version COP 13-2. GOFC-GOLD Project Office, Natural Resources Canada, Alberta, Canada.

GOFC-GOLD Sourcebook, 2010. A sourcebook of methods and procedures for monitoring and reporting anthropogenic greenhouse gas emissions and removals caused by deforestation, gains and losses of carbon stocks in forests remaining forests, and forestation GOFC-GOLD Report version COP16-1, (GOFC-GOLD Project Office, Natural Resource Canada, Alberta, Canada)

Griscom, B., Ganz, D., Virgilio, N., Price, F., Hayward, J., Cortez, R., Dodge, G., Hurd, J., Lowenstein, F.L., and Stanley, B., 2009. The Hidden Frontier of Forest Degradation: A Review of the Science, Policy and Practice of Reducing Degradation Emissions. The Nature Conservancy, Arlington, VA.

Gronsten, H.A., and Lundekvam, H., 2006. Prediction of surface runoff and soil loss in south eastern Norway using the WEPP Hillslope model. Soil & Tillage Research, 85:186–199.

GOI-UNDP- GEF. 2007. Integrated land use management to combat land degradation and deforestation in Madhya Pradesh .Government of Madhya Pradesh.

Gordon, H. R., 1978. Removal of atmospheric effects from Environ. 66:250–272. Satellite imagery of the ocean. Appl. Opt.17:1631–1636.

Haan, C.T., Barfield, B.J., and Hayes, J.C., 1994. Design Hydrology and Sedimentology for Small Catchments. Academic Press, New York.

Hansen, M. C., Stehman, S.V., Potapov, P.V., Loveland, T.R., Townshend, J.R.G., DeFreis, R.S., Pittman, K.W., Arunarwati, B., Stolle, F., Steininger, M.K.,Carroll, M.,DiMiceli, C., 2008. Humid tropical forest clearing from 2000 to 2005 quantified by using multi-temporal and multi-resolution remotely sensed data. Proceedings of the National Academy of Science.105 (27), 9439-9444.

Hansen, M.C., Potapov, P.V., Moore, R., Hancher, M., Turubanova, S.A., Tyukavina, D., Stehman, S.V., Goetz, S.J., Loveland,T.R., Kommareddy, A., Egorov, A., Chini, L., Justice, C.O., and Townshend,

J.R.G., High – resolution global maps of 21st – century forest cover change . Science , 342 (6160): 850-853.

Hanson, D. L„ Steenhuis, T. S., and Walter, M. F., 2004. Effects of soil degradation and management practices on the surface water dynamics in the Talgua River watershed in Honduras. Land Degradation and Development, 15(4): 367–381.

He, Y. H., Franklin, S. E., Guo, X. L., and Stenhouse, G. B., 2011. Object-orientated classification of multi-resolution images for the extraction of narrow linear forest disturbance. Remote Sensing Letters, 2, 147–155.

Hellden, U., 1991. Desertification—Time for an assessment. Ambio 20:372-383

Hessel, R., Messing, I., and Chen, L. D., 2003. Soil erosion simulations of land use scenarios for a small Loess Plateau catchment. Catena, 54(1-2): 289–302.

IPCC Report on Definitions and Methodological Options to Inventory Emissions from 15 Direct Human-induced Degradation of Forests and Degradation of Other Vegetation Types, 2003 (http://www.ipcc.ch/publications_and_data/publications_and_data_reports.htm#2)

Herold, M., Román-Cuesta, R.M., Heymell, V., Hirata, Y., Van Laake, P., Asner, G.P., Souza, C., Avitabile, V. and MacDicken, K., 2011. A review of methods to measure and monitor historical carbon emissions from forest degradation. Unasylva 62(2): 16-24

Horvath, E.H., Post, D.F., and Kelsey, J.B., 1984. The relationships of Landsat digital data to the properties of Arizona Rangeland. Soil Science Society American Journal, 48, 1331- 1334.

Huguenin, R.L., Karaska, M.A., Blaricom, D.V., and Jensen, J.R., 1997. Sub-pixel Classification of Bald Cypress and Tupelo Gum Trees in Thematic Mapper Imagery. Photogramm. Eng. Remote Sens., 63(6): 717-725.

Huete, A.R., Liu, H. , Batchily, K., and van Leeuwen, W., 1997. A Comparison of Vegetation Indices Over a Global Set of TM Images for EOS-MODIS. Remote Sensing of Environment 59(3):440-451.

India's Initial National Communication (INC, 2004). India's Initial National Communication to the United Nations Framework Convention on Climate Change. http://unfccc.int/resource/docs/natc/indnc1.pdf.

INED Population Studies, 2013. French Institute of Demographic Studies, Series Editors: Brian, Éric, Rohrbasser, Jean-Marc ISSN: 2214-2452.

Irrigation Project Report, Narmada Valley Development Authority (An Organisation of Govt. OF Madhya Pradesh, India).

Jain, S.K., and Goel, M.K., 2002. Assessing the vulnerability to soil erosion of the Ukai Dam catchments using remote sensing and GIS. Hydrological Sciences Journal, 47 (1), 31–40.

Janssen, L. L. F., and van der Wel, F. J. M., 1994.Accuracy assessment of satellite derived land-cover data: A review. Photogrammetric Engineering and Remote Sensing, 60, 419-426.

Jensen, J.R., 2005. Digital Change Detection. In: Keith C. Clarke (Series Editor), Introductory Digital Image Processing—A Remote Sensing Perspective, 3rd edition. Prentice Hall Series in Geographic Information Science, pp. 467–494.

Jetten, V., De Roo, A., Favis-Mortlock, D., 1999. Evaluation of field-scale and catchment-scale soil erosion models. Catena 37, 521– 541.

Jeon, S.B., Olofsson, P., and Woodcock, C.E., 2014. Land use change in New England – revising the forest transaction. Journal of Land Use Science.

Joshi, A.K., Pant, P., Kumar, P., Giriraj, A., and Joshi, P.K., 2011. National Forest Policy in India: critique of targets and implementation. Small Scale For. 10 (1), 83–96.

Kirkby, M., Robert, J., Irvine, B., Gobin, A., Govers, G., Cerdan, O., Tompaey, A., Le Bissonnais,Y., Daroussin, J., D. King, L. Montanarella, M. Grimm, V. Vieilefont, J. Puigdefabregas, M. Boer, C. Kosmas, N. Yassoglou, M. Tsara, S. Mantel, G. Van Lynden, J. Hunting , Pan-European Soil Erosion Risk Assesment,Joint Research Centre, ISPRA (2003).

Knight, J.F., and Lunetta, R.S., 2003: an Experimental Assessment of MinimumMapping Unit Size.IEEE Transactions on Geoscience and Remote Sensing, VOL., 41, No 9, September 2003.

Knijff, J. M., Jones, R.J.A., and Montanarella, L., 2000. Soil Erosion Risk Assessment in Europe: report, European Commission directorate general JRC , Joint Research Centre .

Knisel, W. G., 1980. 'CREAMS: A field-scale models for Chemicals, Runoff and Erosion from Agricultural Management Systems', Report No. 26. U.S. Department of Agriculture, Washington, D.C.

Knorn, J., Kuemmerle, T., Szabo, A., Mindrescu, M., Keeton, W. S., Radeloff, V., Abrudan, I .V., Griffiths, P., Gancz, V., and Hostert, P., 2011. Forest restitution and the protected area effectiveness in post-socialist Romania Biol. Cons. Submitted.

Kumar, S., Kumar, A., Saha, S.K., and Kumar, A., 2008. Stereo Cartosat -1 satellite remote sensing data in assessing topographic potential of soil erosion. Journal of the Indian Society of Remote Sensing, 36, (2): 159—165.

Kummerow, C., Simpson, J., Thiele, O., Barnes, W., Chang, A.T.C., Stocker, E., Adler, R. F., Hou, A. , Kakar, R. , Wentz, F. , Ashcroft, P. ,Kozu, T. ,Hong, Y. , Okamoto, K.,Iguchi, T. ., Kuroiwa, E. I. H. ,Haddad, Z. , Huffman, G. , Ferrier , B., Olson , W. S., Zipser, E., Smith, E. A., Wilheit , T. T., North , G., Krishnamurti, T., and Nakamura, K., 2000.The status of the Tropical Rainfall Measuring Mission (TRMM) after two years in orbit. Journal of Applied Meteorology, 39 (12), 1965–1982.

Lambin, E.F., 1999.Monitoring forest degradation in tropical regions by remote sensing: some methodological issues. Global Ecology and Biogeography 8: 191–198

Laflen, J.M., Elliot, W.J., Flanagan, D.C., Meyer, C.R, and Nearing, M.A., 1997. WEPP predicting water erosion using a process-based model. Journal of Soil and Water Conservation. 52: 96-103.

Lehtonen, R., and Pahkinen, E., 1996. Practical methods for Design and Analysis of Complex Surveys. Revised Edition. Chichester: Wiley.

Littleboy, M., Silburn, D.M., Freebairn, D.M., Woodruff, D.R.andHammer, G.L., 1989.PERFECTA computer simulation model of Productivity Erosion Runoff Functions to Evaluate Conservation Techniques. Queensland Department of Primary Industries Bulletin ,QB89005.

Lifen, X., Xuedong, X., and Xiangwie, M., 2012. Risk assessment of soil erosion in different rainfall scenarios by RUSLE model coupled with Information Diffusion Model: A case study of Bohai Rim, China. Catena, 100:74-48.

Londhe, A., 1995. Impact of Water based Interventions of Rajiv Gandhi Watershed Mission on Tribal Livelihood: Case Study of Dhar District in Madhya Pradesh.

Lu, D., Batistella, M., Mausel, P., and Moran, E., 2007. Mapping and monitoring land degradation risks in the Western Brazilian Amazon using multitemporal Landsat TM/ETM+ images. Land Degradation and Development 18, 41–54.

Long, H. L., Heilig, G. K., and Wang, J., 2006. Land use and soil erosion in the upper reaches of the Yangtze River: Some socio-economic considerations on China's Grain-for-Greenn programme. Land Degradation and Development, 17(6): 589–603.

Lu, D., Mausel, P., Brondizios, E., and Moran, E., 2004. Change detection techniques. International Journal of Remote Sensing, 25 (12) : 2365–2407.

Lunetta, R.S., and Elvidge, C.D., 1998. Remote Sensing Change Detection: Environmental Monitoring Methods and Applications, (Ann Arbor Press: Michigan USA).

Manandhar, R., Odeh, I.O., A., and Robert, G.P.J., 2010. Analysis of twenty years of categorical land transitions in the Lower Hunter of New South Wales, Australia Agriculture, Ecosystems and Environment 135:336–346.

Mark, D. M., 1984. Automatic Detection of Drainage Networks from Digital Elevation Models.Cartographica, 21(2/3):168-178.

Margono, B.A., Turubanova, S., Zhuraveva, I., Potapov, P., Tyukavina, A., Baccini, A., Goetz, S., and Hansen, M.C., Mapping and monitoring deforestation and forest degradation in Sumatra (Indonesia) using Landsat time series datasets from 1990 to 2010. Environ. Res. Lett. 7 : 034010 (16).

Martz, L. W., and Garbrecht, J., 1992. Numerical Definition of Drainage Network and Sub-catchment Areas from Digital Elevation Models. Computers and Geosciences, 18(6):747-761.

Manandhar, R., Odeh, O.A., and Robert, G .P. J., 2010. Analysis of twenty years of categorical land transitions in the Lower Hunter of New South Wales, Australia. Agriculture, Ecosystems and Environment 135:336–346.

Madhya Pradesh state Government, forest Department Report 2007. Forest of state.

McRoberts, R. E., 2011. Satellite image-based maps: Scientific inference or pretty pictures? Remote Sensing of Environment, 115:715–724.

Meng, Q. H., Fu, B. J., and Yang, L. Z., 2001. Effects of land use on soil erosion and nutrient loss in the Three Gorges Reservoir Area, China. Soil Use and Management, 17(4): 288–291.

Merritt, W. S., Letcher, R. A., and Jakeman, A. J., 2003. A review of erosion and sediment transport models. Environmental Modelling & Software, 18:761–799.

Mishra, V., 2002. Population growth and intensification of land use in India. Int. J. Popul. Geogr. 8 (5), 365–383.

Morris, D. G., and Heerdegen, R. G., 1988. Automatically Derived Catchment Boundary and Channel Networks and Their Hydrological Applications. Geomorphology, 1(2):131-141.

Mulla, D.J., Sekely, A.C., and Beatty, M., 2000. Evaluation of remote sensing and targeted soil sampling for variable rate application of lime.CD-ROM. In: P.C. Robert et al., (ed) Proc. 5th Intl. Conf. on Precision Agriculture, Minn., MN, Jul 16-19, 2000. ASA, CSSA, and SSSA, Madison, WI.

Mutekanga F.P., Visser S.M. and Stroosnijder L., 2010. A tool for rapid assessment of erosion risk to support decision- making and policy development at the Ngenge watershed in Uganda . Geoderma . (in press).

Miura, T., Huete, A. R., van Leeuwen, W. J. D., and Didan, K.,1998 .Vegetation detection through smoke-filled AVIRIS images: an assessment using MODIS band passes. Journal of Geophysical Research, 103:32001–3201.

Milfred, C.J., and Kiefer, R.W., 1976. Analysis of Soil Variability with Repetitive Aerial Photography.Soil Science Society of America Journal.40 : 553-557.

Miura, T., Huete, A. R., Yoshioka, H., and Holben, B. N., 2001. An error and sensitivity analysis of atmospheric resistant vegetation indices derived from dark target-based atmospheric correction. Remote Sensing of Environment, 78:284–298.

Mutua, B. M., Klik, A., Loiskandl, W., 2006. Modelling soil erosion and sediment yield at a catchment scale: The case of Masinga catchment, Kenya. Land Degradation and Devlopment, 17(5): 557–570.

Myneni, R. B., Maggion, S., Iaquinta, J., Privette, J. L., Gobron, N., Pinty, B., 1995. Optical remote sensing of vegetation: Modelling, caveats and algorithms. Remote Sensing of Environment, 51, 169–188.

Nandy, S., Kushwaha, S.P.S., and Dadhwal, V.K., 2011. Forest degradation assessment in the upper catchment of the river Tons using remote sensing and GIS. Ecological Indicators, 11:509-513.

Naveen, P., 2014. Madhya Pradesh's forest cover shrinking. The Time of India news. http://timesofindia.indiatimes.com/home/environment/developmental-issues/Madhya Pradeshs-forest-cover-shrinking/articleshow/32417177.cms

Nearing, M. A., Lane, L. J., and Lopes, V. L., 1994. Modeling soil erosion. pp 127-156.

Nicks, A.D., Lane, L.J., and Gander, G.A., 1995.Weather generator. In: Flanagan, D.C., Nearing, M.A. (Eds.), Hillslope Profile and Watershed Model Documentation. NSERL Report no. 10, 2.1–2.2. USDA-ARS National Soil Erosion Research Laboratory,West Lafayette, IN, Flanagan, DC.

NRSA (National Remote Sensing Agency, 2007)NRSA (National Remote Sensing Agency) Natural resources census: national land use and land cover mapping using multi-temporal AWiFS data, project report Publication No. NRSA/LULC/1:250K/2007-1National Remote Sensing Agency, Hyderabad, India (2007).

O Callaghan, J. F., and Mark, D. M., 1984. The Extraction of Drainage Networks from Digital Elevation Data. Computer Vision, Graphics, and Image Processing, 28:323-344.

Olofsson, P., Foody, M.G., Stehman, S.V., and Woodcock, C.E., 2013. Making better use of accuracy data in land change studies: Estimating accuracy and area and quantifying uncertainty using stratified estimation. Remote Sensing of Environment .129:122-131.

Olofsson, P., Kuemmerle, T., Griffiths, P., Knorn, J., Baccini, A., Gancz, V., Blujdea, v., Houghton, Abrudan, I.V., and Woodcock, C, E., 2011.Carbon implications of forest restitution in post-socialist Romania.Environmental Research Letters, 6: 045202.

Pandey, A., Chowdary, V. M., Mal, B.C., and Billib M., 2008. Runoff and sediment yield modeling from a small agricultural watershed in India using the WEPP model. Journal of Hydrology 348(3–4): 305–319.

Pandey, A., Chowdary, V. M., Mal, B.C., and Billib, M., 2009. Application of the WEPP model for prioritization and evaluation of best management practices in an Indian watershed. Hydrol.Process. 23:2997–3005.

Pontius, R.G., Shusas, E., and McEachern, M., 2004. Detecting important categorical land changes while accounting for persistence. Agriculture, Ecosystems and Environment 101: 251–268.

Pontius, R.G., Thontteh, O., Chen, H., 2008. Components of information for multiple resolution comparison between maps that share a real variable. Environmental and Ecological Statistics 15, 111–142.

Povilaitis, A., Robichaud, P., Dumbrauskas, A., Tumas, R., and Ruseckas, J., 1995. Erosion prediction in the republic of Lithuania with the WEPP model.In Proc. Water Quality Modeling, 333-340.

Prabaharan, S., Srinivasa Raju, K., Lakshumanan, C., and Ramalingam, M., 2010. Remote Sensing and GIS Applications on Change Detection Study in Coastal Zone Using Multi Temporal Satellite Data, International Journal of Geomatics and Geosciences ,1(2): 159 -166.

Prins, E., and Kikula, I.S., 1996. Deforestation and regrowth phenology in Miombo woodland assessed by Landsat Multispectral Scanner System data. Forest Ecology and Management 84:263-266.

Puyravaud, J.P., 2003. Standardizing the calculation of the annual rate of deforestation. Forest Ecology and Management. 177:593-596.

Prasanna, V., Vijith, H.,Abinod, S., and Geetha, N., 2012. Estimation of soil erosion risk within a small mountainous sub-watershed in Kerala , India , using Revised Universal Soil Loss Equation (RUSLE) and geo – information technology . Geoscience Frontiers , Volume 3 , Issue 2 , pages 209-215.

Rahman, H., and Dedieu, G., 1994. ”SMAC: a simplified method for the atmospheric correction of satellite measurements in the solar spectrum”. International Journal of Remote Sensing, 15(1):123-143.

Rao, K. H. V., Durga, Rao V., Venkateswara, and Roy, P. S., 2005. Water Resources Development – Role of Remote Sensing and Geographical Information System, Proceedings of 12th International Rainwater Catchment Systems Conference.

Ren, W., Tian, H.Q.,Tao, B.,Huang, Y., and Pan, S.F., 2012. China's crop productivity and soil carbon storage as influenced by multifactor global change. Glob. Chang. Biol. 18 (9), 2945–2957.

Renard, K., Foster, G.,Weesies, G., McCool, D., and Yoder, D., 1997. Predicting Soil Erosion by Water: A Guide to Conservation Planning with the Revised Universal Soil Loss Equation (RUSLE), USDA Agr. Handbook, No 703.

Ringrose, S., Matheson, W., Tempest, F., and Boyle, T., 1990.The development and causes of range degradation features in southeast Botswana using multi-temporal Landsat MSS imagery. Photogrammetric Engineering and Remote Sensing 56:1253-1262

Richter, R., 1990. "A fast atmospheric correction algorithm applied to Landsat TM images". International Journal of Remote Sensing, 11(1):159-166.

Richter, R., 1996. "A spatially adaptive fast atmospheric correction algorithm". International Journal of Remote Sensing, 17(6):1201-1214.

Renschler, C., Flanagan, D.C., Engel, B.A., Frankenberger, J.R., 2002. Geo- WEPP The Geo-spatial interface for the Water Erosion Prediction Project. ASAE meeting paper No. 022171, St. Joseph, Michigan.

Renschler, C.S., 2003. Designing geo-spatial interfaces to scale process models: The GeoWEPP approach. Hydrological Processes 17:1005–1017.

Robichaud, P. R., and Brown, R. E., 2002. Silt fences: an economical technique for measuring hillslope soil erosion, General Technical Report RMRS-GTR-94, U.S. Department of Agriculture, Forest Service, Rocky Mountain Research Station, Fort Collins, Colorado, USA (2002).

Robichaud, P.R., and Elliot, W.J., 2003. Erosion Risk Management Tool. Available at:http://forest.moscowfsl.wsu.edu /cgi-bin/fswepp/ermit/ermit.pl. Accessed 21 October 2003.

Rode, M., and Fredo, H.G., 1999.Testing AGNPS for soil erosion and water quality modelling in agricultural catchments in Hesse (Germany) Physics and Chemistry of the Earth (B), 24 (4) : 297–301.

Rouse, J.W., Haas, R.H., Schell, J.A., and Deering, D.W., 1973. Monitoring Vegetation Systems in the Great Plains with ERTS. Third ERTS Symposium, NASA SP-351 I: 309-317.

Rouse, J.W., Benton, A.R., Toler, R.W., Haas, R.H., 1975. Three examples of applied remote sensing of vegetation. NASA. Lyndon B. Johnson Space Center NASA Earth Resources Survey Symposium, 1(C), pp. 1797–1810.

Rozante, J. R, Moreira, D. S., de Goncalves, L. G. G., and Vila, D. A., 2010. Combining TRMM and surface observations of precipitation: technique and validation over South America, Weather Forecast., 25: 885–894.

Running, S.W., 1990. Estimating primary productivity by combining remote sensing with ecosystem simulation. Remote sensing of Biosphere Functioning (ed. by R.J. Hobbs & H.A. Mooney), pp. 65-86. Springer-Verlag, New York.

Saatchi, S., R. Houghton, R. Dos Santos Alvala, J. Soares and Y. Yu. 2007. Distribution of aboveground live biomass in the Amazon basin. Global Change Biology. 13:816-837.

Sarndal, C. E., Swensson, B., and Wretman, J.,1992. Model- togramm. Eng. Remote Sens. 52:839–846. Assisted Survey Sampling. Springer-Verlag, New York.

Saura, S., 2002. Effects of minimum mapping unit on land cover data spatial configuration and composition. International Journal of Remote Sensing, 23:4853–4880.

Savabi, M. R., Klik, A., Grulich, K., Mitcheli, J.K., and Nearing, M.A., 1995. Application of WEPP and GIS-GRASS to a small watershed in Indiana. Journal of Soil and Water Conservation. 50: 477-483.

Sharma, A., Tiwari, K. N., and Bhadoria, P. B., 2011. Effect of land use land cover change on soil erosion potential in an agricultural watershed. Environmental Monitoring and Assessment, 173(1–4): 789–801.

Sharma, K.D., and Singh, S., 1995. Satellite remote sensing for soil erosion modelling using the ANSWERS model. Hydrological Sciences Journal, 40 (2): 259–272.

Sharpley, A.N., Williams, J.R. (Eds.), 1990. EPIC-Erosion Productivity Impact Calculator: 1. Model Documentation. US Department of Agriculture Technical Bulletin No. 1768. US Department of Agriculture, Temple, TX .

Srinivasan, R., Ramanarayanan, T.S., Arnold, J.G., and Bednarz, S.T., 1998. Large area hydrologic modelling and assessment part II: model application. Journalof the American Water Resources Association, 34: 91–101.

Sorooshian, S., 1991. Model validation: conceptual type models. In: Bowles, D.S., O'Connell, P.E. (Eds.), Recent Advances in the Modelling of Hydrological Systems. Kluwer Academic, pp. 443–467.

Sonneveld , BDJS. 2003. Formalizing expert judgments in land degradation assessment: A case study for Ethiopia. Land Degradation & Development 14: 347–361.

Soto, B., and Diaz-Fierros, F., 1998. Runoff and soil erosion from areas of burnt scrub: comparison of experimental results with those predicted by the WEPP model. Catena 31:257-270.

Souza, J. C., and Barreto, P., 2000. An alternative approach for detecting and monitoring selectively logged forests in the Amazon. International Journal of Remote Sensing, 21(1):173-179.

Souza, J. C., Firestone, L., Silva, L.M., Roberts, D., 2003. Mapping forest degradation in the Eastern Amazon from SPOT4 through spectral mixture models. Remote Sens. Environ.87: 494–506.

Souza, J. C., Cochrane, M.A., Sales, M.H., Monteiro, A.L., and Mollicone, D., 2009. Integrating forest transects and remote sensing data to quantify carbon loss due to forest degradation in the Brazilian Amazon. Case Studies on Measuring and Assessing Forest Degradation. Forest Resources Assessment Working Paper 161, Forestry Department, FAO, Rome, Italy.

Sudhakar, C.R., Dutta, K., and Jha, C.S., 2013. Analysing the gross and net deforestation rates in India. Current Science, Volume 105, no.11, 10 December 2013.

Story, M., and Congalton, R.G., 1986. Accuracy Assessment: A User's Perspective. Photo-grammetric Engineering & Remote Sensing, 53(3), 397-399.

Stehman, S. V., Czaplewski, R. C., 1998. Design and analysis for thematic map accuracy assessment: fundamental principles. Remote Sensing of the Environment. 64: 331–344.

Stehman, S. V., 2009. Model-assisted estimation as a unifying framework for estimating the area of land cover and land-cover change from remote sensing. Remote Sensing of Environment, 113(11), 2455–2462.

Symeonakis, E, and Drake, N., 2004. Monitoring desertification and land degradation over sub-Saharan Africa. International Journal of Remote Sensing, 25: 573–592.

Tamgadge, D, B., Gajbhiye K.S., mandal, C., Mandal, D.K., Bankar, W.V., Velayutham, M. and Kaushal, G.S., 2001 .Soil resources atlas of Dhar district (Madhay Pradesh). Natioanal Bureau Of Soil Survey and Land Use Planning, Nagpur, India.NBSS Publication No. 90.

Teferi, E., Bewket, W., Stefan, U., and Jochen, W., 2013. Understanding recent land use and land cover dynamics in the source region of the Upper Blue Nile, Ethiopia: Spatially explicit statistical modeling of systematic transitions Agriculture, Ecosystems and Environment, 165: 98– 117.

Tian, H. A., Kamaljit, B.A., Tao, B., and Vinay, K. D., 2014 . History of land use in India during 1880–2010: Large-scale land transformations reconstructed from satellite data and historical archives, Global and Planetary Change 121: 78–88.

Tian, H.,Lu, C., and Melillo, J., 2012b. Food benefit and climate warming potential of nitrogen fertilizer use in China. Environ. Res. Lett. 7, 044020. http://dx.doi.org/10. 1088/1748 9326/7/4/044020 (8 pp.).

Tiwari, A. K., Risse., L. M., and Nearing, M. A., 2000. Evaluation of WEPP and its comparison with USLE and RUSLE. Trans. ASAE 43(5): 1129-1135.

Tirkey, A.S., Pandey, A.C., and Nathawat, M.S., 2013. Use of Satellite Data, GIS and RUSLE for Estimation of Average Annual Soil Loss in Daltonganj Watershed of Jharkhand, India. Journal of Remote Sensing Technology, 1(1): 20-30.

Townshend, J. R., 2013. High-Resolution Global Maps of 21st-Century Forest Cover Change Science. 342 (6160): 850-853.

Tucker, C., 1979. Red and photographic infrared linear combination for monitoring vegetation, Remote Sensing of Environment, 8:127-150.

Tucker, C.J., Dregne, H.E., and Newcomb, W.W., 1991. Expansion and contraction the Sahara desert from 1980 to 1990. Science, 253:299-301.

Ugur, O., Gunay, E., Mustafa, B., and Emrah, E., 2007. Use of USLE/GIS technology integrated with geostatistics to assess soil erosion risk in different land uses of Indagi Mountain Pass—C¸ankırı, Turkey.

USDA, Agricultural Research Service and USDA Forest Service. 2003. CLIGEN Weather Generator, Expand and Improved. Available at:http://horizon.nserl.purdue.edu/Cligen/. Accessed 9 September 2003.

USDA, 2008. Research/TOPAZ-General Information. Washington, D.C.: USDA-ARS. Available at: www.ars.usda.gov/Research/docs.htm?docid=7835#lt. Accessed 30 March 2009.

Van, O. P.J.A., 2005. Improving land cover change estimates by accounting for classification errors, International Journal of Remote Sensing, 26, 3009-3024.

Van O, P.J.A., 2007. Interpreting the change detection matrix, Remote Sensing of Environment, 108:1-8.

Versace, V.L., Ierodiaconou, D., Stagnitti, F., and Hamilton, A.J., 2008. Appraisals of random and systematic land cover transitions for regional water balance and re-vegetation strategies. Agriculture, Ecosystem and Environment, 123, 328–336.

Viney, N.R., and Sivapalan, M., 1999. A conceptual model of sediment transport: application to the Avon River Basin in Western Australia Hydrological Processes, 13: 727–743.

Vriling, A ., Sterk, G., and Vigiak,O., 2006. Spatial evaluation of soil erosion risk in the West Usambara Mountains, Tanzania. Land Degaridation and Development, 17(3):301-319.

Vrieling, A., Jong , S. M. De., Sterk , G., and Rodrigues, S.C., 2006 .Timing of erosion and satellite data: A multi-resolution approach to soil erosion risk mapping. International Journal of Applied Earth Observation and Geoinformation. 10: 267–281.

Wertz-Kanounnikoff, S., 2008.Monitoring forest emissions – a review of methods. CIFOR Working Paper, 39: 19.

Weng, Q., 2002. Land use change analysis in the Zhujiang Delta of China using satellite remote sensing, GIS and stochastic modelling. Journal of Environmental Management 64:273–284.

Wessels K.J., Prince ,S.D., Frost, P.E., and van Zyl D. 2004. Assessing the effects of human induced land degradation in the former homelands of northern South Africa with a 1 km AVHRR NDVI time-series. Remote Sensing of Environment, 91: 47–67.

White, M.J., and Storm, D.E., 2010. Targeting critical sediment source areas using SWAT and WEPP roads. Prog.Oklahoma Academy of Science, 99:123-132.

Wight, JR., and Skiles , J.W., 1987. SPUR: Simulation of Production Utilization of Rangeland. Documentation and User Guide.USDA, ARS, ARS 63, 366pp.Williams, J.R., C.A. Jones, J.R. Kiniry and D.A. Spanel. 1989. The EPIC crop growth model. Trans. ASAE 32(2):497-5.

Wight, J.R., 1987. ERHYM-II: Model Description and User Guide for the Basic Version, USDA, ARS, ARS, 59:23.

Williams, J. R., Jones, C.A., Dyke, P.T., 1984. A modeling approach to determine the relationship between erosion and soil productivity. Transactions of the ASAE 27: 129–144.

Williams, J.R., Nicks, A.D., and Arnold, J.G., 1985. SWRRB, a simulator for water resources in rural basins. ASCE Hydraulics Journal, 111(6): 970 – 986.

Williams, J.R., Jones, C.A., Kiniry, J.R. and Spanel, D.A., 1989. The EPIC crop growth model. Trans. ASAE, 32(2):497-511.

Wilkinson, G. G., 1996. Soft computing in remote sensing data analysis. Classification algorithms — Where next? (pp. 93–99). Singapore: World Scientific (Ch.).

Wilkinson, G., 2005. Results and implications of a study of fifteen years of satellite image classification experiments. IEEE Transactions on Geoscience and Remote Sensing, 43(3):433–440.

Wolter, K. M., 2007. Introduction to variance estimation. New York: Springer. Xian, G., & Crane, M. (2005). Assessments of urban growth in the Tampa Bay watershed using remote sensing data. Remote Sensing of Environment, 97(2), 203–215.

Xu, Y. Q., Peng, J., and Shao, X. M., 2008. Assessment of soil erosion using RUSLE and GIS: A case study of the Maotiao River watershed, Guizhou Province, China. Environmental Geology, 56: 1643–1652.

Young, A., Onstad, C.A., Bosch, D.D., and Anderson W.P., 1989. AGNPS: a nonpoint-source pollution model for evaluating agricultural watersheds. Journal of Soil and Water Conservation, 168–173.

Yuan, F., Sawaya, K.E., Loeffelholz, B. C., and Bauer, M. E., 2005. Land cover classification and change analysis of the Twin Cities (Minnesota) Metropolitan Area by multitemporal Landsat remote sensing. Remote Sensing of Environment, 98:317– 328.

Yu, B., Ciesiolka, C. A. A., Rose, C. W., and Coughlan, K. J., 2000. A validation test of WEPP to predict runoff and soil loss from a pineapple farm on a sandy soil in subtropical Queensland, Australia, Australian Journal of Soil Research, 38:537-54.

Yu, B., and Rosewell, C.J., 2001. Evaluation of WEPP for runoff and soil loss prediction at Gunnedah, NSW, Australia. Aust. J. Soil Res. , 39:1131–1145.

Zhang, X.C. and Garbrecht, J.D., 2003. Evaluation of CLIGEN precipitation parameters and their implication on WEPP runoff and erosion prediction. Trans. ASAE, 46(2): 311-320.

Zhang, J. X.,Wu J.Q., Chang, K., Elliot, W.J. and Dun, S., 2009. Effects of DEM source and resolution on WEPP hydrologic and erosion simulation: a case study of two forest watersheds in Northern Idaho. American Society of Agricultural and Biological Engineers ISSN 0001-2351, 52(2): 447-457.

Zhu, Z., Yang, L., Stehman, S. V., and Czaplewski, R. L., 2000. Accuracy assessment for the U.S. Geological Survey regional land-cover mapping programme: New York and New Jersey region. Photogrammetric Engineering and Remote Sensing, 66:1425– 1435.

Appendices:

Appendix 6.1: Monthly Average rainfall from 1998 -2012 with TRMM and IMD

Months	Ground (mm)	TRMM (mm)
Jan	0.2	2.43
Feb	0.653	5.26
March	1.85	4.87
April	0.81	2.07
May	4.97	14.99
Jun	106.14	165.83
July	240.58	319.19
Aug	221.77	261.64
Sep	162.32	195.17
Oct	17.01	27.74
Nov	8.041	16.32
Dec	0.574	1.35

Appendix 6.2: Average monthly number of day precipitation occur (NDPO) from 1998 -2012

Months	Ground	TRMM
Jan	0.48	0.095
Feb	0.21	0.207
March	0.53	0.191
April	0.45	0.0814
May	1.11	0.59
Jun	5.92	6.528
July	13.62	12.566
Aug	10.64	10.3
Sep	6.86	7.683
Oct	1.81	1.092
Nov	1.02	0.642
Dec	0.43	0.053

Appendix 6. 3: 15 year cligen based generated TRMM and IMD data monthly data from 1998 -2012

TRMM	TRMM rainfall												
Year	Jan	Fab	Mar	April	May	Jun	Jul	Aug	Sep	Oct	Nov	Dec	Total
2012	0	18.8	0	0	0	27.8	278.4	316.4	213.8	25.6	50.7	0.3	
2011	3.6	0	0	1.3	0	179.7	250.1	242.6	127.4	67.8	0	47.4	
2010	0	0	0	0	0	154.5	317.8	297.8	169.2	18.3	0	0	
2009	3.6	3.9	4.5	0	0	138	225.4	240.6	156.1	17.9	0	0.3	
2008	14.1	0	7.3	0	67.6	180.5	140.4	336.9	161.5	40.9	25.3	0	
2007	1	9.3	5.6	0	0	156.3	208.4	256.4	341.3	15.9	0	0	
2006	18.4	0	0	78.4	0	78.9	238.1	383.7	122.3	35	0	0	
2005	0	25.4	0	24.9	3.6	274.7	379.7	371	128.6	22.4	26.3	0	
2004	0	0	41.7	0.6	6.6	48.5	333.8	341.1	221	70.2	0	55	
2003	1	16.9	0	0	0	95.2	285.9	324.9	222.7	6.9	0	0	
2002	0	0	4.6	0.9	0	151.8	216.4	261.6	227.8	24.4	0	0	
2001	0	0	14.3	0	26.4	111.5	380.6	277.1	209.1	18.5	0	0	
2000	0	15.9	0	24.2	15.5	166.5	195.1	243.4	278.2	17.7	0	0	
1999	0	3.8	12.7	0	5.4	110.5	342.1	276.8	254.1	17.7	0	19	
1998	0	0	6.3	0	16.7	274.9	199.9	352.1	195.6	20.6	1.7	0	
	2.78	6.2	6.4	8.6	9.4	143.2	266.14	301.49	201.91	27.98	6.9	8.1	989.54
	IMD rainfall												
Year	Jan	Feb	Mar	Apr	May	Jun	Jul	Aug	Sep	Oct	Nov	Dec	Total
2012	0	0	0	0	16.7	63	168.8	206.1	152.3	4.2	17.6	0.3	
2011	24.2	0	0	0	0	79.9	37.7	252.5	87	41.3	1.2	0.3	
2010	0.3	0	0	0	5.1	89.3	304.2	173.3	142.6	10.7	0	0	
2009	0.3	0	0.3	0	0	90.1	201.1	253.7	266	9.8	12.8	0.3	
2008	0.6	0	3	0	0.3	113.2	113	209	170	14.1	10.6	0	
2007	0.3	0	2	0	0	120.3	197.6	203.7	180.1	34.8	0.9	0	
2006	0.3	0	0	0	0	64.2	100.1	256.5	170.7	16.5	0	0	
2005	0	0	0	0	9.1	161.6	268.3	299.3	234.5	9.4	5.8	0	
2004	0	0	0.6	0	9.2	80.4	248.4	424.6	138.7	16	0	0	
2003	0.6	0	0	0	0	85.2	201	348.5	64.7	0	0	0	
2002	13	0	57.8	0.9	0	79.1	108.4	284.1	110.5	0	2.8	0	
2001	0	0	5.9	0	15	35.5	341.7	370.9	230.8	43.7	9.7	0	
2000	49.7	10.5	0	0	0	85.5	29	73.1	265.3	11.5	0	0	
1999	0	0	1.9	0	12.8	129.1	222.9	233.8	118.4	19.8	0	36.2	
1998	0	0	3.7	0	2.1	90.6	61.2	242.5	222	15.9	17.2	0	
	5.95	0.7	5.01	0.06	4.69	91.13	173.56	255.44	170.24	16.51	5.24	2.49	731

Appendix 6. 4: TRMM and IMD original monthly rainfall data from 1998 - 2012

		TRMM based monthly rainfall (mm)														
(month)	[mm]98	1999	2000	2001	2002	2003	2004	2005	2006	2007	2008	2009	2010	2011	2012	mean
Jan-98	3.12	1.391	0.67	1.93	0.14	1.69	12.94	5.83	0.16	1.16	0.36	4.13	2.922	0.016	0.051	2.43
Feb-98	0.08	32.41	0.408	0.11	22.0	13.72	0.31	0.20	0.53	3.80	1.14	0.12	3.935	0.011	0.086	5.26
Mar-98	1.62	0.273	0.332	5.44	8.54	0.08	0.03	6.02	43.52	0.11	3.18	2.59	1.091	0.241	0.069	4.87
Apr-98	0.68	0.027	0.201	1.73	13.07	1.98	0.40	2.79	1.17	4.35	0.49	0.52	0.268	1.583	0.861	2.07
May-98	2.92	3.22	41.022	21.41	3.025	0.65	10.09	2.17	41.55	24.47	2.22	51.4	2.472	1.245	17.051	14.99
Jun-98	142.64	195.9	130.77	335.26	174.59	167.63	96.93	64.29	90.69	90.15	134.24	94.3	95.385	181.22	43.441	165.8
Jul-98	310.37	268.9	250.69	199.26	61.66	372.61	348.11	380.04	438.27	315.74	249	424.45	286.64	394.89	487.27	319.1
Aug-98	129.18	130.6	127.85	141.41	381.95	230.33	297.63	133.29	614.50	313.11	203.71	120.75	354.40	508.84	237.09	261.6
Sep-98	400.86	346.6	44.113	60.9	173.36	353.53	89.8	205.35	256.01	145.67	142.93	122.82	170.16	164.40	250.94	195.1
Oct-98	47.77	117.9	4.135	80.8	1.32	1.06	35.38	0.83	22.72	0.23	14.74	60.13	26.777	1.054	1.273	27.74
Nov-98	4.21	1.94	1.335	0.36	4.84	0.39	8.17	1.33	15.38	1.12	7.06	111.25	86.705	0.42	0.349	16.32
Dec-98	0.00	0.004	0.187	0.02	0.00	0.09	0.02	0.21	0.05	0.15	0.26	18.8	0.012	0.377	0.006	1.35
		IMD based monthly rainfall (mm)														
(month)	1998	1999	2000	2001	2002	2003	2004	2005	2006	2007	2008	2009	2010	2011	2012	mean
Jan-98	1.6	0.1	0	0.348	0.013	0	0	0	0	0.4	0	0	0.5	0	0	0.2
Feb-98	0.17	3.04	0.25	0	3.712	2.3	0	0	0	0	0	0	0.3	0	0	0.653
Mar-98	4.65	0	0	3.306	7.824	0.5	0	0	10.3	0	0	0.8	0	0	0	1.85
Apr-98	0.66	0	0	0.105	11.443	0	0	0	0	0	0	0	0	0	0	0.81
May-98	8.06	1.36	22.9	14.518	1.353	0	2.8	0	0	6.5	0	4.6	0.3	0	12.1	4.97
Jun-98	67.9	206.3	97.6	256.824	198.61	159.1	66	30.34	68.4	134.3	71.9	64.6	99.4	46.7	24.1	106.1
Jul-98	205.5	136.2	250.04	137.311	28.747	388.4	196.4	249.02	329.9	432.2	241	314.1	211.7	240.1	248	240.5
Aug-98	161.9	81.5	115.7	82.041	198.91	217.11	390.4	78.93	461.6	373.2	99.5	119	324	378.3	244.4	221.7
Sep-98	239.6	258.5	19.3	13.777	104.16	300	50.9	197.18	205.5	214.4	242.1	105.9	143.1	110.8	229.5	162.3
Oct-98	25.2	70.34	11.4	38.83	0.424	0	14.8	0	5.2	0	32.8	54.7	0	0	1.3	17.01
Nov-98	7.4	0.19	0.87	1.118	2.657	0	0	0	2.5	0	0	56.6	49.2	0	0	8.041
Dec-98	0	1.4	0.1	0	0.372	0	0	0	0	0	0	6.7	0	0	0	0.574

Appendix7.1: WEPP Watershed Simulation for all flowpaths averaged over subcatchments (flowpath method) (FLOWPATH SUMMARY (flowpath method, on-site assesment) (Loniwatershed) .

WEPP Hillslopes	TOPAZ Hillslope	Runoff Valume (m^/yr)	Soil loss (t/yr)	Sediment yield (t/yr)	Area(ha)	Mapped soil loss(t/ha /yr	Sediment yield (t/ha/yr)
1	22	788.7	21.4	21.4	0.1	181.7	181.7
2	23	814.9	23.5	23.5	0.1	239.8	239.8
3	32	1972.4	2.8	2.8	0.5	6.1	6.1
4	33	930.6	6.4	6.4	0	162.7	162.7
5	41	8048.5	3.3	2.6	3.1	1.1	0.8
6	42	8924.2	4.5	4.3	3.1	1.5	1.4
7	43	925.4	2.1	2.1	0.3	6.3	6.3
8	52	56374.3	14.4	14.2	17.8	0.8	0.8
9	53	40809.3	9.7	8.6	10.1	1	0.8
10	61	6622.8	161.8	117.8	7.2	22.4	16.3
11	63	16689.1	3.3	3.1	3.1	1.1	1
12	62	27375.7	10.2	10.2	8.2	1.2	1.2
13	72	2159	6.5	6.5	0.5	13.8	13.8
14	73	1618.4	8.2	8.2	0.2	38.1	38.1
15	83	4209.5	20.9	20.9	0.7	29.6	29.6
16	82	1850.5	2.4	2.4	0.7	3.3	3.3
17	92	5250.9	0.7	0.7	0.6	1.2	1.2
18	93	5464.2	21.2	21.2	0.7	30.1	30.1
19	101	3218.9	66.5	64.4	3	22.2	21.5
20	102	4002	194.4	194.2	2.4	82.7	82.6
21	103	2143.9	20.6	20.6	1.3	16.2	16.2
22	111	3412.7	68.3	64.3	3.3	20.7	19.5
23	112	662.8	1.1	1.1	0.1	8.4	8.4
24	113	2494.2	19.3	19.3	0.3	61.5	61.5
25	121	3376.1	40.2	26.5	3.3	12.1	8
26	123	9069.8	67.2	54.9	7.7	8.7	7.1
27	122	16474.5	81.2	81.2	2.8	29.2	29.2
28	131	10283.2	6.1	6.1	3.7	1.6	1.6
29	132	2555.4	2.9	2.9	0.4	6.7	6.7
30	133	2929.1	9.5	9.5	0.6	15.7	15.7
31	142	12349	6.8	6.8	2.4	2.8	2.8
32	143	24967	5.8	4.8	8.6	0.7	0.6
33	152	8632.2	36	36	1.8	19.5	19.5
34	153	7162.4	2.1	2.1	1.2	1.8	1.8
35	162	30398.1	11.5	11.5	10.1	1.1	1.1
36	163	22669.6	9.8	9.8	6.3	1.6	1.6
37	171	4770	83.3	81.1	4.5	18.4	17.9
38	172	7794.7	100.6	100.6	6	16.9	16.9
39	173	17394.6	38.3	38.3	3.6	10.5	10.5
40	181	3994.6	65.3	64.3	3.9	16.7	16.5
41	182	25396.8	90.4	90.4	6.7	13.4	13.4
42	183	22141.7	27.7	27.7	5.2	5.3	5.3
43	191	18444.2	416.5	405.3	3.9	107.3	104.4
44	192	24628	5.9	5.9	5.6	1.1	1.1
45	193	24513.3	674.4	674.4	5.5	123.3	123.3
46	201	12268.4	5.5	5.5	4.1	1.3	1.3
47	202	21743.2	5.5	5.5	5.5	1	1
48	203	19115.6	4.6	4.6	4.2	1.1	1.1

Appendix 7.2: WEPP Watershed Simulation for Representative Hillslopes and Channel. 40 YEAR AVERAGE ANNUAL VALUES FOR Loni WATERSHED.

Hillslopes	Runoff Volume (m^3)	Subrunoff Volume (m^3)	Soil Loss (kg)	Sediment Deposition (kg)	Sediment Yield (kg)
Hill 1 (22)	788.68	0	21364.27	0	21364.18
Hill 2 (23)	814.9	0	23502.89	0	23502.8
Hill 3 (32)	1972.42	0.07	2763.62	0	2763.62
Hill 4 (33)	930.59	0.22	6378.97	0	6378.96
Hill 5 (41)	8048.47	0.06	3265.21	679.63	2585.55
Hill 6 (42)	8924.18	0.07	4513.73	251.84	4261.85
Hill 7 (43)	925.43	0	2112.47	0	2112.47
Hill 8 (52)	56374.34	0.29	14429.39	196.8	14232.55
Hill 9 (53)	40809.32	0.53	9661.54	1070.51	8591.03
Hill 10 (61)	6622.78	0	161812.3	44032.29	117779.55
Hill 11 (63)	16689.09	0.31	3285.2	210.82	3074.37
Hill 12 (62)	27375.71	0.57	10199.3	0	10199.72
Hill 13 (72)	2159.01	0.11	6485.02	0	6485.03
Hill 14 (73)	1618.38	0.08	8224.62	0	8224.64
Hill 15 (83)	4209.54	0.22	20887.77	0	20887.77
Hill 16 (82)	1850.47	0	2369.43	10.89	2358.54
Hill 17 (92)	5250.94	0.23	746.58	0	746.58
Hill 18 (93)	5464.24	0.38	21218.54	0	21218.56
Hill 19 (101)	3218.91	0	66506.72	2083	64423.95
Hill 20 (102)	4001.98	0	194422.7	207.5	194215.11
Hill 21 (103)	2143.94	0	20612.54	0	20612.49
Hill 22 (111)	3412.71	0	68282.28	4028.31	64254.22
Hill 23 (112)	662.83	0	1147.34	0	1147.34
Hill 24 (113)	2494.21	0.24	19294.97	0	19294.97
Hill 25 (121)	3376.13	0	40181.45	13658.02	26523.46
Hill 26 (123)	9069.78	0	67151.54	12205.04	54946.57
Hill 27 (122)	16474.54	1.12	81198.46	0	81198.45
Hill 28 (131)	10283.22	0.08	6124.17	120.05	6058.85
Hill 29 (132)	2555.41	0.11	2898.79	0	2898.79
Hill 30 (133)	2929.09	0.12	9539.64	0	9539.69
Hill 31 (142)	12349.05	0.35	6828.96	0	6828.97
Hill 32 (143)	24966.96	0.13	5836.06	1027.05	4808.98
Hill 33 (152)	8632.22	0.47	36002.58	0	36002.49
Hill 34 (153)	7162.38	0.22	2125.25	0	2125.25
Hill 35 (162)	30398.1	0.31	11513.27	3.34	11509.97
Hill 36 (163)	22669.57	0.63	9839.54	0	9840.49
Hill 37 (171)	4770.03	0	83312.44	2253.03	81059.56
Hill 38 (172)	7794.69	0	100637.37	0	100637.32
Hill 39 (173)	17394.58	0	38314.68	0	38314.7
Hill 40 (181)	3994.62	0	65291.53	987.6	64303.86
Hill 41 (182)	25396.82	1.09	90429.86	0	90429.87
Hill 42 (183)	22141.71	0.75	27716.07	0	27716.04
Hill 43 (191)	18444.16	0	416517.8	11169.34	405348.67
Hill 44 (192)	24628.03	0.55	5941.22	0	5941.23
Hill 45 (193)	24513.35	2.66	674410.9	0	674410.36
Hill 46 (201)	12268.4	0.18	5475.76	0	5475.71
Hill 47 (202)	21743.2	0.35	5476.33	0	5476.29
Hill 48 (203)	19115.55	0.61	4589.94	0	4589.94

Appendix 7.3: WEPP Watershed Simulation for Representative Hillslopes and Channel. 40 YEAR AVERAGE ANNUAL VALUES FOR Loni WATERSHED.

Channels and Impoundments	Discharge Volume (m^3)	Sediment Yield (tonne)	Soil Loss (kg)	Upland Charge (m^3)
Channel 1 (204)	53331.8	12.5	7649.8	53128.3
Channel 2 (194)	67853.1	271.2	18749.3	67588.8
Channel 3 (184)	51769.4	60.3	8599.1	51535
Channel 4 (174)	30243.9	71.6	5146	29959.3
Channel 5 (164)	135429.6	111.8	26009.8	135082
Channel 6 (154)	219261.2	614.7	295057.1	219078
Channel 7 (144)	310155.0	478.6	20827.3	309909.5
Channel 8 (134)	15805.2	9.7	1044	15768
Channel 9 (124)	29127.5	59.5	5895.5	28921.6
Channel 10 (114)	6612.2	35.1	2048.4	6570
Channel 11 (104)	9397.9	131.8	3459.3	9364.8
Channel 12 (94)	26884.3	111.3	9132.8	26725.9
Channel 13 (84)	62183.5	141.4	54831.5	62072
Channel 14 (74)	81802.3	125	163.7	81766.3
Channel 15 (64)	50902.8	41.9	14866.6	50688.5
Channel 16 (54)	230404.0	152.2	59001.7	229889.6
Channel 17 (44)	17955.9	6.5	1385.8	17898.2
Channel 18 (34)	251042.9	180.7	53386.7	251263.2
Channel 19 (24)	562564.9	742.3	137762.8	562801.5

Appendix 7.4: WEPP Watershed Simulation for Representative Hillslopes and Channel. 40 YEAR AVERAGE ANNUAL VALUES FOR Loni WATERSHED.

- 37 storms produced 702.14 mm. of rainfall on an AVERAGE ANNUAL basis
- 40 events produced 318.87 mm. of runoff passing through the watershed outlet on an AVERAGE ANNUAL basis
- Average Annual Delivery From Channel Outlet:
  - Total contributing area to outlet = 176.42 ha
  - Avg. Ann. Precipitation volume in contributing area = 1238748. m^3/yr
  - Avg. Ann. irrigation volume in contributing area = 0. m^3/yr
  - Avg. Ann. water discharge from outlet = 562565. m^3/yr
  - Avg. Ann. total hillslope soil loss = 2490.8 tonnes/yr
  - Avg. Ann. total channel soil loss = 725.0 tonnes/yr
  - Avg. Ann. sediment discharge from outlet = 742.3 tonnes/yr
  - Avg. Ann. Sed. delivery per unit area of watershed = 4.2 T/ha/yr
  - Sediment Delivery Ratio for Watershed = 0.231

Appendix7.5: GeoWEPP simulation outputs with different scenarios in all three watersheds.

	40YEAR SIMULATION												
Scenario NO	Scenario code	Watershed_name	offsitre Area (ha)	offsite Rainfall	offsite Year of Averag Annual	offsite Produced Stroms	offsite Rainfall (mm)	offsite event produced	offsite Hillslope	offsite Channel	onsite Runoff Volume(m^3)	onsite Soil loss t/yr	onsite soil loss t/ha/yr
1,6,12	MOG_40Y_CRTO_09	Mograba	603.3	GROUND	40	37	702.14		288	121	939694.7	21209.9	35.15
2	MOG_40Y_CRTO_01	Mograba	603.3	GROUND	40	37	702.14		288	121	3002184.6	26369.9	43.7
3	MOG_40Y_CRTO_89	Mograba	603.3	GROUND	40	37	702.14		288	121	2325241	20783.2	34.44
4	MOG_40Y_CRTO_80	Mograba	603.3	GROUND	40	37	702.14		288	121	2393908.7	12775.2	21.17
5	MOG_40Y_CRTO_72	Mograba	603.3	GROUND	40	37	702.14		288	121	921091.2	12716.4	21.07
7	MOG_40Y_ASTER_09	Mograba	603.3	GROUND	40	37	702.14	153	199	82	10174023.8	25191.3	41.75
8	MOG_40Y_FILASTER_09	Mograba	588.3	GROUND	40	37	702.14	170	268	118	8758583.9	23698.3	40.28
9	MOG_40Y_SRTM_09	Mograba	604.8	GROUND	40	37	702.14	148	236	114	11607001.7	19259.7	31.84
10	MOG_15YGRND_CRTO_09	Mograba	603.3	GROUND	15	40	731.03	209	288	121	9806432.2	29880	49.52
11	MOG_15YTRMM_CRTO_09	Mograba	603.3	TRMM	15	70	989.54	212	288	121	9122632	19920.2	33.01

Scenario NO	Scenario code	Watershed_name	offsite Area (ha)	offsite Rainfall	offsite Year of Averag Annual	offsite Produced Stroms	offsite Rainfall (mm)	offsite event produced	offsite Hillslope	offsite Channel	onsite Runoff Volume	onsite Soil loss t/yr	onsite soil loss t/ha/yr
1,6,12	LONI_40Y_CRTO_09	LONI	175	GROUND	40	37	702.14	40	48	19	2064792.4	2217.3	12.67
2	LONI_40Y_CRTO_01	LONI	175	GROUND	40	37	702.14	40	48	19	1092809.7	2327.3	13.29
3	LONI_40Y_CRTO_89	LONI	175	GROUND	40	37	702.14	40	48	19	3563995.4	2182.1	12.46
4	LONI_40Y_CRTO_80	LONI	175	GROUND	40	37	702.14	40	48	19	1058004.3	1779.4	10.16
5	LONI_40Y_CRTO_72	LONI	175	GROUND	40	37	702.14	40	48	19	2678269.2	2178.2	12.44
		LONI											
7	LONI_40Y_ASTER_09	LONI	147.7	GROUND	40	37	702.14	40	46	18	1095296		17.77
8	LONI_40Y_FILASTER_09	LONI	143.3	GROUND	40	37	702.14	40	48	19	911833.2	2027.6	14.14
9	LONI_40Y_SRTM_09	LONI	133.7	GROUND	40	37	702.14	40	56	25	1254369.8	567.7	4.24
		LONI											
10	LONI_15YGRND_CRTO_09	LONI	175	GROUND	15	40	731.03	40	48	19	2306182.2	2313.5	13.22
11	LONI_15YTRMM_CRTO_09	LONI	175	TRMM	15	70	989.54	63	48	19	2129904.2	2117.7	12.1

Scenario NO	Scenario Code	Watershed_name	offsite Area (ha)	offsite Rainfall	offsite Year of Averag Annual	offsite Produced Stroms	offsite Rainfall (mm)	offsite event produced	offsite Hillslope	offsite Channel	onsite Runoff Volume	onsite Soil loss t/yr	onsite soil loss t/ha/yr
1,6,12	SLKN_40Y_CRTO_09	SLKNPUR	150.9	GROUND	40	37	702.14	40	96	39	3128159.5	2365.6	15.67
2	SLKN_40Y_CRTO_01	SLKNPUR	150.9	GROUND	40	37	702.14	40	96	39	1708704	2401	15.91
3	SLKN_40Y_CRTO_89	SLKNPUR	150.9	GROUND	40	37	702.14	40	96	39	938377.4	1737.8	11.51
4	SLKN_40Y_CRTO_80	SLKNPUR	150.9	GROUND	40	37	702.14	40	96	39	1293573.1	1283	8.5
5	SLKN_40Y_CRTO_72	SLKNPUR	150.9	GROUND	40	37	702.14	40	96	39	1126624.9	1192.1	7.8
7	SLKN_40Y_ASTER_09	SLKNPUR	164.7	GROUND	40	37	702.14	40	78	31	2644920.2	4540	27.56
8	SLKN_40Y_FILASTER_09	SLKNPUR	166.6	GROUND	40	37	702.14	40	77	31	2792124.5	3411.1	20.47
9	SLKN_40Y_SRTM_09	SLKNPUR	138.7	GROUND	40	37	702.14	40	116	48	2690821.3	1071.2	7.75
10	SLKN_15YGRND_CRTO_09	SLKNPUR	150.9	GROUND	15	40	731.03	40	96	39	3238084.5	2271.1	15.05
11	SLKN_15YTRMM_CRTO_09	SLKNPUR	150.9	TRMM	15	70	989.54	67	96	39	3023015.9	2240.1	14.84